SEDIMENT TRANSPORT PROCESSES AT A NOURISHED BEACH

By

PAUL A. WORK

A DISSERTATION PRESENTED TO THE GRADUATE SCHOOL
OF THE UNIVERSITY OF FLORIDA IN
PARTIAL FULFILLMENT OF THE REQUIREMENTS
FOR THE DEGREE OF DOCTOR OF PHILOSOPHY

UNIVERSITY OF FLORIDA

1992

UNIVERSITY OF FLORIDA LIBRARIES

ACKNOWLEDGEMENTS

To date I have been blessed with many excellent teachers, advisors, and mentors. My advisor throughout my Ph.D. program, Dr. R.G. Dean, has set a standard which is not likely to be surpassed, however. His unflagging support, enthusiasm, and friendship will always be remembered, appreciated, and emulated. I also owe Mrs. Dean thanks for her generous hospitality on many occasions.

Thanks are due to the staff of the Coastal and Oceanographic Engineering Laboratory, particularly George Chappell, Don Mueller, and Mark Sutherland, for their help with field work, and Sidney Schofield, for assistance in several areas, particularly instrumentation. Many others assisted with field work at some point: Jorge Abramian, Lynda Thompson, Mill Dowd, Dr. Dean, Jon Grant, Sam Houston, Feng Jiang, A. Kadib, Li-Hwa Lin, Emre Otay, Rajesh Srinivas, and Victoria Stone.

I would also like to thank Professor Emeritus R.L. Wiegel of the University of California at Berkeley for introducing me to the field of coastal engineering.

My final acknowledgement is reserved for those to whom I probably owe the most. My parents instilled in me the work ethic and values that have allowed me to make it this far, and have supported me in all my endeavors. And my friend Joni Schmidt has helped me in more ways than she knows, providing me with everything from food to a few lessons in what is and what should be important in life.

TABLE OF CONTENTS

ACKNOWLEDGEMENTS ii

LIST OF TABLES v

LIST OF FIGURES vi

ABSTRACT xi

CHAPTERS

1 INTRODUCTION 1

2 LITERATURE REVIEW 11

2.1 Previous Studies of Beach Nourishment Evolution 12
2.2 Other Studies of the Perdido Key Area 22
2.3 Summary 22

3 FIELD DATA COLLECTION 24

3.1 Topographic/Wading Profile Surveys 32
3.2 Hydrographic Surveys 35
3.3 Waves, Currents, and Tides 42
3.4 Sand Samples 47
3.5 Weather Data 48
3.6 Ft. Pickens Pier Tide Gage 53
3.7 Assessment of Errors 53

4 ANALYSIS AND INTERPRETATION OF FIELD DATA 61

4.1 Wave, Current, and Tide Data 61
4.2 Sediment Transport Processes: Observations Based on Survey Data . 81
4.3 Longshore Sediment Transport Direction 105
4.4 Nourishment Project Volumes 109

5 MODELING LONGSHORE SEDIMENT TRANSPORT PROCESSES . . 111

5.1 Background 111
5.2 Analytical, "One-Line" Approach 114
5.3 Influence of Wave Refraction 119
5.4 Effective Wave Parameters 124
5.5 Comparison of Analytical Model to Measured Changes 126
5.6 Numerical Approach to One-Line Modeling 129

5.7 Determination of Best-Fit Empirical Transport Coefficient 137
5.8 Discussion of Results 145

6 MODELING CROSS-SHORE SEDIMENT TRANSPORT PROCESSES . 153

6.1 Background 154
6.2 Formation of Longshore Bars 160
6.3 Previous Models for Beach Profile Evolution 165
6.4 Desired Characteristics of a Beach Profile Model 168
6.5 Cross-shore Transport Rate vs. Dissipated Wave Energy 170
6.6 Previous Models Compared to Field Data 175
6.7 Summary 195

7 CONCLUSIONS 198

REFERENCES 202

BIOGRAPHICAL SKETCH 213

LIST OF TABLES

3.1	Chronology of Perdido Key Data Collection Efforts.	27
3.2	Coordinates, Elevations and Azimuths for DNR Monuments in Escambia County, FL.	33
3.3	Locations and depths of offshore sand samples.	49
3.4	Sieves used for grain size analysis.	51
3.5	Cross-shore distribution of grain size at various contours (Gulf side). Longshore standard deviation is given following median grain size.	51
4.1	Monthly and annual statistics for significant wave height, H_s. . .	68
4.2	Monthly and annual statistics for wave period corresponding to peak of energy spectrum, T_p.	68
4.3	Monthly and annual statistics for magnitude of mean current, U_c.	69
4.4	Summary of available wave data for Perdido Key area. Data collection for this study is ongoing.	81
5.1	Parameters selected for application of analytical solution for planform evolution.	127
5.2	Effect of various parameters on best-fit K value. $\Delta x \approx 300$ m, $\Delta t = 1$ day for all tests. $\alpha_R < 0$ yields westward transport.	140
6.1	Forces and flows influencing cross-shore sediment transport. . . .	159

LIST OF FIGURES

1.1 Schematic view of planform and profile evolution after beach nourishment. Cross-shore width of project greatly exaggerated in top figure, vertical scale exaggerated in lower figure. 5

1.2 Beach profile evolution in large-scale, two-dimensional wave tank. Data from Kraus and Larson [1988]. 7

1.3 Beach profile evolution in field, after nourishment. Data from Perdido Key, Florida. 8

1.4 Forces influencing beach profile evolution. 9

3.1 Location of field project. 25

3.2 Temporal availability of data at the field site. 29

3.3 Locations of beach profile transects and data collection stations. 31

3.4 Generalized profile geometry and survey methodology. 36

3.5 Surveyed beach profiles at R-58, Perdido Key. 37

3.6 Raw bathymetry data for R-50, October, 1991. Two passes by boat are superimposed. 40

3.7 Bathymetry data for R-50, after spike removal, smoothing, adding proper vertical and horizontal offsets, and patching with wading profile data. 41

3.8 Schematic of wave gage and tripod. 42

3.9 Cross-shore distribution of grain sizes. 52

3.10 Repeatability test at R-46, June, 1992. 56

4.1 Spectra of noise in pressure sensor and current meter, based on 128 points sampled at 1 Hz, Hanning window. Gage in still air in lab. 63

4.2 Spectra from previous figure, transferred to free surface using an assumed depth of 6 m. 64

4.3 Spectra of noise in pressure sensor, based on 1024 points sampled at 100 Hz, Hanning window. Gage in still air in lab. 66

4.4 Number of valid pressure and current data bursts, sorted by month, for the period 1/18/90–6/30/92. 67

4.5 Maximum and mean monthly significant wave heights, $(H_s)_{max}$ and $\overline{H}_s$. 70

4.6 Maximum and mean monthly wave periods at spectral peak, $(T_p)_{max}$ and $\overline{T}_p$. 71

4.7 Maximum and mean monthly mean currents, $(U_c)_{max}$ and $\overline{U}_c$. Calibration suspect for August, September, and October data. . . . 72

4.8 Histogram of significant wave heights measured in the field. . . . 73

4.9 Histogram of wave periods corresponding to spectral peak measured in the field. 74

4.10 Histogram of mean currents measured in the field. 75

4.11 Measured and predicted percent exceedance curves for significant wave height. Measurements from Perdido Key, 1/90–6/92; theory due to Thompson and Harris [1972]. 77

4.12 Measured joint distribution of significant wave height and period corresponding to spectral peak. Based on 2389 observations for 1/18/90–6/30/92. 78

4.13 Directional distribution of waves at the spectral peak, January, 1990–June, 1992. Top of plot corresponds to North. Each bin is ten degrees in width. 79

4.14 Directional distribution of mean currents, January, 1990–June, 1992. Top of plot corresponds to North. Each bin is ten degrees in width. 80

4.15 Coordinate system for sediment transport problem. 83

4.16 Surveyed beach profiles at R–58, November, 1989, through May, 1991. 85

4.17 Surveyed beach profiles at R–58, September, 1991, through June, 1992. 86

4.18 Planform changes since beach nourishment. 87

4.19 Movement of the –4 m contour since beach nourishment. 88

4.20 Planform changes associated with 1985 nourishment project. Data collected by Rutgers University and reported in Dean [1988]. . . 91

4.21 Longshore gradient of longshore sediment transport rate, based on measured profile changes. Positive gradients indicate erosion. Pensacola Pass is adjacent to R–67; the western end of the survey area is to the left. 92

4.22 Average of profiles at ranges 45, 46, 48, 50, 52, 56, and 58. 93

4.23 Average of profiles at ranges 30, 32, 34, 36, and 38. 94

4.24 Cross–shore sediment transport rates computed based on average profile changes within nourishment area for the 1990 and 1991 annual surveys. Offshore transport is positive, longshore gradients of longshore sediment transport assumed negligible. 95

4.25 Cross–shore sediment transport rates computed based on average profile changes west of nourishment area for the 1990 and 1991 annual surveys. Effect of longshore gradients neglected. 96

4.26 Cross–shore sediment transport rates computed based on average profile changes within nourishment area for intermediate survey periods. Effect of longshore gradients neglected. 98

4.27 Cross–shore sediment transport rates computed based on average profile changes west of nourishment area for intermediate survey periods. Effect of longshore gradients neglected. 99

4.28 Cross–shore transport signal after removal of longshore contribution, based on field measurements and computed "average" profiles within the nourished beach. 101

4.29 Changes occurring at profile R–42 for first year. 103

4.30 Computed cross–shore distribution of the longshore gradient of longshore sediment transport, $\partial q_x(x,y)/\partial x$. 104

4.31 Longshore component of radiation stress, $S_{xy}(t)$ computed from all suitable wave data. $S_{xy} > 0$ implies westward sediment transport. 107

5.1 Beach profile geometry for one–line model of planform evolution. 115

5.2 Error function. 117

5.3 Beachfill evolution as predicted by analytical solution. K=0.77, ℓ=4000 m, H_b=0.5 m, $(h_* + B)$=5 m, G=0.0113 m^2/s. 118

5.4 Coordinate system for shoaling/refraction problem. Adapted from Dean and Yoo [in press]. 123

5.5 Comparison of measured and idealized initial planforms. 127

5.6 Longshore gradient of longshore sediment transport rate, as predicted by one–line, analytical solution, vs. measurements, September, 1990, to October, 1991. 130

5.7 Finite–difference definitions for one–line model. 131

5.8 Average retreat of waterline within nourished zone. Changes due, almost exclusively, to cross–shore sediment transport. 135

5.9 "Error surface" indicating error between measured and numerically modeled longshore gradients of longshore transport as a function of K and $(h_* + B)$. 142

5.10 Best–fit (mimimum ε^2) results for several combinations of K and $(h_* + B)$. Curve 2: K=1.0, $(h_* + B)$=2; 3: K=0.33, $(h_* + B)$=4; 4: K=0.15, $(h_* + B)$=8; 5: K=0.14, $(h_* + B)$=10. All results include 3.7 m/yr background erosion. 143

5.11 Best one–line model results describing longshore gradient of longshore sediment transport, $\partial Q_x/\partial x$. 146

5.12 Computed longshore gradient of longshore sediment transport for first and last daily time steps in "best" simulation. 147

5.13 Background erosion rate along Perdido Key, based on shoreline positions indicated on historical maps. Pensacola Pass is to right. 150

6.1 Schematic view of three common distributions for the cross–shore sediment transport rate. Note that each distribution has localized zones of accretion and erosion. 162

6.2 Spatially–averaged minimum depth over bar vs. time, in field. "Inside" implies nourished profiles (R41–R64); "Outside" means "natural" profiles (R25–R40). 163

6.3 Spatially–averaged maximum depth in trough vs. time, in field. "Inside" implies nourished profiles (R41–R64); "Outside" means "natural" profiles (R25–R40). 164

6.4 Decay of cross–shore sediment transport rate with time, based on surveys in large wave tank. (Case 300, Kraus and Larson [1988]). 172

6.5 Total energy dissipated divided by surf zone volume, plotted against average cross–shore transport rate within surf zone for large wave tank data. Points are connected chronologically, with the maximum transport rate in each case corresponding to the first survey interval. 176

6.6 Total energy dissipated divided by surf zone volume, plotted against average cross–shore transport rate within surf zone for field data. 177

6.7 Local cross–shore sediment transport rate vs. local energy dissipation per unit volume for one large wave tank case. Results for other cases exhibiting offshore transport similar. 178

6.8 Local cross–shore sediment transport rate vs. local energy dissipation per unit volume for selected intervals in the field. 179

6.9 Influence of slope term in modified Kriebel model for selected large wave tank test. H_b=1.68 m, T=11.33 sec., D=0.22 mm, A=0.10 $m^{1/3}$, K=1.1x10^{-6} m^4/N. "Alpha" is the coefficient in front of the slope term in the transport equation. Calibration factor, K, chosen to yield best fit for α=1. 184

6.10 R.M.S. error in depth as a function of transport coefficient, K, for large wave tank case illustrated in Figure 6.9. 185

6.11 Modified Kriebel model vs. average nourished profiles based on measurements at Perdido Key, 9/90–2/91. K_{best}=0.2x10^{-6} m^4/N. R.M.S. error in depth=0.15 m. 186

6.12 Modified Kriebel model vs. average nourished profiles based on measurements at Perdido Key, 2/91–5/91. K_{best}=2.0x10^{-6} m^4/N. R.M.S. error in depth=0.15 m. 187

6.13 Modified Kriebel model vs. average nourished profiles based on measurements at Perdido Key, 10/91–1/92. K_{best}=0.2x10^{-6} m^4/N. R.M.S. error in depth=0.14 m. 188

6.14 Modified Kriebel model vs. average nourished profiles based on measurements at Perdido Key, 1/92–6/92. K_{best}=0.1x10^{-6} m^4/N. R.M.S. error in depth=0.26 m. 189

6.15 R.M.S. error in depth as a function of transport coefficient, K, for each field simulation. Note that K=0 corresponds to the R.M.S. depth change measured in the field over the given interval. 190

6.16 On- and offshore average slopes within nourished area, based on measurements at Perdido Key. Onshore slope defined by +1 m contour and waterline; offshore slope by -2 and -4 m contours. . . 191

6.17 Deep water wave steepness, based on mean wave height (monthly average), vs. dimensionless fall speed. Solid line defines switch from offshore to onshore transport in SBEACH model. 193

6.18 Measured and modeled beach profiles, first post–nourishment survey interval at Perdido Key. Model result is based on Larson and Kraus [1989]. K=1.5x10^{-6} m^4/N, ε=0.002 m^2/s. 196

6.19 Measured and modeled beach profiles in field, profile recovery case. Model result is based on Larson and Kraus [1989]. K=0.5x10^{-6} m^4/N, ε=0.001 m^2/s. 197

Abstract of Dissertation Presented to the Graduate School
of the University of Florida in Partial Fulfillment of the
Requirements for the Degree of Doctor of Philosophy

SEDIMENT TRANSPORT PROCESSES AT A NOURISHED BEACH

By

Paul A. Work

December, 1992

Chairman: Dr. Robert G. Dean
Major Department: Coastal and Oceanographic Engineering

Data describing the evolution of a large beach nourishment project on the Gulf of Mexico at Perdido Key, Florida, are analyzed to describe the sediment transport processes governing the behavior of the beach. Analytical and numerical techniques for prediction of the response of the nourished beach to physical forcing arising from incident wind waves are tested.

Repetitive bathymetric and topographic surveys indicated placement of 4.1 million m^3 of sand in the nearshore zone between November, 1989, and August, 1990, and a net loss of 7% from the monitored area after one year. Beach profiles were surveyed every 3–4 months at 33 locations to monitor the evolving beach, providing over 250 profiles describing the spatial and temporal changes at the site. Directional wave data, sediment samples, tide, and weather data were also collected.

Cross-shore sediment transport rates and longshore gradients of longshore sediment transport were computed from the measured changes in the beach profiles. Results indicate that cross-shore sediment transport dominated much of the early evolution of the project. Longshore gradients of longshore sediment transport were found to be strongest on the "shoulders" of the beachfill, where shoreline curvature changes most rapidly.

Longshore and cross–shore sediment transport processes were assumed independent to allow separate investigations. A "one–line", numerical model for planform evolution including the effects of background erosion, cross–shore sediment transport, and spatial and temporal variation in the incident waves gave a reasonable description of the longshore gradient of longshore sediment transport along the nourished beach.

Beach profile changes at the site were modeled by application of two previously developed numerical models that simulate cross–shore sediment transport. One approach reasonably estimated the volumetric redistribution of sediment for the first post–nourishment survey interval but yielded poor results for profile recovery events. Performance of the second model was poor despite a more detailed description of the cross–shore sediment transport rate.

The level of detail included in the assessment and description of long–term sediment transport processes at the site is largely unprecedented. The approach provides information specific to beach nourishment projects as well as more general insight into nearshore sediment transport problems.

CHAPTER 1
INTRODUCTION

The response of a beach to time–varying, physical forcing in the form of waves, fluctuating water levels, nearshore currents, and winds is of significant interest in both the applied engineering and research arenas. Nearshore sediment transport, driven by the complicated and poorly–understood flows in and near the surf zone, has proven to be a particularly durable research problem. This is evidenced in the literature by numerous predictive models and laboratory and field studies regarding coastal sediment transport. Yet no consensus has emerged of an adequate and general predictive model.

Sediment transport in the nearshore zone has traditionally been divided, somewhat arbitrarily but conveniently, into shore–parallel (longshore) and shore–normal (cross–shore) components. Although the two transport modes are clearly driven by some, if not all, of the same forces, the complexity of the problem has generally resulted in studies that either focus on only one mode or assume no coupling between them. This has traditionally led to research that either addresses changes in the planform or the profile of a beach.

The time scales for changes in the planform and profile of the beach are often markedly different. A short period (hours to days) of very energetic waves, particularly if coincident with enhanced water levels, can alter the beach profile drastically. The retreat of the waterline that typically accompanies such an event is sometimes only temporary, as pre–storm conditions may prevail within days of the event. This has made field documentation of storm–induced beach profile changes difficult, since

conditions immediately before the storm are rarely known, and recovery has often commenced by the time post–storm conditions are surveyed.

Major changes in the planform of the beach often occur on a time scale of seasons to years. Such changes are usually attributed to longshore gradients of longshore sediment transport. Many factors can lead to the presence of such gradients. Longshore variation in wave height or wave direction, the presence of natural or man–made littoral barriers, a change in shoreline orientation, and variability in the "erodibility" of the beach (at one extreme because of the natural variability in sediment size, at the other due to man–made structures such as bulkheads or revetments), can all lead to planform changes.

Analytical and numerical models of beach planform evolution are often employed to predict the effects of some human modification of the existing nearshore zone, such as the construction or stabilization of a tidal inlet or placement of sand for beach nourishment. The predictions often employ some simplifying assumptions and require specification of empirically–evaluated coefficients. Field data for verification of the coefficients are sparse, because of the difficulty and expense of the data collection and the relatively large time scale involved. The present state–of–the–art for beach planform modeling is, however, felt to be much better for quantitative predictions than the models describing profile response.

A diverse range of approaches has been developed that fall under the general title of beach profile modeling, from empirical representations of "equilibrium" beach profiles, to unsteady (sometimes unstable) models attempting to include detailed descriptions of nearshore hydrodynamics. Engineering applications of beach profile modeling include prediction of maximum storm erosion (both volumetric and in terms of waterline recession), establishment of "set–back" lines for regulating coastal construction, and investigation of the feasibility and predicted performance of beach nourishment projects.

Most recent models for beach profile response have been tested against wave tank data for calibration. Wave tank tests have several advantages, most significantly the controlled conditions and the quasi–two–dimensional behavior due to the minimization of longshore gradients. The ultimate test of any such model, however, is in comparison to field data. The poor performance of many models for beach profile response when attempting to describe events in the field is generally attributed to an insufficient understanding of the complex physics of the surf zone.

An increase in both the popularity and cost of beach nourishment projects has resulted in the need for better understanding of the processes that shape them over their "lifetimes." The feasibility of a proposed project has often been assessed with inadequate or untested hypotheses about how it will evolve over time. An increased understanding of the post–nourishment behavior will help avoid costly mistakes.

Beach nourishment has been used as a tool to combat erosion for over half a century, and many completed projects have been monitored to allow an assessment of their performance. Monitoring has rarely been sufficient to allow any detailed investigation of the sediment transport processes governing the behavior of the project. Often, only a qualitative assessment of project performance has been possible.

To realistically simulate the evolution of a nourished beach, both longshore and cross–shore sediment transport processes must be addressed. A beach nourishment project may be considered a man–made perturbation to a coast, which may already be affected by human activity. Beach nourishment modifies both the planform and the profile of the beach. This alters the pre–existing sediment transport processes, inducing both longshore and cross–shore transport gradients that result in changes in the shape of the beach.

There are two primary goals of this study. One is to present and interpret field data describing both the evolution of a nourished beach and the forces driving the response. The other is to assess the ability to predict the response, given the forcing.

A large–scale beach nourishment project at Perdido Key, Florida, initiated in November, 1989, provided an opportunity to collect appropriate data. Surveys immediately before and after placement of fill material in the nearshore zone, and at roughly four–month intervals afterward, provided a good description of the evolution of the beachfill in both the profile and planform. Monitoring of environmental parameters such as water level, mean currents, wave conditions, and winds provided knowledge of the forces exerted on the evolving beach.

Most mechanical systems, given constant forcing, will approach an equilibrium condition, often a dynamic equilibrium. Since beach nourishment is usually in response to erosion, it is difficult to argue that the beach is in equilibrium before nourishment, but the nourishment project generally increases the degree of disequilibrium in both the longshore and cross–shore directions. Extending the analogy, it might be expected that the rate of response is proportional to the degree of disequilibrium. By this argument, the rate of change of the beach should decrease with time. It will not reach zero, however, because the processes that made the nourishment project necessary would still be eroding the beach after the perturbation vanishes.

Figure 1.1 provides a schematized view of the planform and profile perturbations and response following a beach nourishment project. Because of the difference in time scales, the profile changes become evident first. Planform changes immediately post–nourishment are often idealized as rectangular, and the as–built, post–nourishment profile is typically much steeper than the pre–nourishment profile. Offshore sediment transport reduces the beach slope and width, while longshore gradients of the longshore sediment transport rate result in losses of sediment from the nourished area.

Figures 1.2 and 1.3 provide examples of wave tank and field measurements of evolving beach profiles. A generalized, qualitative description of the processes causing this evolution in the field provides some insight into the nature of the problem. Waves from deep water propagate towards shore and begin shoaling, with possible energy

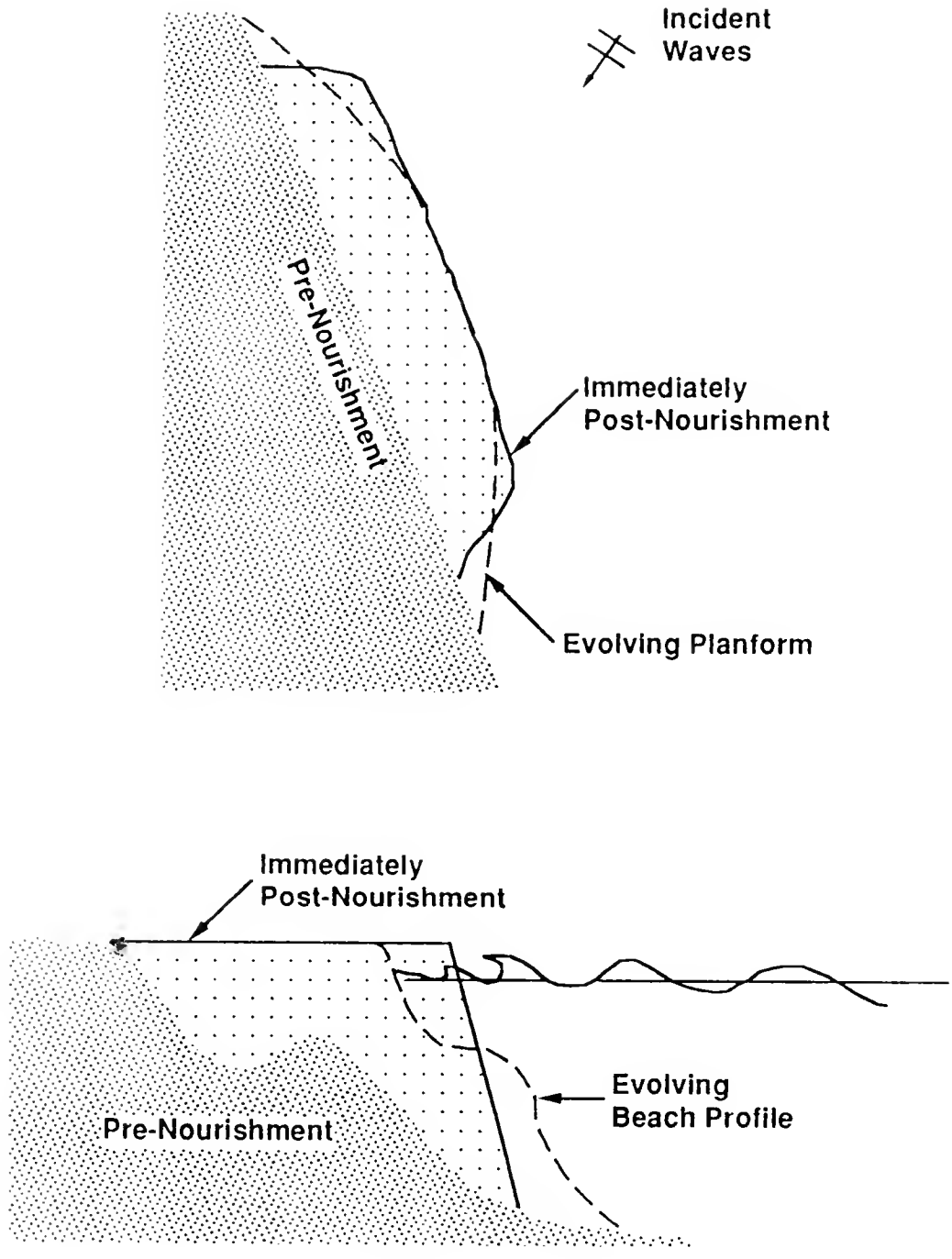

Figure 1.1: Schematic view of planform and profile evolution after beach nourishment. Cross-shore width of project greatly exaggerated in top figure, vertical scale exaggerated in lower figure.

inputs and losses from local winds, whitecapping, bottom friction, etc. Shoaling, refraction, and diffraction can all be important in coastal waters and generally assume increased importance with decreasing depth. Wind, tides, and wave setup/setdown can all modify the local mean water level. The shoaling waves become increasingly nonlinear with reduced relative depth until incipient breaking is reached. At this point, organized wave motion is rapidly converted to turbulent water particle motions, which can mobilize and entrain sediment. The applied stress of the wind and waves acting on the water column will also result in the forcing of quasi–steady flows, both in the longshore and cross–shore directions. These flows can then advect the sediment suspended in the water column and mobilize additional sediment. Deposition of the mobilized sediment provides feedback to the incident waves by modifying the bathymetry responsible for shoaling and wave energy dissipation. These processes are illustrated in Figure 1.4.

Many assumptions are often made to simplify the problem of describing the evolution of a nourished beach. The assumption regarding the independence of longshore and cross–shore sediment transport modes was discussed previously. The incident waves are often parameterized by specification of a single representative frequency and wave height combination. With these simplifications, a fully satisfactory model must still describe the spatial distribution of wave height and mean water level, wave energy dissipation throughout the nearshore zone due to wave breaking, friction, and turbulence, the nearshore velocity field, and the resulting sediment transport.

Recent attempts to develop physics–based models for cross–shore sediment transport have provided insight into the problem and some innovative approaches to describing the processes cited above, but poor quantitative agreement between measured and predicted beach profile response. Additionally, all the models to date that have attempted to retain the maximum amount of physics have been applied only for short–term simulations.

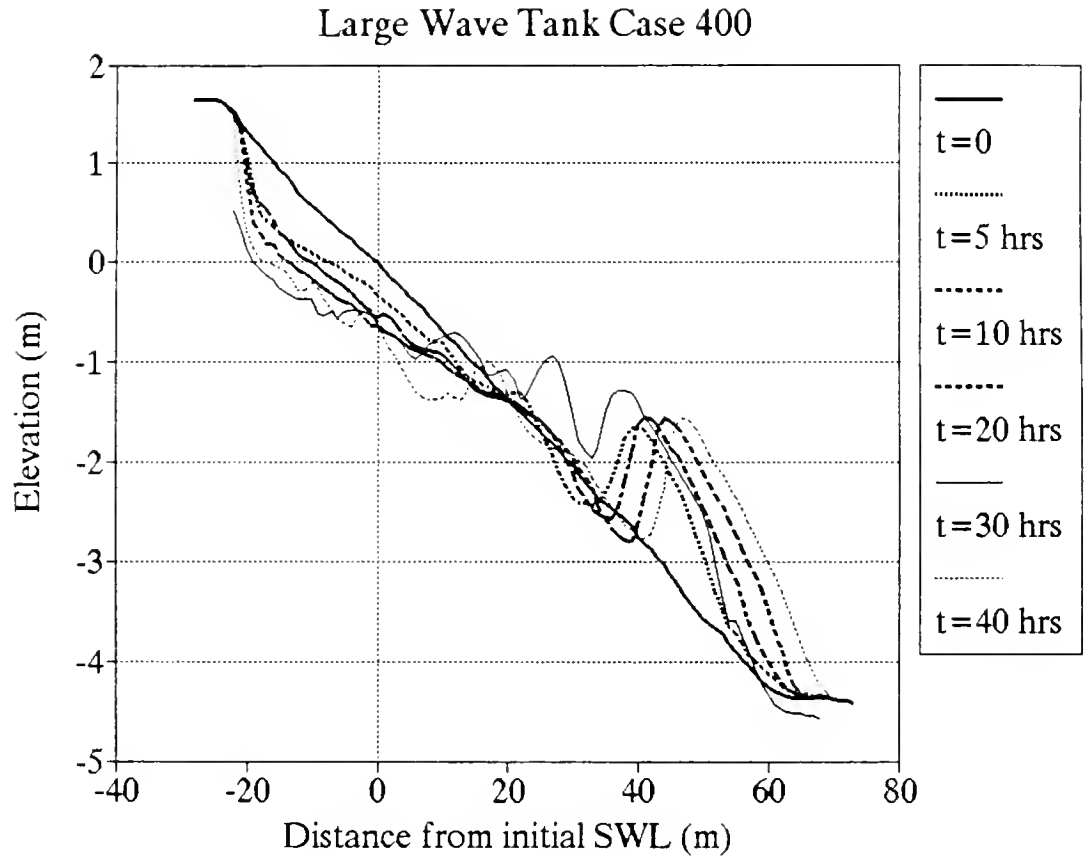

Figure 1.2: Beach profile evolution in large–scale, two–dimensional wave tank. Data from Kraus and Larson [1988].

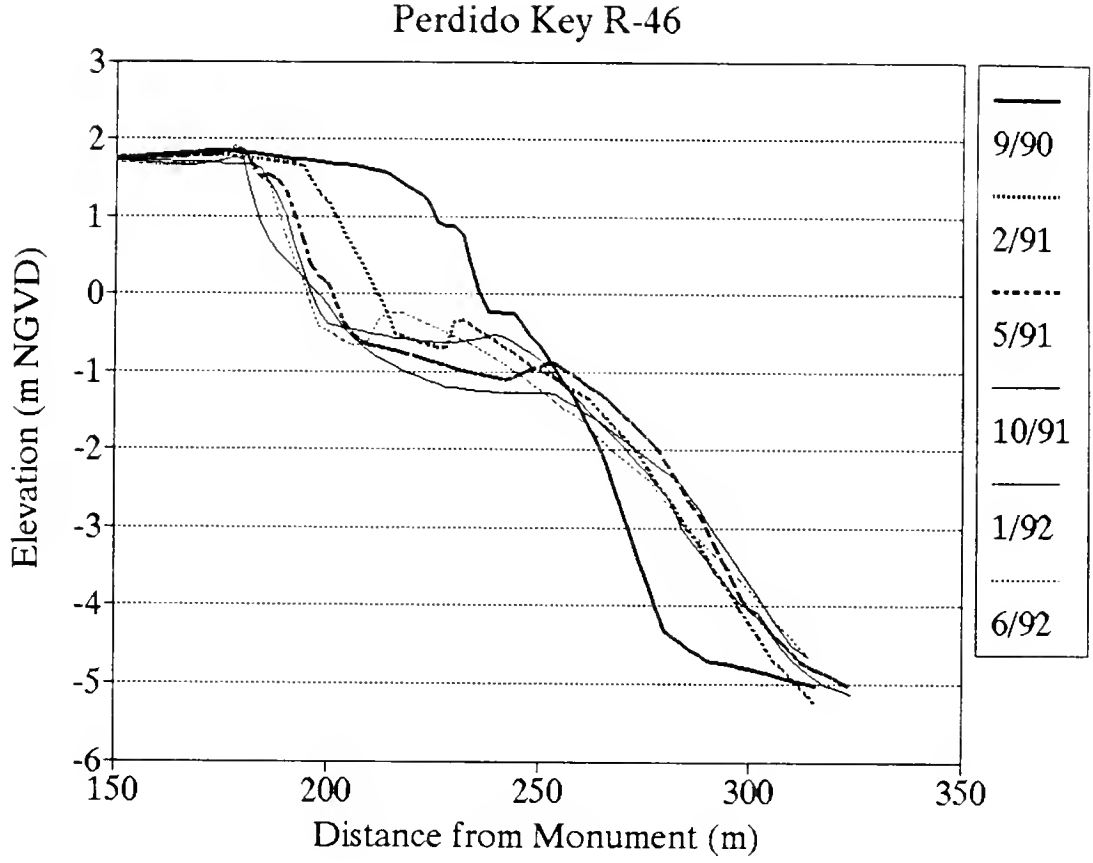

Figure 1.3: Beach profile evolution in field, after nourishment. Data from Perdido Key, Florida.

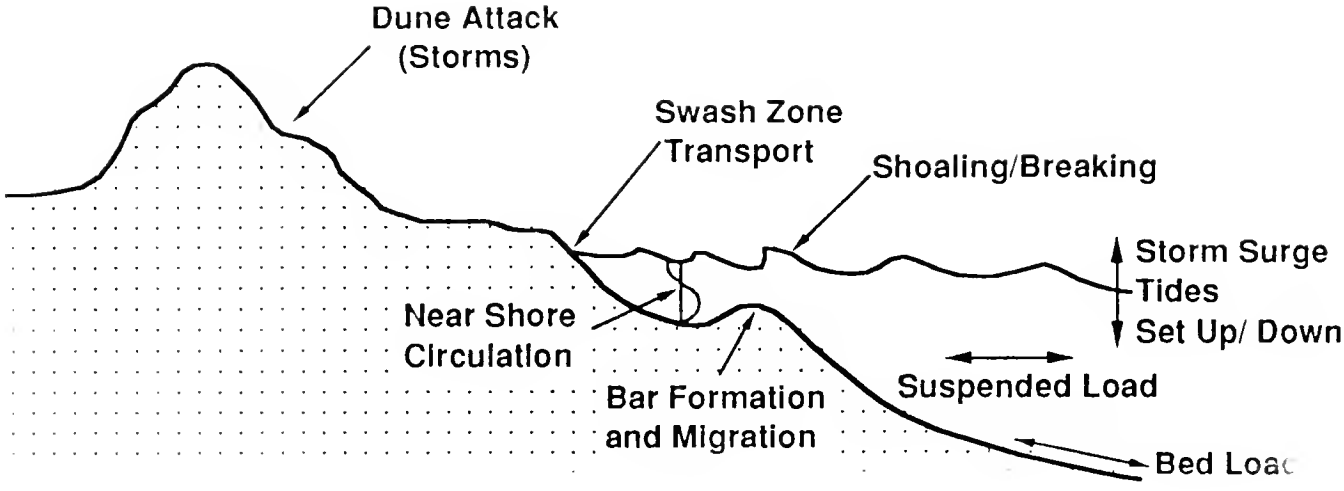

Figure 1.4: Forces influencing beach profile evolution.

In the chapters that follow, the field data collection techniques employed for this study are described and their accuracy assessed. Information extracted from the field data relevant to the sediment transport problem are discussed and summarized. Results from "one–line" models for planform evolution, solved both analytically and numerically, and two numerical models describing beach profile response to varying wave conditions and water levels are compared to field measurements. The accuracy and limitations of each model are evaluated.

The results presented here may be considered a step in the process that should ultimately lead to a three–dimensional model for prediction of the evolution of a beach nourishment project. Until sufficient knowledge and understanding are gained to develop such a model, there will be a continuing need for field, laboratory, numerical, and analytical studies that shed light on the sediment transport processes shaping a beach after nourishment.

CHAPTER 2
LITERATURE REVIEW

The problem of interest is quite complex since what is desired is the response of a system to forces that are themselves poorly understood. Any comprehensive model of coastal behavior must address the processes of wave shoaling and breaking, the spatially–varying elevation of the mean water level (wave setup/setdown), some details of both the fluctuating and mean motions of the fluid within the water column, and the resultant sediment transport. The recent trend in studies of evolving beaches has been toward numerical models describing some or all of these phenomena. Analytical models for special cases, such as planar beaches or rectangular beachfills, are available in some instances, but numerical models are often employed when attempting to simulate more realistic situations. Time–averaged quantities are almost always employed, where the time–averaging is done over many wave periods, to reduce computational requirements.

Because of the importance of each of the component processes influencing the evolution of a beach, an extensive review was made of the literature describing each phenomenon. At this stage, however, the focus will be on prior studies that specifically considered the problem of beach nourishment evolution in the field. Where necessary, previous studies addressing the sub–processes (wave breaking, mean circulation, etc.) will be reviewed.

It should be noted that the field data collected as part of this study do not include any measure of the surf zone hydrodynamics. Wave heights, periods, and directions, tidal stage and local wind speed and direction, which together are generally agreed to include most of the important forces influencing the physical changes observed at a

beach, have all been measured. The response of the beach was also measured. But the intermediate step, the environmentally–forced flows in and near the surf zone, which induce the sediment transport causing the beach to change, have not been monitored. This provides further justification for restricting the scope of the literature review to studies specifically addressing the problem of beach nourishment evolution.

2.1 Previous Studies of Beach Nourishment Evolution

A review of some previous beach nourishment projects which were monitored will help put the problem in perspective. Beach nourishment was being recognized as a potential remedy to chronic erosion problems as early as the 1930's, but many projects were not monitored adequately to quantify their evolution. The goal here is not to assess the value or effectiveness of previous projects, but rather to determine how they were monitored and what the monitoring programs revealed regarding the physical processes important to the evolution.

The number of beach nourishment projects that have been completed is too large to attempt a complete summary. Many projects were not monitored at all after construction, or were monitored for only a short time. Only projects that were monitored sufficiently to allow at least some assessment of their behavior after completion will be discussed here. Many of the studies included surveys of the geometry of the beach at varying levels of complexity, from measurements of beach width to wading profiles to bathymetric surveys. Conclusions about changes in beach volume were often made with little or no information about the subaqueous portion of the project.

Early reports by the Beach Erosion Board of the U.S. Army were visionary in addressing the need for long–term survey data extending from the dry beach out to beyond the limiting depth for sediment motion. Hall and Herron [1950] provided an early example of a well–monitored project at Long Branch, New Jersey. Tide, wave, and wind data, sand samples, aerial photographs, and bathymetric surveys were all employed to study the behavior of 460,000 m^3 of sand placed in 11.5 m of water. The

area was monitored for roughly one year after placement, and no significant movement of the sand was found. Results of similar experiments involving offshore placement of sand for nearshore beach nourishment in 1935 at Santa Barbara, California, and 1935–1942 at Atlantic City, New Jersey, were described. Findings at the three locations were cited as evidence that nourishment material must be placed in shallower depths to exhibit any net shoreward movement. A later investigation of the project at Long Branch by Harris [1954] which included additional data agreed with the findings of the earlier study.

Later projects involved placement of sand on the beachface to increase dry beach width. Hall [1952] discussed beachfill design procedure and summarized over 50 beach nourishment/sediment bypassing projects that had been completed at the time. The majority of the projects were located in California, New Jersey, and Florida; they ranged in volume from 50,000 m^3 to over 14 million m^3 (Silver Strand, Coronado Beach, California, 1940–1944). Five case studies were considered to illustrate alternative approaches to beach nourishment.

Early monitoring projects often resulted in qualitative descriptions of the sediment transport processes at the site, since the accuracy and temporal and spatial resolution of the surveys made quantitative assessment speculative. Watts [1956] described a 1.95 million m^3 beach nourishment project at Ocean City, New Jersey, that was monitored with the aid of bathymetric survey data, aerial photographs, and sand samples. Numerous groins were constructed in the area for shoreline stabilization. An estimated 95% of the fill material was lost from the nourished area in slightly less than two years following nourishment. Lost material moved both up- and downcoast to benefit adjacent areas. The finer grain size of the placed sand and the local shoreline orientation were both concluded to contribute to the high loss rate.

Watts [1958] evaluated a nourishment project in Harrison County, Mississippi, with the aid of sand samples, bathymetric survey data, and wading profile data. A

terminal groin was built at one end of the 4.5 million m^3 project for retention of placed material. A hydrographic survey seven years after project completion revealed that 90% of the 540,000 m^3 "lost" from the beach above the -0.6 m contour (mean low water) was merely transported offshore, adjusting the beach slope. This would indicate a loss of roughly one percent in seven years, although survey errors must be considered in this estimate. The benefit of this offshore material for shore protection was noted.

Watts [1959] gave an account of the 1.0 million m^3 beach nourishment project completed in 1953 at Virginia Beach, Virginia. Emphasis was placed on the importance of adequate spatial resolution in the survey data for estimation of sediment transport rates and directions.

Perdikis [1961] summarized 79 beach nourishment projects in the northeastern United States. Ten projects were discussed in detail, including changes in volumes and beach slopes. The offshore extent of the survey was not given for all cases and it appears that volumetric computations were based primarily on changes in the subaerial beach. Many sites eroded much faster after nourishment than previously. For many cases this was attributed to placement of material that was finer than the native sediment or offshore sediment transport to result in a milder beach slope. The difficulty of predicting post-fill behavior based solely on the knowledge of pre-nourishment conditions was emphasized.

Vesper [1961] monitored a nourished beach on Long Island Sound at Prospect Beach, West Haven, Connecticut. Both the beach and the borrow area from which 335,000 m^3 of sand for nourishment were obtained were studied for roughly three years after placement. The borrow pit was located in only 1.5 m of water 300 m offshore of the waterline. Beach nourishment material did not move into the borrow pit within the three years of project monitoring, and no net loss of material from the

monitored area was found. The most significant adjustment of the fill was found to occur during the first year after placement.

Kramer [1961] noted the rapid initial reduction in beach width associated with an unnaturally steep beach placed on the Island of Norderney in Germany. The importance of seasonal trends was also noted. The later re–nourishment of this beach and a further assessment of the first project was given by Kramer [1972]. The latter paper included a qualitative prediction of the evolution of a proposed "sand groin" on the Island of Sylt on the German North Sea coast. Kunz [1990] discussed several later nourishment projects at Norderney. Volumetric changes were found to be described by an exponential curve. Beach nourishment has been employed at the site for nearly forty years, with an average of 82,500 m^3/yr being placed.

Several studies have included computations of changes in subaerial volumes of nourished beaches, noting that much of the lost material is probably moving offshore because of the unnaturally steep as–built profiles. Everts et al. [1974] (also McCann [1981]) monitored two beach nourishment projects at Atlantic City, New Jersey and concluded that larger fill volumes generally implied more rapid loss rates. A nourishment project at the same site in 1986 was monitored in a similar manner by Sorensen et al. [1988]. The loss rate for the latter project was observed to decrease in the second year of monitoring. This was attributed both to the characteristic behavior of beach fills and a milder wave climate for the second year.

Fisher and Felder [1976] studied a 465,000 m^3 beach nourishment project at Cape Hatteras, North Carolina. High–resolution beach profile data (bi–weekly, 150 m spacing between profiles) and visual wave data were collected to monitor the subaerial portions of the project for eighteen months after placement of the fill. Most of the changes occurring during this time were found within the nourished area, where roughly half of the initial volume above MSL remained after eighteen months. It was acknowledged

that much of the material lost from the subaerial beach was probably moving offshore to deeper portions of the active profile.

A nourished beach at Treasure Island, Florida, was observed for roughly two years to study post-nourishment behavior after placement of 600,000 m^3 of sediment (University of Florida [1971]). Profiles were surveyed to the depth of closure to allow computation of volumetric changes. Twenty months of monitoring revealed a loss of 25% of the project volume, much of it into and near the borrow pit. The fill appeared to "stabilize" after one year, after which the erosion pattern was more uniform.

A study of a proposed 840,000 m^3 beach nourishment project at Delray Beach, Florida, employed monthly littoral drift "roses" (Walton [1973]) and a finite-difference, numerical simulation of planform changes to predict project performance (University of Florida [1973]). The annual volumetric losses from the nourished area were predicted to increase slightly over time for five years after construction.

Shemdin et al. [1976] monitored a 2.6 million m^3 beach nourishment project at Jupiter Island, Florida. Shoreline recession and volumetric gain were both found at both ends of the nourished area. This was attributed to a "groin effect." Predictions of volumetric changes using an empirical longshore drift equation and measured wave data were an order of magnitude larger than measured changes.

Dette [1977] described the evolution of the 770,000 m^3 "sand groin" (Kramer [1972]) placed for beach nourishment purposes on the Island of Sylt in the North Sea. Directional wave data and beach profile surveys to 5 m depths were used to investigate the forcing and behavior. The project initially trapped sediment updrift and thereby increased in volume.

Oertel et al. [1977] monitored a nourished beach at Tybee Island, Georgia. The project involved placement of 1.1 million m^3 of sediment in 1976 on 6 km of beach. Monitoring consisted of time-lapse still photography, movies, and bi-weekly beach profile surveys using a modification of a method due to Emery [1961]. Rapid changes

to the subaerial beach were noted in the first six months after nourishment, with much of the nourished area losing 40% of the subaerial volume. Much of this loss (50–75%) was claimed to be a result of offshore sediment transport. Chu and Posey [1989] described a later project at the same site in 1987 involving 1.0 million m^3 of sediment. Roughly 25% of the project volume was lost from the subaerial beach during the first 21 months after placement.

Walton [1977] summarized available data on beach nourishment projects in Florida and on the lower Atlantic and Gulf coasts. Project performance was briefly assessed where sufficient data existed. Hobson [1981] provided a similar summary for twenty projects located throughout the United States, including the well–known Miami Beach project completed in the early 1980's.

Winton et al. [1981] made a detailed investigation of the sediment transport processes along 42 km of the southern coast of North Carolina. Observed changes after beach nourishment at Wrightsville Beach and Carolina Beach were reported. An exponential loss of beachfill volume was found at Wrightsville Beach following the 1970 beach nourishment project. Eighty percent of the initial fill volume was lost during the first 1–1/2 to 2 years after placement. This was attributed to sediment sorting, slope readjustment, and lateral spreading of the fill.

Hushla [1982] monitored two beach nourishment projects on the eastern coast of Florida with the aid of aerial photography. Subaerial beach widths and areas were used to assess performance. Five years of data for Port Canaveral Beach indicated a loss of beach area equal to 30% of the increase resulting from project construction. A similar calculation for Indialantic/Melbourne Beach based on changes observed in one year revealed a loss of 50%.

Phillips et al. [1984] studied a 720 m segment of South Beach, Sandy Hook, New Jersey, after nourishment with 1.8 million m^3 of sediment. Beach profiles were surveyed and breaking wave and longshore current statistics recorded during site visits.

Volumetric changes were computed based on six surveyed profiles. Some profiles were surveyed to the MSL contour and a constant slope assumed to allow extrapolation to the -4 m contour for volume computations. The magnitude of the annual wind-blown transport out of the study area was estimated at 26,554 m^3/yr, although this was qualified as an upper bound, order-of-magnitude estimate. The effects of wave refraction, wave diffraction, cross-shore sediment transport, and measurement errors were addressed qualitatively. An increased potential for longshore transport out of the monitored area was noted as the shoreline prograded.

Kerkaert et al. [1986] conducted a comprehensive study of a beach nourishment project in Belgium. Predictions of post-nourishment planform changes were made using the analytical approach of Pelnard-Considère [1956]. Repetitive bathymetric surveys showed that six percent of the placed material moved either offshore or into the dunes during two years of monitoring.

Ashley et al. [1987] described the evolution of a nourished beach immediately downdrift of Barnegat Inlet, New Jersey, a tidal inlet that was dredged and stabilized with jetties. The beach was nourished with over one million m^3 of sand and monitored for over seven years, through profile surveys, sand samples, aerial photography, and visual longshore current observations. Beach profile measurements were made at nine stations, some of which were outside of the nourished area. Profiles were surveyed bi-weekly for 3-1/2 years and annually thereafter, using the method due to Emery [1961]. Measured changes in the subaerial beach volume were used to compute a "residence time" for the beachfill of 3-1/2 years, compared to the pre-construction estimate of 8 years.

Pilkey and several colleagues (Pilkey and Clayton [1989], Leonard et al. [1990a], Leonard et al. [1990b], Dixon and Pilkey [1991]) summarized numerous beach nourishment projects in the United States, reporting physical dimensions, costs, and

predicted and measured "lifetimes." The effects of various parameters on the beachfill lifetime were discussed.

Stauble and Holem [1991] documented an eight–year monitoring study of a nourished beach at Indialantic/Melbourne Beach, Florida. The project spanned 3.4 km and included 195,000 m^3 of added sediment. The monitoring plan included wading profile surveys, sand samples, aerial photography, and some wave data. Beach profiles were surveyed weekly immediately after placement of the sand and then at increasing intervals at later times. Offshore portions of the profiles were not monitored. Seven years after placement of the beach nourishment material, the subaerial beach area was found to be 13% greater than the pre–nourishment case.

Recent years have seen an explosion of reports on the evolution of beach nourishment projects (Giardano et al. [1987], Combe and Soileau [1987], Jarrett [1988], Jones and Kana [1988], Aubrey and DeKimpe [1988], Ibe et al. [1991], Spadoni [1992]). Many of these document wave conditions, volume changes, etc., but do not attempt to model the sediment transport processes determining the fate of the project. For economy of space, emphasis will be placed on studies that include empirical, analytical, or numerical predictions of the future changes to the nourished beach.

Analytical and empirical predictions of volumetric changes in nourished beaches have recently become a common component of monitoring studies. Wave height is a dominant forcing term in most analytical investigations, but sufficient measured wave data are rarely available. The analytical approach is often patterned after the one–line theory of Pelnard–Considère [1956]. Volumetric changes for an entire project imply an integrated approach (integrated in both the longshore and cross–shore directions), so details of the sediment transport mechanisms causing the changes are not usually addressed. Beachfill "lifetimes" are often of interest, although definitions vary between studies and are not always given.

Skrabal et al. [1990] estimated the lifetime of a 255,000 m^3 nourishment project at Fenwick Island, Delaware, based on historical shoreline change patterns. The lifetime was defined as the time required for the nourished area to lose an amount of sediment equal to the project volume. One year of post-nourishment data were available for comparison, and revealed that 7.6% of the placed volume was lost from the monitored area during this time. This loss rate was used to estimate a beachfill lifetime of 11.5 years.

de Lange and Healy [1990] monitored a small beach nourishment project (21,000 m^3) in a tidally-influenced bay. Beach profile surveys spanning 3-1/2 years after nourishment indicated that the beach volume above MLW decayed linearly, although the loss rate appeared to be accelerating. It was predicted that all sediment added during renourishment would be lost in 13 years.

Dean and Lin [1990] discussed the measured and predicted performance of a well-documented beach nourishment project at Redington Shores, Florida. A one-line, numerical model for shoreline change, including background losses and measured wave data as inputs, was used to simulate evolution of the project. Comparisons were based on five surveys spanning eighteen months after project completion. The approach is similar to Phlegar [1989], who modeled, both analytically and numerically, the volumetric changes occurring at ten nourished beaches in Florida, some of which had been nourished multiple times.

DeKimpe et al. [1991] modeled the fate of a small (81,000 m^3) beach nourishment project analytically and empirically. The analytical solution followed the one-line approach of Pelnard-Considère [1956] but did not yield volumetric changes as realistic as an empirically-derived exponential curve. After five years of evolution, 43% of the subaerial project volume remained. The lifetime of the project, defined as the time required for the fill to be reduced to 10% of its original volume, was estimated at 13 years.

Larson and Kraus [1991] discussed both analytical and numerical modeling of post–nourishment beach changes. Longshore changes followed the one–line approach of Pelnard–Considère [1956], while cross–shore changes were modeled using a numerical model based on observations from large–scale wave tanks (Larson and Kraus [1989], Larson, Kraus, and Byrnes [1990]). The cross–shore model was tested against field data describing beach profile evolution during a storm.

Mann et al. [1992] modified the one–line approach of Pelnard–Considère [1956] in an ad hoc manner to account for an irregular pre–nourishment planform and background erosion. One post–nourishment survey from a 211,000 m^3 beach nourishment project at Buckroe Beach, Hampton, Virginia, was available for verification. Measurements indicated a much more rapid loss than predicted for the first year after placement.

Stauble et al. [1992, in press] made a detailed investigation of a beach nourishment project at Ocean City, Maryland. Two phases of the project have been completed, the first in 1988 (1.8 million m^3) and the second during the summer of 1991. The scope and goals of the monitoring project were very similar to the Perdido Key project that is the focus of this study, involving bathymetric surveys, in situ wave data collection, and sediment sampling. A detailed investigation of the temporal and spatial changes in sediment size characteristics was made. Additional data collection and analysis associated with this project is currently underway.

Some results became available as this study was nearing completion. Fernández et al. [1992] described a monitoring program at a beach nourished with 1.5 million m^3 of sand much larger than the native material. Visual wave data, bi–monthly beach profile data to the -10 m contour, and sediment samples had been collected for over two years at the time of publication to document changes in the 25 km project.

Ferrante et al. [1992] discussed the construction and monitoring of a beach nourished along 3 km with 1.2 million m^3 of sand. A rubble mound berm breakwater was

built to retain the placed material, which was much coarser than native sediments. The monitoring program included aerial photography, beach profile surveys, sediment samples, and directional wave data. Surveyed profiles indicate an increase in elevation of the dry beach of close to one meter since construction. This gain was nearly uniform in the cross-shore direction.

2.2 Other Studies of the Perdido Key Area

Few studies have addressed the physical forces acting on Perdido Key or the response of the island to these forces. Balsillie et al. [1986] determined long-term shoreline change rates for the area based on historical charts. Psuty [1987, 1988] monitored a 1.86 million m^3 beachfill placed on the eastern end of Perdido Key in 1985. Stone et al. [1992] estimated longshore sediment transport rates for much of western Florida and southern Alabama based on hindcast and visual estimates of wave conditions. A nodal point in the longshore sediment transport rate was predicted on Perdido Key. Clark [1991] provided a bibliography of selected reports regarding coastal processes near Perdido Key. Most of the region monitored as part of the present study was identified as an "erosion problem area."

2.3 Summary

Despite the cost associated with their construction, few beach nourishment projects have been monitored sufficiently to allow a detailed, quantitative assessment of their performance. Where monitoring studies have been sponsored, they have often been of short duration and included a description only of the changes appearing on the dry beach. Many studies have noted the importance of the offshore portions of the profile but based performance assessment only on the condition of the subaerial beach.

The preceding literature review was not totally exhaustive, owing to the number of studies regarding the evolution of beach nourishment projects, but should illustrate the deficiencies in the existing data sets. The complexity of the problem demands a high level of care and expense associated with the data collection process.

High–quality bathymetric survey and directional wave data are obviously important components of the data set.

Many recent studies have employed analytical and numerical tools for the prediction of the response of a nourished beach to waves and currents. Most have taken a volumetric approach, which implies integration in both the longshore and cross–shore directions. The remainder of this study will be devoted to a detailed investigation of the spatially– and temporally–varying sediment transport processes that affect a nourished beach after placement.

CHAPTER 3
FIELD DATA COLLECTION

A significant portion of the research leading to this dissertation consisted of field data collection at Perdido Key, Florida, and subsequent analysis and interpretation of this data. Perdido Key is a barrier island on the Gulf of Mexico in the extreme western "Panhandle" of Florida (Figure 3.1). It trends roughly east–west and is bounded on the east by Pensacola Pass and on the west by Perdido Pass.

The U.S. Navy initiated a dredging project to increase the depth of Pensacola Pass for navigation in November, 1989. Much of the dredge spoil was designated for use as beach nourishment material for Perdido Key. This phase of the dredging project resulted in approximately 4.1 million m^3 of new material being placed on 7 km of the Gulf of Mexico shoreline of Perdido Key, increasing the dry beach width by roughly 140 m. The native and fill sands are similar in color, composition, and size.

The entire nourishment area lies within the Perdido Key area of the Gulf Islands National Seashore and is therefore under the jurisdiction of the U.S. National Park Service. The park contains primarily undeveloped land and no coastal structures except for a small structure abutting Pensacola Pass. The offshore bathymetry of the study area is characterized by very mild slopes seaward of the –5 m contour; the primary exceptions to this are the steep slope adjacent to the dredged channel through Pensacola Pass, and Caucus Shoal, a long, thin, submerged sand spit adjacent to Pensacola Pass at the eastern end of Perdido Key.

A five–year monitoring study containing several elements was sponsored by the National Park Service and the U.S. Navy to investigate the evolution of the project and its effect on pre–existing conditions. Biological, sedimentological, and physical

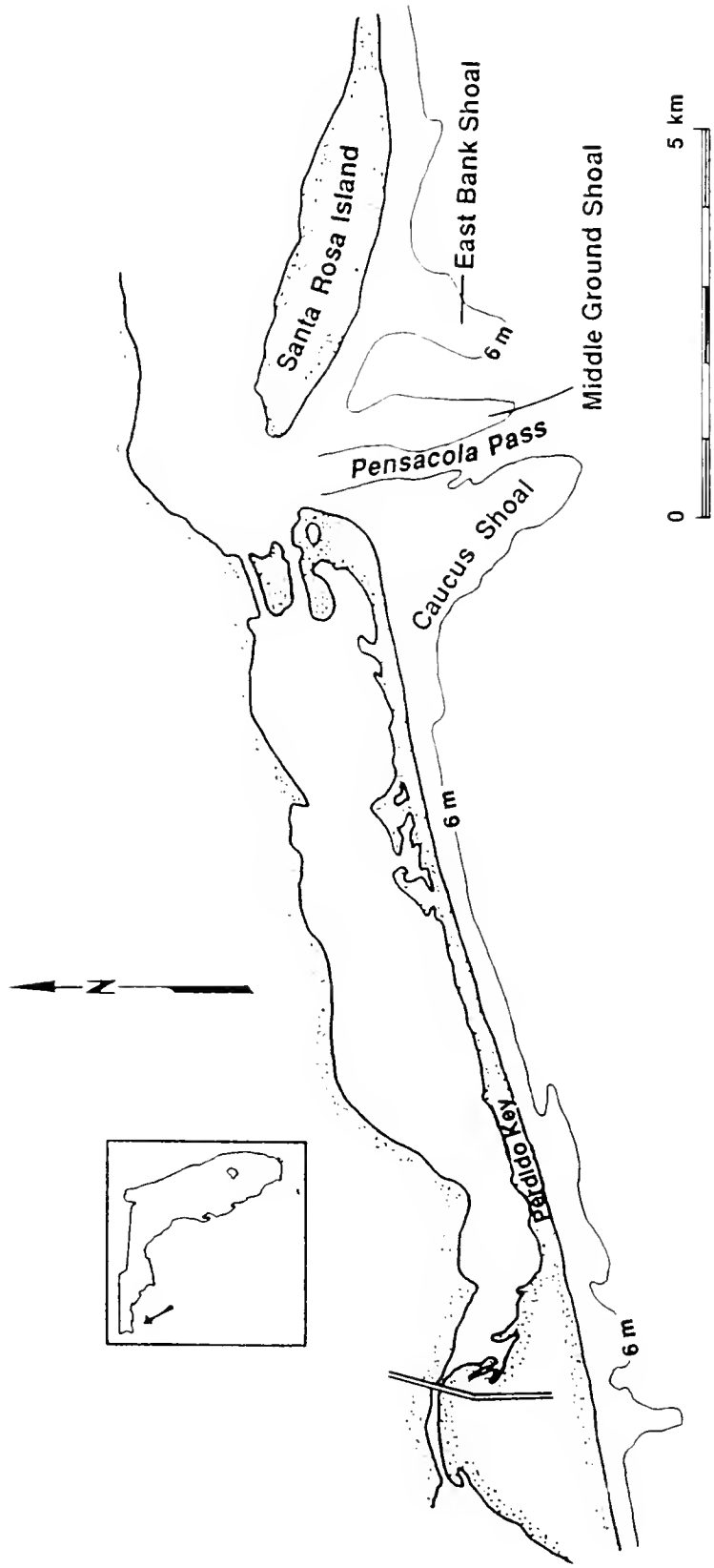

Figure 3.1: Location of field project.

environmental conditions were all incorporated into the study. The Coastal and Oceanographic Engineering Department of the University of Florida was contracted to conduct the physical monitoring study, which will be the focus of this chapter.

The plans for the physical monitoring study called for the collection of several types of data. A physical survey, including both subaerial and subaqueous features of the island, was required yearly by the sponsors. To date, three such surveys have been completed: the pre-nourishment survey of November, 1989, the post-nourishment survey of September, 1990, and the survey of October, 1991. Intermediate surveys extending to water depths of 4 to 5 m were also done to provide better temporal resolution of changes. Five such surveys have been undertaken: February, May, and September of 1991, and January and June of 1992.

Directional wave and current data have been collected offshore of the Perdido Key Ranger Station, and a land-based weather station was installed at the Ranger Station to monitor wind speed and direction, air temperature, and rainfall. A second wave gage was installed near Caucus Shoal at the eastern end of Perdido Key in April, 1992, to investigate the sheltering effect of the shoal. Although the wave gages also provide an estimate of tidal stage, an additional tide gage was installed at Ft. Pickens pier, on Santa Rosa Island near Pensacola Pass. Locations for the instrumentation are shown in Figure 3.3. Oblique photographs of the area were taken to qualitatively document changes as they occurred.

Table 3.1 provides a history of the field work done to date for the physical monitoring study; Figure 3.2 illustrates the temporal availability of the resulting data. The following sections describe the data collection and analysis procedures. Details not found here are available in Work et al. [1990a, 1990b, 1991a, 1991b, 1991c] and Work and Dean [1992]. The wave and bathymetric data are also addressed in the following chapter, because of their particular relevance to the problem of interest.

Table 3.1: Chronology of Perdido Key Data Collection Efforts.

Date	Task
10/28–11/1/89	Pre–nourishment survey: Wading profiles (Gulf and Bay) Offshore bathymetry Sand samples, photos
11/17/89	Placement of nourishment material begins
1/18/90	Wave gage tripod and standalone gage installed Tide gage with small stilling well installed at Ft. Pickens Pier, Santa Rosa Island
1/29/90	Mechanical (analog) weather station installed
1/30/90	Large stilling well installed for Ft. Pickens tide gage
3/7–3/9/90	56 sand samples collected, to replace those destroyed or not collected during pre-nourishment survey
5/2/90	Standalone wave data collection package retrieved; fresh standalone package installed on tripod
6/24/90	Digital weather station installed
8/8/90	Standalone wave data collection package retrieved; fresh standalone package installed on tripod
8/17/90	Placement of nourishment material completed
9/22–9/26/90	First post–nourishment survey: Wading profiles (Gulf side) Offshore bathymetry Sand samples, photos
12/6/90	Standalone wave data collection package retrieved; fresh standalone package installed on tripod Ft. Pickens pier tide gage re–surveyed
1/29–2/3/91	Wading profile survey (Gulf side) Sand samples
3/19–3/21/91	Standalone wave gage retrieved; tripod moved Lightweight data/power transmission cable installed Shore–connected wave gage installed on tripod

Table 3.1: —continued.

Date	Task
4/9–4/10/91	Wave gage cable re–buried
5/15–5/16/91	Wave gage cable re–buried
5/28–6/1/91	Wading profile survey (Gulf side) Sand samples
6/18–6/19/91	Shore–connected wave gage removed; cable cut Standalone wave gage installed on tripod
7/29–7/30/91	Wind vane and anemometer replaced
9/10/91	Standalone wave gage removed from tripod Fresh standalone wave gage installed on tripod
9/28–10/2/91	Wading profile survey (Gulf side) Sand samples, photos Ft. Pickens pier tide gage re–attached
10/12–10/20/91	Yearly survey: Wading profiles and offshore bathymetry (Gulf side) Installed heavyweight data/power cable for wave gage Standalone wave gage removed from tripod Shore–connected wave gage installed on tripod Fresh standalone wave gage installed on tripod
10/23–10/24/91	Shore–connected wave gage replaced
1/16–1/22/92	Wading profile survey (Gulf side) Replaced wind vane/anemometer Replaced shore–connected wave gage on tripod Replaced standalone wave gage on tripod
4/15–4/16/92	Replaced shore–connected wave gage on tripod Removed standalone wave gage from tripod Installed new standalone wave gage near Caucus Shoal
6/12–6/15/92	Wading profile survey (Gulf side) Surveyed 7 profiles to wading depth on Bay side Repeatability check for wading profiles

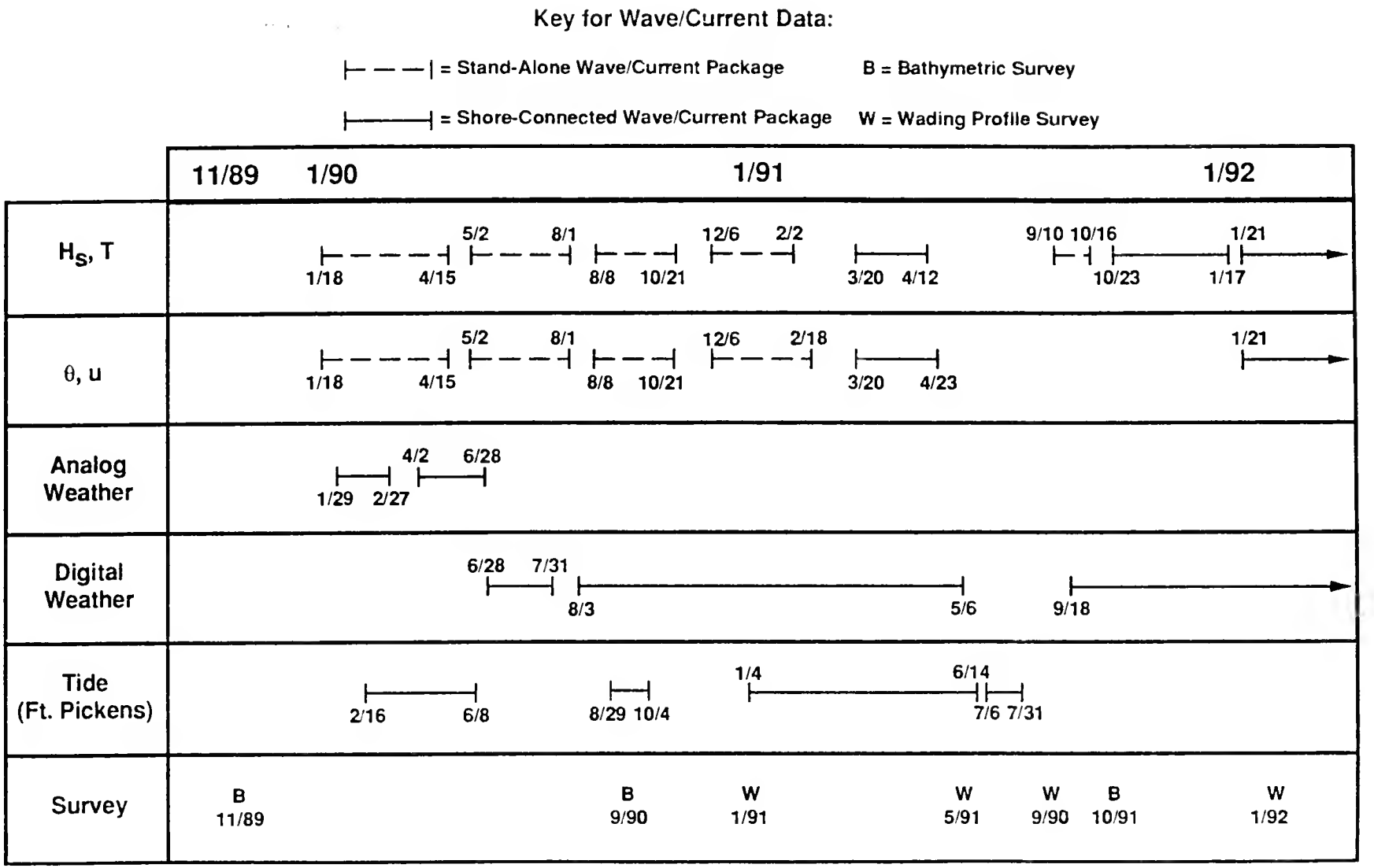

Figure 3.2: Temporal availability of data at field site.

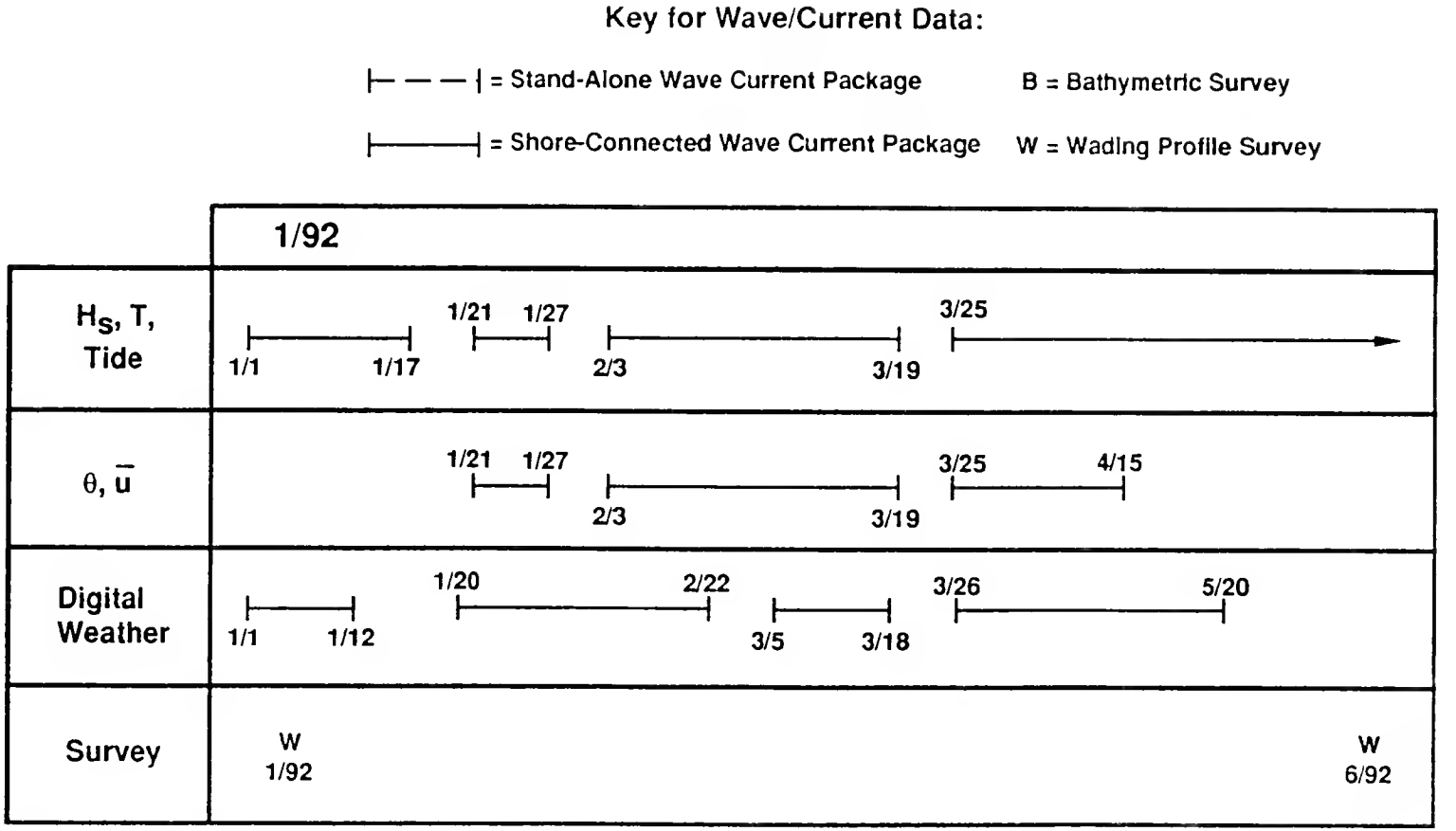

Figure 3.2:--continued.

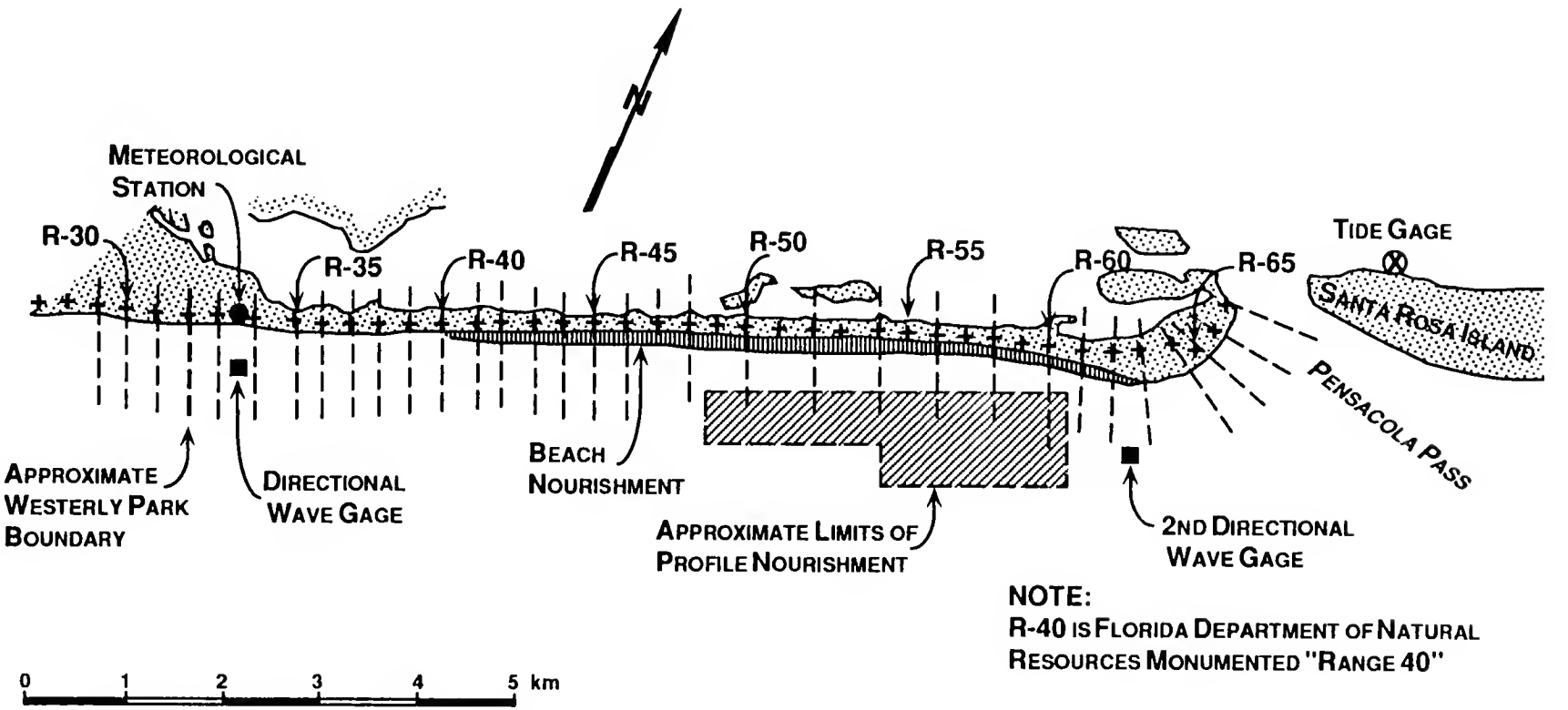

Figure 3.3: Locations of beach profile transects and data collection stations.

The field data collection is an ongoing task; the results discussed in this dissertation will cover the time period from November, 1989, through June, 1992. This allows for the consideration of seven post-nourishment surveys and wave, current, tide, and weather data from a 2-1/2 year time period.

3.1 Topographic/Wading Profile Surveys

A set of 33 beach profile transects was defined to monitor the evolution of the nourished beach. Each transect originated at a State of Florida Department of Natural Resources "permanent" benchmark monument and runs approximately perpendicular to the local shoreline (Figure 3.3). Benchmark elevations and profile azimuths relative to magnetic North were provided by the Department of Natural Resources (Table 3.2). The monuments run the length of the study area and are separated by a nominal distance of 300 m. For the pre-nourishment survey of November, 1989, 16 profiles were also extended north into the bay inland of Perdido Key. An additional 7 profiles were extended into the bay during the June, 1992, survey.

A tripod-mounted theodolite equipped with a magnetic compass was placed directly over each monument in order to establish the path to be followed during the field survey. A wooden stake was used to mark the direction to ensure that later surveys followed the same line. It is estimated, based on repetitive measurements, that this method with the equipment described is accurate to within one degree of the desired azimuth. The theodolite or a hand bearing compass was used to check the azimuth defined by the wooden stake during later surveys to ensure that the stake had not been moved.

The survey monuments at the site are typically found in or near the dunes, well back from the post-nourishment waterline. A standard automatic level and a 7.5 m telescoping, graduated, fiberglass leveling rod were used to measure elevations along the profile. The "rodperson" traversed the profile, pausing at all significant changes in slope for a reading to be made with the level. Elevations were recorded to the

Table 3.2: Coordinates, Elevations and Azimuths for DNR Monuments in Escambia County, FL.

Monument No.[1]	Northing[2] (ft)	Easting (ft)	Elevation (m, NGVD)	Range Azimuth[3] (Degrees)
R-25^{w}	482953.000	1071644.000	3.75	170
R-26	482963.500	1072537.500	3.78	170
R-27^{w}	483193.000	1073517.000	3.90	170
R-28	483323.000	1074635.500	4.48	170
R-29^{w}	483468.000	1075679.500	5.77	170
R-30^{b}	483641.000	1076816.000	4.43	170
R-31^{w}	483786.140	1077860.920	4.77	170
R-32^{b}	483966.820	1078812.720	5.86	170
R-33^{w}	484040.500	1079810.500	6.27	170
R-34^{b}	484575.000	1081013.000	3.99	165
R-35^{w,N}	484615.000	1082233.500	1.74	165
R-36^{b,N}	484834.280	1083221.300	2.35	165
R-37^{w,N}	485039.000	1084078.000	2.34	160
R-38^{b,N}	485332.000	1085078.000	4.07	160
R-39^{w,N}	485573.000	1086029.500	2.61	160
R-40^{b,N}	485924.050	1087119.670	4.27	160
R-41^{w,N}	486256.000	1088156.500	3.66	160
R-42^{b,N}	486537.500	1089122.500	2.62	160
R-43^{b,N}	486786.000	1090213.000	2.83	160
R-44^{b,N}	486922.770	1091143.410	2.87	160
R-45^{b,N}	487257.000	1092157.000	2.18	160
R-46^{b,N}	487350.000	1093014.000	4.14	165
R-47^{N}	487640.000	1094115.500	3.49	165
R-48^{b,N}	487940.770	1095039.730	4.08	165
R-49	488114.500	1096047.000	4.15	165
R-50^{b,N}	488315.000	1097097.000	4.02	165
R-51	488632.090	1098182.820	4.17	165
R-52^{b,N}	489072.500	1099265.000	2.65	165
R-53	488890.500	1100172.000	3.77	165
R-54^{b,N}	489246.500	1101191.000	3.08	165

Table 3.2: —continued.

Monument No.[1]	Northing[2] (ft)	Easting (ft)	Elevation (m, NGVD)	Range Azimuth[3] (Degrees)
R–55	489649.180	1102290.990	2.03	165
R–56^{b,N}	489603.500	1103328.000	2.48	165
R–57	489785.670	1104344.820	2.27	165
R–58^{b,N}	489940.500	1105353.000	2.18	165
R–59	490080.500	1106356.500	1.91	165
R–60^{b,N}	490247.500	1107323.000	2.03	165
R–61^{b,N}	490350.500	1108298.000	2.68	165
R–62^{b,N}	490433.130	1109324.130	2.01	165
R–63^{b,N}	490528.250	1110297.350	2.45	165
R–64^{b}	490836.540	1111090.500	1.82	170
R–65^{b}	491114.930	1111728.450	2.13	105
R–66A^{b}	492016.000	1112143.000	2.68	105
R–67^{b}	492997.990	1112292.510	3.08	90

Notes: 1) Profiles surveyed by boat and wading are marked by a superscript *b*. Profiles marked by superscript *w* were surveyed to wading depth only. Superscript *N* marks those profiles extended north into the bay.
2) Monument coordinates are in units of feet for consistency with common information sources.
3) Azimuths are measured clockwise from magnetic North and correspond to the line–of–sight of an observer at the monument looking offshore along the survey line.

nearest centimeter. Once the rodperson neared the waterline, a turning point was established so that the level could be moved to a lower elevation near the waterline. With a few exceptions, only one turning point per profile was required (Figure 3.4). The leveling loop was not closed, but the waterline elevation and distance were noted for purposes of error checking.

Distances were measured using a fiberglass tape, reading to the nearest decimeter. Offshore distances exceeding 50 m were measured using a simple optical rangefinder. Because of the nonlinear scale that is read by the rangefinder operator, the relative error in the measurement increases with distance, but calibration tests indicated that this error was within 2.5% for the distances measured in the field (<300 m). This

results in a maximum horizontal error of 7.5 m for distances measured by the optical rangefinder.

To maintain correct alignment along the profile while in the water, the rodperson would align himself with two orange traffic cones placed along the upland portion of the profile a distance apart and at different elevations. Strong currents occasionally made exact alignment impossible, but the primary effect of improper alignment is a "stretching" of the measured profile due to overestimates of the distances. The mild bathymetric gradients in the longshore direction reduce the vertical error.

The rodperson would continue his traverse of the profile until the numbers on the graduated rod became indistinguishable through the optics of the level. The profiles measured in the manner described above generally terminated near the –5 m contour, which fortunately lay near the toe of the beach nourishment material. The project site was surveyed in this manner three to four times per year after placement of the beach nourishment material. Figure 3.5 provides an example of a "typical" profile at the site before and after nourishment. For this example, both the nearshore nourishment and the offshore, "profile", nourishment changes are evident.

3.2 Hydrographic Surveys

Hydrographic surveys were conducted at nominal intervals of one year. An 8 m power boat was equipped with a Motorola Mini–Ranger Falcon 484 microwave rangefinder and an Innerspace Technology Model 441 acoustic depth sounder and digitizer for the measurement of distances and depths, respectively. In a test of four currently feasible hydrographic survey techniques, this method was found to be the least accurate (in terms of repeatability, with errors in the vertical of up to 0.30 m) but fastest scheme (Clausner et al. [1986]). Errors will be discussed in a section to follow.

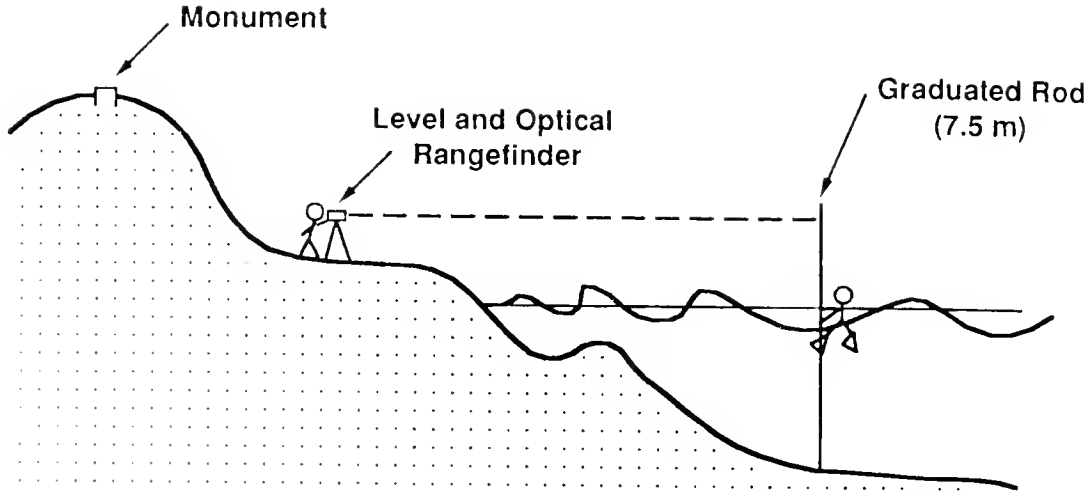

Wading/Swimming Profile

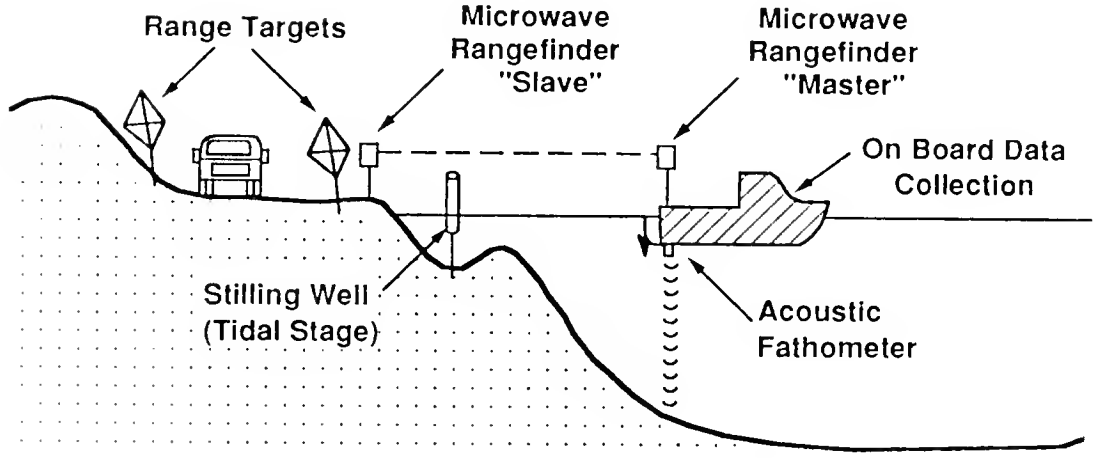

Hydrographic Survey Technique

Figure 3.4: Generalized profile geometry and survey methodology.

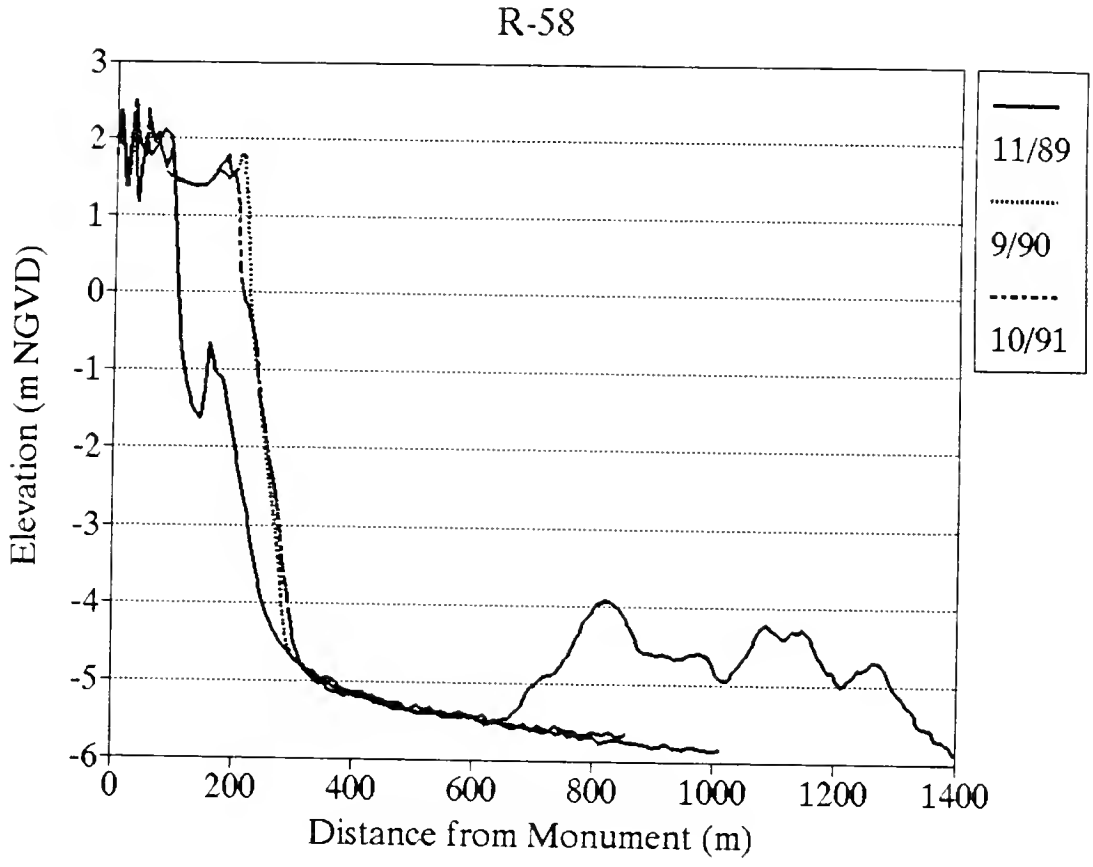

Figure 3.5: Surveyed beach profiles at R–58, Perdido Key.

The boat operator would maintain proper alignment by sighting two large, orange flags placed at different elevations on the profile of interest. The profiling would begin in the shallowest depth reachable by boat in order to provide maximum overlap between wading profiles and boat data. The profile was extended offshore until the depth was at least 8 m or the distance offshore at least 800 m. Distance was usually the controlling factor, because of the very mild slopes offshore of the –5 m contour at Perdido Key. The hydrographic survey technique is illustrated in Figure 3.4.

The electronic rangefinder system includes a battery–powered, shore–based "slave" unit, and a "master" unit aboard the boat. Distances are computed from the time required for a microwave signal to travel between the two units. A small IBM–compatible laptop computer receives the signals from both the rangefinder and the fathometer and stores data on an internal hard drive at a sampling rate of 1 Hz. With a normal boat speed of 5 kt, this yields one data point every 2.5 m.

With the scheme employed, there is no way to determine how accurately the boat followed the desired path for each profile. A second shore–based slave unit would assist the boat operator in staying on–line and provide an additional quality check by permitting computation of the distance between the desired and actual boat path. Data points that were found to be too far "off–line" could then be excluded from the result. This scheme requires a more sophisticated data acquisition program and a faster computer to handle the additional data, so was not pursued for the present study.

The fathometer simply measures the time required for a signal to travel from the transducer down to an acoustically reflective surface and back. The speed of sound through the water, presumed not to vary temporally, vertically, or horizontally within the survey domain, serves as the calibration constant and was adjusted immediately before and after the survey by performing a "bar check." This requires the placement of a large, flat object (in this case an octagonal "stop" sign) at a known depth beneath

the fathometer transducer and adjusting the calibration until the reported and known depths agree. Bar checks done before and after the survey allow for correction for temporal variation of the calibration factor; this was found to be unnecessary. Depths measured by this system are estimated to be accurate to ±3 cm when the system is calibrated properly, exclusive of motion of the fathometer transducer (manufacturer's literature).

Depths measured by fathometer must be converted to a known vertical datum by removing the tidal signal and accounting for the known distance from the transducer to the water surface. The survey boat will also exhibit some "squat", a tendency for the stern to drop as speed increases, but this was considered negligible.

A minimum of two passes were made by the boat along each profile, in order to cancel out the effects of waves. Fortunate timing allowed each hydrographic survey to coincide with minimal seas. This often allowed the boat to cross over the breakpoint bar, maximizing the overlap between the data collected by rod and level and that collected by boat. This also reduced reliance on the optical rangefinder, which is the least accurate of the devices used for distance measurement.

Tidal elevations during the hydrographic survey were measured using a simple stilling well placed in shallow water within the survey area. Readings were recorded manually every 15 minutes. The tidal stage was then removed from the fathometer data to compute elevations relative to NGVD (National Geodetic Vertical Datum).

The raw bathymetry data resemble a noisy signal with a well-defined trend (Figure 3.6 illustrates a representative result). The first step in the data analysis was to remove any obvious "spikes" in the reported distances and depths. The spikes were defined as existing when the bottom slope and change in elevation between successive data points simultaneously exceeded critical values. Spikes were often the result of only one bad data point, so this method was effective for their removal.

Noise was filtered by placing a 10 m-wide "boxcar" window over each data point and assigning the average of all values within the window to that point, conserving sediment. Offsets for tidal stage and slave unit position were then added to the depths and distances, respectively. The wading profile and boat data could then be "patched" together and the results inspected visually for agreement (Figure 3.7).

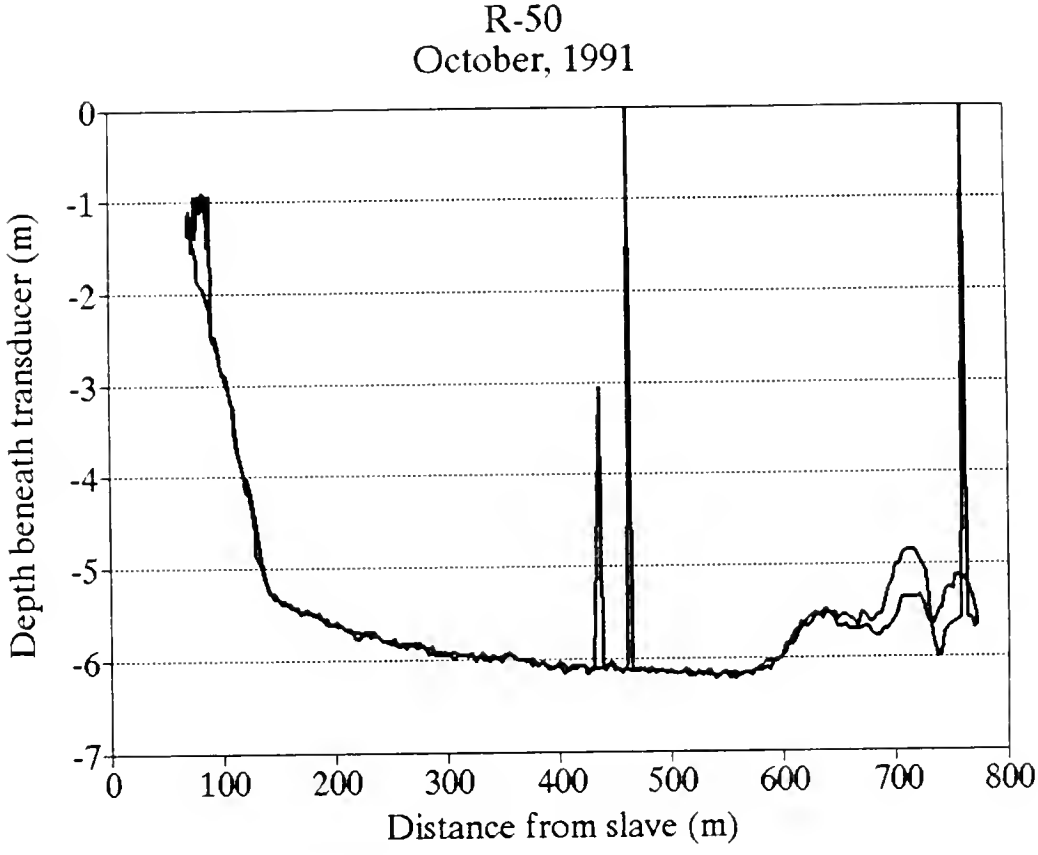

Figure 3.6: Raw bathymetry data for R-50, October, 1991. Two passes by boat are superimposed.

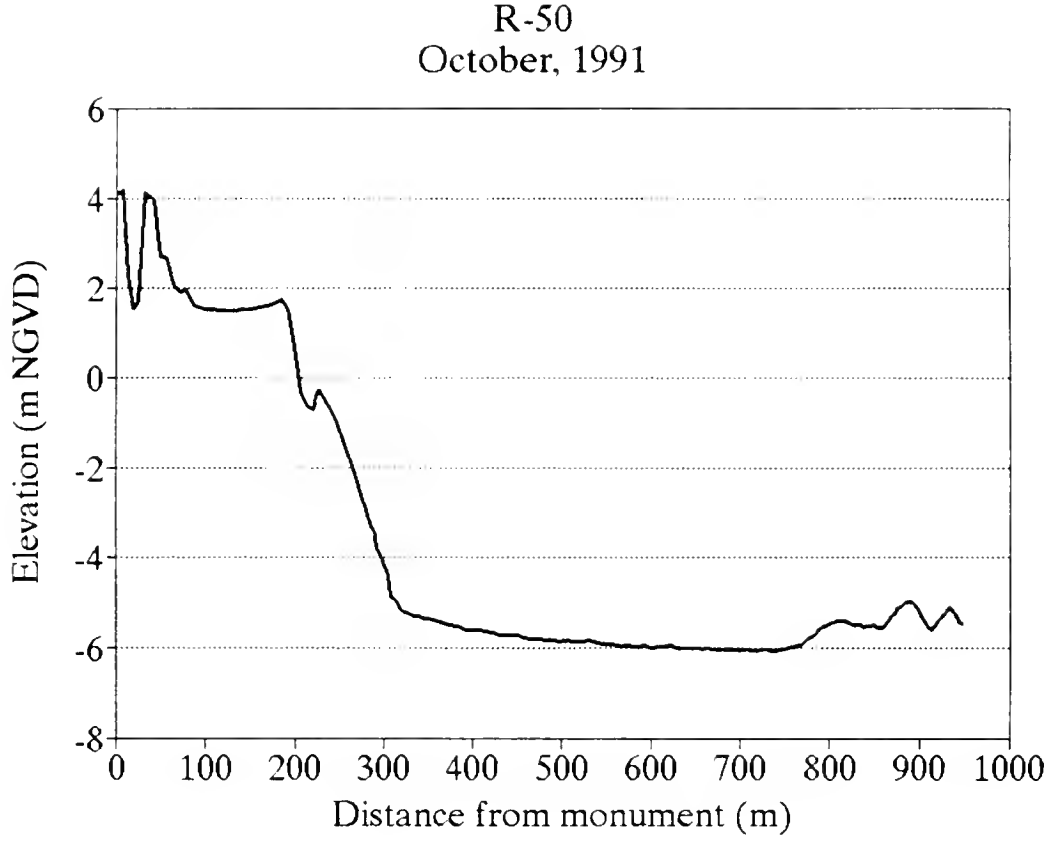

Figure 3.7: Bathymetry data for R–50, after spike removal, smoothing, adding proper vertical and horizontal offsets, and patching with wading profile data.

3.3 Waves, Currents, and Tides

A submersible, self-contained electronic wave gage was installed in 6 m of water in January, 1990. The gage is bolted to a heavy, steel, tetrahedron-shaped frame, held in place on the sea floor by jetted piles (Figure 3.8). The frame has remained on-site since its placement, with the gage being replaced periodically for servicing.

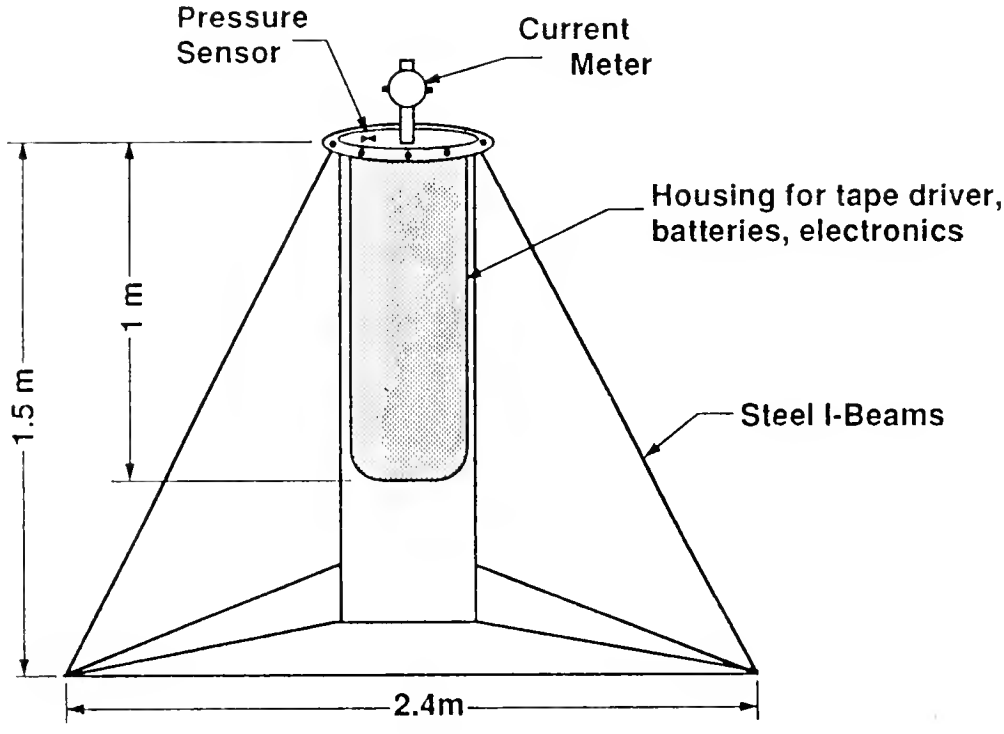

Figure 3.8: Schematic of wave gage and tripod.

Two types of wave data collection packages have been used: one self-contained and the other connected by a cable to a shore station. The data collection and analysis methods are the same for both models. A watertight cylinder, 1 m in length, houses batteries, circuit boards, and some form of data storage device. Magnetic tape drives, hard disk drives, and random-access memory (RAM) storage have all been used at different times. An electromagnetic current meter is mounted externally on the top

of the cylinder; a pressure transducer is mounted on either the top or the bottom, depending on the design.

Data were collected during the early stages of the project using self–contained wave gages. These units must be replaced roughly every three months for battery replacement and data retrieval. A serious drawback to the use of this type of unit is that malfunctions are not evident until the gage is retrieved. For this reason, a data and power transmission cable was installed, leading from the wave gage back to a shore station equipped for modem communications. The shore power maintains a charge on the batteries within the wave gage housing, and data can be downloaded as often as desired over standard telephone lines. Additionally, parameters such as sampling frequency and data burst interval can be altered without retrieval of the gage. Marine fouling is a problem with either type of gage, so neither unit could be considered maintenance–free.

Bursts of pressure and velocity data are collected once every six hours, using a sampling rate of 1 Hz for 1024 seconds. This provides adequate resolution for the waves of interest at the site by yielding a Nyquist frequency of 0.5 Hz, meaning that waves having periods less than 2 seconds cannot be resolved. In practice, high–frequency noise found in both the pressure and velocity time series imposes a more restrictive limit. This is addressed further in the following chapter.

After checking the quality of the data, removing spikes, and correcting flat spots in each time series, the pressure record is analyzed to compute the energy spectrum of the sea surface using spectral analysis methods and linear wave theory. Each 1024–point time series (pressure, u–velocity, v–velocity) is treated as weakly stationary and is time–averaged to determine and remove mean quantities, and then broken up into smaller segments for computation of the energy spectra. Tidal stage is assumed constant for this 17–minute interval, a reasonable assumption given the predominantly diurnal tides and minimal range at the site.

The first 128 points of each time series are passed to a numerical Fast Fourier Transform routine, allowing the computation of the (auto-) spectral density function (energy spectrum) from Equation (3.1). The terms necessary for estimation of wave direction are simultaneously computed. Only the pressure time series is used to compute wave heights and periods; velocities are used for determination of wave direction. A cosine^2 window (or Hanning or Tukey window, Childers and Durling [1975]) is applied to the first 10% and last 10% of the 128 points in each time series segment during the analysis to minimize spectral leakage.

$$E_\eta(f_i) = \frac{2(a_i^2 + b_i^2)}{\Delta f} \frac{1}{\kappa_p^2(f_i)} \tag{3.1}$$

Here $E_\eta(f_i)$ denotes the energy density of the free surface displacement at frequency f_i (Hz), Δf is the frequency resolution, given by the inverse of the number of records (i.e. 1/128), a_i and b_i are the real and imaginary components, respectively, resulting from the Fourier transform of the pressure time-series, and $\kappa_p(f_i)$ is the pressure response factor, given by linear wave theory:

$$\kappa_p(f_i) = \frac{\cosh k(h+z)}{\cosh kh} \tag{3.2}$$

where $k = k(f_i)$ is the wavenumber, h is the mean water depth, and z is the vertical coordinate, with origin at the mean water level and positive upwards.

With the energy spectrum computed based on the first 128 points in the 1024-point time series, the window is shifted 64 points and another spectrum is computed based on the 128 points lying within the shifted window. This is repeated until the end of the 1024-point series is reached. If each of the 1024 points passes the quality test, the resulting spectrum is thus an average of fifteen spectra all computed from a 128-point subset of the 1024 available points.

The significant wave height, H_s, is computed by integrating the energy spectrum and applying Equation (3.3):

$$H_s = 4.01\sqrt{m_0} \tag{3.3}$$

where m_0 is the zeroth moment of the energy spectrum, i.e. the area under the spectrum. Equation (3.3) requires a narrow-banded spectrum and a Gaussian sea surface displacement. These assumptions and the use of linear wave theory are not strictly valid in shallow coastal waters, but are commonly invoked in practice.

During evaluation of the area under the spectrum, m_0, energy found at frequencies higher than a pre-defined cutoff frequency (0.33 Hz) is attributed to noise in the instrumentation and therefore neglected. The effect of the noise and the chosen cutoff frequency will be illustrated in the next chapter.

Computation of the directional wave spectrum largely follows the method of Longuet-Higgins et al. [1963]. The directional spectrum, $E(f_i, \theta)$, is assumed expressible as a truncated Fourier series in terms of wave direction, θ:

$$E(f_i, \theta) = \frac{A_o}{2} + \sum_{n=1}^{2} A_n(f_i) \cos n\theta + \sum_{n=1}^{2} B_n(f_i) \sin n\theta \tag{3.4}$$

where the five Fourier coefficients may be expressed in terms of the available auto- and cross-spectra, $S_{pp}(f_i)$, $S_{uu}(f_i)$, $S_{pu}(f_i)$, $S_{pv}(f_i)$, and $S_{uv}(f_i)$. The auto-spectrum of the v-component of velocity, $S_{vv}(f_i)$, provides redundant information, but could be used to obtain a second estimate of the one-dimensional energy spectrum, $E_\eta(f_i)$.

Several subtleties present themselves when attempting to employ Equation (3.4) to describe the directional spectrum. The result is that a directional spreading function, $H(f, \theta)$, is often introduced, such that:

$$E'(f, \theta) = E(f)H(f, \theta) \tag{3.5}$$

Several forms have been proposed for the spreading function, usually describing $H(f, \theta)$ as a non-negative function, symmetric about some central direction, θ_o, and decreasing with increasing values of $|\theta - \theta_o|$. A central wave direction could be assigned

to each frequency component, but for the present study it was desired to obtain one representative direction for the entire spectrum. This direction was computed using Equation (3.6):

$$\theta_o = \tan^{-1}\left[\frac{B_1(f_m)}{A_1(f_m)}\right] \tag{3.6}$$

where f_m is the modal frequency, i.e. the frequency corresponding to the peak of the energy spectrum.

The magnitude and direction of any quasi–steady currents, and tidal stage were also computed during the wave data analysis procedure. Tidal stage and steady currents are by–products of the de–meaning of the 1024–point bursts of pressure and velocity data, respectively. The pressure gage is not vented, meaning that variations in atmospheric pressure appear as changes in water surface elevation. This does not corrupt the wave data analysis, however, because of the large difference in time scales between the relevant gravity wave periods and atmospheric pressure fluctuations.

Computation of the direction of wave propagation and the direction of the mean current requires knowledge of the orientation of the data collection package in the field. The orientation was measured for each unit immediately after installation and before removal by the diver hovering above it in the water column and sighting with either a diver's magnetic hand bearing compass or a digital compass configured for underwater use. Several of the packages used allow for only one orientation, so repeated measurements aid in assessing the error in the measurement, which is estimated rather subjectively at $\pm 10°$.

The results of the wave/current monitoring program and some additional subtleties of the analysis procedure are discussed in a subsequent chapter. The wave height, period, and direction data will be of primary concern.

3.4 Sand Samples

Close to one thousand sand samples have been collected to date to document the spatial and temporal variability in sediment size within and bordering the study area. Samples were collected during the wading profile surveys and may be considered "grab" samples of surface sediments.

Many of the sampling locations varied slightly with time, since their positions were defined by the locations of elevation contours. Samples were taken along each profile in the dunes, at the berm, on the beachface, and at the –1 m and –2 m contours. An additional sample was added at the "mid-beach" position (halfway across the "new" beach) after completion of the beach nourishment work. Samples were also collected at the –5 m and –8 m contours (or at the end of the survey line) during each hydrographic survey. The pre-nourishment survey of November, 1989, included samples from the north (bay) side of the island, on the beachface and at the –1 m and –2 m contours.

Samples from the –1 m and –2 m depths were collected by a swimmer using a small can as a scoop. The –5 m and –8 m/end-of-line samples were taken from a boat by lowering a steel bucket to the bottom and dragging it until sufficiently full.

The horizontal positions of the sampling points for the –5 m and –8 m samples were established using a Loran navigation system. During the pre-nourishment survey, the boat crew noted the points on each profile where the depth reached 5 m or 8 m and stored the latitude and longitude as a waypoint in the Loran set. Some profiles never reached the –8 m contour, so the coordinates of the offshore limit of the survey line were stored instead. The "–5 m" samples either represent the approximate –5 m contour or an intermediate point along the profile. The same Loran coordinates were used for sampling during later surveys, with the depth recorded for each sample, although the depths were not corrected for tidal stage. When used repeatedly to locate the same points in this manner, accuracies of 50 m are commonly cited for Loran

navigation systems. Table 3.3 presents the location of each offshore sample and the nominal and measured depths.

All sand samples were placed in labelled cloth sacks. They were dried in an oven at 40°C before sieve analysis. Organic content of most of the samples appeared negligible, although no attempt was made to quantify the percentage. Most samples consisted primarily of quartz sand, with the shell fraction increasing near the waterline. Some samples that resembled a fine "ooze" were taken after beach nourishment at the –5 m and –8 m sampling points near the center of the beach nourishment project. These hardened upon drying and were crushed for analysis.

Twelve sieves were used to determine the grain size distribution for each sample (six sieves were used for the pre-nourishment samples). Sieve numbers and sizes are listed in Table 3.4.

After sieving, mean and median grain sizes, sorting index, skewness, and kurtosis were all computed for each sample. Except for the fine samples offshore of the center of the nourishment area, the median grain sizes exhibit little variation in the cross-shore direction (see Table 3.5 and Figure 3.9). Some fining is evident offshore, and the coarsest sediment is found on or near the beachface. Longshore variation in sediment size was also small, and the size characteristics of the "new" and native sands were found to be similar. Sediment size statistics are discussed in more detail in Work et al. [1991a] and Work and Dean [1992].

3.5 Weather Data

A mechanical weather station was installed at the Perdido Key Ranger Station in January, 1990. This unit recorded air temperature and wind speed and direction in analog form on a strip chart. It was replaced in June, 1990, by an electronic weather station that remains at the site. The electronic station includes a series of sensors for wind speed, wind direction, air temperature, and rainfall. The wind sensors were

Table 3.3: Locations and depths of offshore sand samples.

Range No.	Nominal Depth (m)	11/89 Depth (m)	9/90 Depth (m)	10/91 Depth (m)	Latitude (Deg., Min.)	Longitude (Deg., Min.)
R-30	5	4.2	5.5	5.2	30 17.49	87 25.52
	8	6.6	6.7	6.7	30 17.26	87 25.48
R-32	5	5.2	5.8	5.5	30 17.59	87 25.14
	8	5.9	5.5	6.1	30 17.30	87 25.10
R-34	5	5.1	5.2	5.5	30 17.68	87 24.71
	8	5.8	5.8	6.1	30 17.45	87 24.66
R-36	5	4.9	5.0	5.8	30 17.76	87 24.30
	8	6.0	5.9	6.4	30 17.48	87 24.50
R-38	5	5.1	5.8	5.5	30 17.85	87 23.91
	8	6.2	6.1	6.4	30 17.61	87 23.81
R-40	5	5.4	5.5	5.8	30 17.95	87 23.53
	8	5.9	5.8	5.8	30 17.73	87 23.43
R-42	5	4.6	5.6	5.8	30 18.07	87 23.16
	8	6.3	6.4	6.4	30 17.82	87 23.08
R-43	5	5.2	5.2	3.7	30 18.14	87 22.93
	8	6.7	6.9	6.7	30 17.87	87 22.84
R-44	5	5	5.3	4.6	30 18.18	87 22.79
	8	7	6.7	7.0	30 17.90	87 22.67
R-45	5	5.3	5.3	4.6	30 18.19	87 22.57
	8	7.5	7.2	6.7	30 17.93	87 22.47
R-46	5	5.4	5.2	4.6	30 18.23	87 22.43
	8	7.3	7.0	7.0	30 17.94	87 22.36
R-48	5	5.3	5.2	4.6	30 18.32	87 22.05
	8	6.7	6.7	6.4	30 18.06	87 21.98
R-50	5	5.7	5.2	5.5	30 18.38	87 21.65
	8	6.4	6.4	5.5	30 18.13	87 21.54
R-52	5	5.3	5.2	4.9	30 18.49	87 21.24
	8	6.4	6.2	5.5	30 18.24	87 21.17
R-54	5	5.4	4.1	4.3	30 18.55	87 20.88
	8	6.1	5.9	4.9	30 18.30	87 20.79
R-56	5	5	5.3	5.2	30 18.60	87 20.47
	8	6	5.8	5.8	30 18.38	87 20.39

Table 3.3: —continued.

Range No.	Nominal Depth (m)	11/89 Depth (m)	9/90 Depth (m)	10/91 Depth (m)	Latitude (Deg., Min.)	Longitude (Deg., Min.)
R–58	5	5	5.0	5.2	30 18.69	87 20.09
	8	5.8	5.8	4.6	30 18.45	87 20.02
R–60	5	4.5	4.6	4.6	30 18.73	87 19.71
	8	5.6	5.6	4.6	30 18.51	87 19.66
R–61	5	4	4.3	4.3	30 18.75	87 19.53
	8	5.0	5.2	5.2	30 18.53	87 19.47
R–62	5	3.5	3.8	4.0	30 18.78	87 19.34
	8	4.6	4.4	4.6	30 18.55	87 19.27
R–63	5	3	2.4	3.0	30 18.84	87 19.14
	8	3.5	3.5	3.4	30 18.58	87 19.05
R–64	5	2	5.5	2.4	30 18.83	87 19.02
	8	3.1	7.1	3.0	30 18.67	87 18.99
R–65	5	2.7	5.5	4.0	30 19.03	87 18.70
	8	8	9.4	7.3	30 19.00	87 18.61
R–66A	5	5	5	4.6	30 19.21	87 18.72
	8	8	8	7.3	30 19.20	87 18.66
R–67	5	5	8	4.6	30 19.40	87 18.70
	8	5	8	7.0	30 19.30	87 18.69

Notes: 1) All coordinates obtained during pre–nourishment survey of October 28–November 3, 1989, except those for Ranges 66 and 67, which were taken during September, 1990 survey.

2) Measured depths are not corrected for tide, but merely indicate the depth beneath the boat at the time of sampling.

Table 3.4: Sieves used for grain size analysis.

Sieve Number U.S. Standard	Sieve Opening (mm)
10	2.00
20	0.850
30	0.595
40	0.420
50	0.297
60	0.250
70	0.210
80	0.177
100	0.149
120	0.125
140	0.106
160	0.096

Table 3.5: Cross-shore distribution of grain size at various contours (Gulf side). Longshore standard deviation is given following median grain size.

Location	Average D_{50} (mm) November, 1989	Average D_{50} (mm) September, 1990	Average D_{50} (mm) October, 1991
Dune	0.37±0.04	0.36±0.04	0.34±0.03
Mid-Beach			0.34±0.03
Berm	0.39±0.05	0.38±0.03	0.36±0.04
Beachface	0.39±0.05	0.40±0.06	0.36±0.06
-1 m	0.38±0.05	0.36±0.05	0.34±0.04
-2 m	0.30±0.03	0.35±0.07	0.28±0.03
-5 m	0.32±0.03	0.31±0.06	0.30±0.04
-8 m/End of line	0.32±0.05	0.31±0.06	0.31±0.06

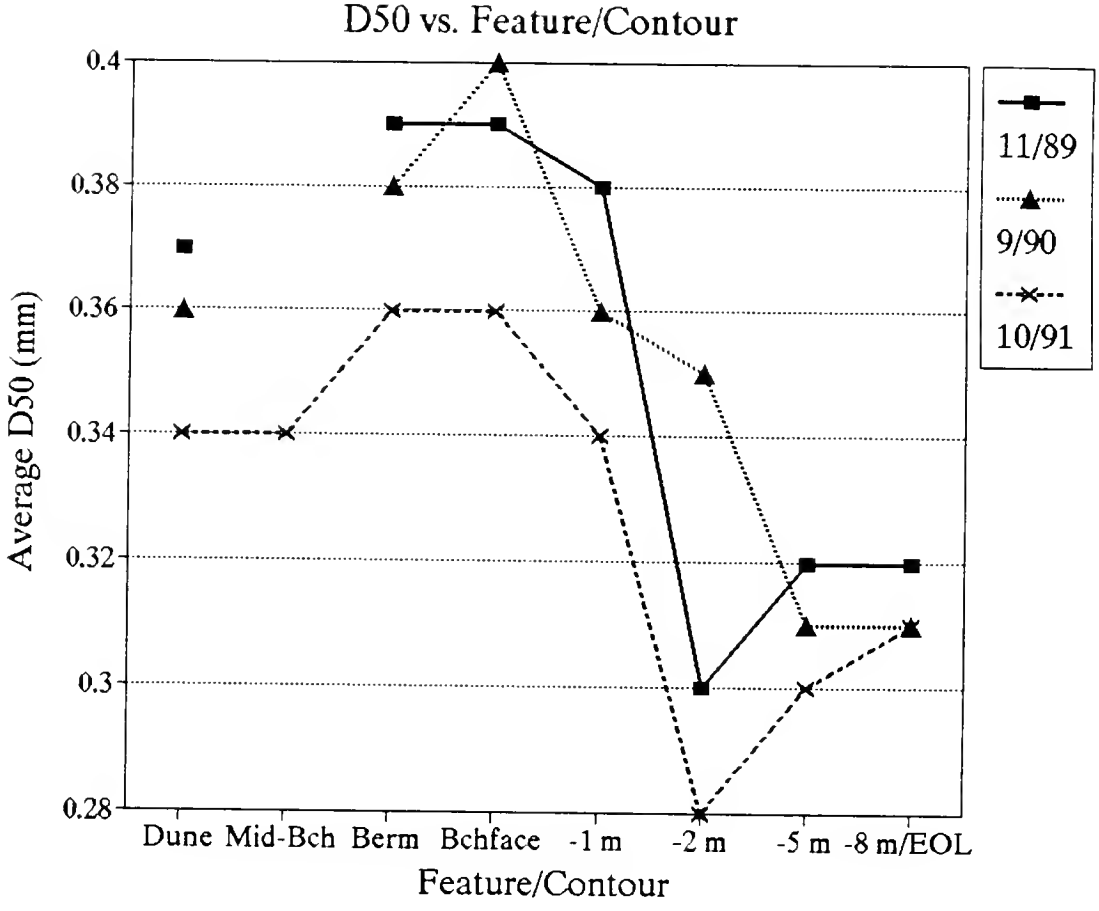

Figure 3.9: Cross-shore distribution of grain sizes.

mounted clear of the roof of the Ranger Station at an elevation of 11.7 m NGVD, and the temperature sensors were shielded from direct sunlight.

Each sensor outputs either a pulse or a voltage to an analog–to–digital conversion board. The digitized signal is sent to a small computer, which stores one set of readings per hour in random–access memory. Once per day, the computer phones a host computer and attempts to dump the stored data via modem. If successful, the memory is cleared and data acquisition re–started. If unsuccessful, data acquisition continues, and a new attempt at data transfer is made the following day.

Weather data are presented and compared with similar data collected by the National Weather Service in Pensacola in Work et al. [1991b]. The weather data were not used in the development or calibration of the beach evolution models presented here, so will not be discussed further.

3.6 Ft. Pickens Pier Tide Gage

A mechanical tide gage was installed on Santa Rosa Island at the Ft. Pickens pier (Figure 3.1). The gage uses a stilling well to damp out high frequency motion and a spring–driven clock to drive a pen across a rotating drum covered with paper. The gage was surveyed to refer all elevations to NGVD. The data do not form an important part of the study because of the numerous gaps in the record and the location of the gage inside Pensacola Bay.

3.7 Assessment of Errors

Many possible sources of error exist in the field data collected, both random and systematic. A few were mentioned during the discussion of the data collection methods. In several cases, it is possible to devise a scheme by which these errors can logically be minimized. Most of the errors have been either treated during data analysis or presumed negligible. It is important, however, to identify all significant sources of error and attempt to assess the magnitude of each. Human errors, such as reading a scale incorrectly, will not be addressed; such errors are often large enough

that they are easily identifiable, and there is rarely a rational way to compensate for them. Emphasis will be placed on errors in the bathymetric and wave/current data, since they are most relevant to the focus of this study.

The beach profiles are defined by horizontal and vertical distance measurements, each having a different error, and each containing several contributions to the total error. Some of the errors are proportional to the magnitude of the distance being measured, while others are independent. Fortunately, most of the errors are not cumulative. Because of the mild slopes involved in beach profile surveying, vertical errors are particularly troublesome.

The portions of the beach profiles surveyed by rod and level contain roundoff errors of up to 0.5 cm in the vertical and up to 5 cm in the horizontal. These are presumed to be random, with zero mean, and will therefore cancel. Insufficient tension in the tape will lead to overestimation of distances. Repeated measurements of the same distance indicated that an error of less than 1.0% could be expected when using the tape. Distances measured by the optical rangefinder were found to be within 2.5%. The stated "probable range error" of the microwave rangefinder system is 2 m, irrespective of range (manufacturer's literature). If the boat maintains the correct alignment along the profile, the maximum horizontal error in the beach profiles surveyed by boat is thus 3 to 4 m. Good overlap between wading profile data and data collected by boat provided some verification and confidence in measured distances.

Incorrect alignment along the profile introduces some error by leading to some "stretching" of the profile, as distances are overestimated (assuming that the correct alignment is perpendicular to the local shoreline). This effect is minimal until well offshore. In some cases, large apparent changes in the profile appear in the dunes when the profile line is not repeated exactly from one survey to the next. This is simply because of the very strong topographic gradients in and near the dunes; i.e.

they are often steep. Fortunately, longshore bathymetric gradients offshore are small for most of the study area. Therefore the primary effect of the boat being off–line during the survey is to overestimate distances by a factor of $1/\cos\theta$, where θ is the angular deviation of the boat from the correct path. With the bathymetric surveying technique employed, there is no way to determine the magnitude of this error or correct for it. The averaging involved in making several passes over the profile should help remove errors of this type.

Vertical errors include those due to not holding the leveling rod vertical, possible settling of the level or rod during the survey, and improper calibration of the level. These sources were considered negligible, as periodic calibration of the level and appropriate caution during each survey should have rendered them so.

An experiment was conducted in June, 1992, to assess the repeatability of the wading profiles. The equipment was deployed at R–46 and the profile surveyed to the maximum depth possible by swimming. The equipment was taken down, all crew tasks were swapped, and the process repeated. This resulted in two surveys of the same profile within one hour, during which wave activity was minimal. Any differences between the two surveys may thus be assumed error.

The results of the repeatability experiment are shown in Figure 3.10. The two realizations of the profile are superimposed and are nearly coincident. The difference between the two surveys is also shown, plotted using a different vertical scale. Not surprisingly, the maximum difference occurs near the dunes, where cross–line gradients are largest. This is not important for the present study, where changes in the submerged portions of the profile are of primary interest. The average difference between the two profiles is slightly more than one millimeter. This average difference will be important for any computations involving a sediment mass balance; the RMS difference (2.6 cm) is more representative of the accuracy with which the elevation

of any particular point may be measured. Wave conditions during this test were favorable, but the same may be said for all but two of the surveys.

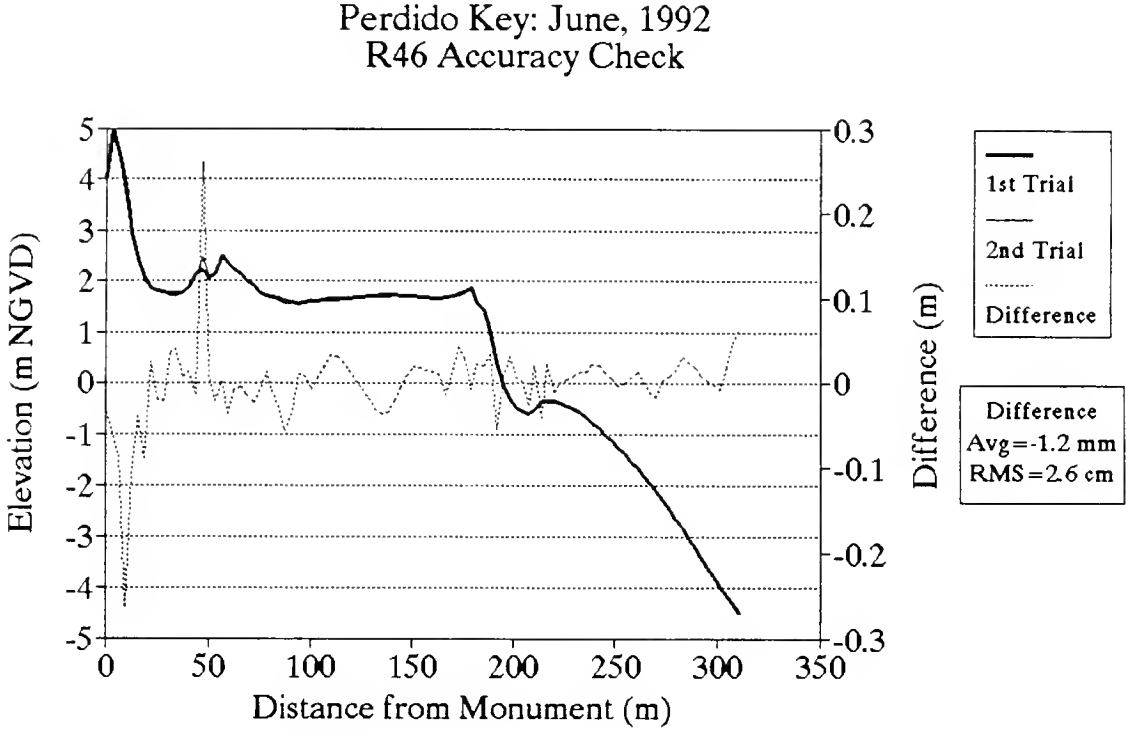

Figure 3.10: Repeatability test at R-46, June, 1992.

The largest potential errors in the surveys in the vertical are found in the regions surveyed by boat. The accuracy of the tide data for correction of depths measured by boat to a common vertical datum is critical. The tide gage was surveyed both before and after the survey to establish its elevation and determine if it had settled during the survey. Tide readings at fifteen-minute intervals provided sufficient temporal resolution of the tidal stage throughout the survey. Error in the computation of the elevation of the water surface *at the tide gage* is thought to be small, on the order of one centimeter. Spatial variation in the instantaneous water surface elevation within

the survey area could be much larger than this (Blair [1983]), but without additional tide data, there is no reasonable way to account for this possibility. The small tidal range at the site (0.3 m at Pensacola Pass, U.S. Department of Commerce [1981]) and their chiefly diurnal nature help to minimize any errors introduced in this manner.

Vertical or angular motion of the fathometer transducer, arising from wave-induced motion of the survey boat, introduces some error in the measured depths. Heaving under- or overestimates depths by the instantaneous vertical excursion of the motion; rolling or pitching will always overestimate depths by the inverse of the cosine of the angular displacement. Commercial systems for the measurement and recording of the heave, pitch, and roll of the survey boat have recently become available and would allow compensation for these effects during data analysis (Downing and Fagerburg [1987]). Such equipment was not available for the present study. The repeated passes over each profile during each bathymetric survey should cancel out the effects of the heaving motion, while the minimal wave activity found during each survey should render the effects of both the heaving and the angular displacement negligible.

Calibration of the fathometer was described earlier. The calibration was assumed to be valid throughout the survey area, and the speed of sound through the water column was considered independent of depth. Improper calibration would lead to a systematic error, always over- or underpredicting depths, while density variations would lead to a more random error. The accuracy of the fathometer, when used in the manner described, was previously estimated at ± 3 cm, exclusive of errors arising from heave, pitch, and roll of the survey boat. This assumes proper calibration; the largest component of vertical error, however, is thought to be fathometer calibration. This is because the bar check is typically done at depths of 1.5 to 3 m, with an uncertainty of 3–4 cm, or roughly 1–2%. During each survey, wading profiles were extended offshore as far as possible to provide maximum overlap for quality checking.

The depths and distances recorded on board the survey vessel are collected independently and both reported as functions of time. "Spikes" occasionally appear in the depth or distance vs. time curves, as was shown in Figure 3.6. Spikes in the depth curve always result in smaller reported depths and are caused by bubbles, fish, or turbid water beneath the transducer. Excessive gain and turbid water are thought to be the cause of the noisy offshore data collected in the middle section of the monitoring area during the September, 1990, survey. Spikes in the distance curve are usually the result of short time intervals when no communication is made between the slave and master units of the range–finding system. Both types of errors are easily spotted and removed during data analysis if the number of bad data points is not too large.

Upon examination of three sets of bathymetric survey data (November, 1989; September, 1990; and October, 1991), some systematic error, most likely due to calibration inaccuracies, was found. The data collected by boat for the October, 1991, survey were found to lie vertically between and nearly equidistant from the profiles from the November, 1989, and September, 1990, surveys. The data collected by boat were adjusted to remove any average error between the offshore portions of successive surveys at one location. More sophisticated schemes for error removal could be devised, such as increasing or reducing depths by a specified percentage, rather than a single depth adjustment, but there will always be a degree of subjectivity in selecting the region over which the profiles should agree, and this subjectivity renders more complicated error correction schemes unjustifiable. Adjustment of the September, 1990, bathymetric data was more difficult because of the noise found in several of the data files.

The result of the vertical adjustment of the hydrographic data was an average raising of the November, 1989, profiles by 14 cm (maximum of 29 cm; standard deviation of 6.7 cm), and a lowering of the September, 1990, profiles by 8 cm (maximum of 20 cm; standard deviation of 6.9 cm). One of the October, 1991, profiles was lowered

by 6 cm, the rest were left unmodified. Note that only the data points collected by boat were modified in this manner; wading profile data were unaffected.

It could be argued that the average of all three data sets should be computed, and then each profile adjusted to agree with the computed average offshore. The chosen method instead weights the most recent survey more heavily than the previous surveys, assuming that the quality of the data improved with experience in the data collection process. The difference between the two adjustment methods is not particularly relevant when considering sediment transport, since profile differences are much more important than absolute depths.

Saville and Caldwell [1953] and Nordstrom and Inman [1975] both discussed the vertical accuracy of beach profiles surveyed using acoustic fathometers. Based on repetitive surveys of the same beach profile over a short time interval, Saville and Caldwell [1953] concluded that the probable vertical error in one profile is 2.5 cm, but also conceded that this was probably an optimistic estimate. All measurements were made in one day, tide range was minimal, no crew changes were made, and the surveying equipment was mobilized only once. Nordstrom and Inman [1975] compared profile changes measured by fathometer and permanent vertical reference rods placed at various locations in the surf zone and concluded that fathometer measurements were accurate to ± 30 cm. The results of the Perdido Key monitoring program suggest that the error estimated by Nordstrom and Inman [1975] is a reasonable upper bound for the absolute vertical error in the boat data. It is the author's belief, however, that adjusting the profiles to agree in the offshore segments can reduce this error by nearly an order of magnitude, leaving a vertical error of 3–5 cm.

The wave and current data have two primary sources of error: calibration and orientation. The maximum error in the orientation of the data collection package was earlier estimated at $\pm 10°$. Wave and current directions are directly dependent on

this orientation. This is a serious problem, because a ten degree difference in wave direction can have a significant effect on nearshore sediment transport.

Errors in the calibration of the pressure sensor or current meter will affect the computed mean quantities, such as tidal stage and mean currents, and significant wave height. Calibration problems will in general not corrupt computed wave or current directions or the wave period corresponding to the spectral peak. Pressure sensors were calibrated prior to installation; the calibration factors supplied by the manufacturer of the current meters were used for lack of suitable calibration facilities. With one exception, the various current meters each reported similar steady currents when deployed in the field, providing some confidence in the supplied calibration constants.

Electronic noise in the pressure sensor and the hardware "downstream" from it will lead to an overestimate of the energy in the wave spectrum. A simple experiment was conducted to determine the amplitudes and frequencies associated with this noise. The experiment is discussed in the following chapter.

Errors in the weather data are limited to calibration factors, although wind direction is dependent on accurate alignment of the wind vane in the field. The error in this angle is estimated at $\pm 5°$. The remaining sensors (wind speed, rainfall, temperature) were calibrated prior to deployment and presumed invariant. Two temperature sensors were deployed side–by–side; they typically agreed within 1° F.

CHAPTER 4
ANALYSIS AND INTERPRETATION OF FIELD DATA

The primary goal underlying much of the field program was to obtain data documenting the sediment transport processes at a nourished beach, as well as the forces influencing the processes. The sediment transport at the site has not been measured directly, but can be inferred from the measured changes in the bathymetry. Many environmental parameters have been monitored, but the data provided by the wave gage (incident wave spectrum, water level, and mean currents) are thought to include all the dominant environmental forces modifying the bathymetry at the site. The goal of this chapter is to extract from the field data all qualitative and quantitative trends that are important to the sediment transport problem of interest.

4.1 Wave, Current, and Tide Data

Analysis of the data from the offshore P–U–V (pressure and two components of horizontal velocity) gage was described in the previous chapter. This analysis provided, for every six hours of satisfactory operation, one realization of each of the following parameters: energy spectrum (from which significant wave height, H_s, and wave frequency corresponding to the peak of the energy spectrum, T_p, are computed), wave direction corresponding to the peak of the spectrum, magnitude and direction of any mean current, and tidal stage.

Some quality checking was done in order to establish confidence limits on the data collected by the wave gage. The first issue addressed was the level of noise in the pressure sensor and the current meter and the associated electronics. To investigate this, one of the wave gages was activated in the lab, in still air, and a 1024–point burst of data collected. Figure 4.1 shows the resulting energy spectra of the pressure and

velocity signals, $E_p(f_i)$ and $E_v(f_i)$, respectively. The spectra shown in Figure 4.1 have not been transferred to the surface to enable computation of a significant wave height. To determine the energy spectrum of the sea surface, each frequency contribution must be divided by the square of its response function:

$$E_\eta(f_i) = \frac{E_p(f_i)}{\kappa_p^2(f_i)} \tag{4.1}$$

and

$$E_\eta(f_i) = \frac{E_v(f_i)}{\kappa_v^2(f_i)} \tag{4.2}$$

where $\kappa_p(f_i) = \cosh k_i(h + z)/\cosh k_i h$ and $\kappa_v(f_i) = 2\pi f_i \cosh k_i(h + z)/\sinh k_i h$. Since the response functions $\kappa_p(f_i)$ and $\kappa_v(f_i)$ are much smaller for high frequencies, noise at high frequencies will be much more troublesome.

The noise shown in Figure 4.1 was transferred to an assumed free surface, using Equations (4.1) and (4.2) with an assumed water depth of 6 m, to yield the surface energy spectra shown in Figure 4.2. The energy in the velocity signal is seen to be minimal and will not be of further concern since it is not used in the wave height or wave frequency estimation.

The next step was to compute the significant wave height, H_s, based on the energy spectrum of the free surface, $E_\eta(f_i)$, derived from the pressure time series. The significant wave height is assumed to be equal to 4.01 times the square root of the area under the spectrum. The cutoff frequency for evaluation of this area is clearly important: with a cutoff frequency of 0.5 Hz (the Nyquist frequency), the significant wave height for this case is 0.14 m, while a cutoff frequency of 0.33 Hz yields H_s=0.05 m. Since the data collected in the field were analyzed with a cutoff frequency of 0.33 Hz, it was assumed at this stage that the contribution of the noise to the reported significant wave heights was negligible.

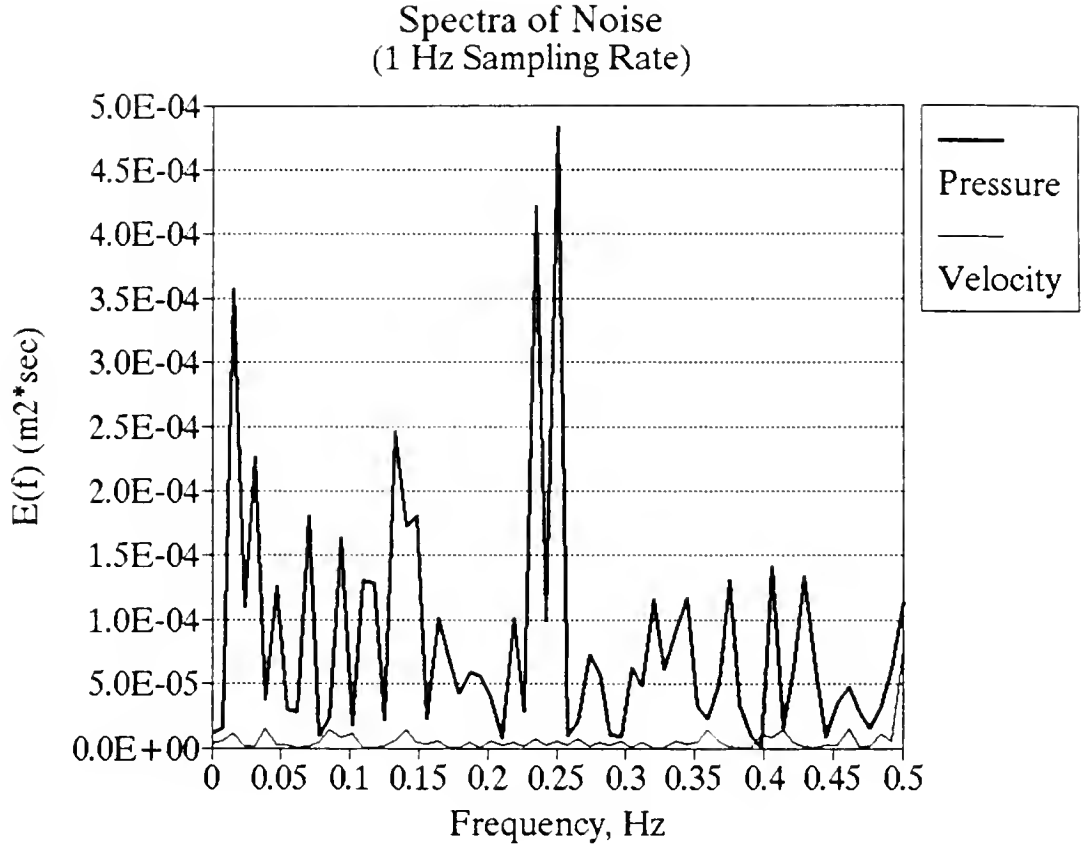

Figure 4.1: Spectra of noise in pressure sensor and current meter, based on 128 points sampled at 1 Hz, Hanning window. Gage in still air in lab.

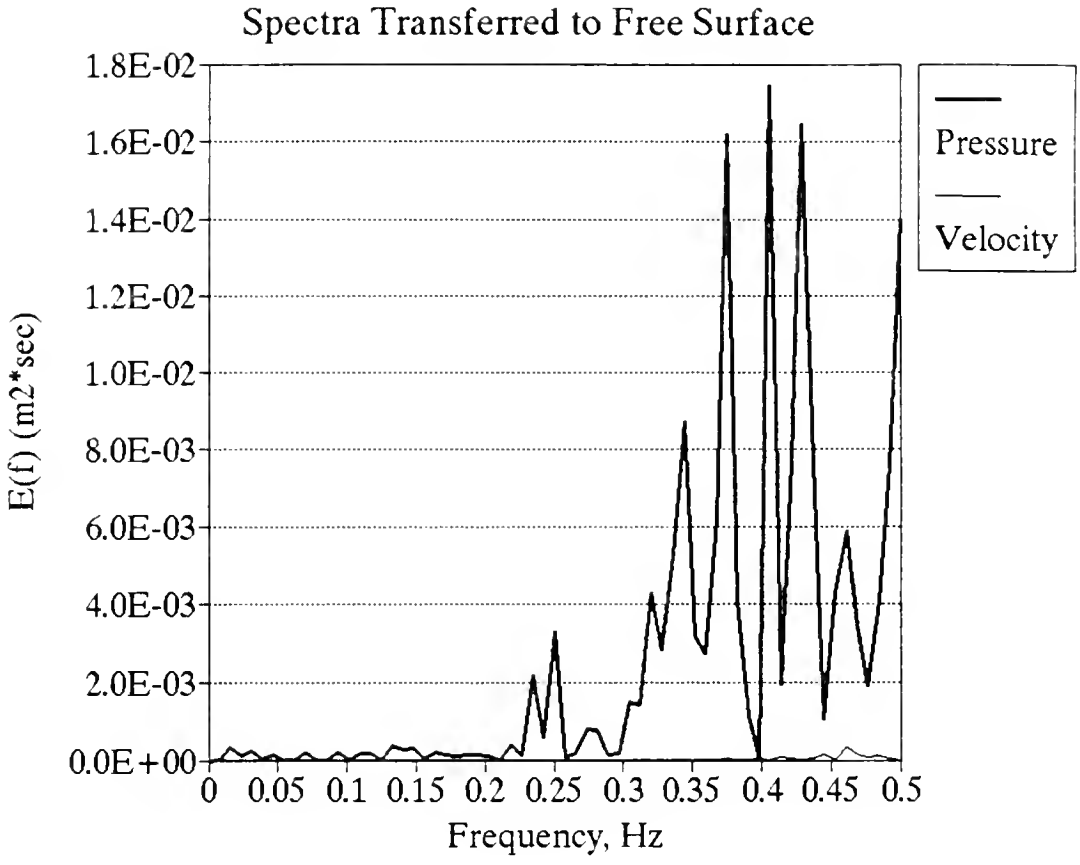

Figure 4.2: Spectra from previous figure, transferred to free surface using an assumed depth of 6 m.

The noise can also bias the computation of the wave period corresponding to the peak of the energy spectrum, T_p. If most of the signal is due to noise, and the noise is distributed fairly evenly over all frequencies (i.e. white noise), then the reported value for T_p will correspond to the cutoff frequency, regardless of the chosen value. Wave and current directions can also be affected by noise: if the signal is very small, the computed directions lose their significance. When interested in average values, these problems can generally be avoided by weighting each quantity (T_p, wave direction, or current direction) by the magnitude of the parameters used to estimate them. The computed waves and mean currents may both be thought of as vectors, each having a magnitude and direction. The confidence level of the computed directions decreases as the magnitudes of the vectors decrease.

Some data files revealed failure of the current meter while the pressure sensor was still functioning properly. Often this was attributable to fouling of the current sensor by marine organisms. For this situation, only wave height and period data are available. Wave direction is not available.

Although the results above suggested that the effect of the noise was negligible, a second time series was generated by sampling the pressure at 100 Hz. The idea was to determine if high-frequency noise was being aliased and appearing at lower frequencies. The spectrum of this pressure time series is shown in Figure 4.3. A dominant signal is evident at 40 Hz, most likely arising from the power supply or amplification circuitry. Based on this result, sampling at 80 Hz or more and then computing the significant wave height using a cutoff frequency lower than 40 Hz could reduce the influence of noise on the result. This approach would greatly increase storage requirements, however, and would not have a large effect on the results. A much larger range of frequencies would be included in the analysis, but most of these, corresponding to wave periods less than two seconds, are not of interest and can't be scaled up to the free surface with confidence due to large amplification factors.

Only one gage was tested in the manner described above. Other gages might display different noise characteristics, but the one tested is thought to be fairly representative. The tests essentially investigated only the effects of electronic noise. Since the gage itself modifies the flow that it is monitoring, hydrodynamic noise could also introduce some error into computed wave and current characteristics. The magnitude of this error cannot be assessed with the available data, but is thought to be relatively small.

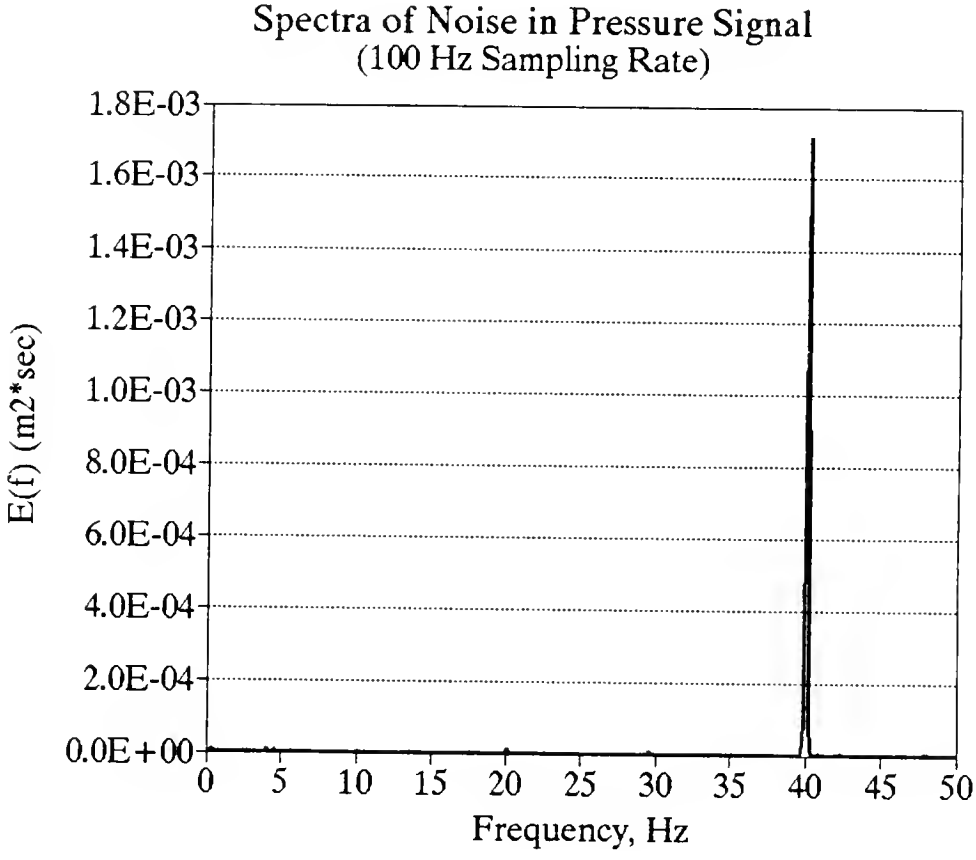

Figure 4.3: Spectra of noise in pressure sensor, based on 1024 points sampled at 100 Hz, Hanning window. Gage in still air in lab.

Long-term behavior of the wave climate (seasons to years) at the site will be important to describing the evolution of the beach nourishment project. Observation of the wave climate at the site for 2-1/2 years has provided some insight into

the typical conditions and seasonal trends at Perdido Key. Tables 4.1 through 4.3 summarize the monthly and annual statistics for significant wave height, wave period at the spectral peak, and mean current from the wave gage offshore of Perdido Key. Figure 4.4 illustrates the number of successful data bursts collected for each month.

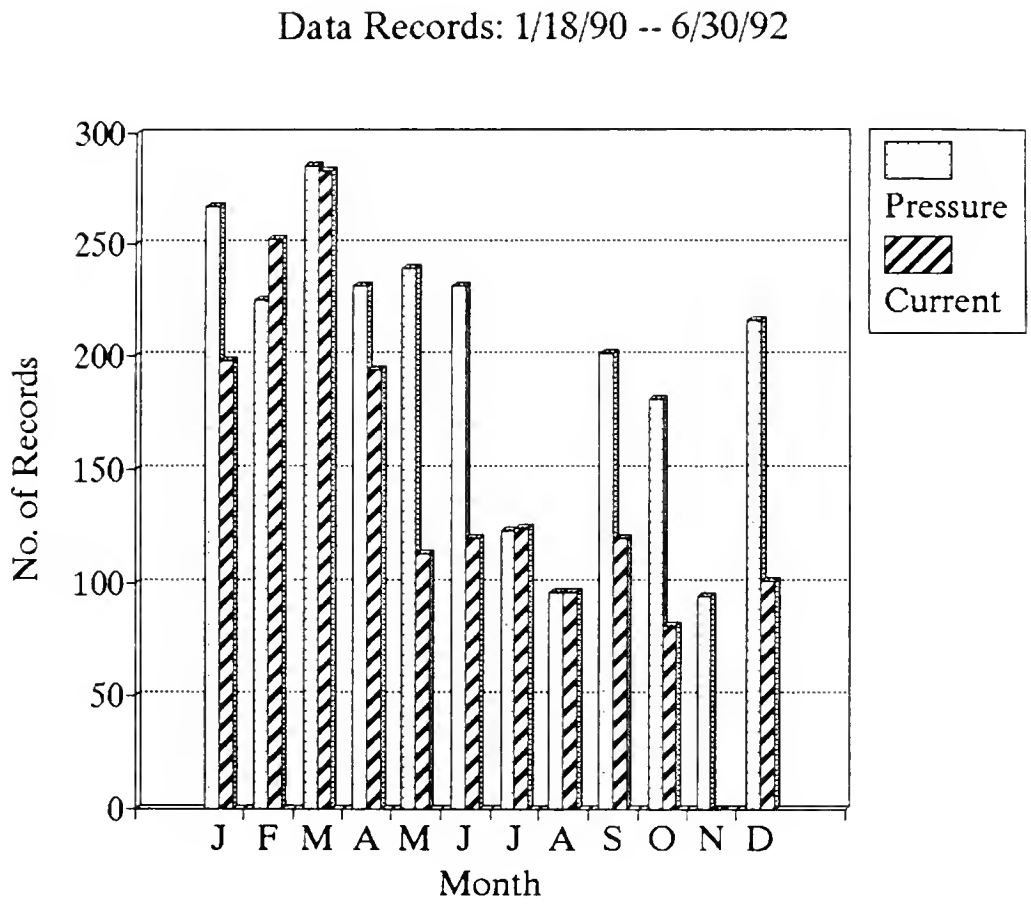

Figure 4.4: Number of valid pressure and current data bursts, sorted by month, for the period 1/18/90-6/30/92.

Table 4.1: Monthly and annual statistics for significant wave height, H_s.

Month	Maximum (m)	Date of maximum	Mean (m)	Standard Deviation (m)	Number of Records
January	2.34	1/14/92	0.46	0.34	267
February	2.61	2/3/91	0.59	0.36	225
March	1.76	3/29/91	0.51	0.35	285
April	1.46	4/9/90	0.48	0.32	231
May	1.45	5/9/90	0.38	0.26	239
June	0.99	6/30/92	0.27	0.21	231
July	1.00	7/5/90	0.33	0.18	123
August	0.58	8/23/90	0.27	0.09	96
September	1.74	9/30/91	0.40	0.30	201
October	1.58	10/30/91	0.68	0.33	181
November	1.51	11/1/91	0.44	0.36	94
December	2.20	12/20/91	0.48	0.36	216
All	2.61	2/3/91	0.45	0.33	2389

Table 4.2: Monthly and annual statistics for wave period corresponding to peak of energy spectrum, T_p.

Month	Maximum (sec)	Date of maximum	Mean (sec)	Standard Deviation (sec)	Number of Records
January	9.8	1/23/90	5.8	1.6	267
February	10.6	2/6/92	6.0	1.5	225
March	9.8	3/19/90	6.4	1.7	285
April	9.2	4/1/91	5.8	1.5	231
May	9.2	5/8/90	5.7	1.8	239
June	9.8	6/24/90	5.6	1.9	231
July	9.8	7/30/90	5.8	1.8	123
August	11.6	8/8/90	6.4	2.3	96
September	9.8	9/14/91	4.7	1.5	201
October	8.0	10/31/91	4.8	1.4	181
November	9.8	11/4/91	5.1	1.9	94
December	12.8	12/8/90	6.0	1.9	216
All	12.8	12/8/90	5.7	1.8	2389

Table 4.3: Monthly and annual statistics for magnitude of mean current, U_c.

Month	Maximum (m/s)	Date of maximum	Mean (m/s)	Standard Deviation (m/s)	Number of Records
January	0.33	1/27/90	0.09	0.04	198
February	0.69	2/15/90	0.09	0.06	252
March	0.93	3/8/90	0.08	0.08	283
April	0.60	4/8/90	0.08	0.06	194
May	0.27	5/13/90	0.09	0.05	113
June	0.16	6/4/90	0.06	0.03	120
July	0.16	7/4/90	0.05	0.03	124
August	0.40	8/31/90	0.27*	0.06	96
September	0.40	9/22/90	0.29*	0.04	120
October	0.46	10/18/90	0.35*	0.05	81
November					0
December	0.22	12/27/90	0.08	0.04	101
All	0.93	3/8/90	0.12	0.10	1682

*All data for 8/90–11/90 from one deployment; current meter calibration appears suspect.

Seasonal trends in the data are illustrated in Figures 4.5, 4.6, and 4.7. Both mean and maximum monthly significant wave heights are quite small during the summer; the same is also true of the mean currents. Wave period exhibits little variation month–to–month.

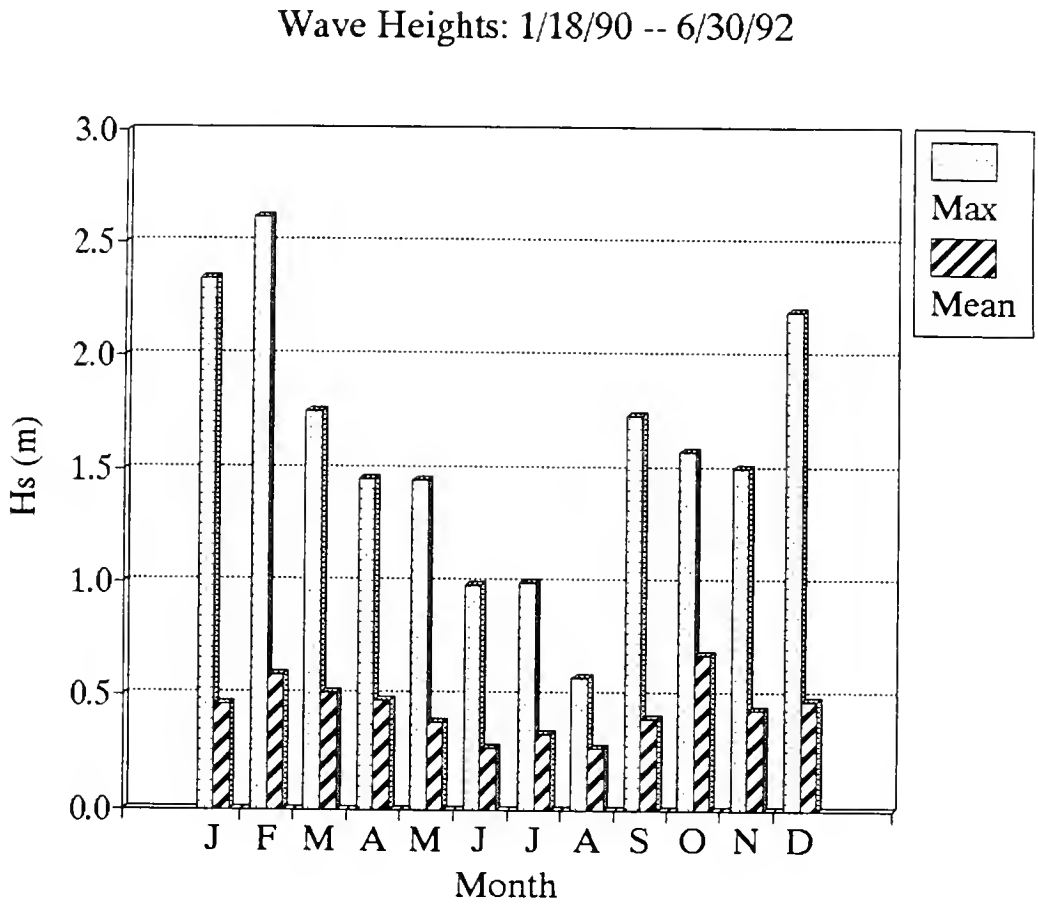

Figure 4.5: Maximum and mean monthly significant wave heights, $(H_s)_{max}$ and $\overline{H}_s$.

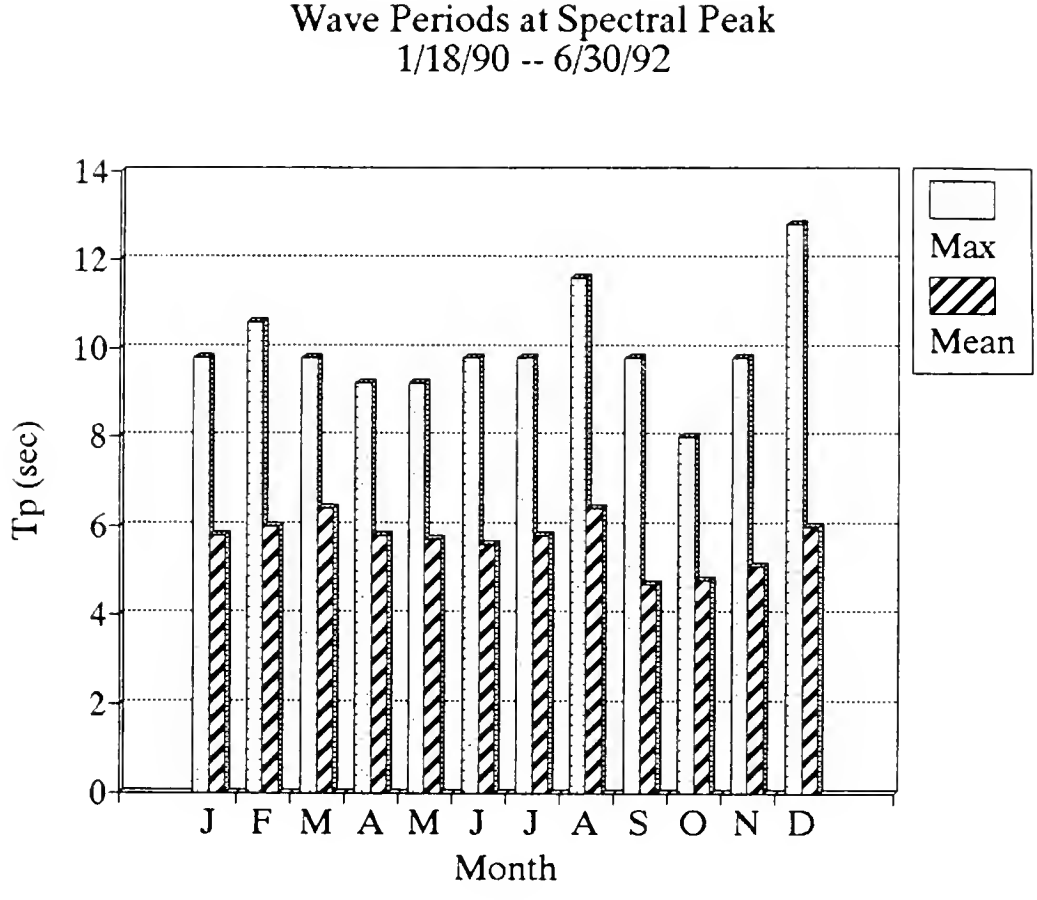

Figure 4.6: Maximum and mean monthly wave periods at spectral peak, $(T_p)_{max}$ and $\overline{T}_p$.

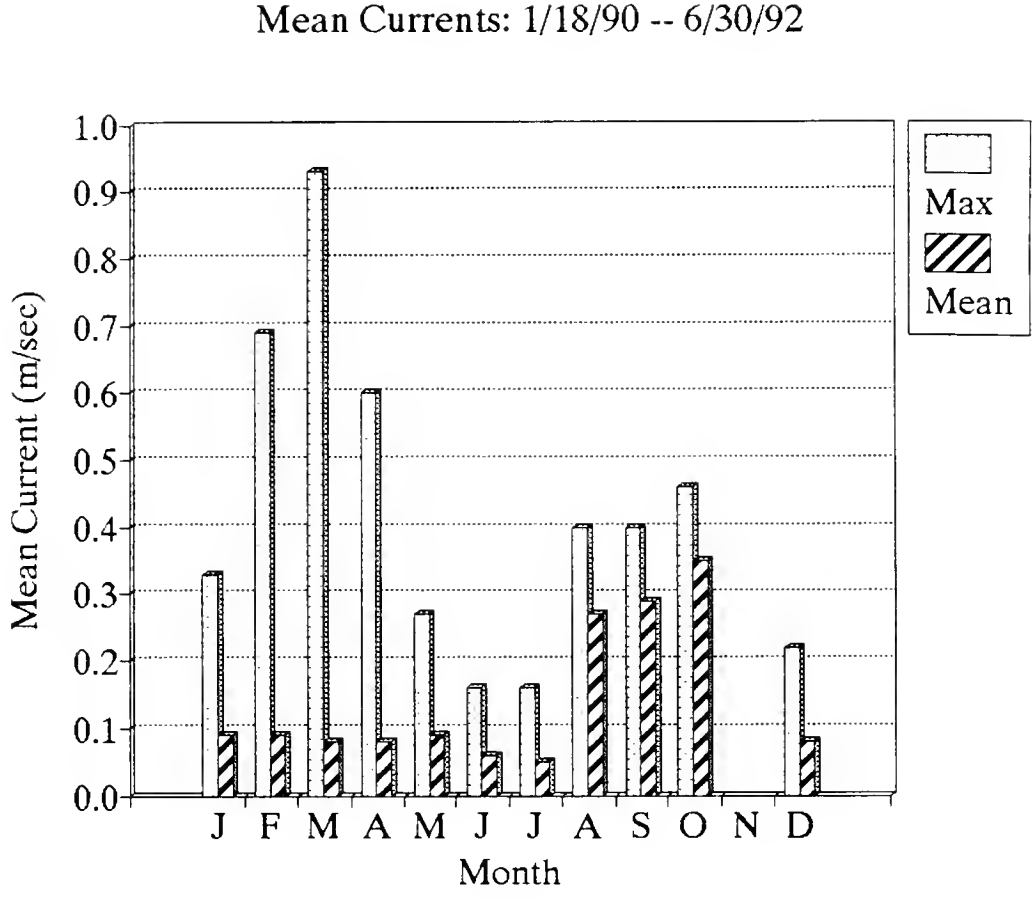

Figure 4.7: Maximum and mean monthly mean currents, $(U_c)_{max}$ and $\overline{U}_c$. Calibration suspect for August, September, and October data.

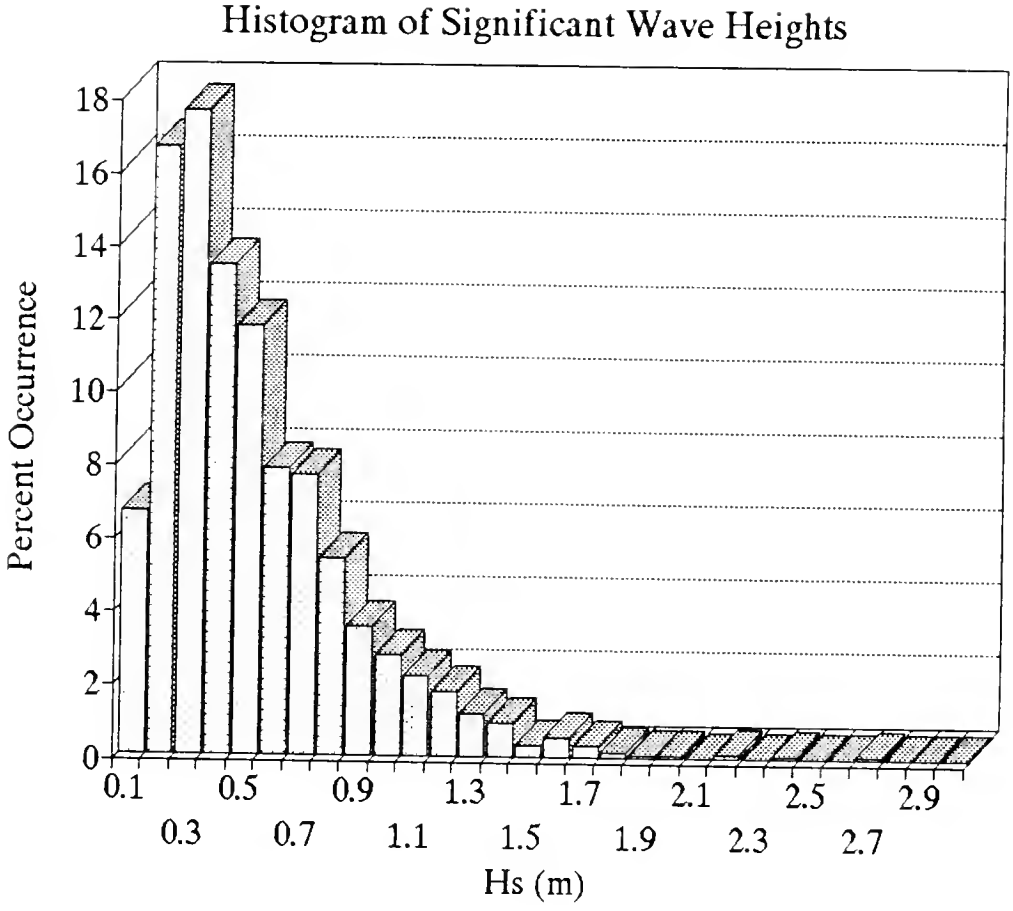

Figure 4.8: Histogram of significant wave heights measured in the field.

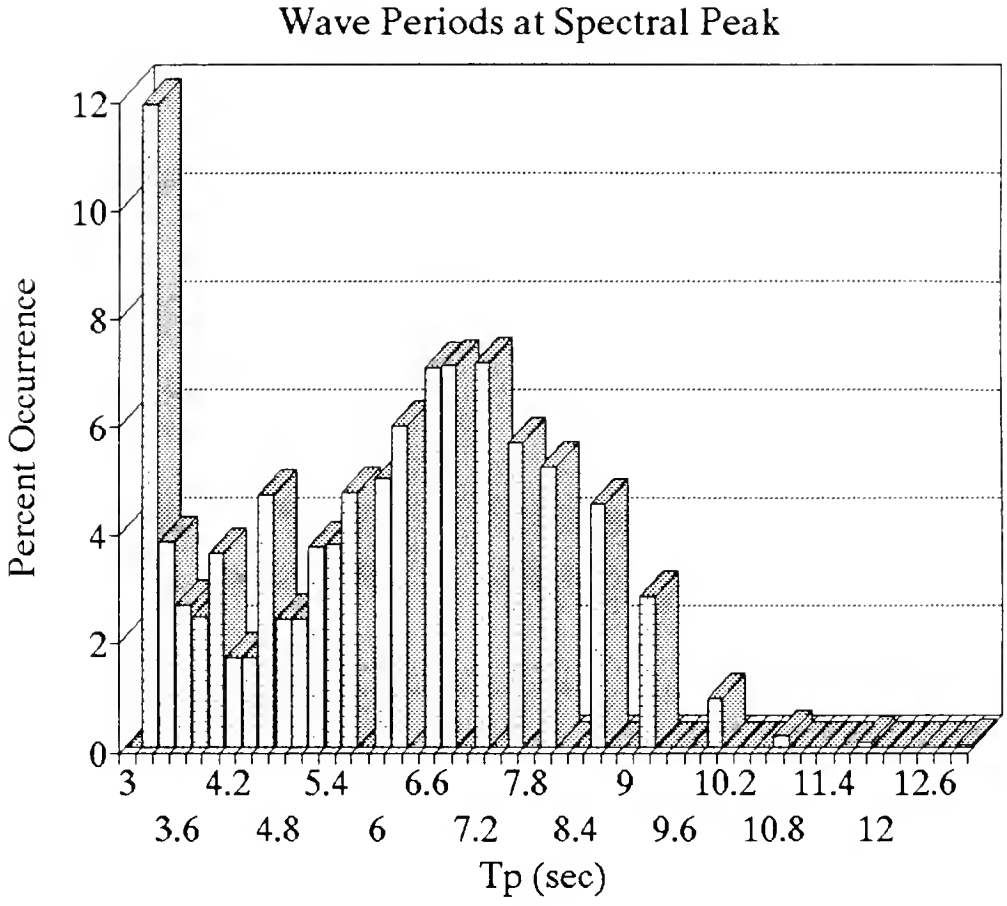

Figure 4.9: Histogram of wave periods corresponding to spectral peak measured in the field.

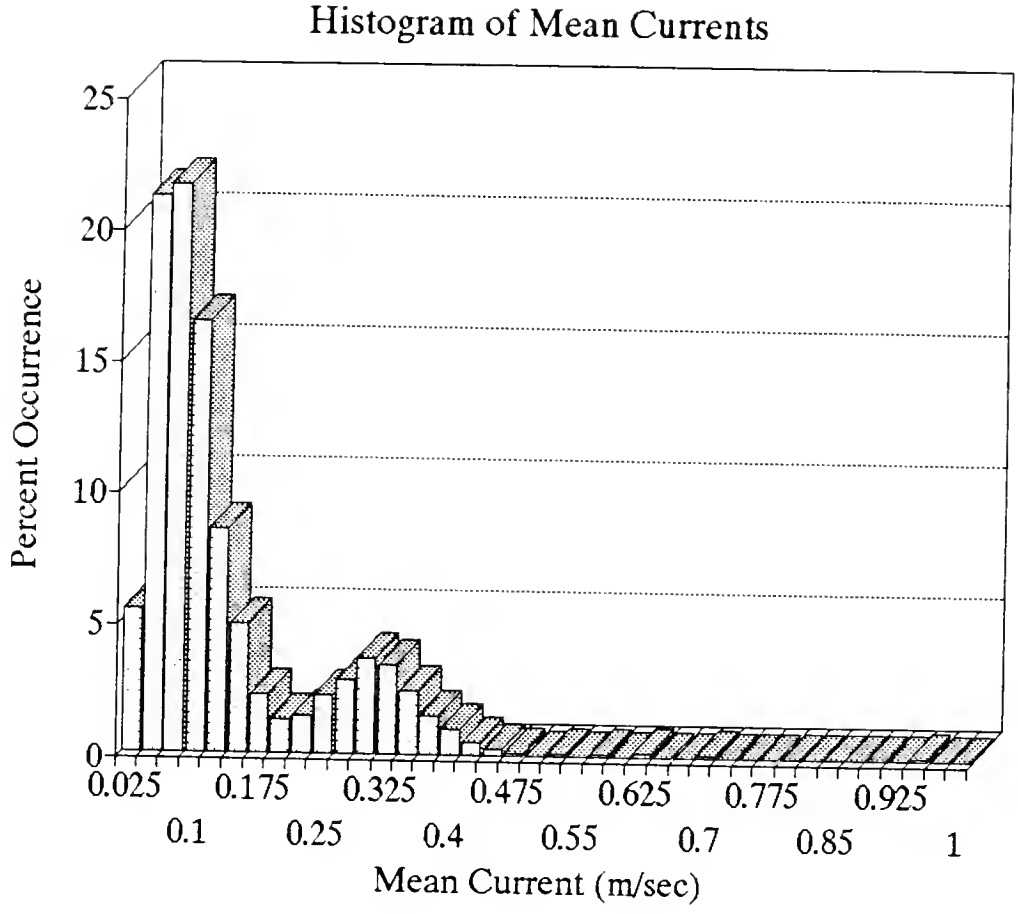

Figure 4.10: Histogram of mean currents measured in the field.

Figures 4.8, 4.9, and 4.10 present histograms of the significant wave heights, wave periods at the spectral peak, and mean currents, respectively. Previous researchers have addressed the long-term distribution of significant wave heights (Goda [1990], Houmb [1989]), either explicitly or implicitly corresponding to deep-water conditions. Shallow-water waves are less linear and may not follow the same distribution function. The Shore Protection Manual (U.S. Army Corps of Engineers [1984]) presents a modified exponential distribution function for significant wave height, H_s:

$$F(H_s > \hat{H}_s) = \exp\left[-\frac{1.61\hat{H}_s - 0.61\overline{H}_s}{\overline{H}_s}\right] \tag{4.3}$$

where $\overline{H}_s \approx 2.63 H_{s_{min}}$ so that $F(H_s > H_{s_{min}}) = 1$. $\overline{H}_s$ and $H_{s_{min}}$ are the mean and minimum significant wave heights, respectively. Equation (4.3) has been compared to nearshore wave measurements made in water depths of three to thirty meters and was concluded to give a reliable wave height distribution function for as little as one year of data containing six observations per day (Thompson and Harris [1972]). The results from this study are plotted and compared to Equation (4.3) in Figure 4.11. Agreement is good except for the largest wave heights, where the effects of the limited record length become apparent.

Prediction of the extreme wave climate at the site is not as important to the purposes of this study as is knowledge of the conditions that have actually been experienced. Estimation of extreme conditions will be important when attempting to predict future changes.

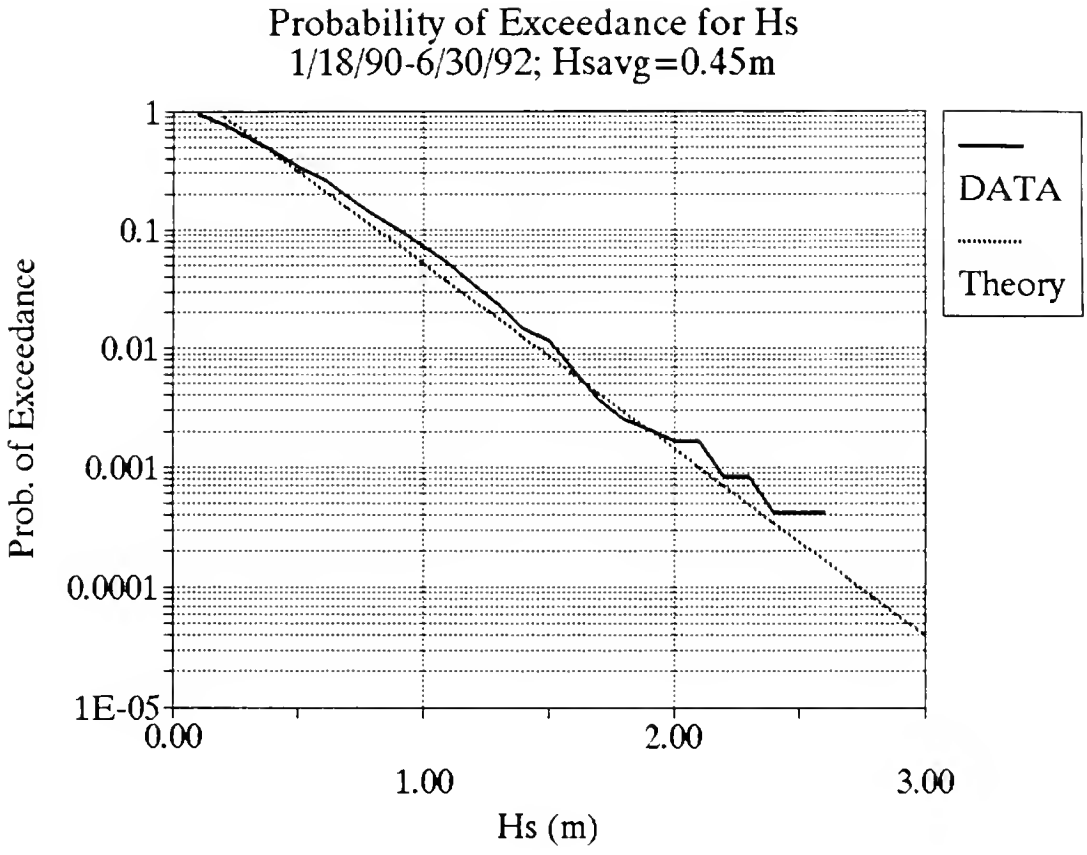

Figure 4.11: Measured and predicted percent exceedance curves for significant wave height. Measurements from Perdido Key, 1/90-6/92; theory due to Thompson and Harris [1972].

The histogram of wave periods at the spectral peak is clearly influenced by the chosen cutoff frequency. The cutoff frequency of 0.33 Hz ($T_p = 3.03$ sec) corresponds to the wave period having the highest frequency of occurrence. This is due to the large number of records where the wave energy is very small. As explained earlier, very small waves will generally result in the computation of a peak frequency that matches the cutoff frequency. The measured joint distribution of significant wave height and peak period shown in Figure 4.12 supports this claim.

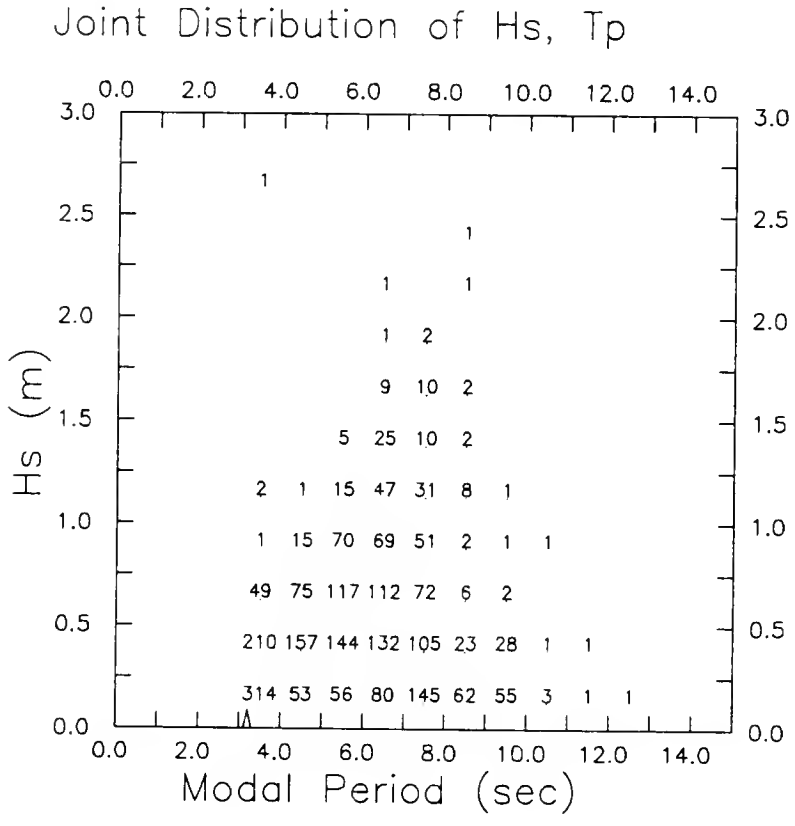

Figure 4.12: Measured joint distribution of significant wave height and period corresponding to spectral peak. Based on 2389 observations for 1/18/90–6/30/92.

The distribution of the mean currents appears somewhat anomalous, but the secondary maximum in the vicinity of 0.3 m/s is a result of the incorrectly calibrated current meter that was in place during the summer of 1990. If not for this problem, the shape of the distribution would resemble that for the wave heights.

Figures 4.13 and 4.14 illustrate the directional distributions of the waves at the spectral peak and the mean currents. The results agree with published references (see Work et al. [1991c]) and field observations in indicating that the waves and mean currents are dominantly directed toward the compass quadrant lying between West and North. This suggests that the net longshore transport of sediment at the site will be directed westward. A subsequent section will be devoted to proof of this supposition.

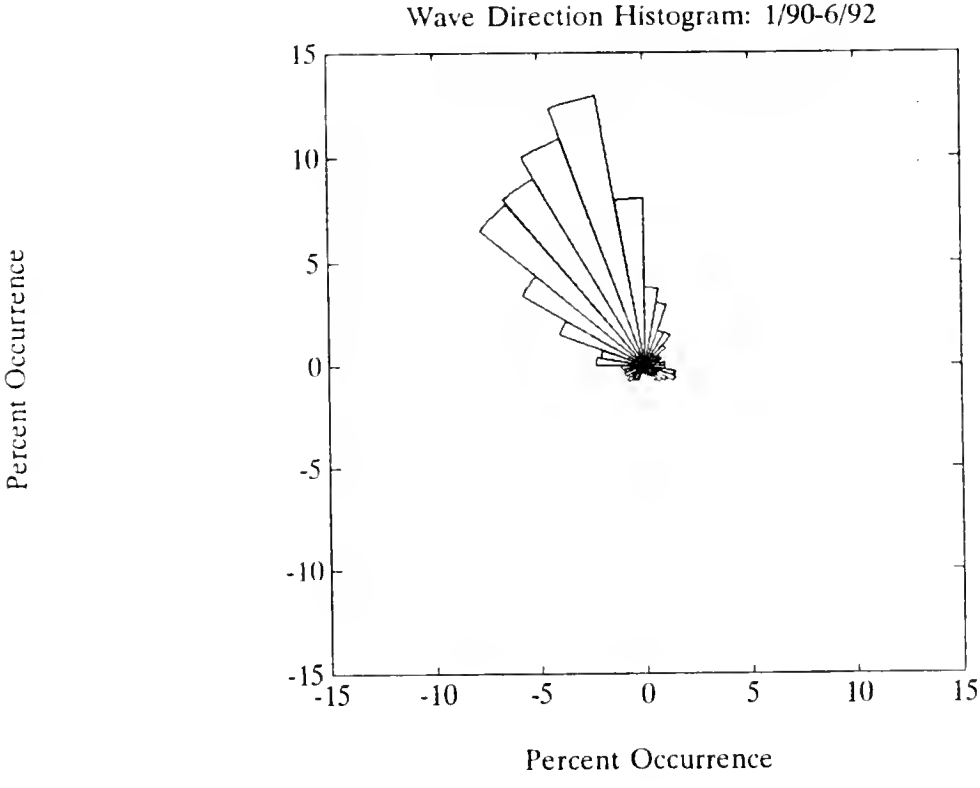

Figure 4.13: Directional distribution of waves at the spectral peak, January, 1990–June, 1992. Top of plot corresponds to North. Each bin is ten degrees in width.

Some additional sources of wave data for the Perdido Key/Pensacola area are available. The quality and utility of the data vary widely, from offshore visual observations to nearshore, in situ pressure measurements.

Hindcast wave heights, directions, and periods for several offshore stations are available through the Wave Information Study (WIS) sponsored by the Coastal Engineering Research Center of the U.S. Army Corps of Engineers (Hubertz and Brooks [1989]). Wave parameters were reported for each three–hour interval during the years 1956–1975. A separate study addresses tropical storm and hurricane conditions (Abel et al. [1989]).

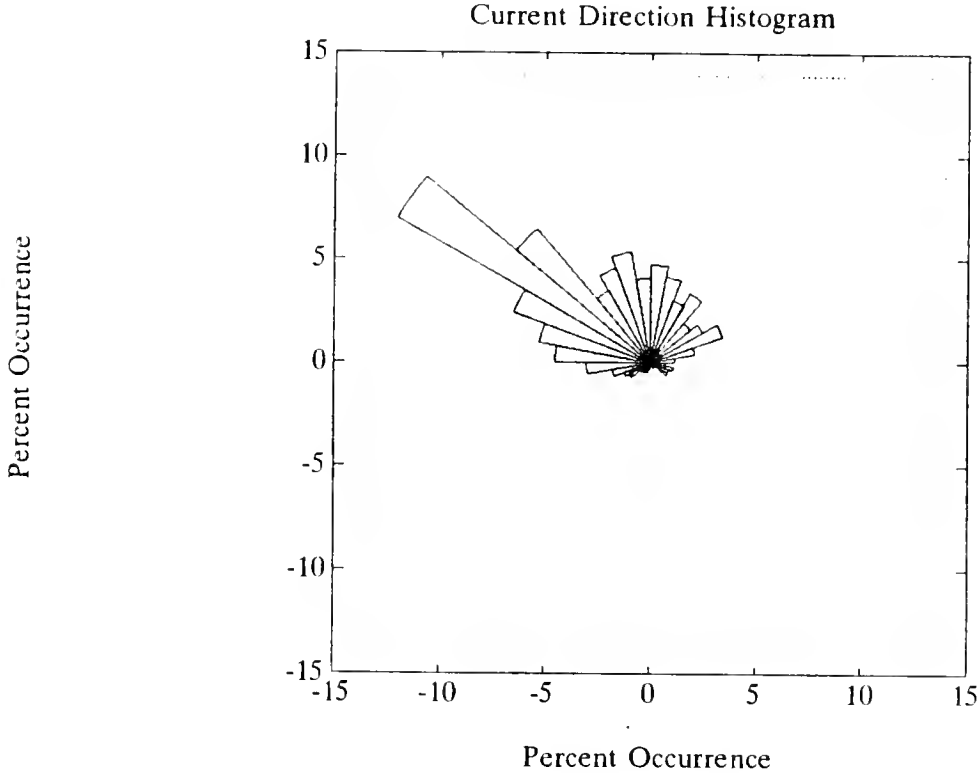

Figure 4.14: Directional distribution of mean currents, January, 1990–June, 1992. Top of plot corresponds to North. Each bin is ten degrees in width.

Table 4.4: Summary of available wave data for Perdido Key area. Data collection for this study is ongoing.

Data Source	Location	Technique	Period of Record	H_s, m		Period, sec	
				Max.	Avg.	Max	Avg.
USNWSC (1975)	Area 26 (Pensacola)	Visual	1949–1971	8–10	1.1	>13	
Balsillie (1975)	Ft. Pickens State Park	Visual	9/69–8/70		0.66 (H_b)		5.78
Hubertz/Brooks (1989)	Station 29 (Pensacola)	Hindcast	1956–1975	3.7	1.0	9.6–10.5	5.2
This study	Perdido Key	In situ	1/90–6/92	2.6	0.45	12.8	5.7

Visual observations from ships are available through a program coordinated by the U.S. Naval Weather Service Command (USNWC [1975]). The Summary of Synoptic Meteorological Observations (SSMO) data provide visual estimates of wave height, direction, and period representative of regional conditions. Nearshore, visual observations were reported by Balsillie [1975], for several sites on Santa Rosa Island, east of Perdido Key. Wave heights, directions, periods, and the speeds and directions of longshore currents were recorded 20 to 30 times per month for a total of eight months in 1969 and 1970.

The only known wave data for the Perdido Key area that were measured in situ, prior to this study, were collected by Psuty [1987]. Nearshore pressure and velocity records were collected at several nearshore sites along Perdido Key for a total of five days, making the overall record length too short for application to this study. Statistics of the wave data sources are summarized in Table 4.4.

4.2 Sediment Transport Processes: Observations Based on Survey Data

It is generally convenient to divide sediment transport processes, somewhat arbitrarily, into longshore and cross-shore components. The relative importance of both modes of transport will often vary both temporally and spatially when some form of shoreline perturbation is produced. This will be shown to be the case for the Perdido Key beach nourishment project, where both longshore and cross-shore sed-

iment transport gradients are responsible for the changes observed to date, with the cross–shore processes exerting the most influence for the early stages of the evolution.

Although it was stated earlier that the study area is essentially undeveloped, this does not imply that it has not been affected by human activities. Dredging of Pensacola Pass has taken place for over 100 years (Dean [1988]); the resulting channel serves as a partial barrier to longshore sediment transport, serving more as a "sink" than a "bridge" for the sediment. The reduced sediment supply to the eastern end of Perdido Key has resulted in a positive longshore gradient of longshore sediment transport and a corresponding erosional trend. One goal of the beach nourishment project was to offset the erosion that is the by–product of the deepened navigation channel. A smaller beach nourishment project (1.86 million m^3) was undertaken in 1985 (Psuty [1987]) for the same reason. The history of the site is discussed in more detail in Work et al. [1991c]. Some results from the earlier (1985) nourishment project will be discussed, but the primary focus here will be on changes occurring since completion of the latest beach nourishment project.

The concept of an "equilibrium" configuration for a beach is often useful, whether or not it is ever actually reached. Cross–shore and longshore equilibria may be considered separately, in keeping with the arbitrary division of the sediment transport into orthogonal components. Following this convention and the coordinate system of Figure 4.15, the equation expressing continuity of sediment is given as follows:

$$\frac{\partial h}{\partial t} = \nabla \cdot \vec{q} = \frac{\partial q_x}{\partial x} + \frac{\partial q_y}{\partial y} \tag{4.4}$$

where $q_x = q_x(x, y, t)$ is the volumetric longshore sediment transport rate, $q_y = q_y(x, y, t)$ the cross–shore component, and $h(x, y, t)$ the depth. Note that positive sediment transport gradients imply local erosion. At equilibrium, gradients in both directions vanish. Conversely, large perturbations away from the equilibrium con-

dition, in either direction, would be expected to induce large sediment transport gradients.

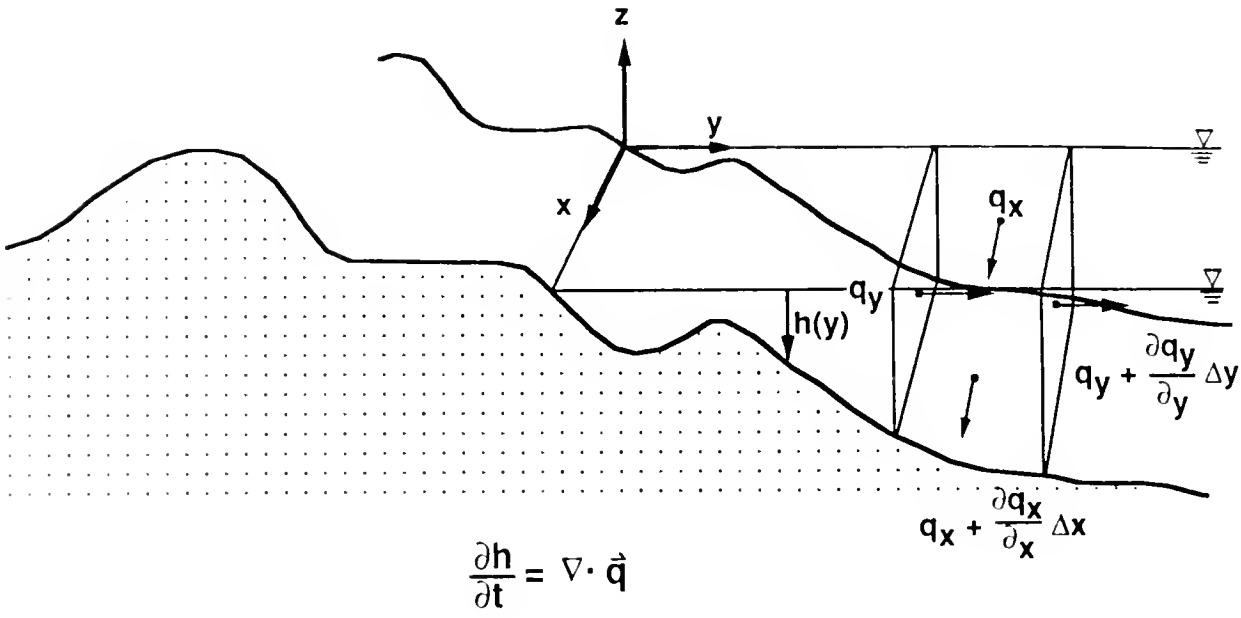

Figure 4.15: Coordinate system for sediment transport problem.

If the same beach profile is surveyed at two different points in time, then a value for the left–hand side of Equation (4.4), averaged in time over the survey interval, may be determined for any point along the profile. If Equation (4.4) is integrated between two points at the extreme onshore and offshore limits of the active profile, such that there are no profile changes at either of the integration limits, then all changes in the cross–sectional area of the profile may be assumed due to longshore gradients of longshore sediment transport:

$$\frac{\partial A}{\partial t} = \int_0^{y_*} \frac{\partial h}{\partial t} dy = \int_0^{y_*} \frac{\partial q_x}{\partial x} dy = \frac{\partial Q_x}{\partial x} \tag{4.5}$$

Here $A = A(x,t)$ denotes the cross-sectional area of the profile and $Q_x(x,t)$ is the longshore sediment transport rate, integrated across the active profile. The distance to the point where the depth reaches the "depth of closure", or limiting depth for sediment motion, is denoted by y_*. Any temporal variation in $A(x,t)$ is thus indicative of a longshore gradient in longshore sediment transport, $\partial Q_x/\partial x$.

If an assumption is made regarding the cross-shore dependency of the local longshore gradient of longshore sediment transport, $\partial q_x(x,y)/\partial x$, the sediment continuity equation can be integrated with indefinite limits to determine the local cross-shore sediment transport rate:

$$q_y(y) = \int_0^y \frac{\partial h}{\partial t} dy - \int_0^y \frac{\partial q_x}{\partial x} dy \tag{4.6}$$

where a boundary condition of $q_y(0) = 0$ has been invoked. Very little information exists regarding the y-dependence of the longshore gradient of longshore sediment transport, $\partial q_x(x,y)/\partial x$. The most convenient assumption is that this term does not contribute to the mass balance, i.e. $\partial q_x(x,y)/\partial x$=0 for all y. If the cross-shore mean value of $\partial q_x/\partial x$ is non-zero, then $\partial Q_x/\partial x$ will also be non-zero, and a net increase or decrease in cross-sectional area will be evident. Additional factors could lead to apparent changes in the cross-sectional area of the profiles, such as sediment compaction, survey error, and wind-blown sediment transport. These contributions will be discussed in a subsequent section.

Figures 4.16 and 4.17 present examples of the surveyed beach profiles at Perdido Key before and after the nourishment project. Most of the pre-nourishment profiles had a similar shape, with a pronounced breakpoint bar and very mild slopes offshore of the –5 m contour. The profile immediately post-nourishment is drastically different and by the previous argument, assuming that the pre-nourishment condition is

more indicative of equilibrium cross-shore conditions, strong cross-shore transport gradients would be expected. Profile data collected at later times indicate that there has been some slumping and a breakpoint bar is forming; the profile shape is evolving toward the pre-nourishment condition.

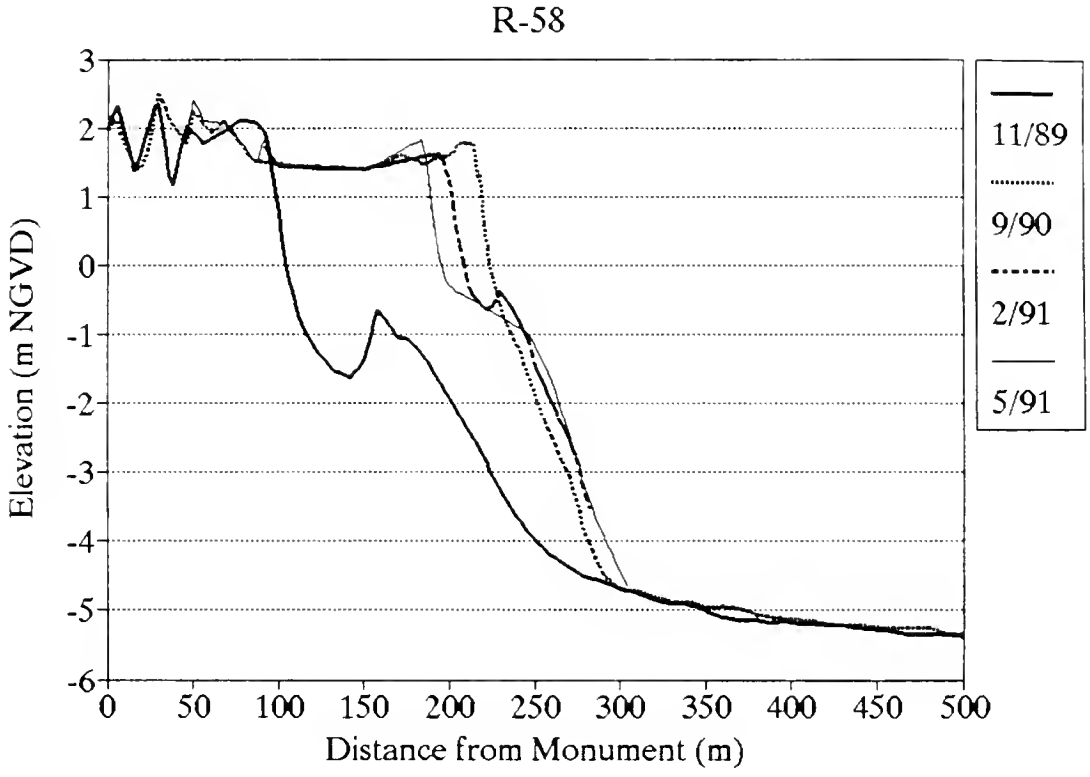

Figure 4.16: Surveyed beach profiles at R-58, November, 1989, through May, 1991.

Examination of the planform changes of the new beach provides an indication of the rates of cross-shore and longshore equilibration. Figure 4.18 illustrates the spatial extent of the longshore perturbation that the beach nourishment project represents; the cross-shore perturbation has already been illustrated. It can be seen that the most dominant early change in the planform was a rapid retreat of the waterline within the nourished area.

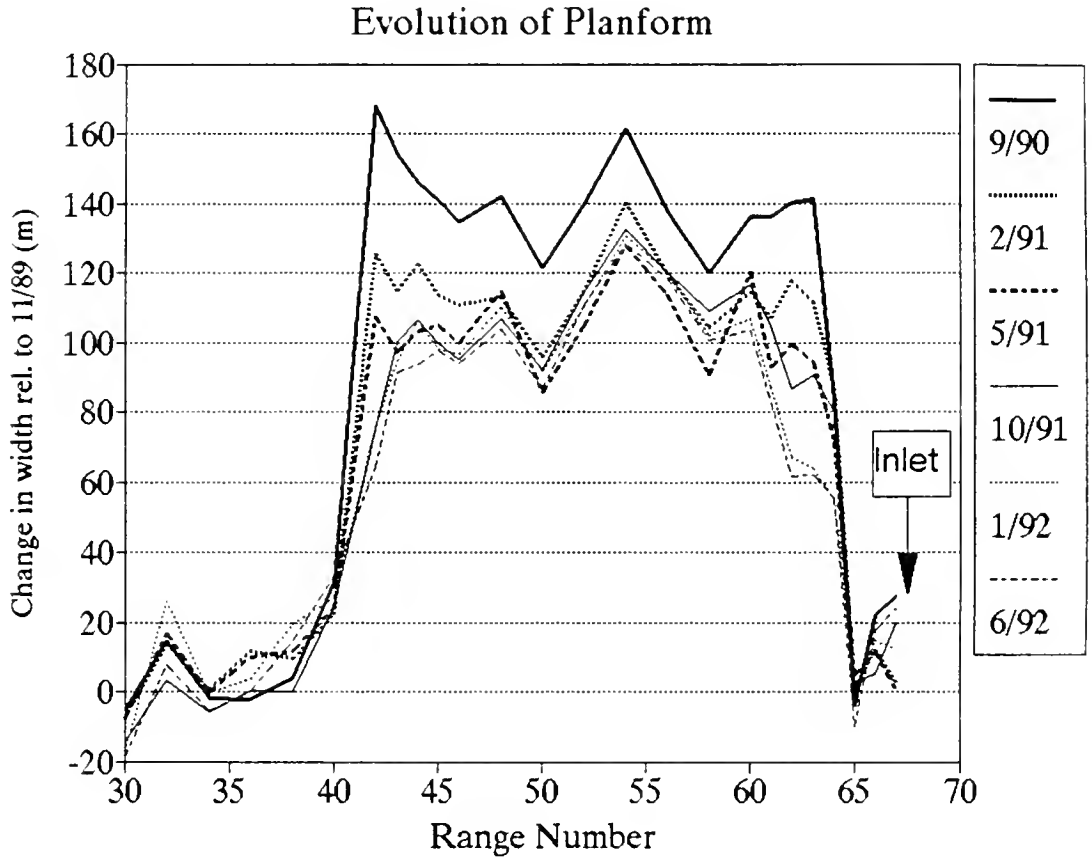

Figure 4.18: Planform changes since beach nourishment.

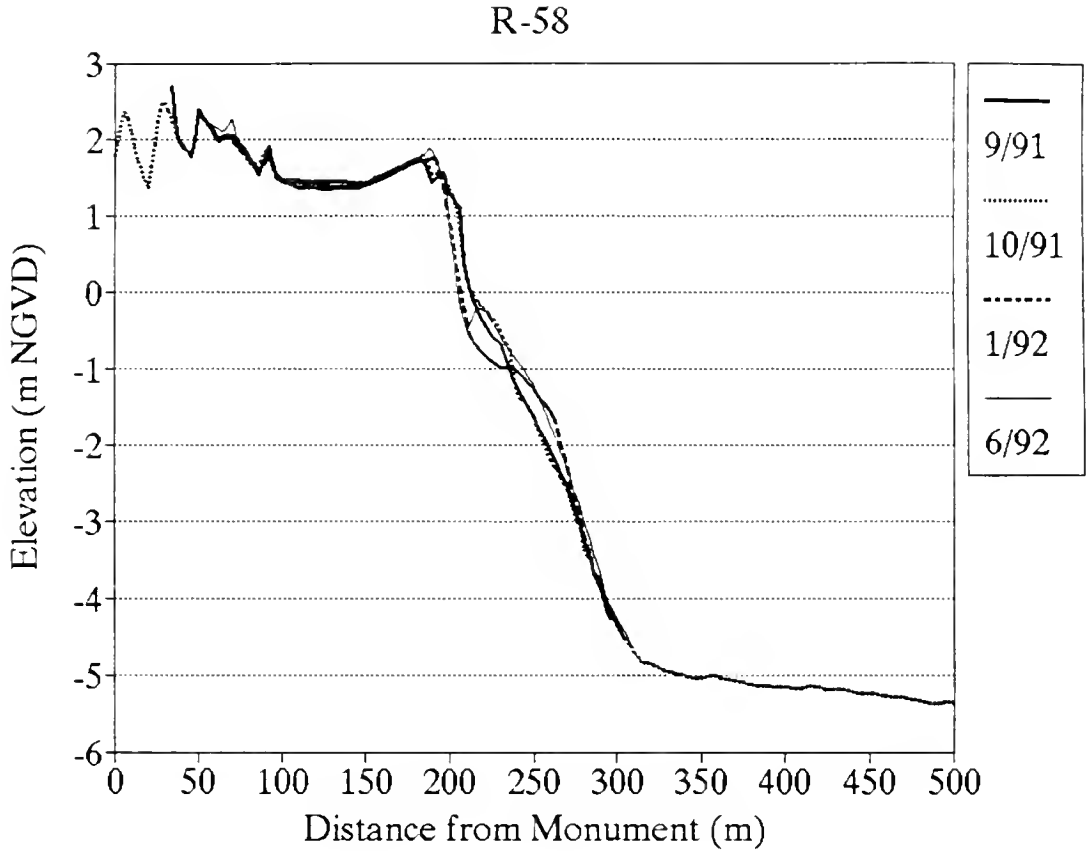

Figure 4.17: Surveyed beach profiles at R-58, September, 1991, through June, 1992.

Figure 4.19 presents a similar result for the movement of the –4 m contour. Although less pronounced, the –4 m contour has moved seaward within the project domain. This is simply another way of looking at the "unsteepening" illustrated in Figures 4.16 and 4.17: there is a net movement of sand offshore, causing erosion of the waterline and accretion of the –4 m contour.

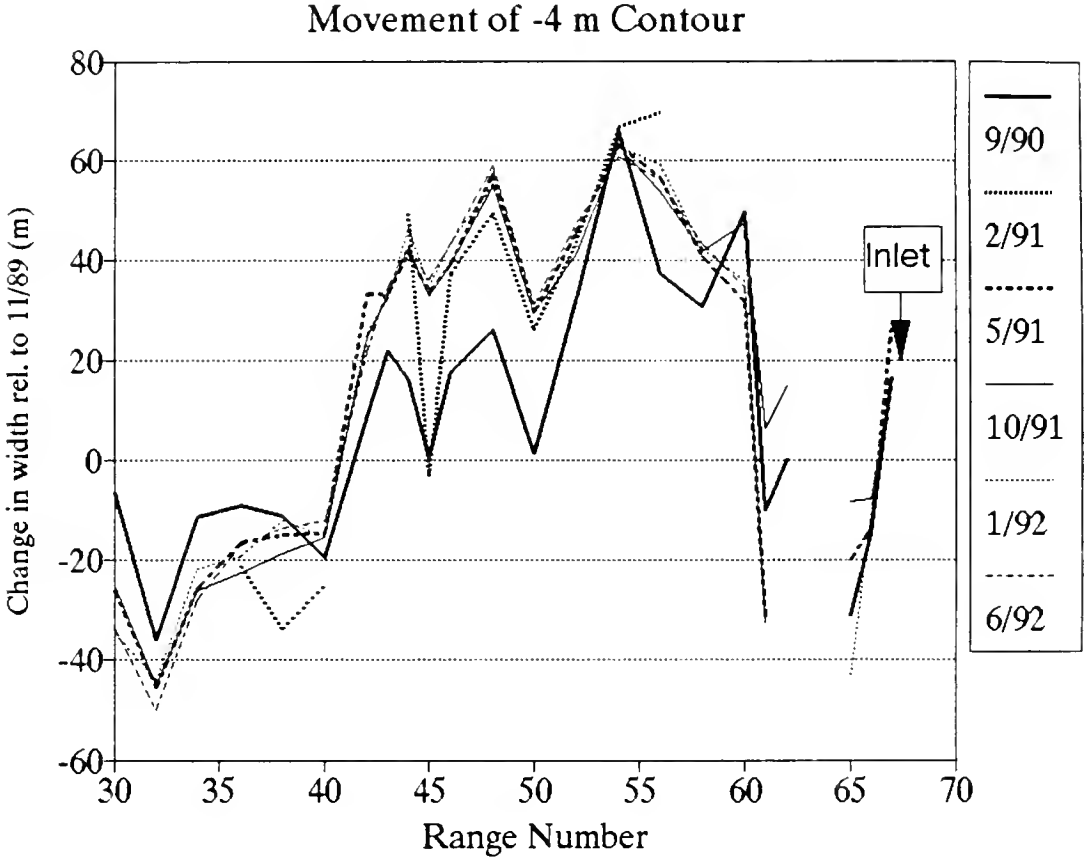

Figure 4.19: Movement of the –4 m contour since beach nourishment.

Evidence of longshore gradients of longshore sediment transport may be found in both of the previous plots. Figures 4.16 and 4.17 indicate a slight loss of sediment over time, resulting from a positive longshore gradient in the local longshore sediment transport rate. In Figure 4.18, the "shoulders" of the beachfill appear to be losing sediment, and the planform immediately downdrift (west) of the beach nourishment project is seen to be building seaward (e.g. R–40). This area is gaining sand from the nourished area. The area updrift (east) of the beachfill is affected by both Pensacola Pass and Caucus Shoal, making interpretation more difficult.

Figure 4.20 illustrates the planform changes associated with the previous Perdido Key beach nourishment project, which took place in July, 1985. The first curve (10/84) is thus well before nourishment, and the next is both post–nourishment and post–Hurricane Elena. The nourished area spanned from R–61 to R–64, so it was roughly one–eighth the length, yet nearly half the volume, of the most recent project (Dean [1988]). Beach profile and wave data are not available for the earlier project, so it is not possible to accurately estimate volumetric changes, sediment transport rates, or transport gradients.

The changes illustrated in Figure 4.20 bear some resemblance to those shown in Figure 4.18, as should be expected. Some accretion is evident west of the fill (to the left in both figures), and the most marked changes are within the nourished area. It is speculated that much of the change seen in the nourished area of the 1985 project corresponds to cross–shore transport that does not imply a loss of sediment within the nourished zone.

Beach nourishment projects are often studied with the assistance of so–called "one–line" models, to be discussed in more detail in the next chapter. Such models assume that all contours remain parallel to one another (but not necessarily straight). This approach would therefore not be totally appropriate for application to the present case, because the dominant behavior, the "unsteepening" of the beach profile, would

be neglected. It is for this reason that the cross-shore behavior is also of interest. As the cross-shore sediment transport molds the profile and reduces the degree of disequilibrium, the cross-shore and longshore sediment transport gradients should at some point assume equal importance. Over a longer time scale, the beach should return to the pre-nourishment scenario, where the longshore gradients of longshore sediment transport are dominant.

Figure 4.21 was generated by applying Equation (4.5) to all the profiles surveyed by boat. For the first year (November, 1989 — September, 1990), only the results outside of the nourished zone are shown, since changes elsewhere for this time period were a result of dredging, not natural processes. The results confirm expectations: there are strong positive gradients of longshore sediment transport on the "shoulders" of the beachfill, implying rapid erosion, with corresponding negative gradients just outside the nourished area. The anomalous peak at R-54 is interpreted as being due to the "bump" in the post-nourishment planform; this feature would be expected to erode faster.

Similar results may be generated for other time periods, using the intermediate wading profile data. Since some of the wading profiles do not reach the offshore limit of the active profile, changes in cross-sectional area cannot be computed accurately. Emphasis will therefore be placed on the surveys that include data collected by boat.

For investigation of the cross-shore sediment transport mechanisms in the field, several profiles were chosen where longshore gradients of longshore sediment transport appeared small. These profiles were then superimposed and "pinned" at the position of the September, 1990, waterline. Depths were averaged to determine a representative "average" profile. Within the nourishment zone, profiles at R-45, R-46, R-48, R-50, R-52, R-56, and R-58 were selected, avoiding the shoulders of the beachfill and the anomaly at R-54. The results are shown in Figure 4.22. The slight elevation of the offshore sections of the September, 1990, average profile relative to the other

two surveys is due to the previously discussed noise in the 1990 survey. This noise was ignored when adjusting the profile data to minimize the average error between offshore sections of the profiles.

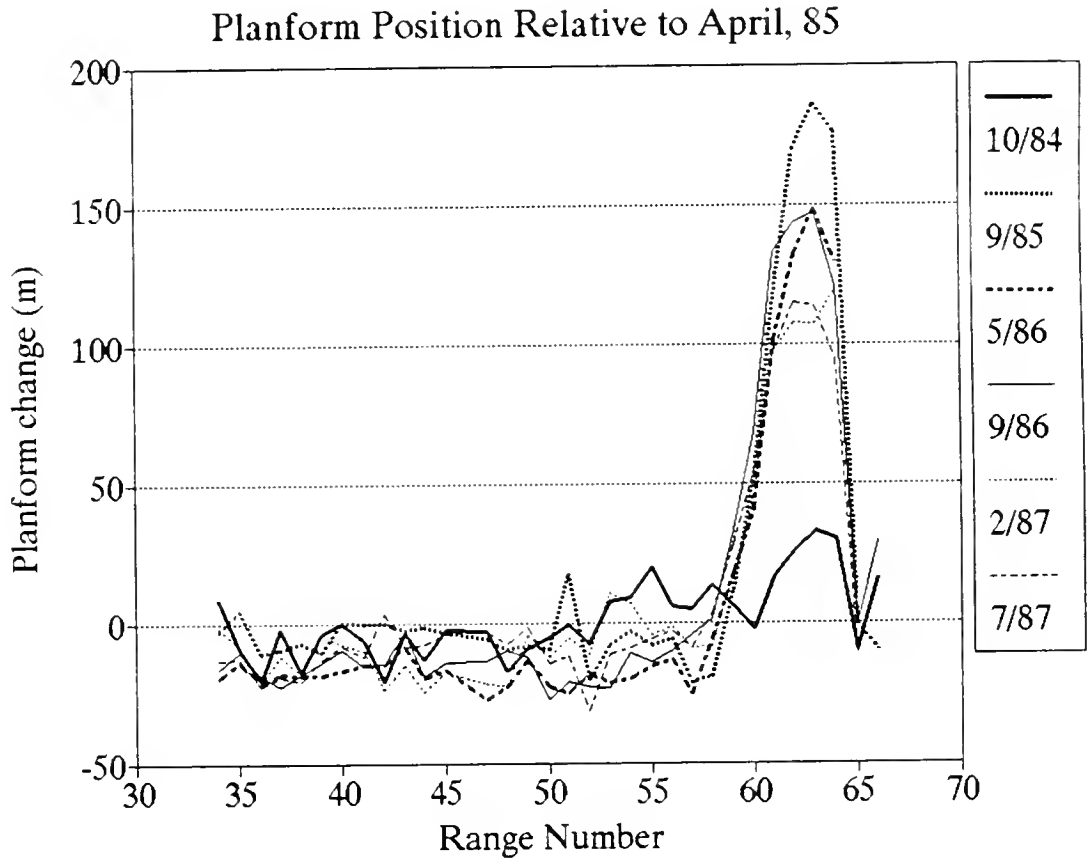

Figure 4.20: Planform changes associated with 1985 nourishment project. Data collected by Rutgers University and reported in Dean [1988].

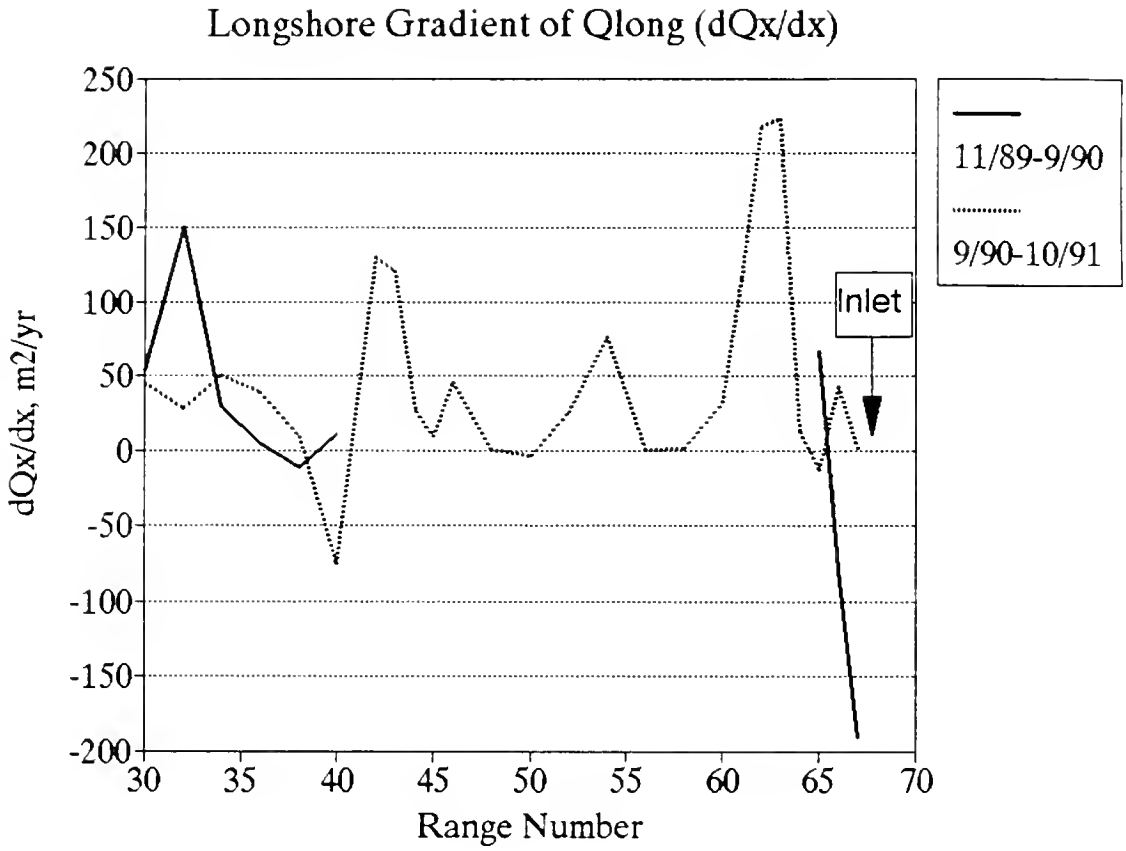

Figure 4.21: Longshore gradient of longshore sediment transport rate, based on measured profile changes. Positive gradients indicate erosion. Pensacola Pass is adjacent to R-67; the western end of the survey area is to the left.

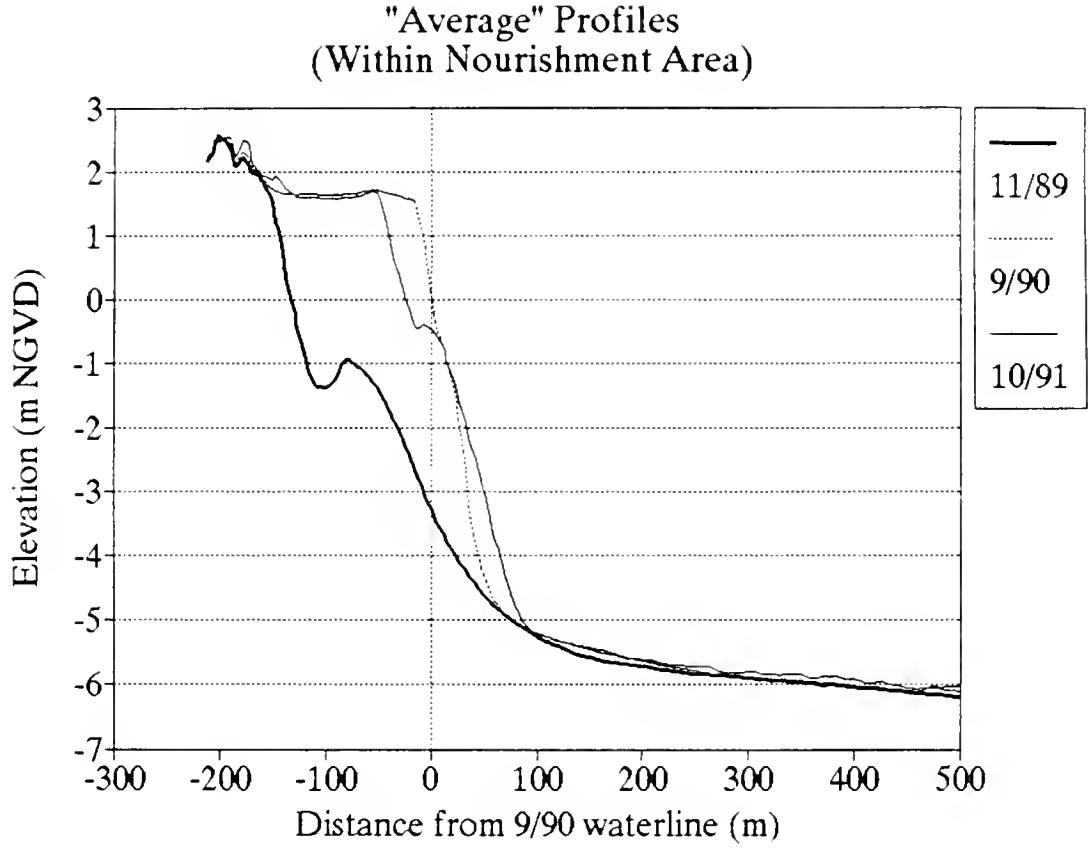

Figure 4.22: Average of profiles at ranges 45, 46, 48, 50, 52, 56, and 58.

Average profiles for the region west of the nourished beach are shown in Figure 4.23. For this analysis, profiles at ranges 30, 32, 34, 36, and 38 have been included.

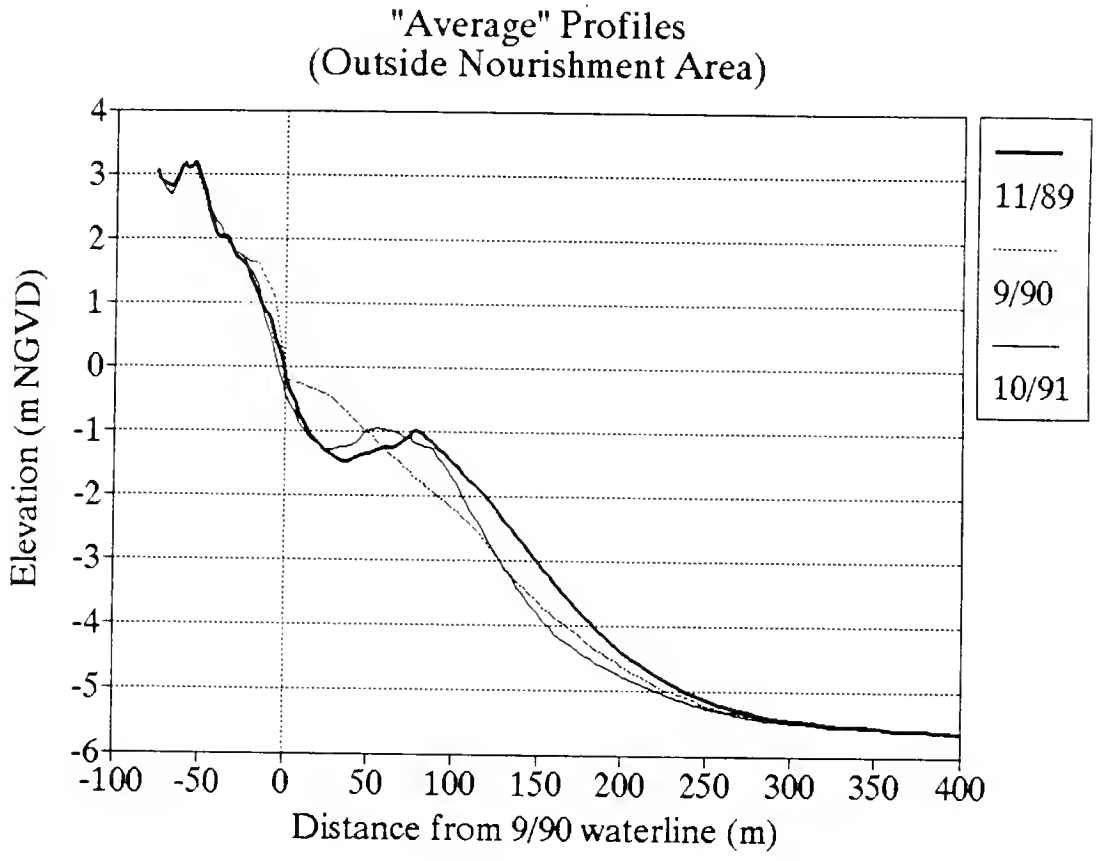

Figure 4.23: Average of profiles at ranges 30, 32, 34, 36, and 38.

Equation (4.6) was applied to the average profiles from the three annual surveys to determine the cross-shore sediment transport rate, assuming the longshore contribution, $\partial q_x/\partial x$, to be zero. The results are shown in Figures 4.24 and 4.25. Upon inspection of the figures, it is seen that the neglect of the longshore contribution was not fully justified; each plot of $q_y(y)$ has an upward trend, indicating some loss of sediment as a result of longshore gradients of longshore sediment transport.

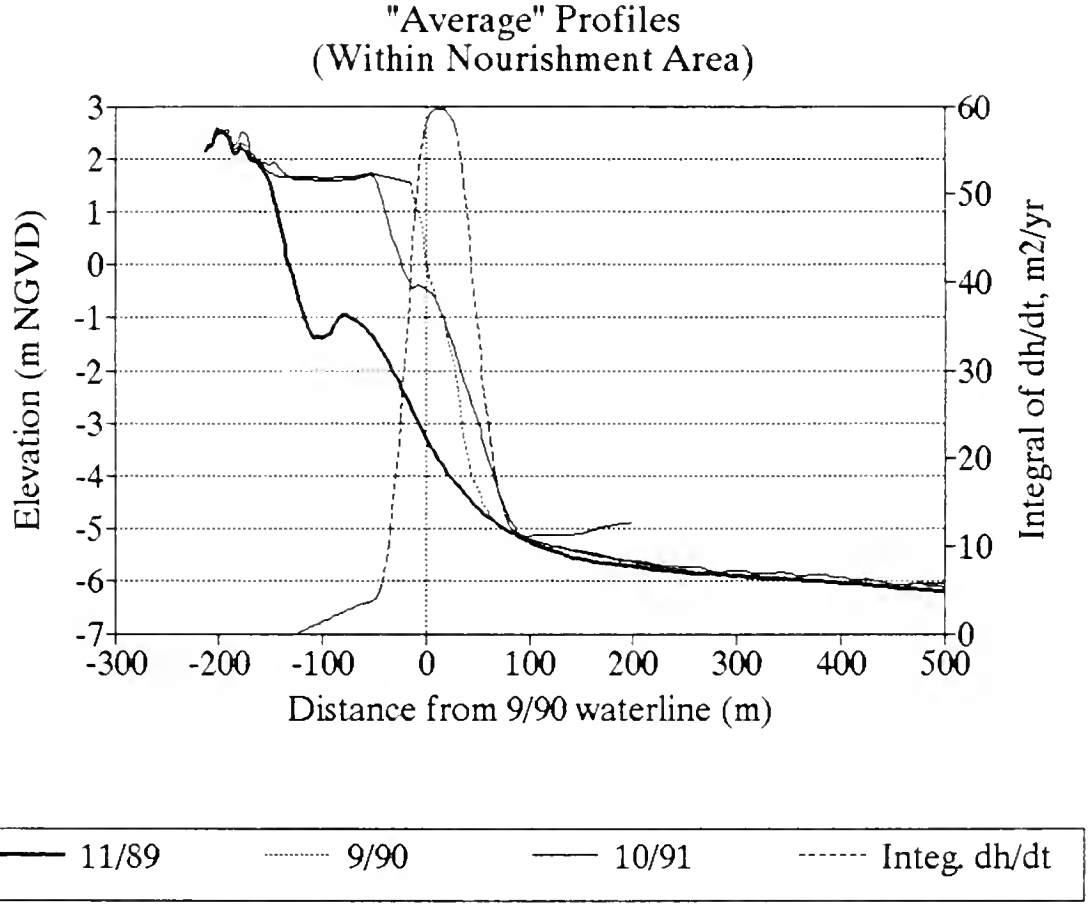

Figure 4.24: Cross-shore sediment transport rates computed based on average profile changes within nourishment area for the 1990 and 1991 annual surveys. Offshore transport is positive, longshore gradients of longshore sediment transport assumed negligible.

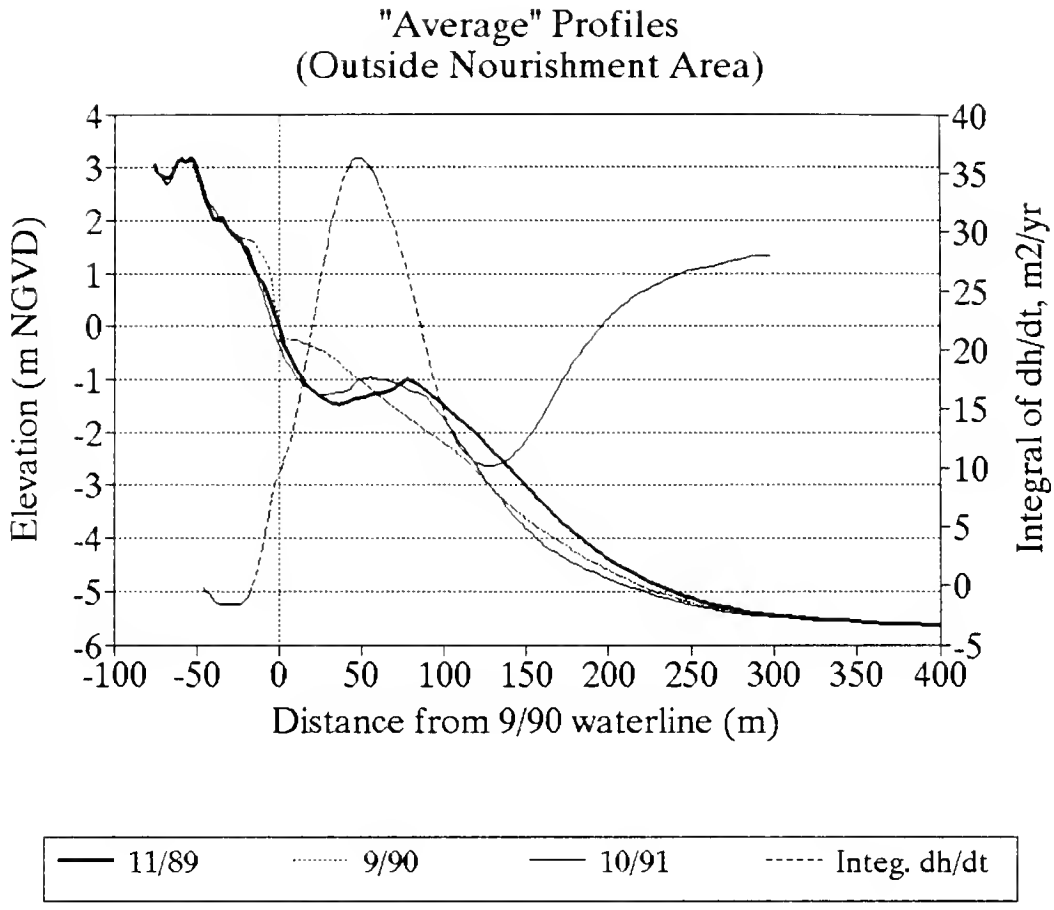

Figure 4.25: Cross–shore sediment transport rates computed based on average profile changes west of nourishment area for the 1990 and 1991 annual surveys. Effect of longshore gradients neglected.

The loss of sediment within the nourished zone is expected as the project evolves. The loss west of the nourished area may be considered "remnant", or "background" erosion, as this region has not yet benefitted from the beach nourishment project.

Several important points should be made regarding Figures 4.24 and 4.25. First is the overall magnitude of the cross-shore transport rate for each case. The transport rate within the nourished zone is much larger (roughly a factor of two) than that to the west. Secondly, the relative magnitude of the changes attributable to cross-shore transport gradients vs. those resulting from longshore gradients of longshore sediment transport is much higher within the nourished zone. This agrees with the earlier argument that the transport rate should be proportional to the degree of disequilibrium, and that the cross-shore rate of equilibration should exceed that of the longshore direction. A third point regards the differences in the shapes of the distributions. The transport within the nourished area is clearly directed offshore, while the distribution for the western profiles resembles the summer to winter, bar-forming shape.

Figures 4.26 and 4.27 present similar results for the intermediate survey periods. Some seasonal effects are evident, but the overall results are consistent with the results based on the three annual surveys. Within the nourished zone, offshore sediment transport dominates, with some recovery during the summer. Outside of the nourishment area, the signals correspond to a migrating bar with no dominant trend.

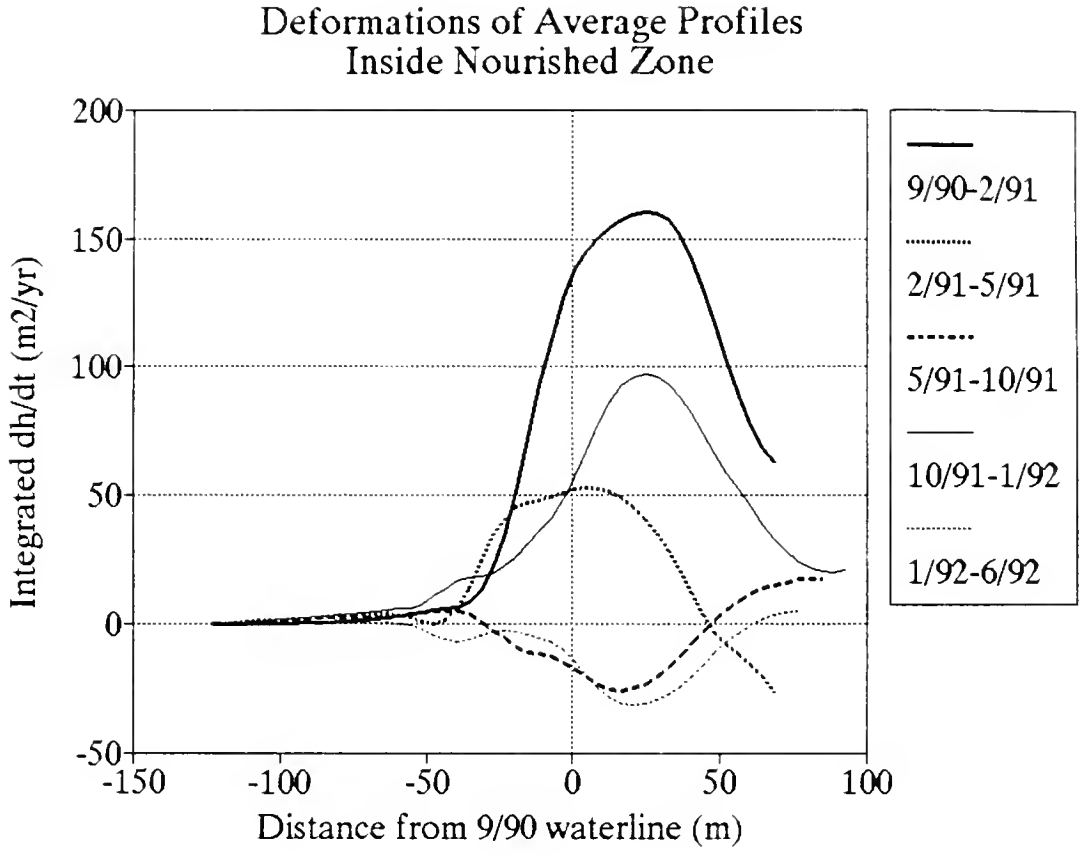

Figure 4.26: Cross-shore sediment transport rates computed based on average profile changes within nourishment area for intermediate survey periods. Effect of longshore gradients neglected.

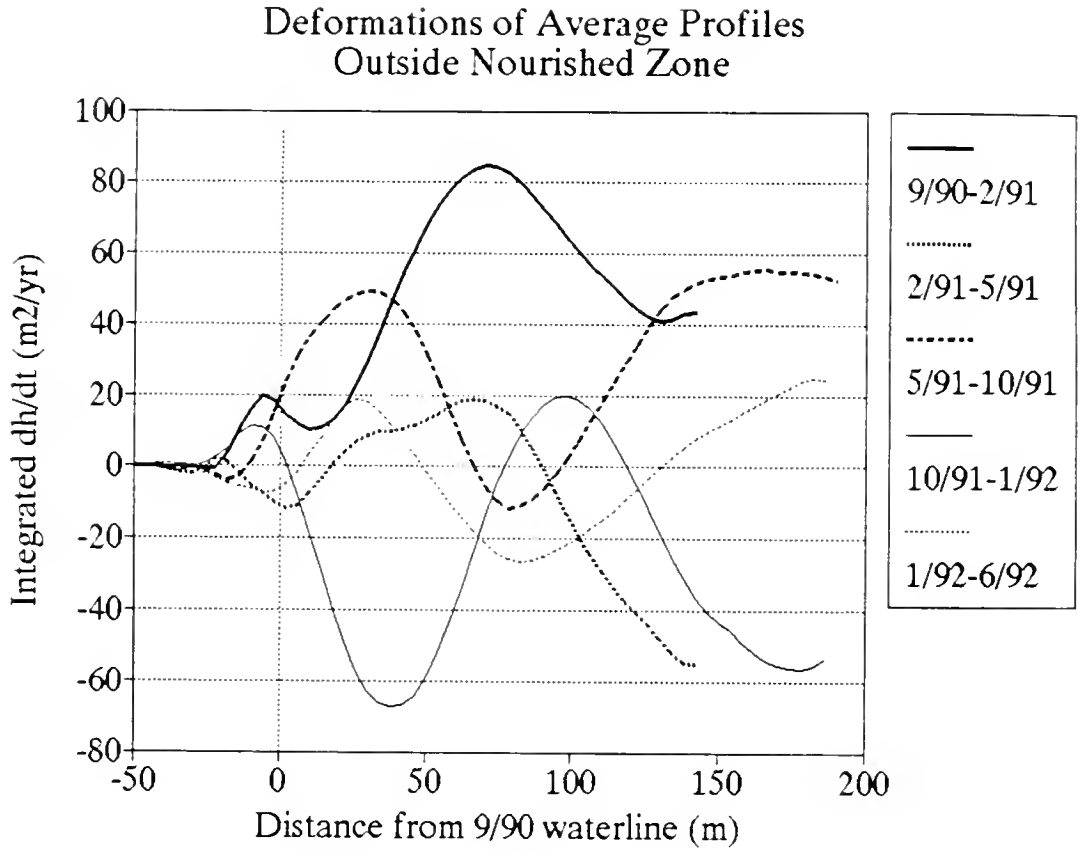

Figure 4.27: Cross–shore sediment transport rates computed based on average profile changes west of nourishment area for intermediate survey periods. Effect of longshore gradients neglected.

The results presented to this point have considered the longshore and cross-shore transport mechanisms separately. The results obtained describing the longshore gradient of longshore sediment transport, $\partial Q/\partial x$, removed the effects of the cross-shore transport by integrating across the entire active profile, and the derived cross-shore transport neglected the influence of longshore sediment transport, but longshore gradients were clearly removing sediment from the profiles. Ideally, the two transport distributions could be considered separately without any overly restrictive assumptions. Unfortunately, only one of the three terms in the sediment continuity equation (Equation (4.4)) has been directly measured.

The results shown in Figure 4.24 indicated that the cross-shore sediment transport within the nourished beach, away from the "shoulders", was the dominant process causing the observed changes. The profile deformations indicated some loss of sediment, and this was interpreted as being due to longshore gradients of longshore sediment transport. If this lost sediment could be added back to the signal, the result would be the changes due solely to the cross-shore transport. The cross-shore distribution of longshore sediment transport ($q_x(x,y)$) is not well known however; it is generally assumed to be proportional to some power of the longshore current (Bodge [1986]), but the longshore current distribution for a barred profile is also not well known. However, since the effects of the longshore transport gradients in Figure 4.24 are so small compared to the cross-shore processes, the assumed distribution for the longshore transport gradients will not be very important.

The sediment loss illustrated in Figure 4.24 was divided into three components. The first, corresponding to -123 m $< y <$-45 m, was assumed to be due to compaction of the added sediment and/or eolian (wind-blown) transport into the dunes. This is assumed to be uniform across this region, and corresponds to a vertical loss of 6.4 cm/yr.

The second region includes the entire active profile (i.e. acted upon by hydrodynamic forces). This region is taken to extend to 100 m offshore of the September, 1990, waterline. Sediment losses in this region are assumed due solely to longshore gradients of longshore sediment transport. Compaction could also be a factor here, but it is not as important to know the mechanism causing the change as it is to account for its effect. If the longshore gradient of longshore sediment transport is assumed not to vary in the cross-shore direction, then this region corresponds to $\partial q_x(x,y)/\partial x$=4.6 cm/yr. This assumption, that $\partial q_x(x,y)/\partial x$=constant, is not particularly satisfying, but, given the small magnitude, will not be particularly important.

The third region extends offshore from y = 100 m, where changes are assumed to be due to bathymetric survey error. If uniform, this corresponds to a vertical error of 1.3 cm. With the longshore contributions removed from the signal shown in Figure 4.22, the result shown in Figure 4.28 is obtained.

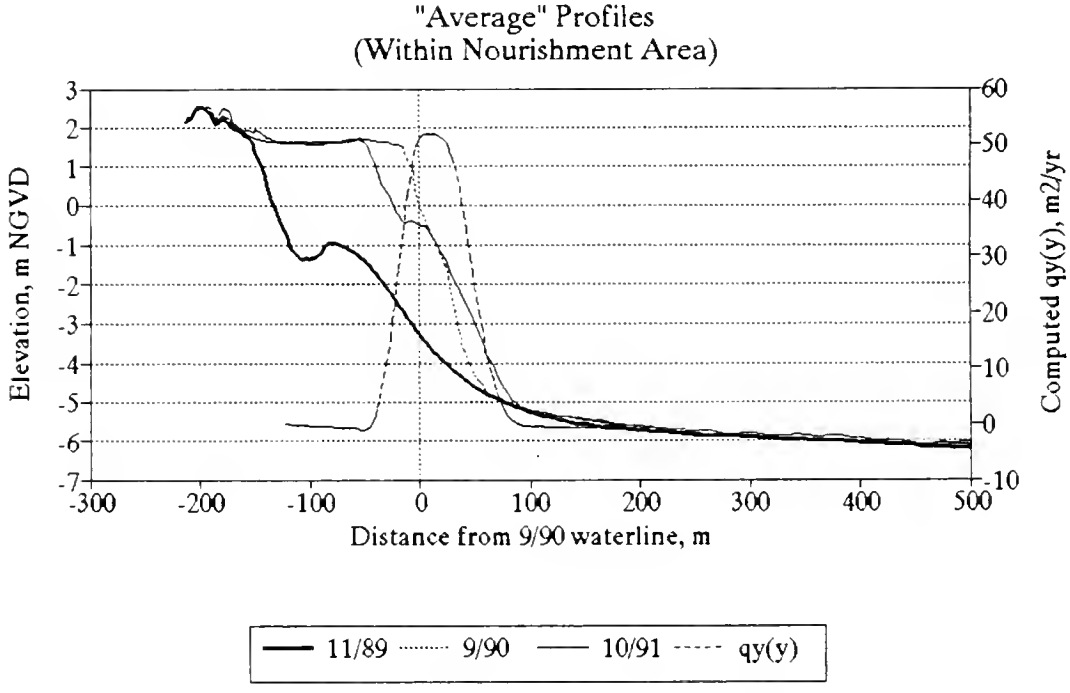

Figure 4.28: Cross-shore transport signal after removal of longshore contribution, based on field measurements and computed "average" profiles within the nourished beach.

The next step was to consider a profile where the effects of the longshore sediment transport were much more significant. The shoulders of the beachfill were shown to be the areas where the longshore gradient of longshore sediment transport was largest. Figure 4.29 shows the profile changes occurring at R–42 for the first year after placement of the fill. The computed areal changes are also shown, and for this case, the dominant change seems to be the loss of sediment due to the longshore processes. An important assumption was made at this stage: that the cross–shore signal here should be the same as the cross–shore signal for the average profiles inside the nourished beach, since the profiles immediately after nourishment were very similar in shape.

Because of the strong, positive, longshore gradient of longshore sediment transport on the shoulder of the beachfill at R–42, the profile has retreated an average of approximately 19 m relative to the average nourished profile, which has retreated only 2 m over the same time interval. This recession occurred gradually (refer to Figure 4.18). The width of the signature at each profile is approximately the same, although it is translated landward at R–42. To remove the cross–shore component from the signal at R–42, the cross–shore signal derived from the average profiles was therefore assumed to be representative of the cross–shore changes at R–42 if translated landward a distance of (19-2)/2=8.5 m. The fourth curve in Figure 4.29 shows the result after the cross–shore signal is removed in this manner.

Since one term from the continuity equation has been measured (the profile deformation, $\partial h/\partial t$), and a second (the cross–shore gradient of cross–shore transport, $\partial q_y/\partial y$) assumed based on the results from the average profiles, the remaining term, the local longshore gradient of longshore transport, $\partial q_x/\partial x$, can be computed. The result is shown in Figure 4.30. Computation of $\partial q_x/\partial x$ required evaluation of the slope of the fourth curve in Figure 4.29; this was done numerically, employing a triangular averaging window to remove the high–frequency oscillations.

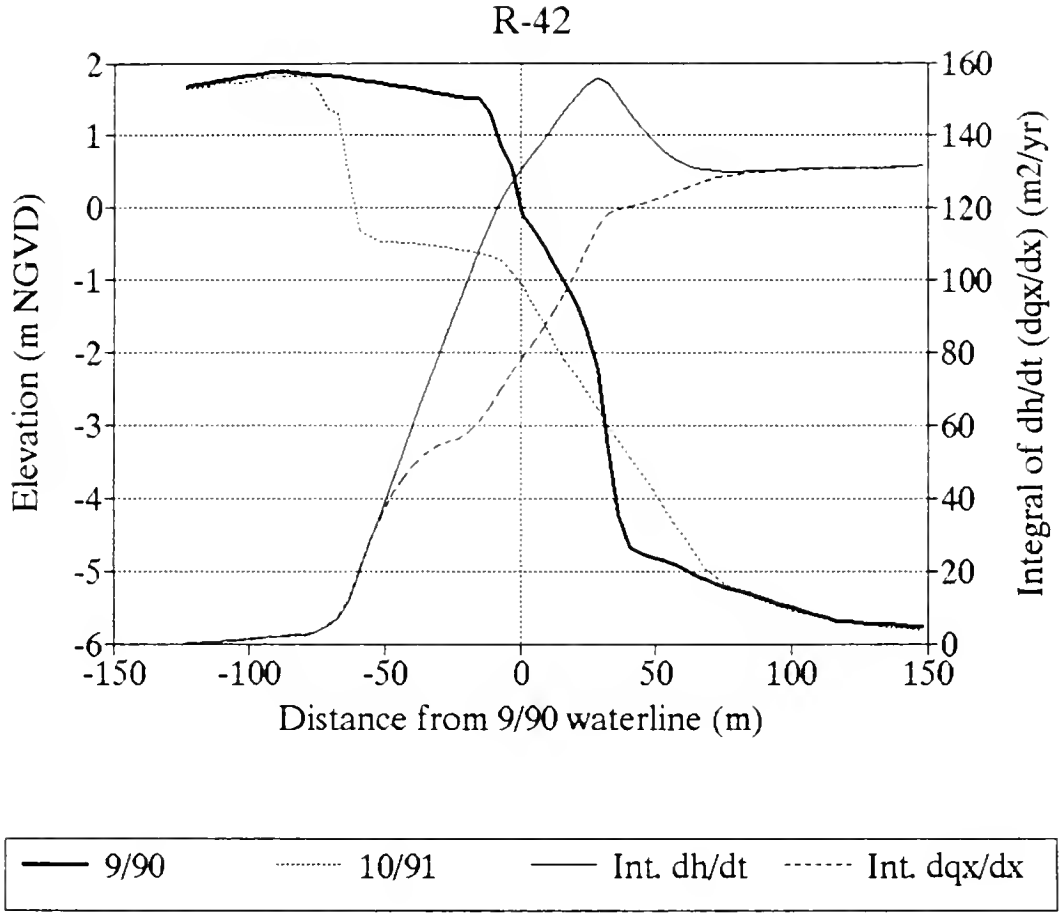

Figure 4.29: Changes occurring at profile R-42 for first year.

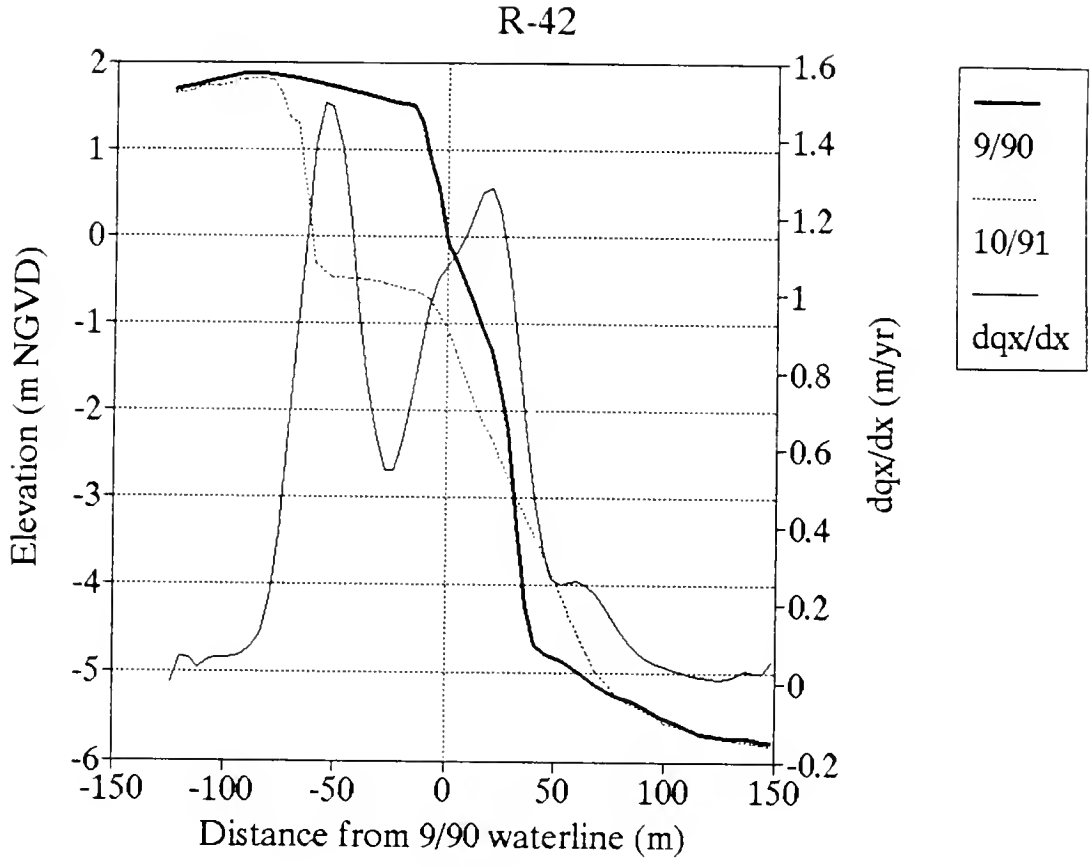

Figure 4.30: Computed cross-shore distribution of the longshore gradient of longshore sediment transport, $\partial q_x(x,y)/\partial x$.

It is reasonable to expect that the longshore sediment transport rate, $q_x(x,y)$, and its longshore gradient, $\partial q_x(x,y)/\partial x$, should exhibit similar behavior in the cross-shore direction. This would imply that $q_x(x,y) \propto [\partial q_x(x,y)/\partial x]^n$. To make the next step to determine $q_x(x,y)$ would require the assumption of both a constant of proportionality and an exponent. The available data preclude such a step, but some qualitative observations may be made.

The bimodal nature of the distribution shown in Figure 4.30 is in agreement with measured results from both the laboratory and the field (Bodge [1986], Kamphius [1991]). Previous studies have led to the conclusion that there is a maximum in the transport distribution in the swash zone and a secondary maximum near the breakpoint. This agrees well with the result presented here. Definition of the breakpoint is difficult when considering random waves incident on a rapidly eroding beach profile for over one year, but the secondary maximum is located at a point where water depths ranged from one to two meters over this time period. The primary maximum does correspond to the swash zone.

4.3 Longshore Sediment Transport Direction

Two of the most fundamental parameters needed to predict or interpret the behavior of a coastal area are the longshore sediment transport direction and rate. Correct determination of either is deceptively difficult. Beach profile data provide a good measure of the rate at which the beach is eroding or accreting, but do not indicate the magnitude or sign of the longshore sediment transport rate, only its gradient.

Most data regarding sediment transport rate and direction have been obtained either by observation of the impoundment rate adjacent to a littoral barrier or by inference from wave data. With no structures present within the study area, the wave data collected as a part of this study provide the best available information regarding the direction of the longshore transport. Both the long-term and seasonally-varying wave directions are of interest.

Longshore sediment transport has often been related to the longshore component of radiation stress, S_{xy}:

$$S_{xy} = En\cos\theta\sin\theta \tag{4.7}$$

where θ is the angle between the wave rays and the local shore-normal vector. $E = \rho g H^2/8$ is the wave energy density, and n is the ratio of the wave group velocity to the wave celerity, C_g/C. Note that E, n, and θ will all be functions of time. Komar and Inman [1970] expressed longshore sediment transport as being proportional to a longshore energy flux factor, which is the product of S_{xy} and the wave celerity, at breaking. With the assumptions of straight and shore–parallel bathymetric contours and no energy inputs or losses between the location of the wave gage and the breakpoint, it can be shown that S_{xy} is constant between the gage and the breakpoint. The assumption regarding the bathymetry is reasonable for the wave gage offshore of the Perdido Key Ranger Station.

The value of $S_{xy}(t)$ was determined for each wave data burst that included reasonable data for both pressure and velocity. The resulting time series was then integrated over time to investigate the cumulative effect of this stress on the beach. The results are shown in Figure 4.31. Wave direction has been defined such that a positive value for the longshore component of the radiation stress implies that this stress, and hence the longshore sediment transport, is directed westward. In this analysis, wave records where the computed wave direction differs from the local shore–normal by more than 90° are assumed to be in error and have not been included. This generally occurs when velocities (and therefore wave heights) are very small, and noise dominates the velocity signal, from which wave direction is computed.

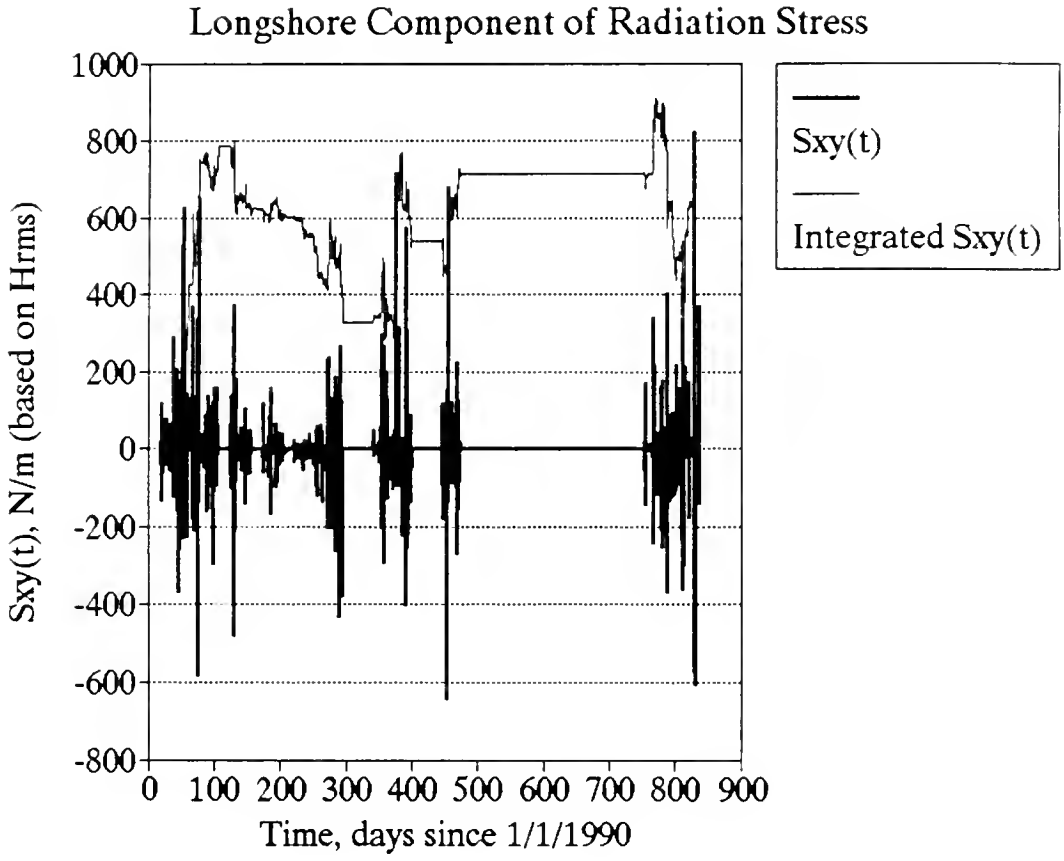

Figure 4.31: Longshore component of radiation stress, $S_{xy}(t)$ computed from all suitable wave data. $S_{xy} > 0$ implies westward sediment transport.

Unfortunately, of the 2-1/2 years covered by the wave monitoring program, only 1-1/2 years of data are available where both the pressure sensor and the current meter were functioning. This makes quantitative estimation of the longshore sediment transport rate based on the wave data difficult, but some qualitative observations are possible. In agreement with the author's field observations, Figure 4.31 indicates that the net longshore sediment transport is directed to the west, with periodic reversals, primarily during the less-energetic summer months.

Previous studies have estimated the direction and magnitude of the longshore sediment transport rate for the area (Johnson [1956], Gorsline [1966], U.S. Army [1972], Walton [1973], Dean [1988], Stone et al. [1992]). All have concluded that the net transport direction for Perdido Key is westward, although one study suggests a nodal point where the direction reverses. Estimated magnitudes vary widely.

Stone et al. [1992] determined net longshore sediment transport rates for much of the Florida Panhandle. A numerical refraction model was used to transfer offshore wave data from hindcasts and visual observations to nearshore values for computation of transport rates. Their results indicated a reversal in the direction of the net transport, with the net transport on the eastern end of Perdido Key directed eastward. The wave gage deployed for the present study offshore of the Perdido Key Ranger Station is located slightly west of the nodal point predicted by Stone et al. [1992].

Determination of the existence and location of a nodal point is not simple, requiring accurate directional wave data, bathymetric data, and a good model describing the refraction and shoaling processes. The bathymetry and shoreline orientation within the Perdido Key study area do not change drastically except in the vicinity of Caucus Shoal. Since the longshore sediment transport in the vicinity of the wave gage is directed westward, other portions of the study not influenced by the shoal should also have westward net transport. This would imply that the nodal point, if it exists, should lie somewhere within the "wave shadow" created by the shoal. The steep

bathymetric gradients and strong currents in the neighborhood of the shoal make refraction analysis of this area challenging at best. An ongoing wave monitoring program near Caucus Shoal should provide some information regarding the wave climate near the shoal. Considering the drastic change in shoreline orientation at the shoal (nearly 90°), a nodal point in the longshore transport rate near the shoal is likely, although its position should vary with time as the incident wave field changes.

Consideration of the temporal variation in the incident wave climate will be important to the sediment transport problem because of what is commonly believed to be a nonlinear relation between the wave height and the longshore sediment transport rate. Application of the time–dependent wave conditions for a given time period will not necessarily yield the same results as the average conditions applied over the same time interval.

4.4 Nourishment Project Volumes

With survey data blanketing the entire nourishment project, it is fairly simple to compute the volume of sediment placed on the beach. For each surveyed, nourished beach profile, the change in cross–sectional area was determined by numerically integrating the measured depths across the entire active profile. The trapezoidal rule was then applied to establish the change in volume.

Comparison of the profiles surveyed in November, 1989, and September, 1990, yielded a project volume of 4.07 million m^3. A similar calculation for the September, 1990, through October, 1991, period indicated a loss of 350,000 m^3, or approximately nine percent. Profiles at R–40 and R–64 defined the longshore boundaries of the computational domain for this analysis.

An apparent, but not true, change in the volume of sediment within the survey domain could arise from survey errors or inadequate survey resolution. Survey errors could appear as either a loss or gain, depending on the sign of the errors. Inadequate

longshore resolution of the survey (i.e. not enough profiles surveyed) could similarly indicate sediment gain or loss.

The only processes that could cause a true change in the volume would be compaction or a net flux of sediment into or out of the survey area. The apparent sediment "loss" rate due to compaction and eolian transport for the first survey interval was estimated at 6.4 cm/yr (vertical drop) on the dry beach. If this is assumed uniform throughout the nourished zone, multiplication by the project length (6900 m) and cross-shore width (average of 140 m) yields an apparent loss of 62,000 m^3/yr. This would imply an actual loss of 288,000 m^3 from the nourished area for the period 9/90–10/91, or seven percent of the volume of the sediment added for beach nourishment.

The apparent loss rate due to sediment compaction and/or transport by wind should decrease with time as the sediment becomes compacted and selective eolian transport leads to coarsening of the dry beach sediment. Offshore directed eolian transport was observed in the field at times, but onshore winds are much more commonplace.

Based upon inspection of the computed longshore gradient of longshore sediment transport (Figure 4.21) it does not appear that project-induced gradients have affected the region west of the domain chosen for the volumetric computations, as of 10/91. The eastern boundary of the domain is significantly more complicated, due to the presence of Pensacola Pass and Caucus Shoal, and the sharp change in shoreline orientation. The surveyed beach profiles do not clearly resolve changes in the shape and volume of the shoal. Some of the material that appears to have been lost could be collecting in the vicinity of the shoal.

The following chapter will provide a detailed look at the longshore sediment transport processes and the degree to which they can be described through the use of analytical and numerical models. The net longshore sediment transport rate may then be estimated.

CHAPTER 5
MODELING LONGSHORE SEDIMENT TRANSPORT PROCESSES

Modeling of the longshore and cross-shore sediment transport processes will be considered separately. The results of the previous chapter suggested that both transport modes were influencing the response of the beach, with the relative magnitude of the changes due to the different modes varying both temporally and spatially. The effects of the longshore sediment transport will be considered first.

5.1 Background

Longshore sediment transport is commonly expressed as proportional to some measure of the longshore wave energy flux. Komar and Inman [1970], for example, related the immersed weight longshore sediment transport rate, I, to the longshore component of wave energy flux at breaking, P_ℓ:

$$I = KP_\ell \tag{5.1}$$

where K is a non-dimensional coefficient of proportionality. The numerical value of this coefficient and the factors influencing it have been the subject of much debate; Komar and Inman [1970] determined K=0.77.

The immersed weight sediment transport rate may be related to the volumetric transport rate, Q:

$$I = Q\rho g(s-1)(1-p) \tag{5.2}$$

where ρ is the fluid density, s is the specific gravity of the sediment (the ratio of sediment density to water density), g is the acceleration of gravity, and p is the

porosity of the sediment in the bed. One notable missing parameter is sediment size. Several researchers have suggested that the longshore transport rate should be dependent on sediment size (Dean et al. [1982], Kraus et al. [1982], Kamphius [1991]), but a consensus does not exist. Komar [1991] argues that while K in Equation (5.1) should decrease with increasing sediment size, the existing field data sets do not verify this hypothesis.

The longshore component of wave energy flux, P_ℓ, is evaluated using linear wave theory:

$$P_\ell = E_b C_{G_b} \sin\theta_b \cos\theta_b \tag{5.3}$$

Following convention, a subscript "b" will be used to denote quantities evaluated at the wave breakpoint. Hence $E_b = \rho g H_b^2/8$ is the wave energy density at breaking (average energy per unit surface area), H_b is the breaking wave height, C_{G_b} the wave group velocity at breaking, and θ_b is the angle between the wave crests and the bathymetric contours at breaking. Note that P_ℓ is equal to the product of the longshore component of radiation stress, S_{xy}, and the wave celerity, C. For straight, parallel bathymetric contours, S_{xy} is conserved up to the breakpoint, but P_ℓ is not. Use of the proper definition for P_ℓ is thus important.

Definition of the wave height in Equation (5.3) is also important. Because of the nonlinear wave height term, use of a temporally–averaged wave height will not yield the same result as an approach accounting for the temporal variation. If only one wave height is to be used to compute the sediment transport rate for a given period, that wave height should be an "effective" value that considers the power of the wave height term in the transport equation. If computed correctly, the sediment transport rate based on the effective wave height will match the mean of the sediment transport rates based on the individual wave heights.

Komar and Inman [1970] used the R.M.S. wave height to define P_ℓ and determine the value of K=0.77 for the empirical coefficient. The value of 0.39 for K cited in the Shore Protection Manual (U.S. Army Corps of Engineers [1984]) arises from use of the significant wave height, H_s, and the assumption of a Rayleigh distribution to describe the distribution of breaking wave heights.

If shallow water, linear wave theory is used, it can be shown that the group velocity and celerity of the wave at the breakpoint are the same, i.e. $C_{G_b} = C_b = \sqrt{gh_b}$. Employing a similarity law for the wave height ($H_b = \kappa h_b$), and combining Equations (5.1), (5.2), and (5.3), the following result is obtained:

$$Q = \frac{K H_b^{5/2} \sqrt{g/\kappa}}{8(s-1)(1-p)} \sin\theta_b \cos\theta_b \qquad (5.$$

The proper effective wave height to use for this case would thus be:

$$H_{b_{eff}} = \left[\frac{1}{N} \sum_{n=1}^{N} H_{b_n}^{5/2} \right]^{2/5} \qquad (5.5)$$

where n denotes the nth of N wave observations for the time period of interest.

Note that Equation (5.4) expresses the total longshore sediment transport rate, integrated across the surf zone. The cross-shore distribution of the longshore sediment transport is therefore not resolved. Any attempt to employ this result to model the response of a beach will thus also have to retain the integrated approach.

Other equations have been proposed relating longshore sediment transport to the incident wave field, including some that describe the cross-shore distribution. The method outlined here represents the most common approach and therefore serves as a good basis for comparison.

Bodge and Kraus [1991] point out several potential pitfalls when attempting to compare results from different studies obtained using Equation (5.1). Even with "perfect" field data, there are enough assumptions involved that computed, best-fit

values for the empirical transport coefficient, K, vary by nearly an order of magnitude, from 0.2 to 1.6, with much scatter in the data.

The porosity and specific gravity of the sediment are often assumed, rather than measured, introducing possible (small) sources of error when determining a best value of K to fit the observed planform changes at a site. The nonlinear contribution of the wave height in Equation (5.4) is probably the most significant source of error, in part because of the accuracy with which breaking wave heights can be estimated, but also because of the temporal variation. Wave direction could cause similar, although less drastic, problems since, for small angles, transport varies nearly linearly with wave angle. In summary, any comparison of results from different studies should include careful consideration of how the results were obtained and possible sources of error

5.2 Analytical, "One–Line" Approach

If the wave conditions at the breakpoint are known, then Equation (5.4) may be combined with a sediment continuity equation to describe the planform evolution of a beach. If the shape of the beach profile is assumed to not vary with time, the beach planform may be completely described by the position of one contour. This has resulted in the term "one–line" model. The contour coincident with the waterline is generally most convenient for description of the planform changes. The continuity equation describing the motion of this (or any other) contour was discussed in the previous chapter to assist in interpretation of the changes observed in the field:

$$\frac{\partial y}{\partial t} = \frac{-1}{h_* + B} \frac{\partial Q_x}{\partial x} \tag{5.6}$$

The geometry associated with this continuity equation is shown in Figure 5.1. The variable $y(x,t)$ denotes the shore–normal, horizontal distance from an arbitrary datum to the contour of interest, x is the longshore coordinate, h_* is the water depth at the limit of active motion due to the longshore sediment transport, and B is the height of the berm immediately landward of the waterline. Note that although the

beach profile shape is assumed to not vary with time, no assumption has been made regarding its form. Selection of an appropriate value for h_* is often difficult, and unfortunately this term exerts a strong influence on model results.

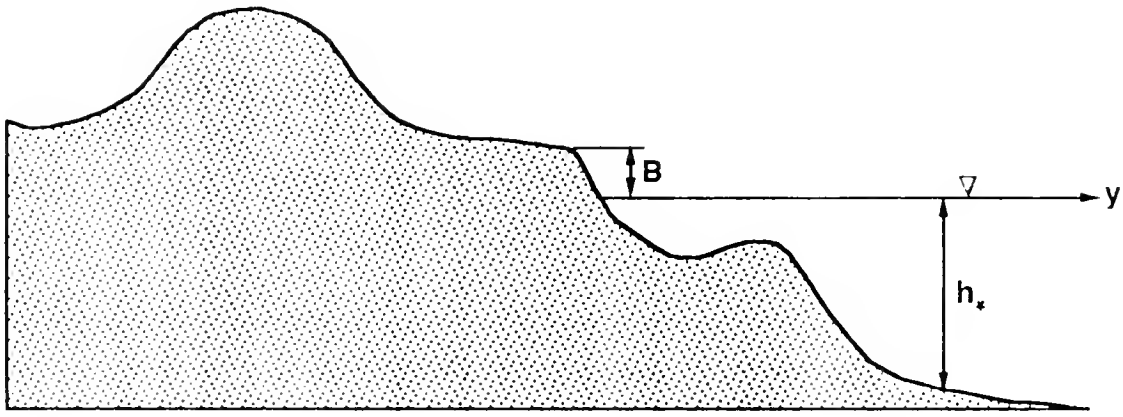

Figure 5.1: Beach profile geometry for one–line model of planform evolution.

Pelnard-Considère [1956] derived a diffusion equation governing the behavior of the coast to a planform perturbation. This was done by linearizing Equation (5.4) describing the longshore sediment transport rate by assuming that the aspect ratio of the planform perturbation is small (i.e. the cross-shore width is much less than the longshore length, tending to make θ_b small). The linearized transport equation was then combined with the sediment continuity equation (Equation (5.6)) to yield:

$$\frac{\partial y}{\partial t} = G\frac{\partial^2 y}{\partial x^2} \tag{5.7}$$

where G is a "longshore diffusivity" parameter:

$$G = \frac{K H_b^{5/2}\sqrt{g/\kappa}}{8(s-1)(1-p)(h_* + B)} \tag{5.8}$$

in which it has been assumed that $\partial\theta_b/\partial x$=0. Equations (5.7) and (5.8) demonstrate the limited role of mean wave direction in planform evolution of a beach nourishment project.

Many solutions to Equation (5.7) are readily available (Larson et al. [1987]), but an analytical approach is generally suitable only when initial and boundary conditions are relatively simple. If the beach nourishment project is idealized as a rectangle having a longshore length ℓ and cross-shore width w, placed on an initially straight shoreline with no barriers to longshore sediment transport, the resulting solution may be expressed in terms of error functions:

$$y(x,t) = \frac{w}{2}\left\{\mathrm{erf}\left[\frac{\ell}{4\sqrt{Gt}}\left(\frac{2x}{\ell}+1\right)\right] - \mathrm{erf}\left[\frac{\ell}{4\sqrt{Gt}}\left(\frac{2x}{\ell}-1\right)\right]\right\} \tag{5.9}$$

where "erf" denotes the error function (Abramowitz and Stegun [1972]; Figure 5.2):

$$\mathrm{erf}(z) = \frac{2}{\sqrt{\pi}}\int_0^z \mathrm{e}^{-u^2}\,du \tag{5.10}$$

and u is a "dummy" variable.

Note that the solution given by Equation (5.9) has no dependence on wave direction (due to the linearization) or period (because of the shallow–water assumption, which renders the waves non–dispersive). The wave height, depth of closure, h_*, and berm height, B, are all assumed spatially and temporally uniform, although an effective value could be substituted in the manner described earlier to account for the temporal variation in breaking wave height.

Figure 5.3 provides an example of the evolution predicted by Equation (5.9). Note that the solution is symmetric about the center of the project regardless of wave direction and that the planform area is preserved as the beach evolves. There is no "loss" of sediment. Sediment leaving the nourished zone benefits adjacent areas.

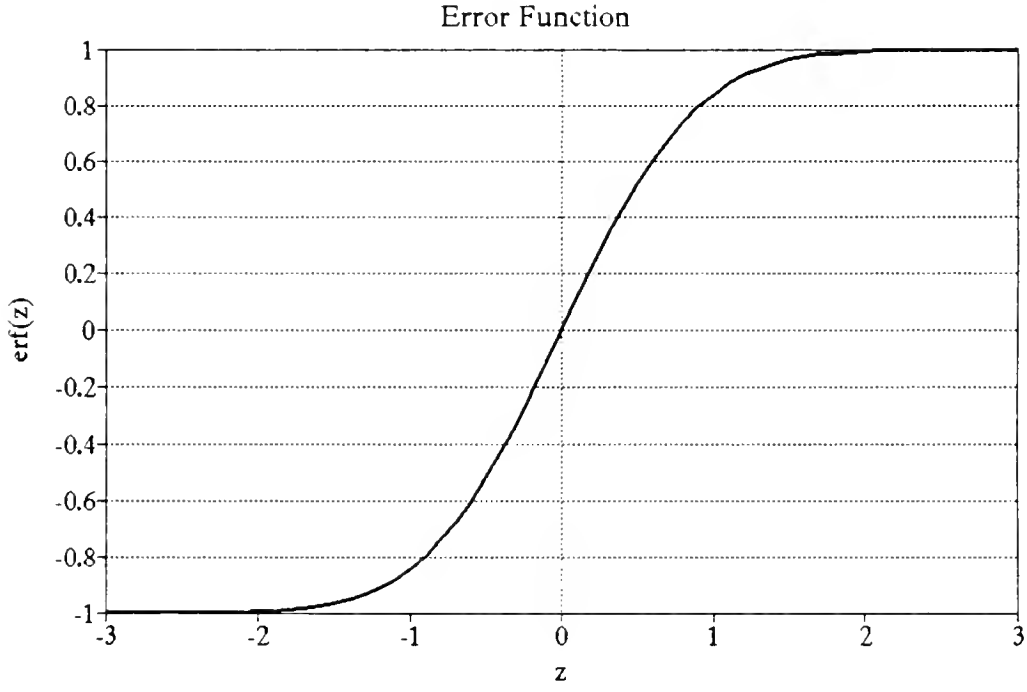

Figure 5.2: Error function.

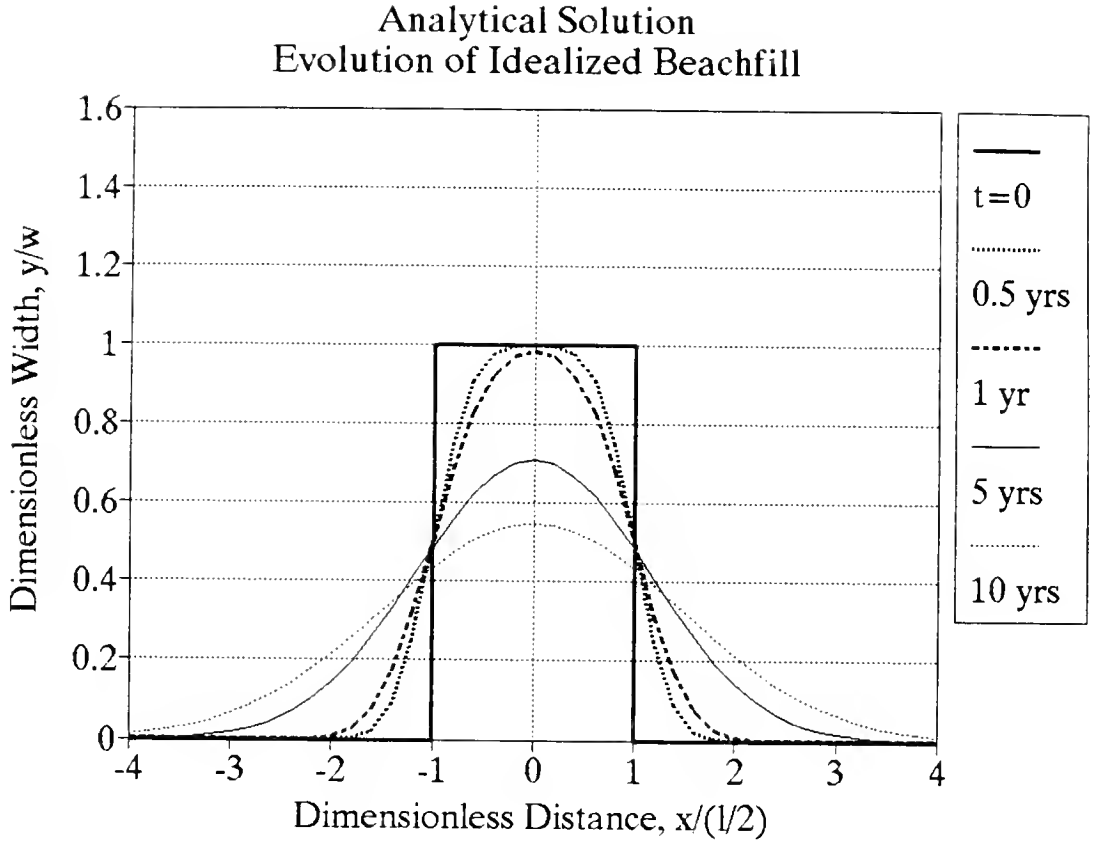

Figure 5.3: Beachfill evolution as predicted by analytical solution. K=0.77, ℓ=4000 m, H_b=0.5 m, $(h_* + B)$=5 m, G=0.0113 m^2/s.

5.3 Influence of Wave Refraction

Before applying the analytical, one–line solution to investigate its ability to predict changes measured in the field, some consideration must be given to the type of wave data available. The wave gage is well offshore of the surf zone (600 m), so both shoaling and refraction must be considered to compute an effective breaking wave height for simulation of the planform evolution.

One approach would be to develop a numerical refraction model to determine H_b and θ_b as functions of time and longshore distance, given the wave conditions at the offshore gage. This would only be valid for numerical solution of the equations governing the planform evolution, since the analytical approach requires a constant wave climate. There are several additional drawbacks to this approach. First, the results of Dean and Yoo [in press] comparing a detailed finite–difference model for refraction to one employing what will be termed "analytical refraction" revealed that the detailed refraction method did not yield significantly different results. Their results addressed the effects of an incident spectrum, but modeled the refraction of only one frequency component and one incident wave height (the effective wave height) at any given time. The results of Work and Dean [1990], employing the same finite–difference model for refraction over a shoal, also support the conclusion that the use of the simpler refraction scheme is reasonable, particularly in light of some of the other assumptions invoked.

The second point concerns the wave data collected as part of the Perdido Key monitoring study. As illustrated in the previous chapter, wave direction is only available for 1-1/2 years, vs. 2-1/2 years for wave height and period, and there is a fairly large degree of uncertainty in the directions when available. This uncertainty alone accounts for more than the differences between the two refraction schemes discussed by Dean and Yoo [in press].

The analytical refraction scheme to be used follows Dean and Grant [1989] and is based on linear wave theory. It corresponds to the simpler of the two refraction schemes considered by Dean and Yoo [in press]. The method will be detailed to some degree in the interest of completeness.

Energy flux is assumed to be conserved between the wave gage and the breakpoint. The neglect of energy input from wind and loss due to bottom friction is justified by the limited distance between these points. A simple calculation following Dean and Dalrymple [1984] indicated that the expected decay in wave height between the gage and the toe of the beachfill is less than one percent. This assumes a rigid, flat bottom and a turbulent boundary layer.

The coordinate system and geometric definitions for the problem are illustrated in Figure 5.4. All angles are referenced to North as shown. The general trend of the shoreline is denoted by μ, while β indicates the local azimuth of the bathymetric contours, and α is the azimuth of the local wave ray.

If the local bathymetric contours do not vary in the longshore direction, x, the equation expressing conservation of wave energy flux reduces to:

$$EC_G \cos(\beta - \alpha) = \text{Constant} \tag{5.11}$$

This assumption regarding the bathymetry is reasonably valid for most of the study area, offshore of the toe of the beach fill, becoming less valid near the inlet.

A subscript "R" will be used to denote a variable evaluated at the offshore (reference) gage location, where the contours are assumed to be straight and parallel to the pre-nourishment shoreline. A subscript "$\star$" implies evaluation at the toe of the beachfill. The symbol β_s will be used to indicate the local azimuth of the shoreline within the influence of the nourishment project. The contours between the waterline and the toe of the beachfill, although not necessarily straight, are assumed parallel to

the shoreline. This implies that the shape of the beach profiles does not vary along the beach.

The irrotationality condition on the wavenumber vector provides the additional equation necessary for the refraction analysis:

$$\vec{\nabla} \times \vec{k} = 0 \tag{5.12}$$

or, for the straight, parallel contours of interest, Snell's law results:

$$\frac{\sin(\beta - \alpha)}{C} = \text{Constant} \tag{5.13}$$

Equation (5.11) may be rewritten as:

$$E_R C_{G_R} \cos(\beta_R - \alpha_R) \approx E_* C_{G_*} \cos(\beta_* - \alpha_*) \approx E_b C_{G_b} \cos(\beta_s - \alpha_b) \tag{5.14}$$

The shallow water approximation and wave height similarity condition may then be invoked to yield:

$$C_{G_b} = C_b = \sqrt{g h_b} = \sqrt{g H_b / \kappa} \tag{5.15}$$

Equations (5.14) and (5.15) may be combined and solved for the wave celerity at breaking:

$$g^2 H_R^2 C_{G_R} \cos(\beta_R - \alpha_R) \approx g^2 H_b^2 C_b \cos(\beta_s - \alpha_b) \approx C_b^5 \kappa^2 \cos(\beta_s - \alpha_b) \tag{5.16}$$

or

$$C_b = \left[\frac{g^2 H_R^2 C_{G_R} \cos(\beta_R - \alpha_R)}{\kappa^2 \cos(\beta_s - \alpha_b)} \right]^{0.2} \tag{5.17}$$

Application of Equation (5.13) within the nourished area yields:

$$\frac{\sin(\beta_s - \alpha_*)}{C_*} = \frac{\sin(\beta_s - \alpha_b)}{C_b} \tag{5.18}$$

Equations (5.14), (5.17) and (5.18) may be substituted into Equation (5.4) to express the longshore sediment transport rate primarily in terms of wave parameters evaluated at the offshore gage location:

$$Q = \frac{K H_R^{2.4} C_{G_R}^{1.2} g^{0.4} \cos^{1.2}(\beta_R - \alpha_R)}{8(s-1)(1-p) C_* \kappa^{0.4}} \sin(\beta_s - \alpha_*) \tag{5.19}$$

Here it has been assumed that the wave obliquity at breaking is small, so that $\cos(\beta_s - \alpha_b) \approx 1$. This approach accounts for the longshore variation in wave direction at breaking, α_b, resulting from wave refraction.

Combination of Equation (5.19) with the sediment continuity equation (Equation (5.6)) and linearization will again lead to the diffusion equation (Equation (5.7)). In this instance, the "diffusivity", analogous to Equation (5.8), will be expressed primarily in terms of wave parameters evaluated at the gage location:

$$G = \frac{K H_R^{2.4} C_{G_R}^{1.2} g^{0.4}}{8(s-1)(1-p) C_* \kappa^{0.4} (h_* + B)} \left[\frac{\cos^{1.2}(\beta_R - \alpha_R) \cos 2(\beta_R - \alpha_*)}{\cos(\beta_R - \alpha_*)} \right] \tag{5.20}$$

Equations (5.19) and (5.20) suggest the manner in which effective wave heights should be computed in terms of wave parameters measured at the gage.

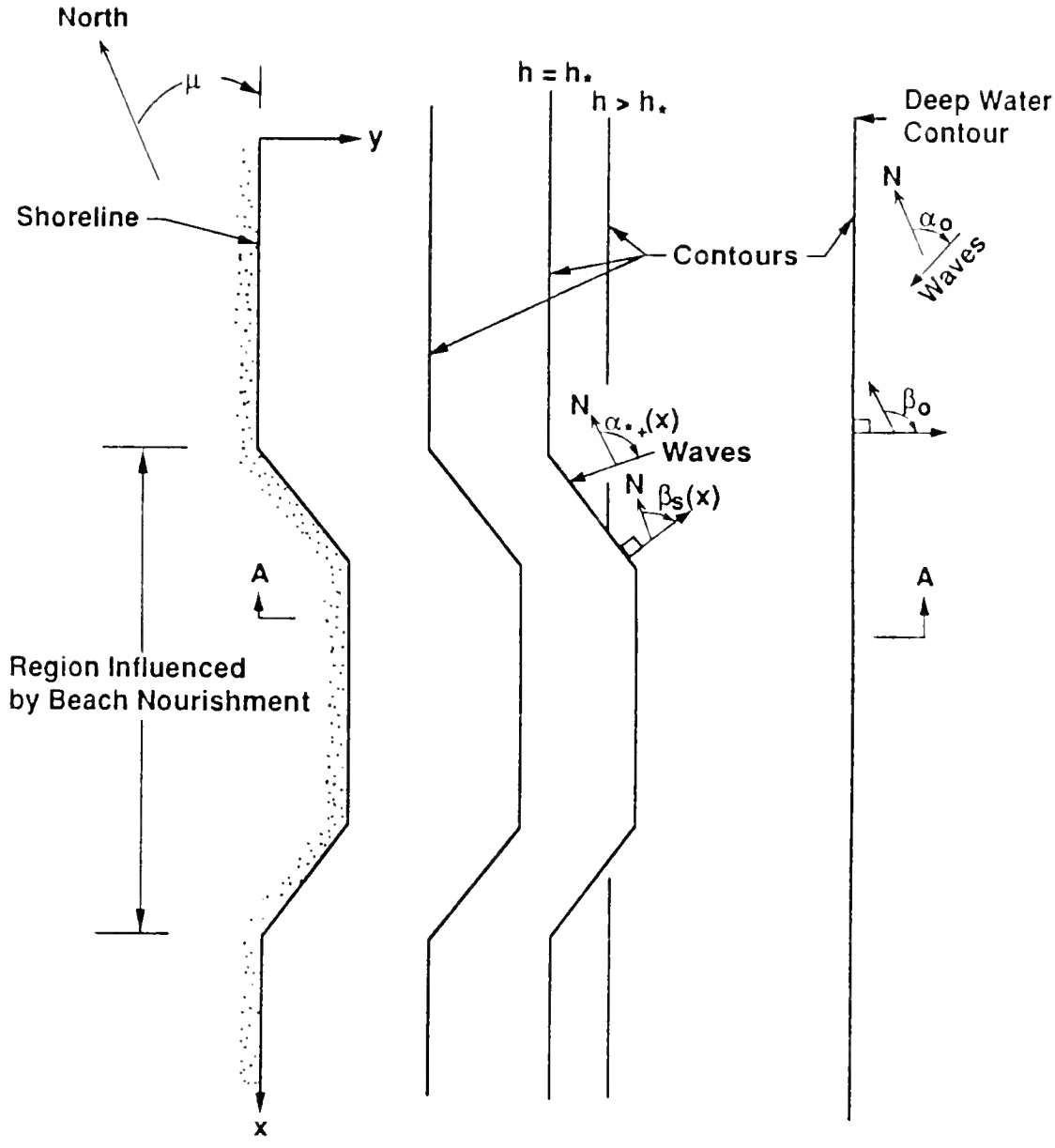

Figure 5.4: Coordinate system for shoaling/refraction problem. Adapted from Dean and Yoo [in press].

5.4 Effective Wave Parameters

The motive for defining an effective wave height is to parameterize both the temporal variation in the wave climate and the spectral nature of the waves. The importance of the temporal variation in the wave climate has already been discussed. The parameterization will neglect complicated (and poorly understood) wave–wave interactions, in keeping with the assumptions invoked to this point.

The equations of interest for modeling the response of the planform are the sediment transport and continuity equations (Equations (5.19) and (5.6)). To parameterize the spectral nature of the waves, wave height, celerity, group velocity, and wave direction should all be considered.

Inspection of Equation (5.19) indicates that the dominant fluctuating term will be $H_R^{2.4} C_{G_R}^{1.2} / C_*$. Since the angular deviation between the wave direction and the local shore–normal will generally be small, temporal variation in the trigonometric terms will be less important. The chosen method for selecting representative, or "effective" values for the wave height and group velocity follows Dean and Grant [1989], and assumes that, for a statistically stationary spectrum, the wave heights may be reasonably described by a Rayleigh probability density function:

$$f(H) = \frac{2H}{H_{rms}^2} \exp[-(H/H_{rms})^2] \tag{5.21}$$

Note that significant wave height and R.M.S. wave height, H_{rms}, are related (retaining the Rayleigh distribution assumption): $H_s \approx \sqrt{2} H_{rms}$. The long–term distribution of *significant* wave heights at the gage was earlier found to be poorly–described by the Rayleigh distribution. If the sea surface displacement is a Gaussian random process, however, individual waves should follow the Rayleigh distribution.

Employing the Rayleigh distribution, an effective wave height at the wave gage location, representative over a time interval short enough to allow assumption of a stationary spectrum, may be defined as follows:

$$(H_R)_{eff} = \left[\int_0^\infty H^{2.4} f(H) dH\right]^{1/2.4} = K_{rms}(H_R)_{rms} = K_s(H_R)_s \tag{5.22}$$

where $H_{R_{rms}}$ and H_{R_s} are the root–mean–square and significant values of the wave height at the gage, respectively. The coefficients, K_{rms} and K_s may be evaluated numerically as 1.04 and 0.735, respectively. The exponent is suggested by the form of Equation (5.19).

The method outlined above provides one effective wave height representative of the entire spectrum for use in the sediment transport equation. A more practical result is the effective wave height for some longer time interval of interest. Temporal variation in the wave climate may be accounted for in a similar manner, if the effective wave height is defined as follows:

$$(H_R)^n_{eff} = \frac{\left[\frac{1}{N}\sum_{n=1}^{N}[K_s(H_R)^n_s]^{2.4}\left(\frac{C^{1.2}_{G_R}}{C_*}\right)^n\right]^{1/2.4}}{\left[\frac{1}{N}\sum_{n=1}^{N}\left(\frac{C^{1.2}_{G_R}}{C_*}\right)^n\right]^{1/2.4}} \tag{5.23}$$

The superscript "n" denotes the nth of N records available for the time period for which the effective wave height is desired.

For each valid burst of wave data in the field, a significant wave height and a wave period corresponding to the peak of the energy spectrum were available. When operating correctly, this resulted in four values for both parameters every day. One day is a reasonable time step for numerical modeling of beach planform response, so an effective wave height, $(H_R)_{eff}$, and an effective value of the term $C^{1.2}_{G_R}/C_*$ were determined for each day. Effective values for longer time periods were computed for use in the analytical model, which does not allow any temporal variation. Where daily data were unavailable, monthly means were substituted.

The remaining terms in Equation (5.19) involving wave parameters are the two wave directions, α_R and α_*, which may be related using Equation (5.13). For the case of interest, the depth at the wave gage is approximately 6 m, and the depth at

the toe of the beach fill averages 5.2 m. Under these conditions, particularly with the short-period waves measured at the site, the difference between α_R and α_* will be quite small. It was therefore assumed that $\alpha_* \approx \alpha_R$. Effective wave directions were not computed. It will be shown later that the results are relatively insensitive to mean wave direction. This result is consistent with the analytical solution, where the longshore diffusivity, G (Equation (5.8)), is not dependent on wave direction.

The resulting refraction scheme approximately conserves wave energy flux between the wave gage and the breakpoint, and assumes that the wave direction does not change until the wave reaches the toe of the beachfill. Linear wave theory, with shallow water approximations invoked near the breakpoint, has been used throughout the development. The important assumption of straight, parallel offshore contours has also been employed.

5.5 Comparison of Analytical Model to Measured Changes

To compare the analytical solution to the planform changes measured at Perdido Key, appropriate values for the effective wave height, initial planform shape, etc., must be selected. Most of these are well-defined, based on the field measurements.

The parameters selected to compare the analytical solution to the measured planform changes are summarized in Table 5.1. Where possible, values are based on measurements. The chosen value of 0.77 for the empirical sediment transport coefficient, K, is based on the value found by Komar and Inman [1970]. Following rather standard procedures, the "depth of closure", h_*, is taken as the depth beyond which sediment is observed to be immobile, even though longshore sediment transport processes were not necessarily responsible for motion of the sediment to that depth.

The change in shoreline width, w, is taken as the average of the measured changes within the nourished area. The measured initial condition is compared to the resulting idealized initial condition for application of the analytical solution in Figure 5.5.

Table 5.1: Parameters selected for application of analytical solution for planform evolution.

Parameter	Value	Measured (M) or Assumed (A)
Project width, w	136 m	M
Project length, ℓ	6900 m	M
Transport coefficient, K	0.77	A
Effective wave height, $(H_R)_{eff}$	0.51 m	M
Effective celerity term, $[C_{GR}^{1.2}/C_*]_{eff}$	1.06 $(m/s)^{0.2}$	M
Breaking Wave height/water depth ratio, κ	0.78	A
Sediment specific gravity, s	2.65	A
Bed Porosity, p	0.35	A
Depth of closure, h_*	5.2 m	M[1]
Berm height, B	1.5 m	M
Relative wave direction, $\beta_R - \alpha_R$	0	A
Time interval, Δt	388 days	M

Note: [1]Depth of closure inferred from measured profile deformations.

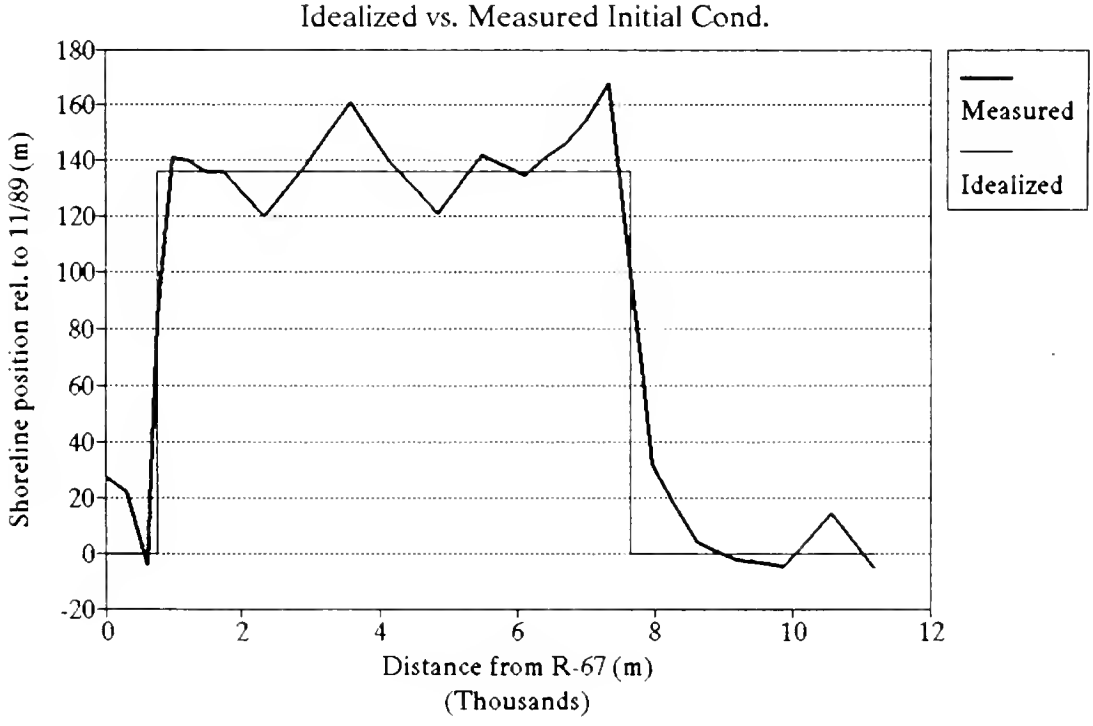

Figure 5.5: Comparison of measured and idealized initial planforms.

The assumption of a rectangular planform perturbation is not well justified for this case. As evidenced by Equation (5.7), the product of shoreline curvature and the local "diffusivity", G, drives planform changes. Neglect of the strong curvature present within the nourished section of the post-nourishment planform should be expected to cause problems when comparing the analytical solution to the measured changes.

The boundary condition at the eastern end of the field site, at Pensacola Pass, is not well known. The boundary condition assumed to arrive at the analytical solution, that of a straight, uninterrupted shoreline, is not a very satisfactory choice. Both the inlet and Caucus Shoal may be expected to exert a significant effect on the downdrift shoreline behavior. More complicated boundary conditions are best suited to a numerical approach, to be discussed shortly.

Figure 5.6 compares the analytical solution for this simple case to the actual measured changes occurring at Perdido Key for the first year following placement of the new material. The longshore gradient of the longshore sediment transport rate has been used as the basis for comparison, since this removes the effects of cross-shore transport, known to be important in the field data (Chapter 4) and neglected in the derivation of the analytical result.

The poor agreement between the analytical result and the measurements appears to arise primarily from three factors. The idealized initial condition results in a "smooth" curve representing the longshore gradient of longshore sediment transport. The smaller-scale anomalies found in the result derived from the field data are not apparent in the model result. The spatially-averaged value of the longshore gradient of longshore sediment transport, $\partial Q_x/\partial x$, is zero for the analytical solution, while the field result exhibits a positive mean value, indicative of a net loss of sediment.

Discussion of the third problem regarding application of the analytical solution requires inspection of the behavior of Equation (5.9) near the ends of the beachfill

($x = \pm\ell/2$). Note that the dominant term in this equation is $\ell/(4\sqrt{Gt})$. For large values of this term (e.g. for small t) the shoreline displacement at either end of the beachfill, $y(\pm\ell/2, t)$, is simply $w/2$. For $x = \pm\ell/2 \pm \delta$, where δ is infinitesimally small, this implies a change in cross-sectional area of $\pm(w/2)(h_* + B)$, relative to the initial condition. The time-averaged longshore gradient of longshore sediment transport at these points, averaged from t=0 up to any time such that $\ell/(4\sqrt{Gt})$ is still large, will thus be $|\overline{\partial Q_x/\partial x}| = (w/2)(h_* + B)/(\Delta t)$. The unrealistically strong planform gradient at $x = \pm\ell/2$ thus leads to an unrealistically strong gradient of longshore sediment transport. Note that for the parameters in Table 5.1, $\ell/(4\sqrt{Gt})$ is roughly 3.3, so the argument of the error function terms for $x = \pm\ell/2$ in Equation (5.9) are $\pm$6.6. Figure 5.2 indicates that this still corresponds to "small" time.

5.6 Numerical Approach to One-Line Modeling

The approach described to this point allows a complete description of the spatially- and temporally-varying longshore sediment transport rate. Numerical solution of the equations for sediment transport and continuity will allow a description of the beach evolution in space and time, and remove the restrictions on initial and boundary conditions implicit in the analytical approach.

For the numerical scheme, the longshore transport rate throughout the domain at a point in time is computed, and then the continuity equation is applied over some small time interval to determine the new shoreline position. This is repeated until the desired simulation time has been reached. Equations (5.19) and (5.6) were expressed in finite difference form to allow implementation of this approach. The geometry for the finite difference solution is shown in Figure 5.7.

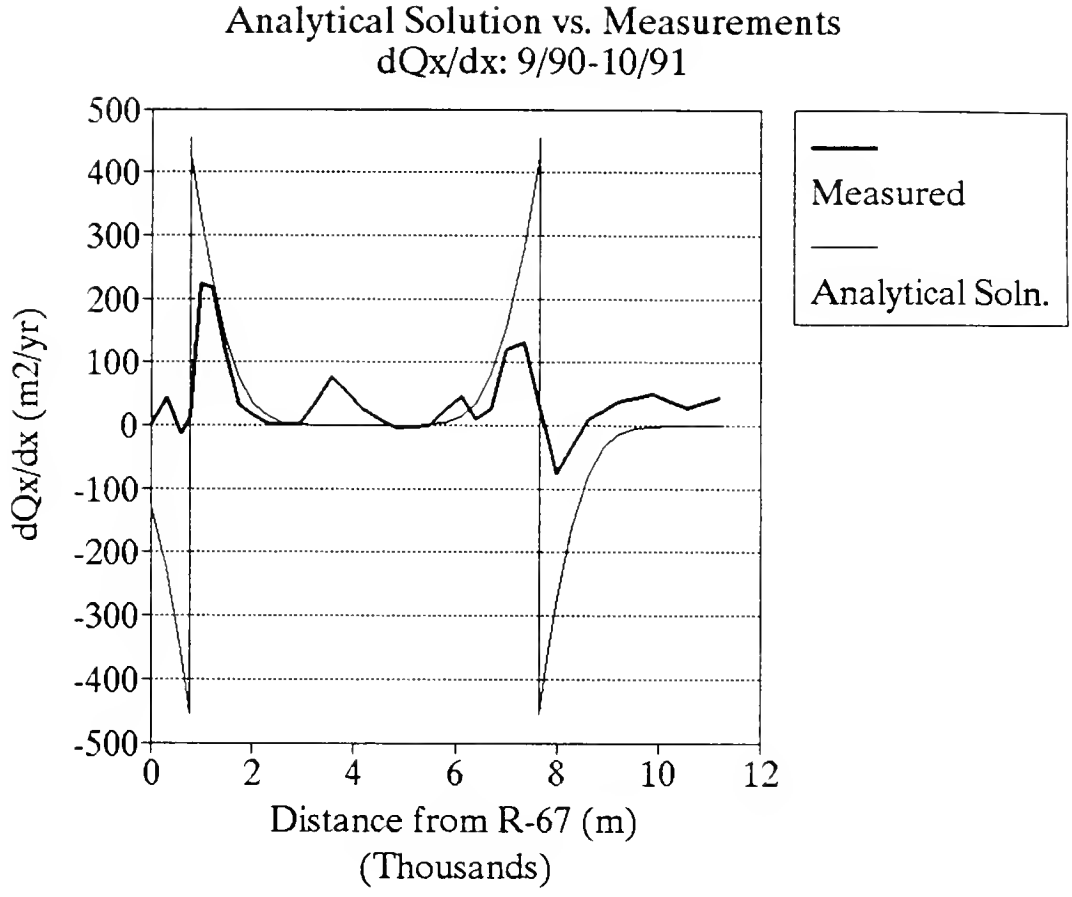

Figure 5.6: Longshore gradient of longshore sediment transport rate, as predicted by one-line, analytical solution, vs. measurements, September, 1990, to October, 1991.

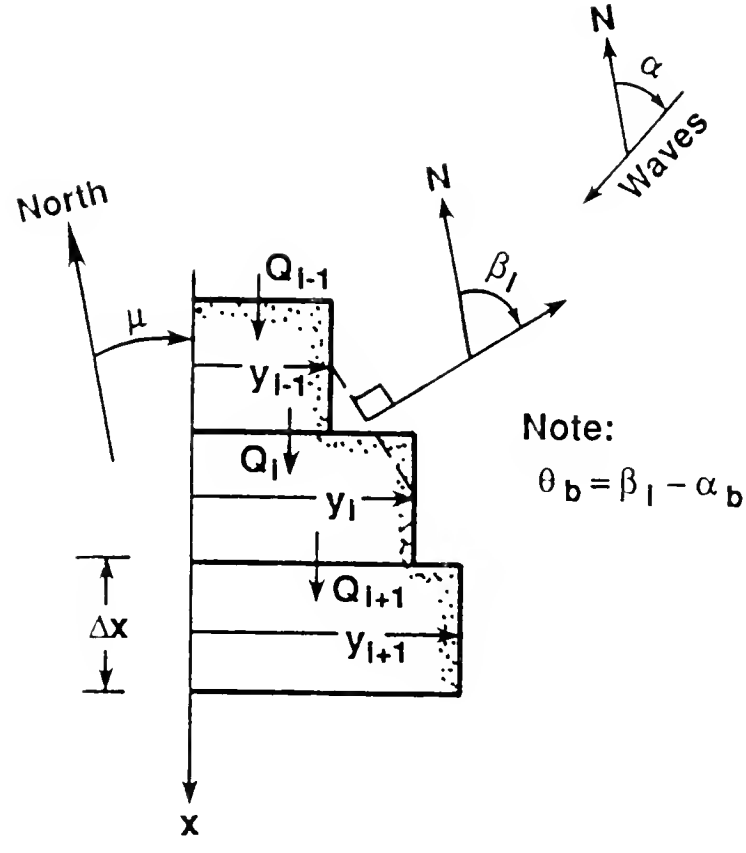

Figure 5.7: Finite–difference definitions for one–line model.

The local shoreline orientation, β_s, may be expressed in terms of longshore gradients of shoreline position, $y(x,t)$. Dropping the "s" subscript and replacing it with a subscript "i" denoting the ith computational node number,

$$\beta_i^n = \mu + \frac{\pi}{2} - \tan^{-1}\left(\frac{y_i^n - y_{i-1}^n}{x_i - x_{i-1}}\right) \tag{5.24}$$

Here the superscript "n" has been used to denote the nth time level.

The transport and continuity equations may then be discretized. An explicit formulation was used, which provides a very simple solution scheme and has as its primary drawback a maximum allowable time step. Exceedance of the maximum allowable time step results in numerical instability in the model. For the linearized governing equation (Equation (5.7)), this critical time step is a function of the diffusivity and the finite–difference space step:

$$\Delta t_{crit} = \frac{(\Delta x)^2}{2G} \tag{5.25}$$

Although not exact, this has also been found to provide a good estimate of the stability limit for the numerical model, which does not use the combined, linearized equations.

A fully–implicit or semi–implicit solution scheme would allow the use of larger time steps, but the explicit model, because of the small number of computational nodes and the simplicity of the equations required for this simulation, requires very little computational time. Most model results were obtained using time steps of one day. Because of the spatial resolution of the survey data, model space steps, Δx, smaller than 300 m were not justified. (Smaller space and time steps reduce error, but sensitivity tests indicated that the chosen values were adequate). Large wave heights reduce stability by increasing the diffusivity, G, so represent the worst case as far as model stability is concerned. For the parameters summarized in Table 5.1 and a space step, Δx, of 300 m, the estimated critical time step is 52 days. Alternately, for a time step of one day, the minimum allowable space step is roughly 42 m.

The discretized transport and continuity equations, based on Equations (5.19) and (5.6), respectively, are as follows:

$$Q_i^n = \frac{K[(H_R)_{eff}^n]^{2.4} g^{0.4} \cos^{1.2}(\beta_R - \alpha_R)}{8(s-1)(1-p)\kappa^{0.4}} \left(\frac{C_{GR}^{1.2}}{C_*}\right)_{eff}^n \sin(\beta_i^n - \alpha_R) \tag{5.26}$$

$$y_i^{n+1} = y_i^n - \frac{\Delta t}{(h_* + B)} \frac{Q_{i+1}^n - Q_i^n}{\Delta x} \tag{5.27}$$

Equations (5.26) and (5.27) provide a description of the effects of the planform anomaly produced when the beach is nourished. At many sites, persistent background erosion exists because of longshore gradients of longshore sediment transport unrelated to the nourishment project. The background erosion must be accounted for to realistically describe the sediment transport processes. The background transport, Q_{B_i}, assumed steady, and the project–related transport, Q_i^n will be assumed independent, allowing linear superposition to determine the total longshore transport rate, $Q_{T_i}^n$:

$$Q_{T_i}^n = Q_i^n + Q_{B_i} \tag{5.28}$$

The background transport, Q_{B_i}, must vary spatially to induce any planform changes. Generally, it is the rate of planform change, $\partial y_{B_i}/\partial t$, that is known, rather than Q_{B_i}. The two are related by the equation describing continuity of the background transport:

$$\frac{\partial Q_{B_i}}{\partial x} = -(h_* + B)\frac{\partial y_{B_i}}{\partial t} \tag{5.29}$$

In theory, if the description of longshore sediment transport equation is fully adequate, any background erosion should already be incorporated and there is no need for the extra term in Equation (5.28). The modification described above essentially accounts for limitations in the description of the longshore sediment transport. The

spatial variation in the term $\partial y_{B_i}/\partial t$ should be minimal to maintain credibility of both the model and the model results. Background erosion was assumed both temporally and spatially constant ($\partial y_{B_i}/\partial t$=Constant) for all model results to be discussed.

The primary effect of changes due solely to cross-shore sediment transport were removed from the previous results by considering the longshore gradient of longshore transport, which involves integration across the profile. An additional modification to the governing equations was made to investigate possible coupling between the two processes. The field data presented in the previous chapter illustrated the rapid recession of the waterline due to cross-shore sediment transport as the profile shape began to equilibrate. This could have the effect of reducing the planform anomaly (w in the analytical solution), and therefore longshore gradients of longshore transport (since $\partial Q_x/\partial x \propto w$ near the ends of the beachfill).

With the modifications to account for background erosion and planform changes attributable to cross-shore transport, the continuity equation may be written as:

$$y_i^{n+1} = y_i^n - \frac{\Delta t}{(h_* + B)} \frac{Q_{T_{i+1}}^n - Q_{T_i}^n}{\Delta x} + \frac{\partial y_{c_i}}{\partial t} \Delta t \tag{5.30}$$

where $\partial y_{c_i}/\partial t$ is the rate of change of shoreline position attributable solely to cross-shore sediment transport.

The data measured in the field were employed to assess the magnitude of the cross-shore term in Equation (5.30). Figure 5.8 indicates the change in the distance to the waterline within the nourished area as a function of time, based on the previously computed average profiles. The measured curve was parameterized by a hyperbolic tangent for application in the model:

$$y_{c_i} = \begin{cases} a \tanh bt & \text{within nourished zone} \\ 0 & \text{elsewhere} \end{cases} \tag{5.31}$$

where $a < 0$.

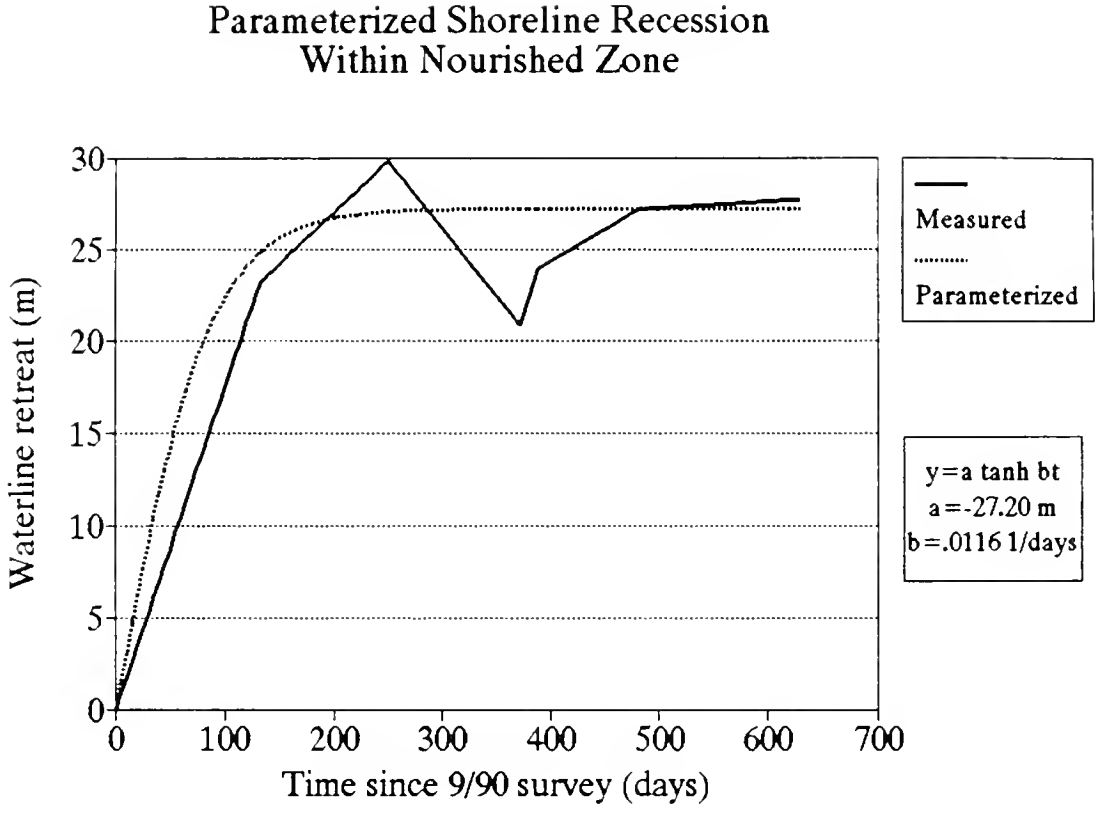

Figure 5.8: Average retreat of waterline within nourished zone. Changes due, almost exclusively, to cross-shore sediment transport.

While the background erosion term in Equation (5.28) removes sediment to account for processes not described in the model, the cross–shore transport should not modify the sediment budget and therefore does not contribute directly to $\partial Q_x/\partial x$. To compute the longshore gradient of longshore sediment transport from the model results, the changes due to cross–shore transport must be added back in:

$$\left(\frac{\partial Q_{x_i}}{\partial x}\right)_{model} = -\frac{(h_* + B)}{(t_{end} - t_{start})}\left[y_i(t_{end}) - y_{c_i}(t_{end}) - y_i(t_{start})\right] \tag{5.32}$$

Note that with this approach, it would be equally valid to compare the measured and predicted shoreline positions, instead of the longshore gradient of longshore sediment transport. The term y_{c_i} accounts for the initial differences in the shapes of the profiles within and outside the nourished sections of the beach.

A simple example may help justify this approach. Consider a beach that is in a dynamic equilibrium, both in planform and profile, extending to infinity both up– and downdrift, with no littoral barriers. Then a section of the beach is drastically steepened by moving sediment from the lower to the upper limit of its active profile. The effect of this will be to displace the shoreline seaward within the altered region, solely because of a cross–shore process, with no change in cross–sectional area. If the waves are then allowed to re–work the beach, the steep section of the beach would be expected to return to its earlier profile shape. When the profile returned to its former shape, the planform anomaly would no longer exist, and there would be no longshore gradient of longshore sediment transport.

For the Perdido Key beach nourishment project, as with most such projects, the added sand places the beach out of "equilibrium" in both the planform and profile. The method detailed above is simply a way of removing the effects of the cross–shore transport to examine the effects of the longshore sediment transport.

5.7 Determination of Best-Fit Empirical Transport Coefficient

Numerical solution of the equations governing the evolution of the nourished beach provides the most realistic results and assists in investigating the effects of different parameters and assumptions. Because of its importance for the prediction of the longshore sediment transport rate, it is of interest to determine the value of the empirical transport parameter, K, that provides the best fit to the measured changes.

If the planform changes due solely to cross-shore transport are accounted for, the basis for a comparison between measurements and model results could be the shoreline position, the longshore gradient of the longshore transport rate, or the change in volume within a given domain. Differences between the first two measures are insignificant. In either case, the spatially-averaged error between curves representing the model and measured results, respectively, will be minimized. The third approach involves minimizing an integrated quantity, and is therefore slightly less strict.

Comparison of the longshore gradient of the longshore transport rate, $\partial Q_x/\partial x$, is slightly preferable to shoreline position, since cross-shore effects need not be considered in the measured results. To compare the model to the measured gradient, a non-dimensional error, ε^2, was defined:

$$\varepsilon^2 = \frac{\frac{1}{I}\sum_{i=1}^{I}\left[\left(\frac{\partial Q_{x_i}}{\partial x}\right)_{meas} - \left(\frac{\partial Q_{x_i}}{\partial x}\right)_{model}\right]^2}{\frac{1}{I}\sum_{i=1}^{I}\left[\left(\frac{\partial Q_{x_i}}{\partial x}\right)_{meas}\right]^2} \tag{5.33}$$

where I is the number of data points describing $\partial Q_x/\partial x$ that are being used for the comparison, which is somewhat subjective. Fortunately, the best-fit value for K will be shown to be only weakly dependent on the domain used for comparison. Note that ε^2=0 implies perfect agreement, and K=0 is an upper limit corresponding to ε^2=1.

If volumes are to be used as the basis for the comparison, then the error may be defined by Equation (5.34):

$$\varepsilon = \frac{|\Delta V_{meas} - \Delta V_{model}|}{|\Delta V_{meas}|} \tag{5.34}$$

Volumetric changes are determined by integrating the longshore gradient of longshore transport over x, the longshore coordinate.

$$\Delta V = \Delta t \int_{x_{start}}^{x_{end}} \frac{\partial Q_x}{\partial x} dx \tag{5.35}$$

The same subjectivity regarding the domain for comparison of model and measured quantities thus applies to volumes.

The first definition for the error, Equation (5.33) was chosen to determine the best-fit transport coefficient, K. Comparison was based on measured results for the period 9/90–10/91. This interval is defined by two bathymetric surveys, assuring that profiles reached the depth of closure. The dates chosen for comparison should also help reduce seasonal variation.

The value of K that minimized the error between the measurements and the model results was found essentially by trial-and-error. Values of all other parameters were selected, and the error was computed for enough values of K to define the best fit.

The effects of each of the following parameters on the results were tested: wave height (both absolute magnitude and constant vs. unsteady), updrift and downdrift boundary conditions, incident wave direction, background erosion rate, domain for comparison, magnitude of cross-shore transport term, and active depth ($h_* + B$). The effects of some of these parameters are suggested by the governing equations and the idealized solution, but the coupled equations, when combined with more complicated boundary conditions and temporally-varying forcing, make a numerical investigation most practical.

The input and results of most of the tests performed to investigate the effects of each parameter are summarized in Table 5.2. Based on the results, several factors

may be ruled unimportant to the model output. The boundary condition at the inlet exerts little influence on the downdrift solution for this relatively short time interval (one year). Essentially the same results were obtained with $y_1 = f(t)$ (where $f(t)$ is determined from the field measurements), y_1=constant, and Q_1=0.

Wave direction is not important until unrealistically oblique angles are encountered. Even reversing the direction does not alter the results significantly. This is fortunate, since wave direction is the measured wave parameter containing the largest degree of uncertainty.

The term added to account for cross-shore transport, $\partial y_c/\partial t$, was found to exert a negligible effect on the results until the magnitude of y_c approached the cross-shore width of the beach nourishment project. This is fortunate because, in practice, this term is difficult to predict. The implication then is that the longshore gradient of longshore sediment transport may be estimated almost without consideration of the cross-shore sediment transport. This is because cross-shore transport, by itself, will not cause a change in cross-sectional area of the profile.

The spatial domain for comparison of the model to the measurements becomes important when the ends of the beachfill are added to or removed from the domain. Note that changing the domain while holding all other parameters constant will affect the resulting error, because of the way the error has been defined by Equations (5.33) and (5.34).

Temporal variation in wave height is very important because of the nonlinear wave height term appearing in the sediment transport equation. Using an average wave height as representative of a long time period results in less transport and therefore a larger value for K to yield the same planform changes. Use of the correct, constant, "effective" wave height in the manner outlined previously will give the same results as the fluctuating wave height.

Table 5.2: Effect of various parameters on best-fit K value. $\Delta x \approx$300 m, Δt=1 day for all tests. $\alpha_R < 0$ yields westward transport.

Trial	Wave Height (m)	Inlet B.C.	α_R deg.	$\partial y_B/\partial t$ m/yr	x_{start} m	x_{end} m	$(h_* + B)$ m	ε^2	K_{best}
1	Daily	$y = f(t)$	0	0	2922	8621	6.7	0.498	0.20
2	Daily	$y = f(t)$	-5	0	2922	8621	6.7	0.498	0.21
3	Daily	$y = f(t)$	-10	0	2922	8621	6.7	0.498	0.21
4	Daily	$y = f(t)$	-30	0	2922	8621	6.7	0.496	0.30
5	Daily	$y = f(t)$	0	-1	2922	8621	6.7	0.448	0.20
6	Daily	$y = f(t)$	0	-2	2922	8621	6.7	0.407	0.20
7	Daily	$y = f(t)$	0	-3	2922	8621	6.7	0.383	0.19
8	Daily	$y = f(t)$	0	-4	2922	8621	6.7	0.383	0.19
9	Daily	$y = f(t)$	0	-5	2922	8621	6.7	0.407	0.19
10	$H_s = 0.45$ $C_{G_R}^{1\,2}/C_* = 1$	$y = f(t)$	0	0	2922	8621	6.7	0.497	0.33
11	$H_s = 0.45$ $C_{G_R}^{1\,2}/C_* = f(t)$	$y = f(t)$	0	0	2922	8621	6.7	0.497	0.32
12	Daily	Pinned	0	0	2922	8621	6.7	0.498	0.20
13	Daily	$Q_1 = 0$	0	0	2922	8621	6.7	0.498	0.20
14	Daily	$Q_1 = 0$	0	0	754	7972	6.7	0.339	0.41
15	Daily	Pinned	0	0	754	7972	6.7	0.339	0.41
16	Daily	$y = f(t)$	0	0	754	7972	6.7	0.339	0.41
17	Daily	$y = f(t)$	0	0	1731	7972	6.7	0.514	0.19
18	Daily	$y = f(t)$	0	0	1731	7972	2	<0.166	>1
19	Daily	$y = f(t)$	0	0	1731	7972	10	0.555	0.15
20	Daily	$y = f(t)$	0	-4	1731	7972	6.7	0.372	0.17
21	Daily	$y = f(t)$	0	-4.5	1731	7972	6.7	0.381	0.17
22	Daily	$y = f(t)$	0	-3.5	1731	7972	6.7	0.371	0.18
23	Daily	$y = f(t)$	0	-3.4	1731	7972	6.7	0.372	0.18
24	Daily	$y = f(t)$	0	-3.7	1731	7972	6.7	0.371	0.18
25	Daily	$y = f(t)$	0	-3.7	1731	6709	6.7	0.730	0.13
26	Daily	$y = f(t)$	0	-3.7	1731	7972	6.7	0.371	0.18
27	Daily	$y = f(t)$	0	-3.7	1731	7972	6.7	0.371	0.18

Notes:
1) Downdrift B.C. for all tests: $y_{imax} = y_{imax-1}$, where $y_{imax} \approx$6500 m (21 nodes) downdrift (west) of fill.
2) Trials 1–26 include $y_c = a \tanh bt$ within the nourished area, with a=-27.20 and b=0.0116 1/days. Trial 27 has y_c=0.
3) For trial 26, length of domain has been doubled by adding nodes downdrift.
4) $y = f(t)$ boundary condition means measured change at inlet was input.

Inclusion of the background erosion term improves the degree of fit between the model predictions and the measured changes. It does not alter the shape of the predicted distribution, but merely adjusts the mean value. Note that the active depth, $(h_* + B)$, and the background erosion rate, $\partial y_B/\partial t$, are closely related, since their product defines the longshore mean value of $\partial Q_x/\partial x$.

For some ranges of variables, the active depth, $(h_* + B)$, exerts a strong influence on K. This prompted further investigation of the nature of the dependency between K and $(h_* + B)$. Figure 5.9 illustrates this dependency for the case of interest by indicating the shape of the "error surface", a contour plot of ε^2 vs. K and $(h_* + B)$. This result indicates that for small values of $(h_* + B)$, the best-fit value for K is very-poorly defined, whereas it is well-defined for large values of $(h_* + B)$. Best-fit results for several combinations of K and $(h_* + B)$ are shown in Figure 5.10.

The relationship between K and $(h_* + B)$ is difficult to predict from the analytical solution (Equation (5.9)). For a given value of K, increasing the active depth, $(h_* + B)$, will reduce the diffusivity, G, and therefore reduce $\partial y/\partial t$. The longshore gradient of longshore transport is then the product of two terms, one increasing and the other decreasing: $\partial Q_x/\partial x = -(h_* + B)(\partial y/\partial t)$.

The method employed to determine the appropriate value for the depth of closure, h_*, in the model may be considered the "standard" definition: the depth beyond which changes are negligible. In reality this merely represents an upper bound for h_*, since it is possible that cross-shore transport is solely responsible for the changes occurring at the offshore limit of the active profile. The depth of closure for modeling the changes induced by longshore sediment transport gradients would have to be reduced for realistic results under this scenario.

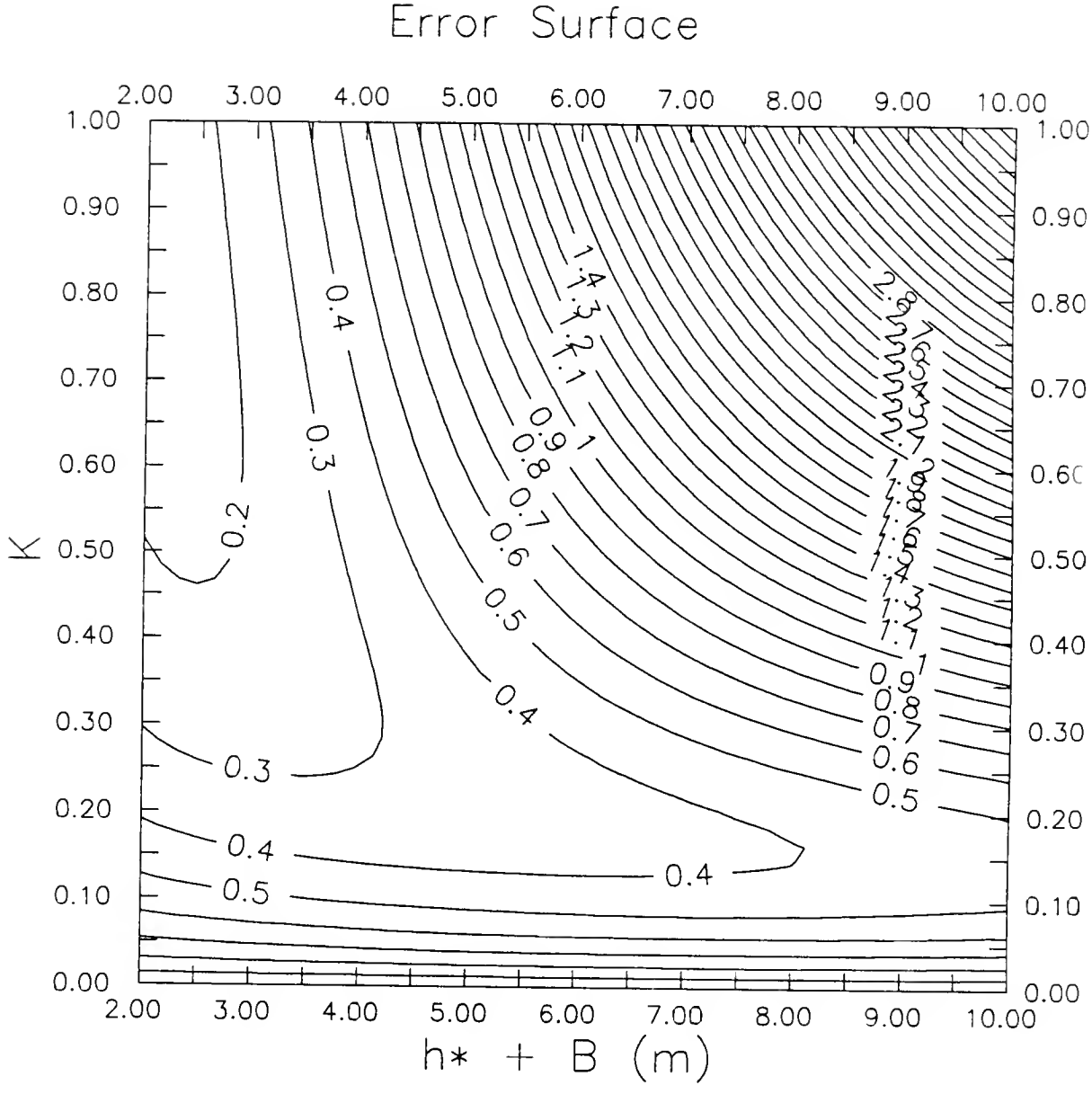

Figure 5.9: "Error surface" indicating error between measured and numerically modeled longshore gradients of longshore transport as a function of K and $(h_* + B)$.

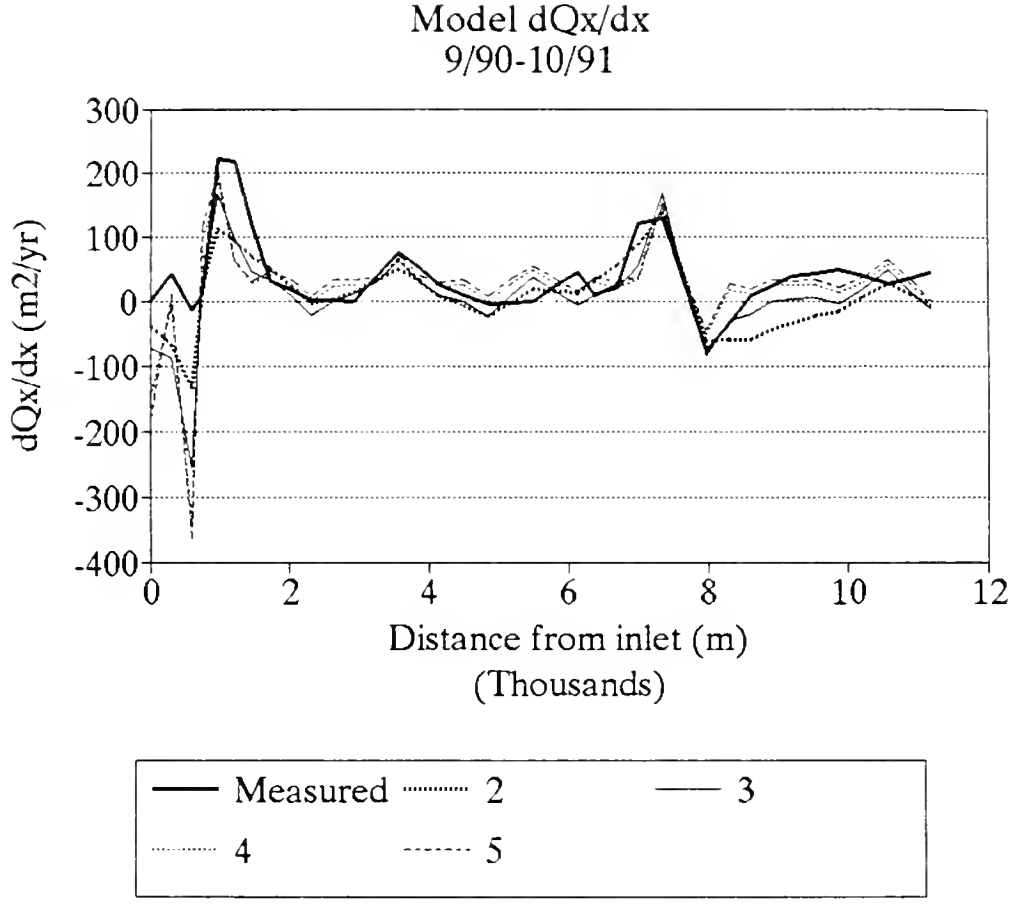

Figure 5.10: Best-fit (mimimum ε^2) results for several combinations of K and $(h_* + B)$. Curve 2: K=1.0, $(h_* + B)$=2; 3: K=0.33, $(h_* + B)$=4; 4: K=0.15, $(h_* + B)$=8; 5: K=0.14, $(h_* + B)$=10. All results include 3.7 m/yr background erosion.

A second approach to the refraction problem was tested to see if inadequate description of the wave climate was influencing the model results. The approach may be considered a "two-line" scheme, since two contours, the waterline and the deepest contour affected by the project, influence the computed sediment transport rates. Unlike the one-line approach, these contours need not parallel each other. The contour defining the limiting depth of motion for longshore sediment transport is assumed to lie in between, and parallels the waterline. With this approach, the offshore contour influences the wave direction, but is not affected by the sediment transport.

Letting h_{*_1} and C_{*_1} denote the depth and celerity, respectively, at the deepest contour of interest, and h_{*_2} and C_{*_2} indicate conditions at the depth of closure, the longshore sediment transport rate resulting from the project may be shown to be:

$$Q = \frac{K E_o C_{G_o} \cos(\beta_o - \alpha_o)}{\rho g (s-1)(1-p)} \frac{C_b}{C_{*_2}} \left[\left(\frac{C_{*_2}}{C_{*_1}} - 1 \right) \beta_{s_1} + \beta_{s_2} - \beta_o \frac{C_{*_2}}{C_{*_1}} \right] \tag{5.36}$$

where β_{s_1} is the orientation of the offshore contour and β_{s_2} that of the waterline.

The results of the two-line approach were not significantly different from the earlier approach, and the ambiguity regarding the depth of closure is still present. Even with this more advanced approach to the refraction problem, the ends of the beachfill are probably the areas where the description of the nearshore wave climate is weakest.

An additional test was made to investigate the effect of longshore variation in the active depth, $(h_* + B)$ on the numerical model results. Rather than a single, representative value for all profiles, a distinct value was determined for each profile and included in the model. Since the longshore variation in this term is significant only near Caucus Shoal, near the updrift limit of the model domain, little change was found.

It is expected that future field measurements, when combined with those presently available, will result in improved confidence regarding the depth of closure for longshore sediment transport. As the profile shape equilibrates, cross-shore sediment transport should assume less importance, and a larger percentage of the changes will be attributable to gradients of longshore sediment transport.

5.8 Discussion of Results

The goal of all the tests described in the previous section was to determine a "best" value for the empirical longshore sediment transport coefficient, K. In Table 5.2, the minimum error between measurements and model, excluding case 18, which included an unrealistically low value of 2 m for $(h_* + B)$, corresponds to cases 14–16, which differ only in their updrift boundary conditions. As mentioned previously, the error definition employed here is affected by the domain chosen for comparison. Cases 14–16 included the large measured changes near Caucus Shoal, which increase the denominator in Equation (5.33). The effect is evident upon comparison of cases 16 and 17, which differ only in the chosen domain for comparison. Discarding cases 14–16 from consideration, case 24 provides the best agreement.

Figure 5.11 presents the best result (case 24) describing the longshore gradient of longshore sediment transport, as modeled by the one-line, numerical scheme. The result for the commonly-used value of K=0.77 is also shown. Results for the first and last time steps in this simulation are shown in Figure 5.12. The gradients of longshore transport are seen to decrease with time as the planform anomaly is "smoothed." The strong gradients near x=0 arise from the boundary condition at the inlet of $y_1 = f(t)$.

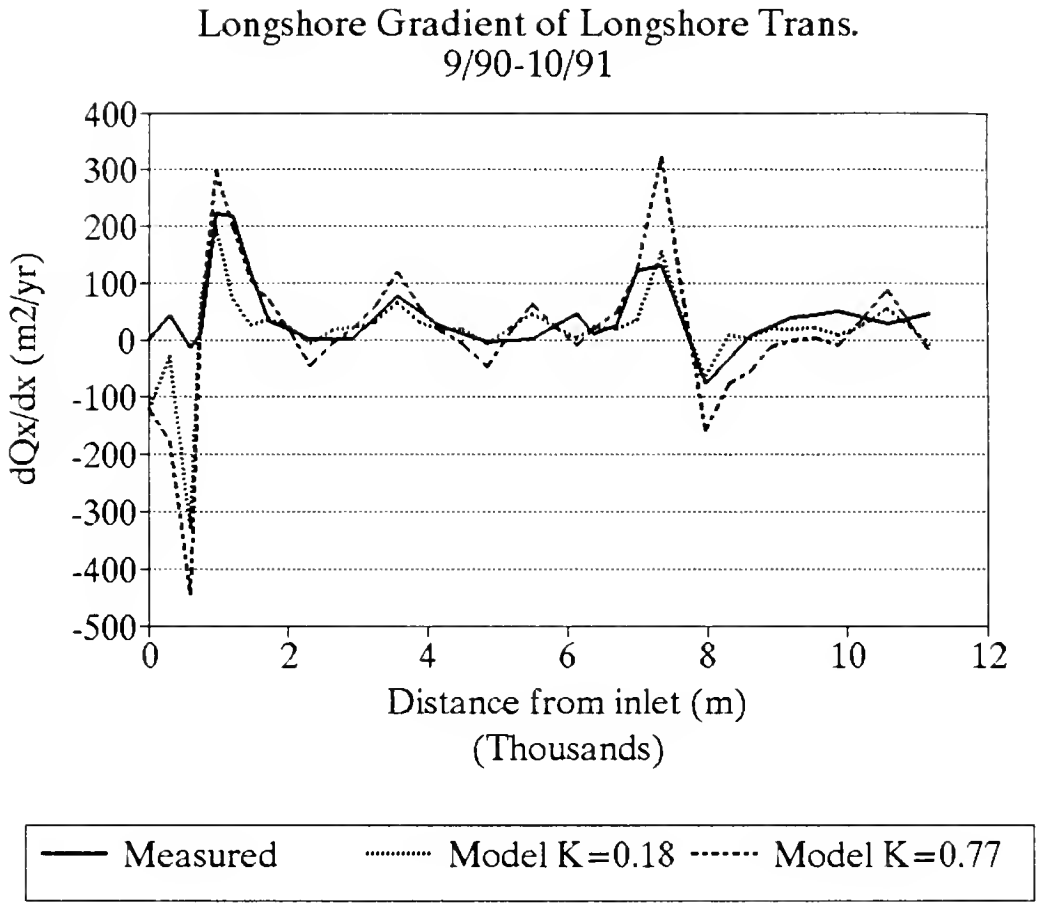

Figure 5.11: Best one-line model results describing longshore gradient of longshore sediment transport, $\partial Q_x/\partial x$.

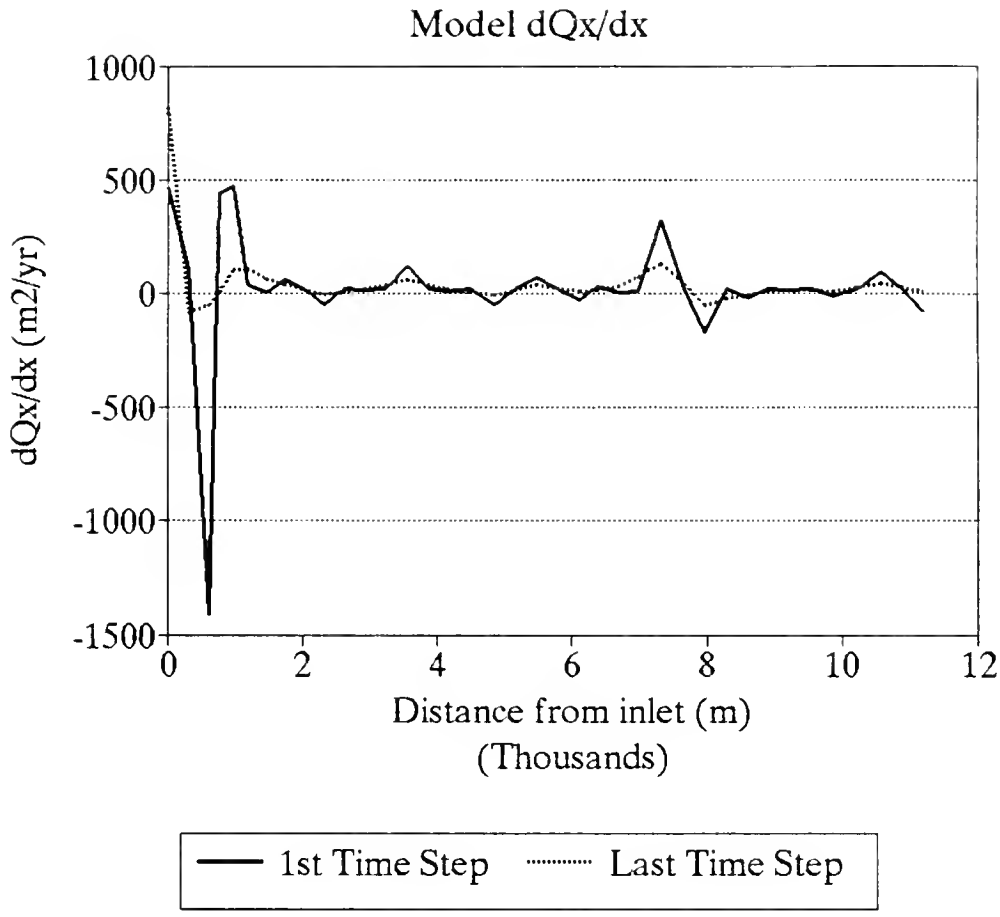

Figure 5.12: Computed longshore gradient of longshore sediment transport for first and last daily time steps in "best" simulation.

The agreement between measured and modeled distributions of $\partial Q_x/\partial x$ is reasonable, with a few notable exceptions. Recalling that a positive gradient of longshore sediment transport implies erosion, it is seen that the maximum erosion, as expected, occurs on the "shoulders" of the beachfill. This trend is in agreement with the analytical solution.

Not surprisingly, the point where agreement is worst is near the inlet and shoal (to the left in Figure 5.11). The model predicts substantial accretion just outside the nourished zone, near Caucus Shoal, while very little is actually observed. The predicted and measured erosion rates on this shoulder of the beachfill are similar, however. Considering that Caucus Shoal lies between the two points defining the predicted switch from erosion to accretion, two explanations of the discrepancy may be advanced. One possibility is that sediment is moving off the shoulder of the beachfill, but not moving as far as the next surveyed profile, therefore appearing as a loss. It could be that sediment is moving as far or beyond the next surveyed profile, but is then slumping into the inlet or being transported away by tidal currents. Because of the sharp change in shoreline orientation, the complicated bathymetry and confused wave climate due to the shoal, and the strong currents and steep slopes associated with the tidal inlet, it is not possible to explain this discrepancy with any certainty.

The width of the erosional features at the shoulders of the beachfill reveals a consistent discrepancy between measurements and model results. The measurements indicate that the "end effect" of the beachfill propagates farther into the planform anomaly than the model predicts. It might be expected that model results would be least accurate where the assumptions implicit in the model are least valid. Wave refraction should be most important at the ends of the nourished area and may be at least part of the cause of the discrepancy. Simple numerical tests conducted to investigate the effects of wave height variation near the ends of the beachfill did not improve the agreement between the measurements and model results. The resolution

of both the survey and the model results would probably have to be improved to fully investigate the behavior in this area.

The erosional zone found at $x = 3600$ m corresponds to the as-built planform anomaly at R-54 (refer to Figure 5.5). This feature would be expected to erode faster than the surrounding area. The discrepancy near $x = 6000$ m is not well understood. Large, cuspate features have been observed in the field during many of the surveys. If a surveyed profile at one time passes across the horn of a cusp, and then at a later time passes through the embayment of a cusp, it will appear that erosion has occurred. Unless very high resolution is maintained by surveying many more profiles in the field, problems such as this must be accepted as contributing noise to the measured signal. Future surveys should help assess the effect of this noise.

Historical shoreline position data provide some information about the background erosion rates existing before the latest beach nourishment project, and suggest that background erosion has accelerated in recent years. Figure 5.13 illustrates the background erosion rate, averaged over more than 80 years, along a large section of Perdido Key. The region near Pensacola Pass which faces the Gulf of Mexico is seen to be eroding most rapidly, and the eastern half of the domain is accreting, leaving a stable point near R35. The mean erosion rate for R35–R60 is 0.73 m/yr. With an assumed active profile depth of 6.7 m based on the recent measurements, the erosion shown in Figure 5.13 corresponds to a loss of 120,000 m^3/yr. Note that this material may be directed either east or west, and the erosion may be affected by bypassing across the Pass or sediment transport into the Pass. The figure and the previous analysis of the wave data appear to indicate that most of the sediment is moving to the west.

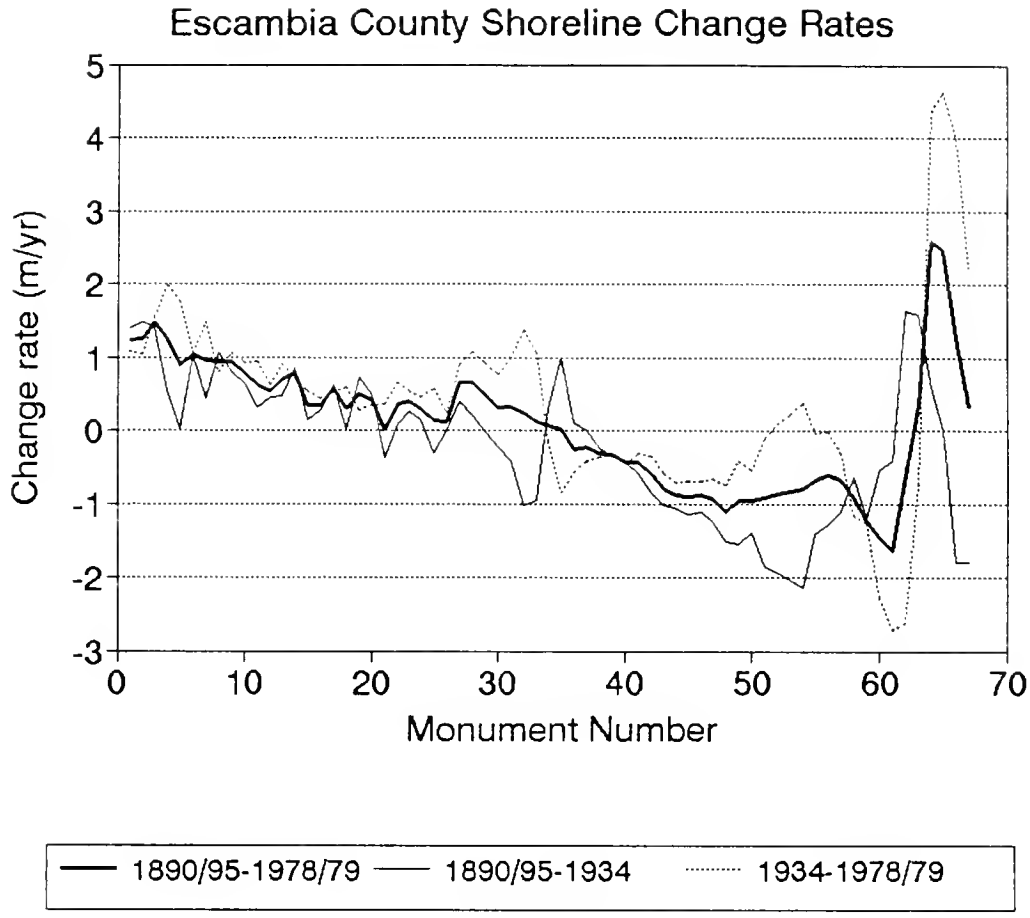

Figure 5.13: Background erosion rate along Perdido Key, based on shoreline positions indicated on historical maps. Pensacola Pass is to right.

Results for 1974–1984 (Dean [1988]) indicate that the stable point previously located at R35 has moved west of R30, and the average erosion rate has increased to nearly 1.5 m/yr. Note that these results are based on shoreline position and may include seasonal effects. The increased erosion rate most likely reflects the enhanced ability of the Pass to trap sediment as a result of dredging.

The background erosion providing the best fit between measurements and model, 3.7 m/yr, is significantly higher than both previous estimates for the same region, but note that this includes the contributions of compaction and eolian transport, which, within the nourished area, would appear as at least 1.3 m/yr of background erosion, depending on the chosen depth of closure. If all sediment west of the updrift shoulder of the beachfill is assumed to move westward, and no sediment is supplied across Pensacola Pass or by the shoal, the remaining background erosion would imply a loss of 160,000 m^3/yr from the monitored area. If losses west of the monitored area are small, as suggested by the historical data, this should be indicative of the net longshore sediment transport rate. Note that this estimate is independent of the depth of closure, since it is based on measured changes in cross-sectional area, and it falls within the range of previous estimates for the area, which vary from 50,000 to 223,000 m^3/yr. The difficulty associated with estimating the net longshore sediment transport rate at a site and the fact that all previous estimates are either not for the same location or are not based on direct measurements may explain some of the variation in the estimates.

The estimated longshore sediment transport rate provides a check on the best-fit value for the empirical parameter, K, determined earlier. The active depth, $(h_* + B)$, need not be considered, since it appears only in the continuity equation. With a longshore transport rate of 160,000 m^3/yr, the best-fit value of K=0.18, and other parameters as given in Table 5.1, the corresponding relative wave direction at the gage location is nearly 30 degrees. For K=0.77, the relative wave direction is six degrees,

which seems much more reasonable. This would support the earlier conclusion that the best–fit value of K=0.18 is a lower bound, and hence $(h_* + B)$=6.7 m is an upper bound. Again, data that become available through future surveys should help resolve this problem.

CHAPTER 6
MODELING CROSS-SHORE SEDIMENT TRANSPORT PROCESSES

Analysis of the field data from Perdido Key indicated that cross-shore sediment transport was the mechanism for much of the early redistribution of sediment after nourishment. The rate of cross-shore change was seen to decay with time as the beach profile shape adjusted to the ambient wave climate. An understanding of the forces driving the cross-shore transport and the resulting profile changes will be important for predicting both the initial response and the long-term beach profile shape.

Historically, attempts to quantify nearshore sediment transport rates, particularly within the surf zone, have been hindered by a limited understanding of the fluid mechanics of this region. The approach adopted in the previous chapter regarding longshore sediment transport was to simplify the problem somewhat by integrating across the entire active profile. The simplification generally invoked in the study of cross-shore sediment transport is the assumption of negligible longshore gradients. Emphasis will also be placed on profiles modified by offshore transport as witnessed in the field after beach nourishment.

An overview of the surf zone processes thought to be important to the problem of beach profile evolution will be followed by a review of previous models for beach profile evolution. This will illustrate some of the difficulties typically encountered and point out some of the limitations of previous approaches. Field data will then be compared to two previous models for beach profile response that have been calibrated for short-term (days) simulations.

6.1 Background

A fully comprehensive model for cross–shore sediment transport in the field must address the effects of the mean and fluctuating velocities throughout the water column, driven by incident waves at many frequencies, with possible interaction between waves of different frequencies. The wave height and water level distributions across the profile must be described, as well as the turbulence and sediment entrainment resulting from wave breaking. Most of these processes have been addressed individually because of the difficulty associated with coupling them.

Computation of the wave height and water level distributions across the surf zone is typically the first step in a model for beach profile evolution. Both monochromatic and spectral models have been developed and tested against laboratory and field data, although suitable field data sets are sparse and difficult to obtain. The simplest monochromatic model is due to McCowan [1894], and states that the ratio of wave height to water depth at breaking is a constant:

$$H_b = \kappa h_b \tag{6.1}$$

The empirical coefficient, κ, is often taken as 0.78. Subsequent studies have related κ to wave period and beach slope (e.g. Weggel [1972]).

Equation (6.1) has seen much use in engineering studies because of its simplicity. It is not directly applicable for computation of wave heights across a barred profile because it will predict an increase in wave height (and energy flux) in the trough.

Dally et al. [1984, 1985] developed a widely–used model for propagation of monochromatic waves across arbitrary bathymetry. Linear wave theory was used to shoal the waves up to a pre–defined breaking condition. Subsequent to breaking, it was assumed that for a given water depth, there is a "stable" wave height that, once attained, will result in no further energy dissipation. Energy dissipation was assumed proportional to the difference between the actual and stable values of the local energy

flux, evaluated using linear wave theory:

$$\frac{\partial EC_g}{\partial x} = \frac{-K}{h}[EC_g - (EC_g)_s] \tag{6.2}$$

Here EC_g and $(EC_g)_s$ denote the actual and stable values of the wave energy flux, respectively, and h is the local mean water depth. The x–axis is directed onshore from an arbitrary origin. The coefficient, K, which bears no relation to the coefficient in the longshore transport equaiton, was evaluated empirically by comparison to laboratory data.

A balance between the onshore component of radiation stress, S_{xx}, and the applied pressure gradient due to wave setup was employed to determine the mean water level $\overline{\eta}$ (Longuet–Higgins and Stewart [1962, 1964]):

$$\frac{\partial \overline{\eta}}{\partial x} = \frac{-1}{\rho g h}\frac{\partial S_{xx}}{\partial x} \tag{6.3}$$

Note that the mean water depth, h, is the sum of the still water depth and the wave setup.

Equation (6.3) is derived from the time–averaged, depth–integrated, horizontal momentum equation and is theoretically well–founded. It assumes that dissipated wave energy is converted instantaneously to heat, so that the local setup gradient is given explicitly in terms of the local radiation stress gradient. Several researchers have suggested that the waves must travel through a "transition zone" extending landward from the breakpoint before exerting any significant influence on the wave setup, an idea which appears to be supported by laboratory measurements (Svendsen [1984a], Basco and Yamashita [1986], Nairn et al. [1990]). This implied "lag" is of importance for sediment transport computations by affecting the local mean water depth, and also suggests that models describing the cross–shore sediment transport in terms of only the local wave height or wave height gradient may be missing an important feature of the surf zone dynamics.

The next level of complexity regarding the wave height and water level distributions across the surf zone involves the description of random wave propagation. Two fundamentally different types of models have been developed. The first approach is probabilistic, assuming a distribution of wave heights at some offshore reference point, and modeling the evolution of this distribution as the waves move onshore (Battjes and Janssen [1978], Guza and Thornton [1983], Battjes and Stive [1985]). The second approach shoals the waves individually to points of interest to allow determination of statistics of the local distribution such as significant or R.M.S. wave height (Dally [1990, 1992]). Details of the two approaches may be found in the cited references.

The surf zone wave energy dissipation models discussed above do not explicitly address the water particle motions forced by the waves. Output from the wave models often serves as input for models of surf zone hydrodynamics. Surf zone flows are commonly decomposed into slowly–varying and fluctuating components:

$$u(x,z,t) = \overline{u}(x,z) + \tilde{u}(x,z,t) + u'(x,z,t) \tag{6.4}$$

where $\overline{u}$ is the mean flow, averaged over several wave periods, $\tilde{u}$ is the organized, fluctuating motion due to the waves, and u' denotes the turbulent fluctuations. The effects of turbulence are usually parameterized by use of an eddy viscosity. Description of the fluctuating component requires selection of an appropriate wave theory, and no consensus has emerged regarding the definition of "appropriate" within the surf zone.

Description of the mean cross–shore flow in the surf zone, often called undertow, is derived from the observations of Dhyr–Nielsen and Sorensen [1970], who noted that there is a local imbalance in the vertical between the applied pressure gradient due to wave setup and the contribution to the onshore component of radiation stress. This implies a torque on the water column and a shoreward flux of mass in the upper portion of the water column within the surf zone. For the two–dimensional

problem (horizontally 1–D), conservation of mass requires a seaward mass flux of equal magnitude in the lower layer.

Dally [1980] developed the first quantitative model for the vertical distribution of the undertow, using linear wave theory. The derivation involves time–averaging the horizontal equation of motion and integrating over the vertical. Selection of appropriate boundary conditions for this problem has been debated at length (Svendsen [1984b], Stive and Wind [1986], Dally and Dean [1986], Svendsen and Hansen [1988]).

One bottom boundary condition that has been applied to the undertow problem is an onshore streaming velocity at the bottom boundary. This was theorized to exist for the case of progressive waves on a flat bottom by Longuet–Higgins [1953], who later suggested that the streaming could be overwhelmed by the undertow inside the surf zone (Longuet–Higgins [1983]). Laboratory measurements suggest that this may indeed be the case (Nadaoka and Kondoh [1982], Hansen and Svendsen [1984], Okayasu et al. [1988]).

Börekçi [1982] gave a detailed description of the vertical structure of the radiation stress, based on linear wave theory, and suggested that the sharp horizontal gradient found at the break point might be important for formation of longshore bars. Several models for eddy viscosity were tested.

Each of the three contributions to the velocity field mentioned to this point could contribute to sediment transport, either as bed load or suspended load. Since bed load transport is driven by the near–bottom flow, and the suspended sediment concentration decays very rapidly with distance from the bed (Hanes [1990]), the near–bed flow is most significant to the sediment transport problem.

Wave breaking will enhance turbulence and induce time–dependent sediment suspension, both inside and outside the surf zone. Sediment in suspension can be advected by all components of the flow until it falls to the bed. The oscillatory flow, which by definition time–averages to zero, contributes if the sediment falls back to the

bed in less than a full wave period. The important quantity is the time average of the vertically–integrated product of the instantaneous horizontal velocity and sediment concentration, which gives the mean flux of suspended sediment, $\overline{q}_s$:

$$\overline{q}_s(x) = \overline{\int_{-h(x,t)+\delta}^{\eta(x,t)} u(x,z,t)c(x,z,t)dz} \tag{6.5}$$

Here $\eta(x,t)$ denotes the water surface elevation, $h(x,t)$ is the still water depth, $c(x,z,t)$ the concentration of suspended sediment, and δ the thickness of the layer in which bed load sediment transport is dominant. Note that the velocity, $u(x,z,t)$, includes all contributions. The fall speed of the sediment is expected to serve as an important parameter in Equation (6.5) by influencing the time required for the sediment to return to the bed, hence controlling the time–dependence in the suspended sediment concentration.

The mean and oscillatory components of the flow can both contribute to transport of sediment as bed load. Bed load transport is often assumed proportional to some power of the difference between actual and critical values of the bed shear stress (commonly non–dimensionalized to yield a Shields parameter), with the actual value determined via a quadratic shear stress relation:

$$\tau_b = \frac{\rho f}{8}\overline{|u_b(t)|u_b(t)} = \frac{\rho f}{8}\overline{|\overline{u}_b + \tilde{u}_b(t) + u_b'(t)|(\overline{u}_b + \tilde{u}_b(t) + u_b'(t))} \tag{6.6}$$

where a subscript "b" indicates evaluation just above the bottom boundary layer and f is an empirical friction factor.

In the case of linear (sinusoidal) waves, the time average of $|\tilde{u}(t)|\tilde{u}(t)$ is zero, but this will not be true for waves that exhibit a skewness about the mean water level. The result is that the oscillatory component of the horizontal velocity beneath nonlinear waves will cause an onshore shear stress. If the undertow does indeed overwhelm the onshore streaming inside the surf zone, then the mean flow will result in a shear stress directed offshore. This may also be true for some distance offshore of the breakpoint.

Table 6.1 summarizes the forces and flows contributing to cross-shore sediment transport described above, with the obvious addition of gravity. Knowledge of the time dependence of each process is important, because the use of time-averaged quantities is preferable for numerical modeling to reduce computation time.

Table 6.1: Forces and flows influencing cross-shore sediment transport.

Force/Flow	Slowly (S) or Rapidly (R) varying	Transport Direction (On- or Offshore)
Gravity/slumping	S	Both; primarily offshore
Nonlinear orbital velocities $u(t)$	R	Onshore
Streaming at bottom	S	Onshore, if present
Mean flow (undertow), $\overline{u}(z)$	S	Offshore (near bed)
Intermittent suspension	R	Both
Advection of suspended sediment	S	Predominantly Offshore
Diffusion of suspended sediment	S	Both
Longshore currents	S	?
Fluid accelerations	R	?

It has been suggested that there is coupling between longshore and cross-shore sediment transport (e.g. Bailard [1981]), which is logical since differences in cross-shore behavior at adjacent profiles will induce longshore bathymetric gradients. This has almost always been assumed negligible in models for beach profile evolution. The effects of fluid accelerations have also been neglected; most researchers have assumed that the sediment responds instantaneously to the fluid velocity, regardless of the acceleration.

Diffusion of suspended sediment is usually neglected. For non-cohesive, sand-sized particles, the importance of diffusive transport relative to advection of suspended sediment or transport as bed load should be quite small.

6.2 Formation of Longshore Bars

The processes that lead to formation of longshore bars are not well understood. Bar formation is generally attributed to either long wave motion or the wave breaking process. Larson and Kraus [1989] gave a thorough review of previous studies regarding bar formation. The wave data collected as a part of this study do not allow verification of a particular hypothesis for bar formation.

Bar formation is a dominant feature of the post-nourishment response at Perdido Key and many other sites. Although there is uncertainty regarding which factors determine the cross-shore distribution of cross-shore sediment transport, some insight may be gained by inspecting different types of distributions and the corresponding profile changes.

Several classification schemes have been proposed for beach profile changes and cross-shore transport distributions (Kajima et al. [1983], Larson and Kraus [1989]). Three of the most commonly observed transport distributions are schematized in Figure 6.1.

Referring back to the transport distributions derived from the "average" profiles based on the field data from the Perdido Key beach nourishment project (Figures 4.26 and 4.27), some conclusions may be drawn. Within the nourished area, some seasonal effects are evident, with onshore transport during periods of lower wave heights, and offshore transport the rest of the time. The dominant behavior is offshore transport. Outside of the nourished area, the signals are much more complicated, indicating both on- and offshore transport, but the strength of the signal is significantly less than within the nourished beach.

A first-order look at the behavior of the bars in the field indicates that the minimum depth over the bar (and similarly, the maximum depth in the trough) is well-correllated with trends in the seasonally-averaged breaking wave height (Figures 6.2 and 6.3). The difference in behavior between the nourished profiles and those

outside of the nourished area indicates that the profile shape is also important. Note that the averaging performed to arrive at Figures 6.2 and 6.3 included all profiles that had distinct bar/trough features. No profiles for the September, 1990, post-nourishment survey met this condition.

A few observations based on the continuity equation (Equation (4.4)), repeated here for reference, aid in interpreting the transport rate distributions.

$$\frac{\partial h}{\partial t} = \frac{\partial q_x}{\partial x} + \frac{\partial q_y}{\partial y} \tag{6.7}$$

Recall that the x-axis is coincident with the waterline and the y-axis is directed offshore for the sediment transport problem. Note that the second term on the right hand side of the continuity equation is simply the gradient of the cross-shore transport distribution. If longshore gradients are zero, then a point in the distribution where the slope is zero implies no net change at the location of the point. A uniform slope over a region implies either uniform erosion (slope>0) or accretion (slope<0) over that region.

Bar formation does not require any singular type of cross-shore transport distribution. It can result from offshore or onshore sediment transport, or a combination of both. In nature, a common scenario is offshore transport during storm conditions, forming a bar, followed by onshore transport as the waves subside, smearing or removing the bar. If a model is capable of simulating the cross-shore transport distributions illustrated in Figures 4.26 and 4.27, it will yield the profile changes observed in the field. The next section will address the ability of existing, available models for beach profile change to reproduce the correct transport rate distributions.

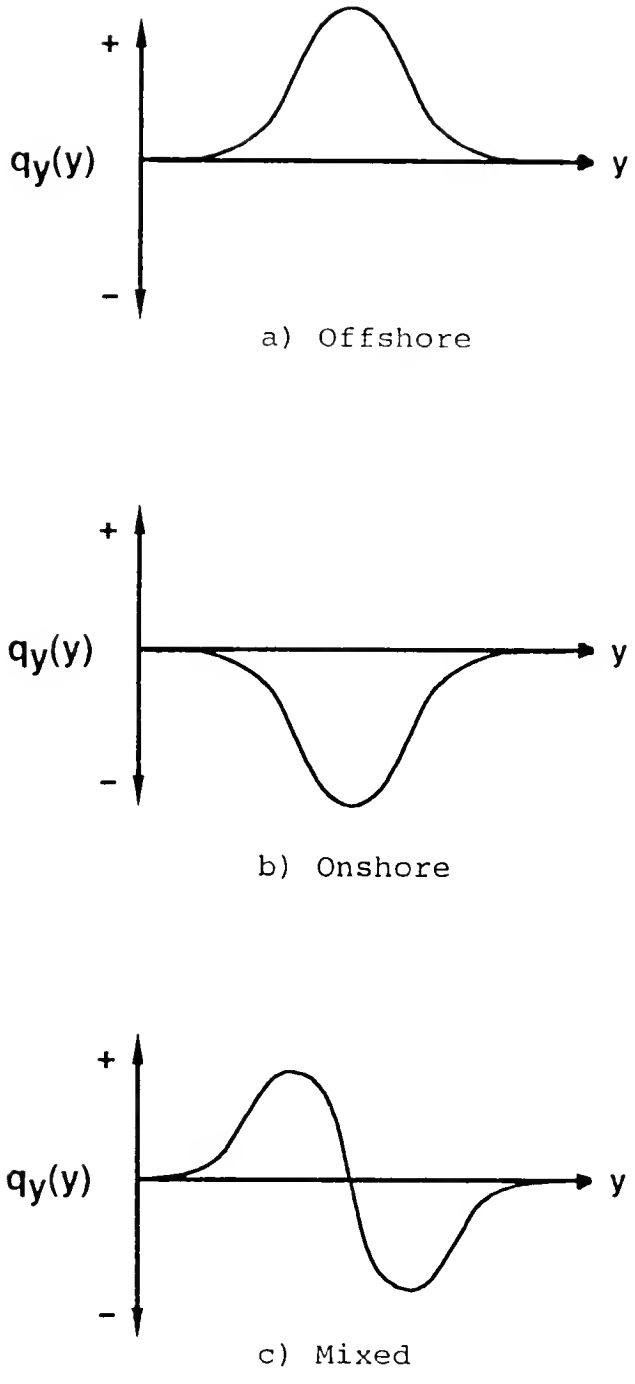

Figure 6.1: Schematic view of three common distributions for the cross–shore sediment transport rate. Note that each distribution has localized zones of accretion and erosion.

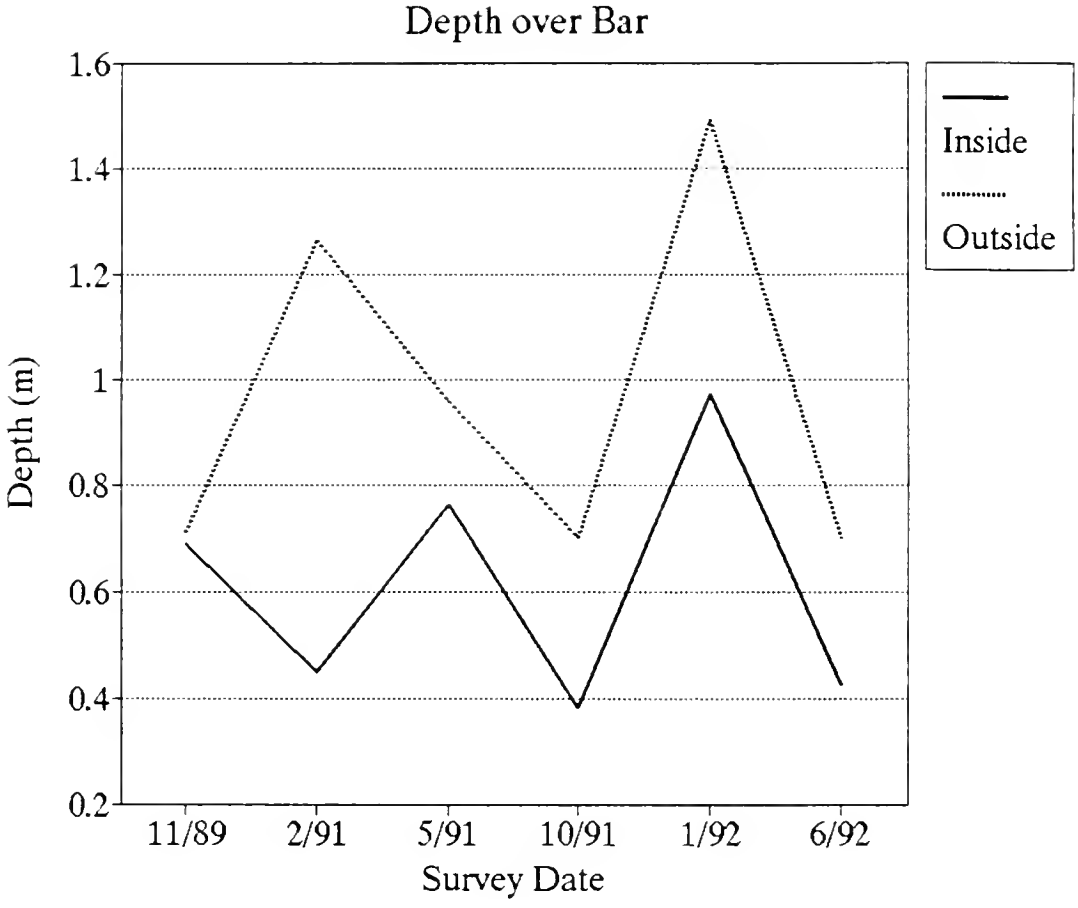

Figure 6.2: Spatially-averaged minimum depth over bar vs. time, in field. "Inside" implies nourished profiles (R41-R64); "Outside" means "natural" profiles (R25-R40).

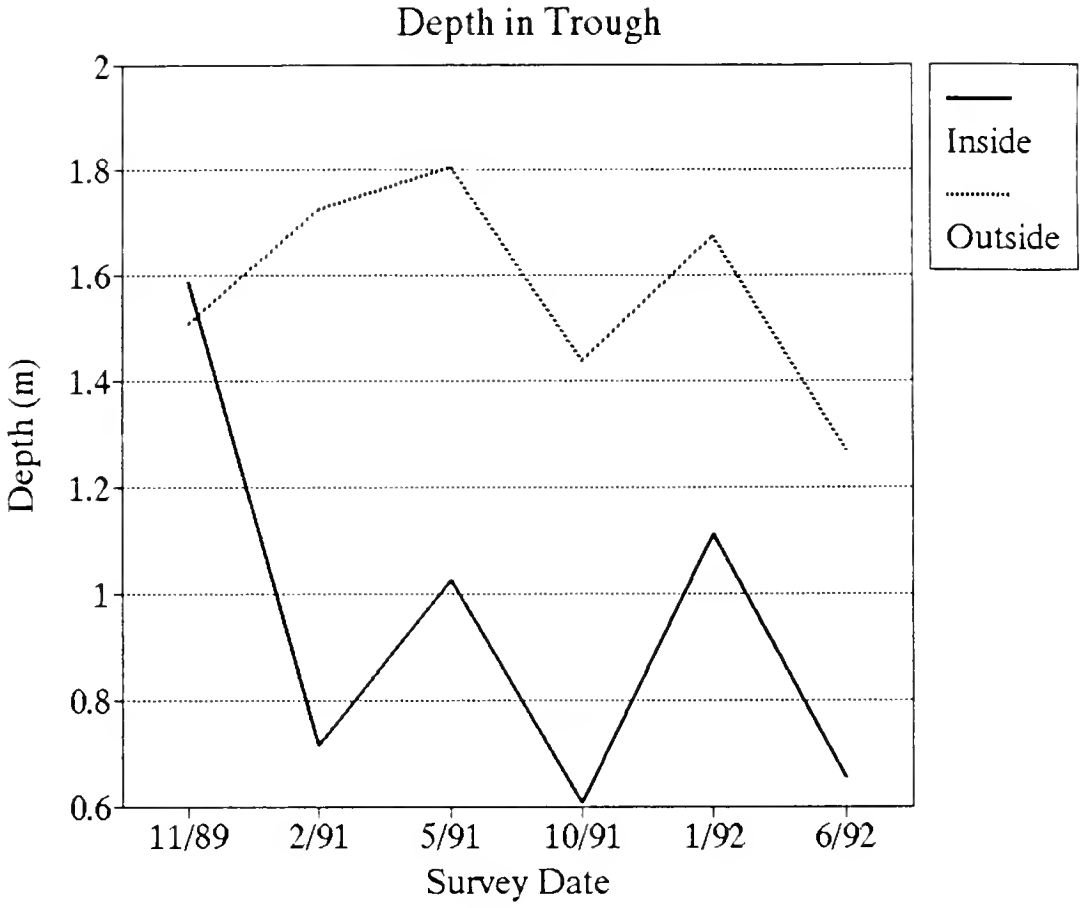

Figure 6.3: Spatially–averaged maximum depth in trough vs. time, in field. "Inside" implies nourished profiles (R41–R64); "Outside" means "natural" profiles (R25–R40).

6.3 Previous Models for Beach Profile Evolution

Many models for beach profile evolution have been proposed, but at present none are considered reliable for quantitative prediction of beach profile evolution. This is particularly true when predictions for longer time periods (months to years) are desired. Inspection of previous models for beach profile evolution will illustrate some of the difficulties associated with the cross–shore sediment transport problem. This is not intended to serve as an exhaustive literature review, but rather as an illustration of the fundamental approaches to the problem of describing beach profile evolution.

Because of the difficulty and uncertainty associated with description of the near-shore flows, several levels of beach profile models have evolved. These will be addressed in order of increasing complexity. Increased sophistication has generally provided more scientific gratification, but has not always led to improved results.

The most fundamental approach is the assumption of an equilibrium beach profile, to which the profile will evolve given sufficient time (Bruun [1954]). The equilibrium beach profile is not explicitly dependent on any wave parameters or surf zone hydrodynamics, but has proven to be a useful concept and is commonly used for engineering assessments. One advantage is simplicity. For a coordinate system with origin at the still water line, one form of the equilibrium beach profile is given by Equation (6.8):

$$h(y) = Ay^{2/3} \tag{6.8}$$

where h is the water depth at distance y offshore. The scale parameter, A, has been evaluated empirically by Dean [1977] and Moore [1982], and demonstrated to be an increasing function of sediment size or, more appropriately, fall speed (Dean [1991]). Equation (6.8) thus reproduces two trends commonly observed in the field by predicting beach profiles that are concave upward, and tend to be steeper for larger sediment sizes. Dean [1977] demonstrated that the 2/3 exponent appearing

in Equation (6.8) corresponds to uniform wave energy dissipation per unit volume across the equilibrium beach profile.

By definition, the equilibrium beach profile hypothesis does not provide any description of beach profile evolution. The concept of the equilibrium beach profile has been used, however, as a "target" profile in time–dependent models. One model to employ this idea was developed by Kriebel [1982], who expressed the cross–shore sediment transport rate as proportional to the degree of disequilibrium:

$$q_y(y) = K[D(y) - D_*] \tag{6.9}$$

Here D and D_* are the local and equilibrium values of the energy dissipation per unit volume, respectively. The coefficient, K, serves as a calibration factor and was evaluated empirically. The local energy dissipation per unit volume (the negative of the onshore gradient of wave energy flux divided by water depth) was evaluated using shallow water, linear wave theory, while the equilibrium value was derived based on the assumption of an equilibrium beach profile, as given by Equation (6.8). A similarity law was employed to describe the wave height envelope within the surf zone ($H = \kappa h$).

The model developed by Kriebel [1982] (see also Kriebel and Dean [1985], Kriebel [1986]) provides a time–dependent description of the beach profile, and accounts for the effects of temporally–varying wave heights and water levels. It has seen a large number of applications, particularly for simulation of short–duration events (i.e. time scale of days) similar to those that were used for calibration. It is computationally robust and relatively easily applied, but simulates only profiles without breakpoint bars. It does not require or include any description of the surf zone velocity field. The a priori assumption of a "target" profile toward which the model evolves results in what has been termed a "closed loop" model.

Larson and Kraus [1989] divided the beach profile into four distinct zones, with the limiting depth for sediment motion, the wave break point, plunge point, onshore limit of wave height calculations, and limit of runup defining the zone boundaries. The sediment transport rate in the broken wave zone was given by Equation (6.9) with the addition of a slope-dependent term; transport rates in the remaining regions were evaluated empirically based on large scale physical model tests. An empirical relation was used to determine the transport direction (on- or offshore), and the sign on the transport equation reversed where appropriate. The breaker decay model of Dally et al. [1984, 1985] was used to describe the wave height distribution. The form of the sediment transport equations outside of the broken wave zone allows simulation of breakpoint bars.

The previously described models for beach profile evolution did not explicitly address the hydrodynamics of the surf zone, and thus predicted the total sediment transport rate, without subdivision into bed load and suspended load fractions. Dally [1980] (also Dally and Dean [1984]) considered sediment entrained into the water column by wave breaking, resulting in a concentration of suspended sediment that decayed exponentially with vertical distance from the bed. Advection of the suspended sediment by both the mean and fluctuating components of the fluid motion was described by results derived from linear wave theory. Considerable smoothing of the calculated cross-shore suspended sediment transport distribution was required to provide stable model results. The model allowed formation of breakpoint bars but did not stabilize given constant forcing. Transport of sediment as bed load was not included.

Models have been developed recently that include detailed descriptions of the hydrodynamics of the surf zone and consider the transport of sediment both as bed load and suspended load. Two recent examples (Roelvink and Stive [1989], Nairn [1992]) employ the so-called "energetics" approach as given by Bailard [1981], which

is based on the approach for uni-directional flow due to Bagnold [1963] for description of the sediment transport rates in terms of the velocity field. The higher moments of the horizontal velocities that must be evaluated to employ this approach make accurate description of the surf zone hydrodynamics critical.

The variety of approaches to the description of cross-shore sediment transport serves as an indication of the difficulty of the problem. Field conditions present the most formidable problem by including random waves, tides, longshore currents, etc. Seymour and King [1982] investigated eight models for the prediction of cross-shore sediment transport and compared the predictions to field data collected during the Nearshore Sediment Transport Study at Torrey Pines Beach, California. Measured transport rates were based on short-term changes appearing in surveyed beach profiles between the +2 and -1 m contours, relative to the mean sea level. The best model predictions were based on wave energy, power, or steepness, but none of the models were able to predict more than a third of the variance in the time history of the measured changes in beach volume.

Unfortunately the state-of-the-art for numerical modeling of beach profile evolution still contains a high degree of "art." Most models require empirical smoothing of the computed wave height envelope, the cross-shore sediment transport distribution, or the bathymetry. Simulations rarely exceed the time scale of a storm (i.e. hours to days).

6.4 Desired Characteristics of a Beach Profile Model

There are some general requirements which any model for beach profile evolution should satisfy. It should be physics-based and include a sufficient level of detail to resolve the behavior of interest. It should respond appropriately to all the parameters thought to govern the behavior: wave height, period, water level, sediment size, etc. Both erosion and recovery should be simulated, and mid-scale morphological features such as bars and berms must also be included. Subjected to constant forcing, the

model should approach a quasi-equilibrium condition, as is commonly witnessed in laboratory studies, although it is desired to avoid specification of this "target" profile a priori. Computationally, the model should be robust, easy to apply, and fast, attributes which are often at odds with the other requirements. Sediment should obviously be conserved.

A nourished beach represents a good test case for models for beach profile evolution, since the initial profile is typically very steep, resulting in strong offshore sediment transport. When attempting to model beach profile evolution in the field over a long time period (months to years), the available data and desired level of detail to be included in the model must be considered carefully. The approaches described in the previous section were each evaluated to determine their suitability to the problem at hand.

The field data available at the Perdido Key site immediately impose some restrictions that rule out some of the approaches to beach profile modeling. Since the elapsed time between surveys averages 3–4 months, during which incident wave conditions vary widely, the model must be very stable numerically. The lack of data regarding the nearshore hydrodynamics suggests the use of a simpler approach which will not require calibration of terms describing the surf zone velocities. Despite the availability of spectral wave data, a monochromatic description is desired, both to reduce computational requirements and because of insufficient justification for the addition of more terms and calibration factors in the model.

Considering the variability in the forcing terms between surveys at the field site, and the fact that beach profile changes have been observed at depths as great as five meters, despite mean wave heights an order of magnitude smaller, it should be expected that both suspended sediment transport and bed load transport are governing the response. The steep slopes and offshore transport to fairly large depths also suggest that gravity is an important forcing term.

In light of the aforementioned requirements and limitations that must be considered to model the long-term profile evolution at a nourished beach, the models proposed by Kriebel [1982] and Larson and Kraus [1989] represent the most suitable of the existing approaches. They are both based on the premise that there is an equilibrium profile that will result if constant forcing is applied for a sufficient time, and that the cross-shore sediment transport rate is proportional to the degree of disequilibrium. Both have been calibrated against several data sets and yielded reasonable results for short-term simulations.

6.5 Cross-shore Transport Rate vs. Dissipated Wave Energy

The fundamental equation in both the models of Kriebel [1982] and Larson and Kraus [1989] (slightly modified) is Equation (6.9), which states that the local cross-shore sediment transport rate is proportional to the difference between the local and equilibrium values of energy dissipation per unit volume. It is thus of interest to investigate the correlation between the energy dissipation per unit volume and the cross-shore sediment transport rate across the beach profile. Large-scale wave tank data are well-suited to this problem, since the wave conditions may be assumed nearly constant between the surveys that will be used to compute the sediment transport rates.

Both of the models under consideration have been calibrated against the large-scale wave tank data collected by Saville [1957] (tabulated in Kraus and Larson [1988]) and selected field data sets describing storm events. The wave tank data include beach profile surveys at selected times and breaking wave heights and locations. Several combinations of incident wave height and period were chosen and tested with two different sediment sizes, resulting in the formation of both bar and berm profiles. The initial condition for most tests was a planar beach with a slope of 1 on 15. Larson and Kraus [1989] also employed a more recent data set from a large wave

tank in Japan, which differs primarily by including a description of the wave height distribution across the profile.

The importance of Equation (6.9) in both models prompted some investigation of the relationship between energy dissipation and cross-shore sediment transport rate. Of the 19 tests in the large wave tank reported by Kraus and Larson [1988], six cases (300, 400, 500, 401, 501, 901) were chosen that each started from a planar slope, included breaking wave height data, and exhibited dominant offshore transport. Wave data for one case (501) appeared suspect, leaving five cases for investigation.

For each selected case, the cross-shore sediment transport rate was computed by integrating the profile deformations occurring between two consecutive surveys across the profile using Equation (4.6). A uniform vertical adjustment was applied to the latter of the two surveys to force the transport rate to zero at the offshore limit of the surveys, where necessary. In each case there was a rapid initial decrease in the maximum sediment transport rate, which eventually decayed to a small but finite value, in general agreement with the premise that the response is proportional to the degree of disequilibrium. Figure 6.4 illustrates the temporal decay of the transport rate for one case. Note that this behavior is at least qualitatively similar to results derived from the field measurements (Figure 4.26), although recovery was observed in the field for some time intervals.

Two approaches to the energy dissipation were considered for comparison to the measured cross-shore transport rates. The first considered energy dissipation in a gross sense, by examining the correlation between the energy flux at breaking divided by the surf zone area (or volume per unit width) and some measure of the observed cross-shore sediment transport rate. The second approach investigated the correlation between the local values of the energy dissipation and cross-shore sediment transport rate.

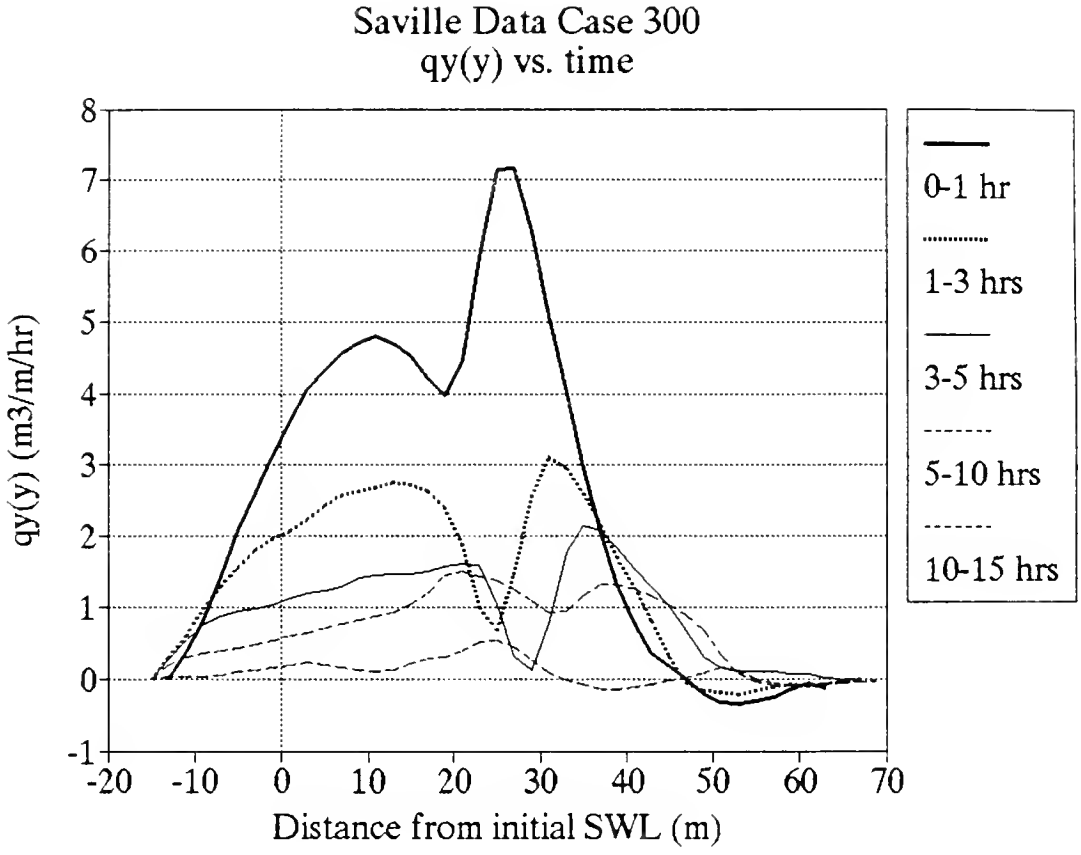

Figure 6.4: Decay of cross–shore sediment transport rate with time, based on surveys in large wave tank. (Case 300, Kraus and Larson [1988]).

Energy dissipation was computed using the monochromatic model developed by Dally et al. [1984, 1985]. The bathymetry used to compute the wave height envelope was in each case an average of the two surveys defining the time interval of interest. This approach does not address the previously discussed lag between the onset of wave energy dissipation and the sign change on the setup gradient.

Figure 6.5 illustrates the correlation between the total wave energy dissipation and the average cross-shore sediment transport rate within the surf zone for the cases selected from the large wave tank data reported by Kraus and Larson [1988]. Note that the points plotted in this figure include a range of incident wave conditions and two sediment sizes. If Equation (6.9) is valid, and the empirical transport coefficient K not dependent on wave conditions or sediment properties, then each case should fall on a straight line of slope K in Figure 6.5. A different sediment size should shift the curve laterally by modifying the energy dissipation required to initiate transport.

The case designation employed for the large wave tank data in Figure 6.5 indicates both wave conditions and sediment size. The first digit denotes wave conditions and the last digit signifies sediment size. Thus cases 400 and 401 have the same incident wave conditions, but different sediment sizes (0.22 mm and 0.40 mm, respectively). It appears that the larger sediment size does indeed increase the level of energy dissipation required to initiate cross-shore transport. Because of scatter in the data, however, it is difficult to determine the slope of each curve or even assess whether each is linear. Four of the five cases indicate that the average transport is initially higher than would be estimated by a best-fit line through the points describing each case.

A similar comparison may be made using the data collected in the field describing the evolution of the nourished profiles. The results are rather speculative because of the limited number of data points and the wide variation in the wave climate over the time period describing the profile changes. Data were available for three inter-survey

periods that showed dominant offshore transport after nourishment. The average profiles described in Chapter 4 were chosen for analysis on the premise that most longshore effects have been averaged out.

For each chosen interval, the effective breaking wave height and temporally–averaged profile were determined. This allowed estimation of the temporally–averaged energy dissipation and transport rates. Results are shown in Figure 6.6. Note that this approach implies both spatial and temporal averaging. Average transport rates computed for the field intervals are two orders of magnitude smaller, but at least show the same trend as the laboratory data. The discrepancy may be considered a by–product of the long time interval employed in the computations for the field conditions, when the wave climate varied widely and transport was likely minimal for many sub–intervals.

The second investigation of the relationship between cross–shore sediment transport rates and energy dissipation per unit volume removed the spatial integration of the first approach. The wave model employed allows computation of the local value of the energy dissipation per unit volume, and this has been plotted in Figure 6.7 against the local cross–shore sediment transport rate for one of the five large wave tank data sets selected previously. Similar results were obtained for the remaining wave tank tests. Analogous results for the three intervals in the field exhibiting offshore transport are shown in Figure 6.8. Both figures reveal two distinct zones where behavior differs. In each case, the zone corresponding to higher levels of wave energy dissipation per unit volume is derived from calculations within the surf zone, while the zone to the left in each figure corresponds to offshore transport occuring seaward of the breakpoint.

Figures 6.7 and 6.8 suggest that the energy dissipation per unit volume is an important parameter influencing the cross–shore sediment transport rate for cases exhibiting offshore transport, but that the assumed linear relationship between the

two may not be totally appropriate. Some consideration was given to determining an appropriate nonlinear relationship between the cross-shore transport rate and the energy dissipation per unit volume, such as given below:

$$q_y(y) = K[D(y) - D_*]^n \tag{6.10}$$

Because of scatter in the data, however, this quickly degenerated to an unproductive exercise in curve-fitting.

The hypothesis that the cross-shore transport rate is proportional to the excess energy dissipation per unit volume appears to have merit. Based on previous studies and the results presented here, however, it seems best suited for prediction of volumetric changes since individual features of the profile are poorly described. For engineering situations, volumetric changes and the movement of the waterline are usually of primary interest.

6.6 Previous Models Compared to Field Data

Since the primary goal was to model the evolution of the nourished profiles, the "average" profiles after nourishment were chosen as the basis for comparison for the tests of the beach profile models. The model developed by Kriebel [1982], with minor modifications, was tested first against a calibration run reported by Kriebel [1986] to assess the need for re-calibration after modification. The primary modification introduced was intended to provide a more realistic finite slope at the still water line, rather than the infinite slope predicted by Equation (6.8). This change alters the form of the equilibrium beach profile and hence the sediment transport equation:

$$q_y(y) = K\left[D(y) + \frac{D_*}{m}\frac{\partial h}{\partial y} - D_*\right] \tag{6.11}$$

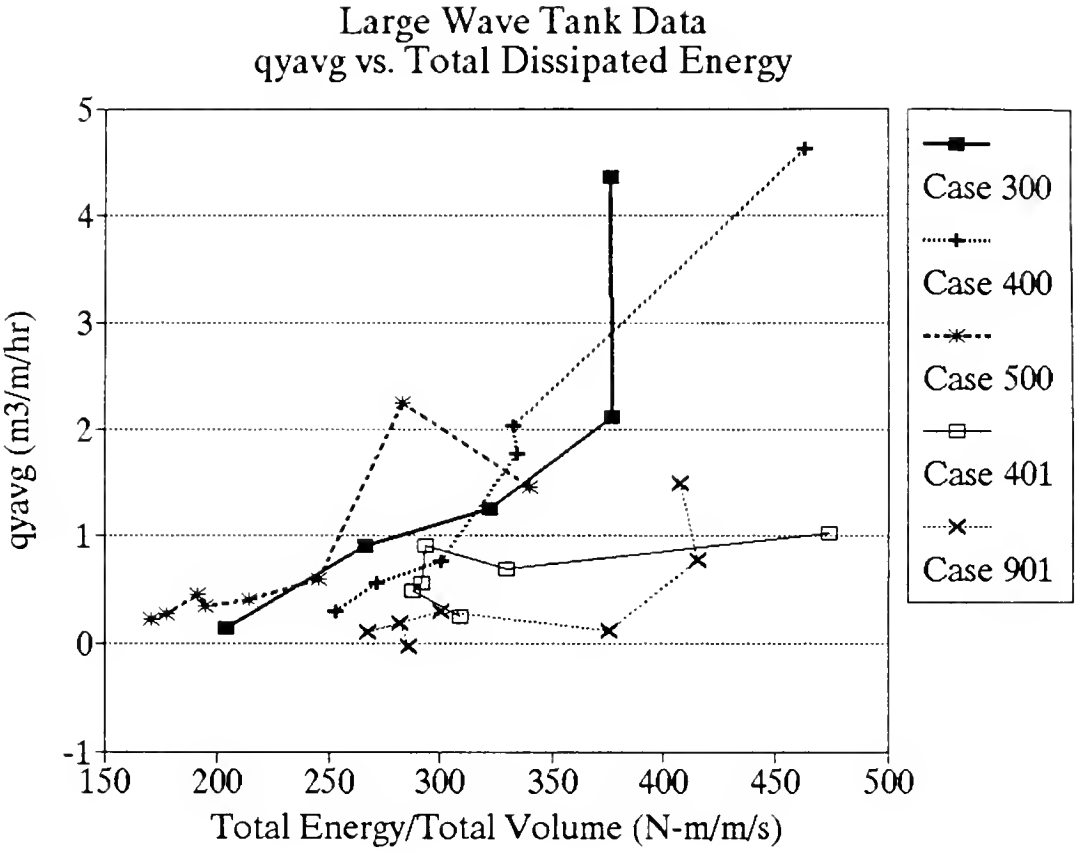

Figure 6.5: Total energy dissipated divided by surf zone volume, plotted against average cross-shore transport rate within surf zone for large wave tank data. Points are connected chronologically, with the maximum transport rate in each case corresponding to the first survey interval.

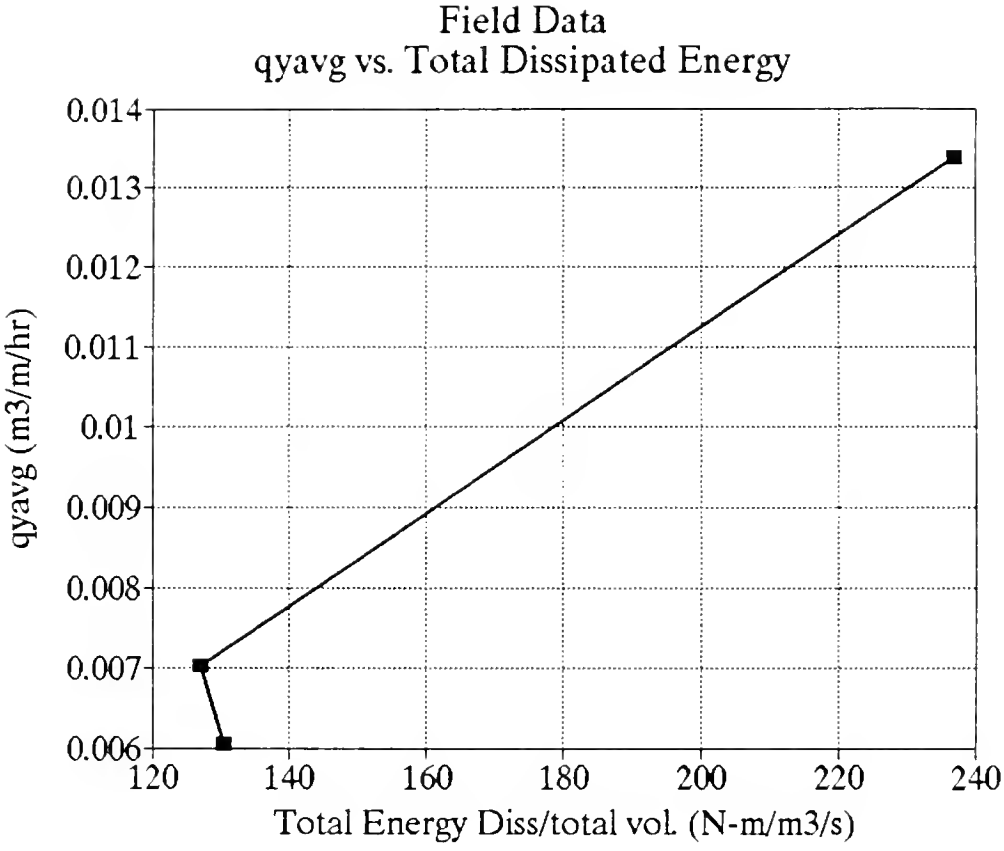

Figure 6.6: Total energy dissipated divided by surf zone volume, plotted against average cross-shore transport rate within surf zone for field data.

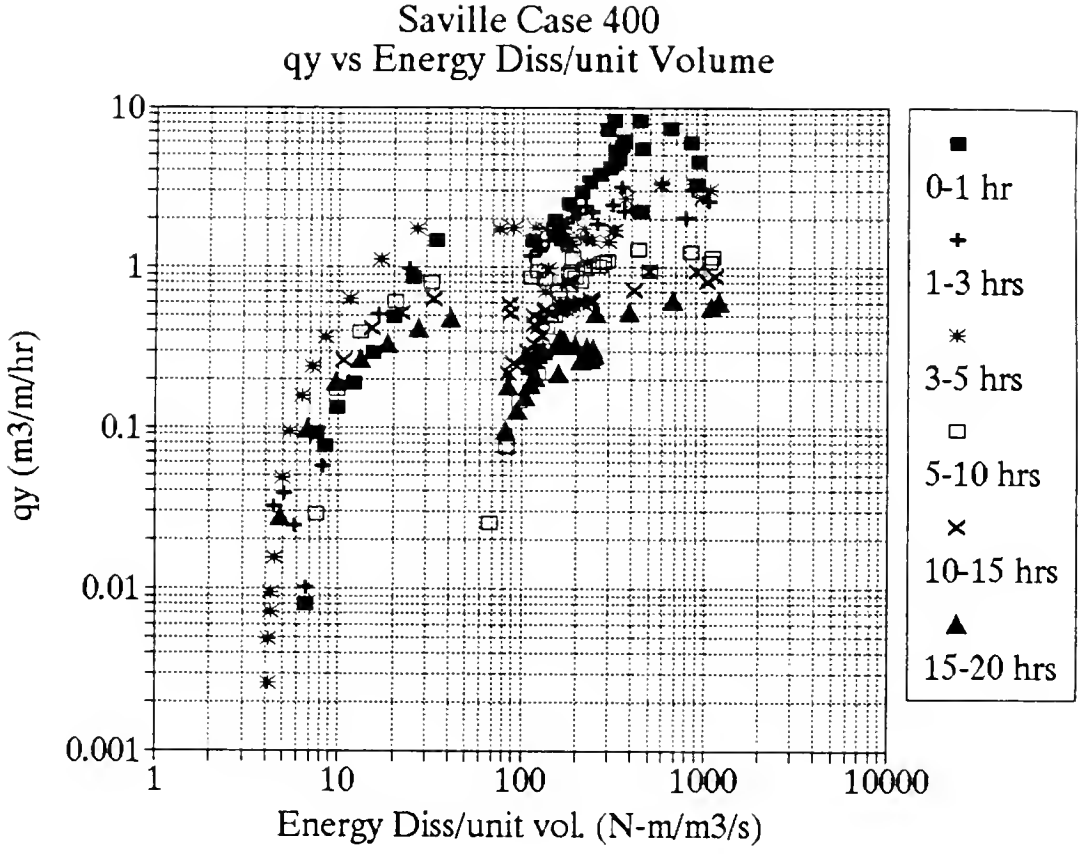

Figure 6.7: Local cross–shore sediment transport rate vs. local energy dissipation per unit volume for one large wave tank case. Results for other cases exhibiting offshore transport similar.

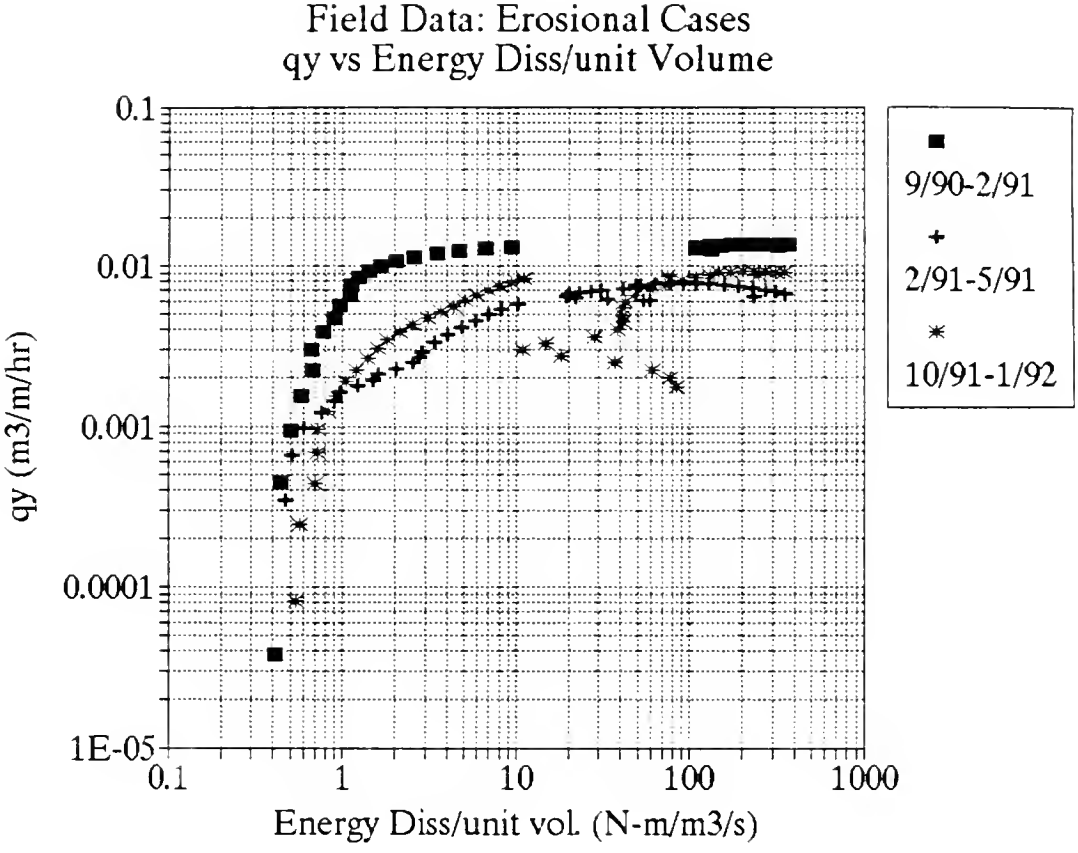

Figure 6.8: Local cross-shore sediment transport rate vs. local energy dissipation per unit volume for selected intervals in the field.

where m is the beachface slope. This implies that both the energy dissipation per unit volume and gravity influence the equilibrium profile by acting as destabilizing forces. The equilibrium beach profile will thus have a slightly milder slope. Note that the added term in the transport equation should be expected to affect the model calibration, since $\frac{1}{m}\frac{\partial h}{\partial y} \sim O(1)$ near the waterline. The modification incorporates the influence of gravity through the addition of only one adjustable parameter, the beachface slope, m, which is readily estimated.

Setting $q_y(y) = 0$, Equation (6.11) may be integrated to solve for the resulting equilibrium profile (Dean [1991]):

$$y = \frac{h}{m} + \frac{1}{A^{3/2}} h^{3/2} \tag{6.12}$$

where the scale factor, A, is expressed in terms of the equilibrium value of the wave energy dissipation per unit volume, as before:

$$A = \left[\frac{24 D_*}{5 \rho g^{3/2} \kappa^2} \right]^{2/3} \tag{6.13}$$

and D_* varies with sediment characteristics. Note that the shallow and deep water asymptotes for this form of the equilibrium beach profile are $h = my$ and $h = Ay^{2/3}$, respectively.

Using shallow water, linear wave theory, and assuming that the ratio of wave height to water depth is constant within the surf zone, Equation (6.11) may be rewritten:

$$q_y(y) = K \frac{5}{24} \rho g^{3/2} \kappa^2 \left[\frac{\partial h^{3/2}}{\partial y} + A^{3/2} \left(\frac{1}{m} \frac{\partial h}{\partial y} - 1 \right) \right] \tag{6.14}$$

The resulting form of the sediment transport equation is fundamentally the same as that employed by Larson and Kraus [1989], although the coefficient in front of the slope term has been related to physical quantities.

Kriebel [1986] reported a test against one of the large wave tank experiments of Saville [1957]. The test is repeated here in Figure 6.9, using a best-fit calibration factor of 1.1×10^{-6} m^4/N, to illustrate the influence of the additional term in the sediment transport equation. As anticipated, the slope term results in milder slopes within the surf zone, which in this case also implies enhanced offshore transport. The numerical solution scheme employed is a double-sweep, implicit formulation, following Kriebel and Dean [1985], although a modification has been introduced to allow specification of boundary conditions in terms of either transport rates or contour positions. The R.M.S. error as a function of the transport coefficient, K, is plotted in Figure 6.10.

The solution scheme divides the profile into three distinct zones. Sediment transport in the zone of broken waves is governed by Equation (6.14), and it is redistributed offshore of this zone by a geometric control. Avalanching at the onshore limit of the profile similarly is governed by a geometric argument.

Ideally, one would include tests under many conditions to determine the best-fit calibration factor, K, and consider its dependence on other parameters. This was done using the same basic governing equation by Larson and Kraus [1989], who found that the best-fit calibration value ranged from $0.3\text{–}2.2 \times 10^{-6}$ m^4/N for wave tank data, and recommended an overall best value of $K = 1.6 \times 10^{-6}$ m^4/N. The best-fit value for four field simulations was found to be 0.7×10^{-6} m^4/N. Also note that with $K \sim O(10^{-6})$, $D_* \sim O(10^2)$, and $m \sim O(10^{-1})$, the resulting coefficient in front of the slope term is $O(10^{-3})$, in agreement with the results of Larson and Kraus [1989].

A comparison was made against beach profile data from the field for each inter-survey period after beach nourishment for which transport was dominantly offshore, and one interval exhibiting onshore transport. Comparison to the field data introduces an additional problem, since the longshore gradients of longshore sediment transport ($\partial q_x / \partial x$) that are present result in a net change in cross-sectional area.

The magnitude of the change is known and is small for each case when the average profiles are used as the basis for comparison. This implies that the manner of accounting for longshore effects will not be important. It was therefore assumed that this contribution was distributed uniformly across the active profile so that the entire profile could be translated uniformly.

Comparisons of the modified Kriebel model results to the field data are shown in Figures 6.11 through 6.14. The effect of the tide is also illustrated in the first comparison. Measured wave data have been used to describe the forcing in each case. Tidal effects have also been included in each simulation. The chosen value of A=0.13 $m^{1/3}$ represents the best-fit to the pre-nourishment average profile and agrees well with the predicted value based on the sediment size.

The results of the model simulations are reasonably good for two of the three cases exhibiting offshore transport and slightly poorer for the third. The primary disagreement is in the shape of the active profile. The model predicts the concave-upward shape dictated by Equation (6.8), whereas the profiles in the field are for each case concave-downward over this region. This may be indicative of profile recovery at the time of the latter survey, but cannot be resolved because of the large time period between surveys. The case including onshore transport in the field is not predicted well by the model, which predicts offshore transport over this interval.

Best-fit transport coefficients for the field simulations are smaller for three of the four simulations than values determined from wave tank tests. The error for the one case (2/91-5/91) yielding a larger coefficient is relatively insensitive to the chosen coefficient, as illustrated in Figure 6.15. Since the transport coefficient, K, primarily affects the time scale of the response, this implies that the model is in a near-equilibrium condition by the end of the simulation.

It should also be noted that nearly two-thirds of the active profile for each simulation is governed purely by geometrical considerations. The assumption of linear

beach profile slopes bordering each end of the active profile yields good agreement, but the slopes will vary with time and must be described to use the model in a predictive fashion. Figure 6.16 shows the average on- and offshore slopes measured in the field after beach nourishment. It is seen that within five months after nourishment, both slopes had decreased almost to their pre-nourishment values. Since that time they show primarily seasonal changes.

Simulations of changes occurring over longer time periods than illustrated here were largely unsuccessful. It is clear that profile recovery (onshore sediment transport) is inadequately described by this approach, and the accuracy of long-term simulations will remain poor until profile recovery is satisfactorily modeled.

The beach profile response model developed by Larson and Kraus [1989], provided to the author by the U.S. Army Corps of Engineers, Coastal Engineering Research Center, in the form of a compiled, interactive program known as "SBEACH", was also tested against the field data from Perdido Key. As discussed previously, the model employs the same primary equation governing the magnitude of the cross-shore sediment transport rate as the previous model, within the zone of broken waves. The SBEACH model includes some important differences, however, such as a more realistic description of the distributions of wave height and water level across the profile and the capability to describe the evolution of breakpoint bars. Another difference that will be important for interpretation of the results to follow regards the determination of the direction of the cross-shore sediment transport.

Many researchers have attempted to determine a dimensionless combination of wave and beach parameters to serve as a predictor of erosion or accretion. The most frequently appearing parameters are deep water wave height, steepness (H_o/L_o), beach slope, sediment diameter, and sediment fall speed. Larson and Kraus [1989] empirically determined an expression that appeared to provide good delineation between erosion and accretion in both field and large wave tank situations:

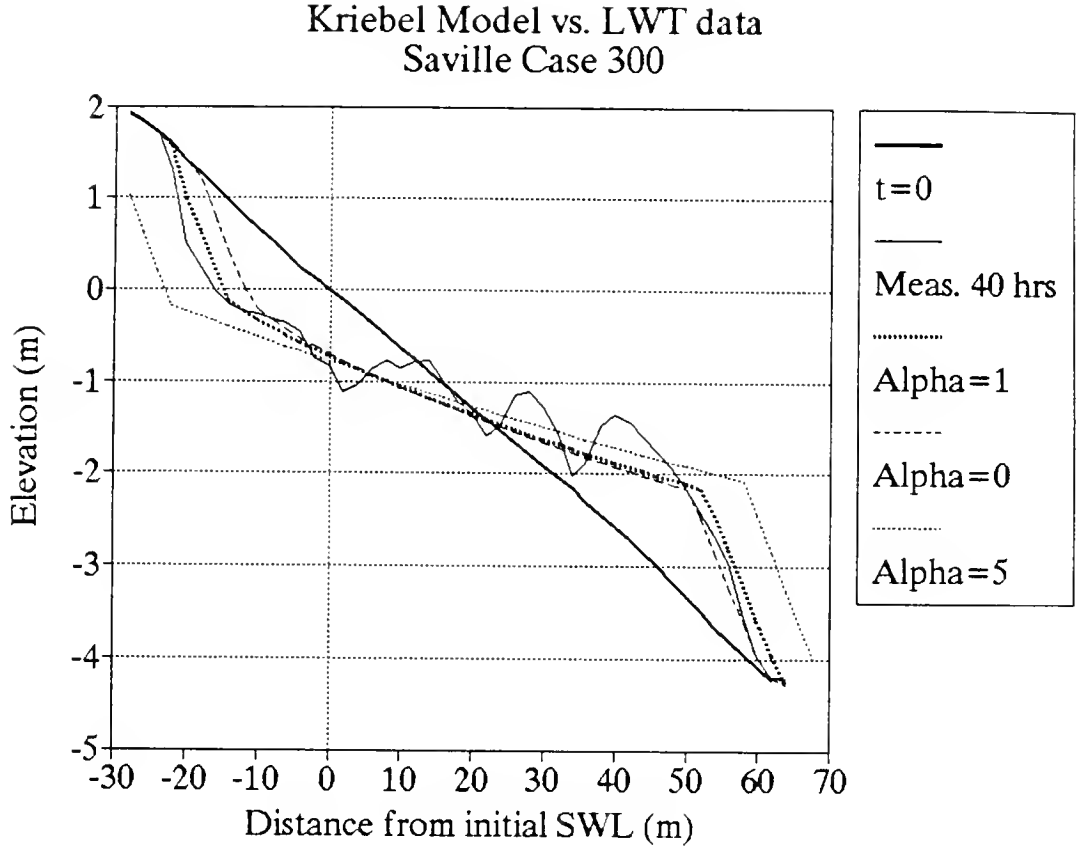

Figure 6.9: Influence of slope term in modified Kriebel model for selected large wave tank test. H_b=1.68 m, T=11.33 sec., D=0.22 mm, A=0.10 $m^{1/3}$, K=1.1x10^{-6} m^4/N. "Alpha" is the coefficient in front of the slope term in the transport equation. Calibration factor, K, chosen to yield best fit for α=1.

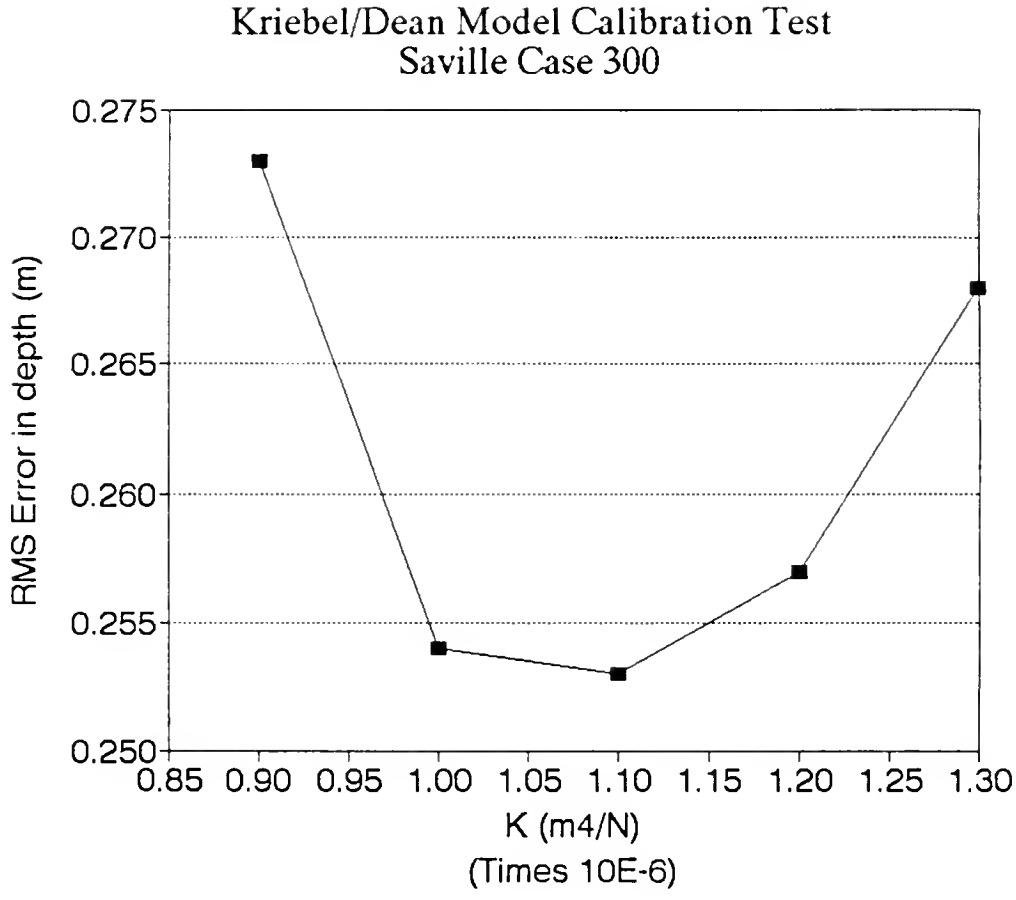

Figure 6.10: R.M.S. error in depth as a function of transport coefficient, K, for large wave tank case illustrated in Figure 6.9.

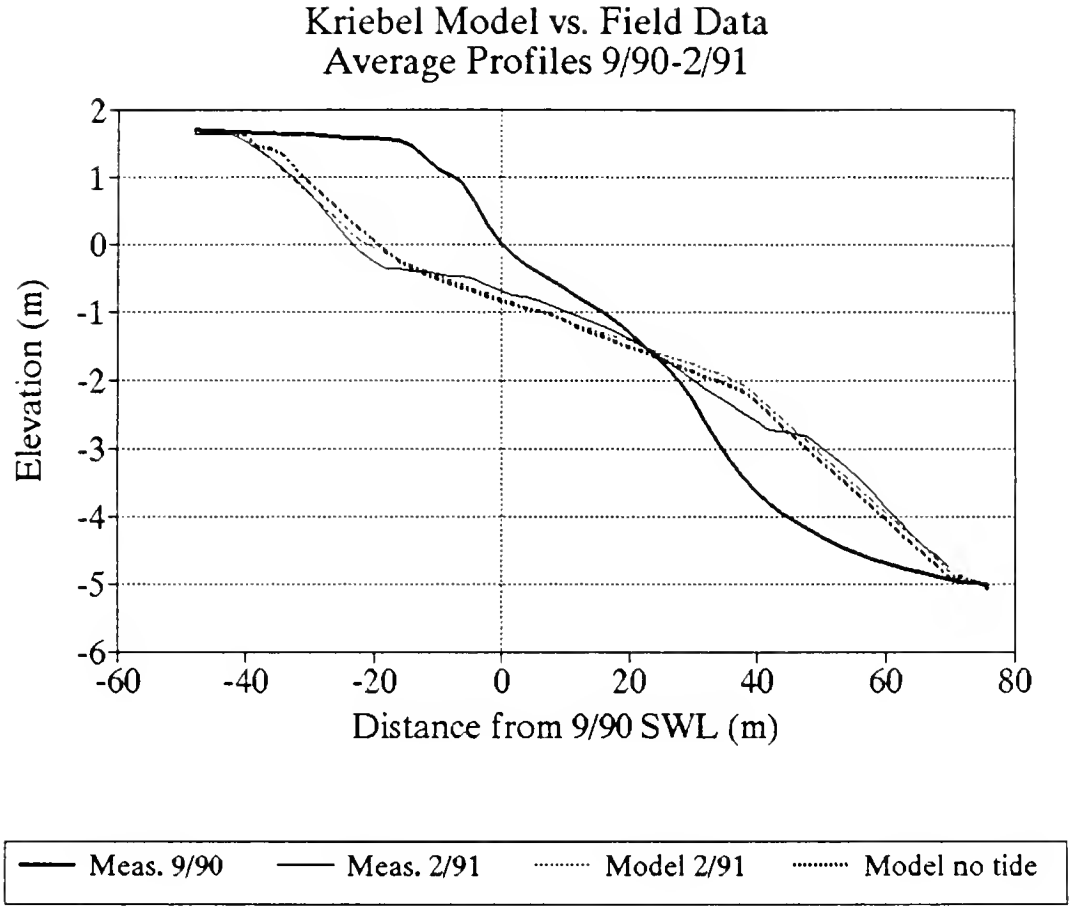

Figure 6.11: Modified Kriebel model vs. average nourished profiles based on measurements at Perdido Key, 9/90–2/91. K_{best}=0.2x10^{-6} m^4/N. R.M.S. error in depth=0.15 m.

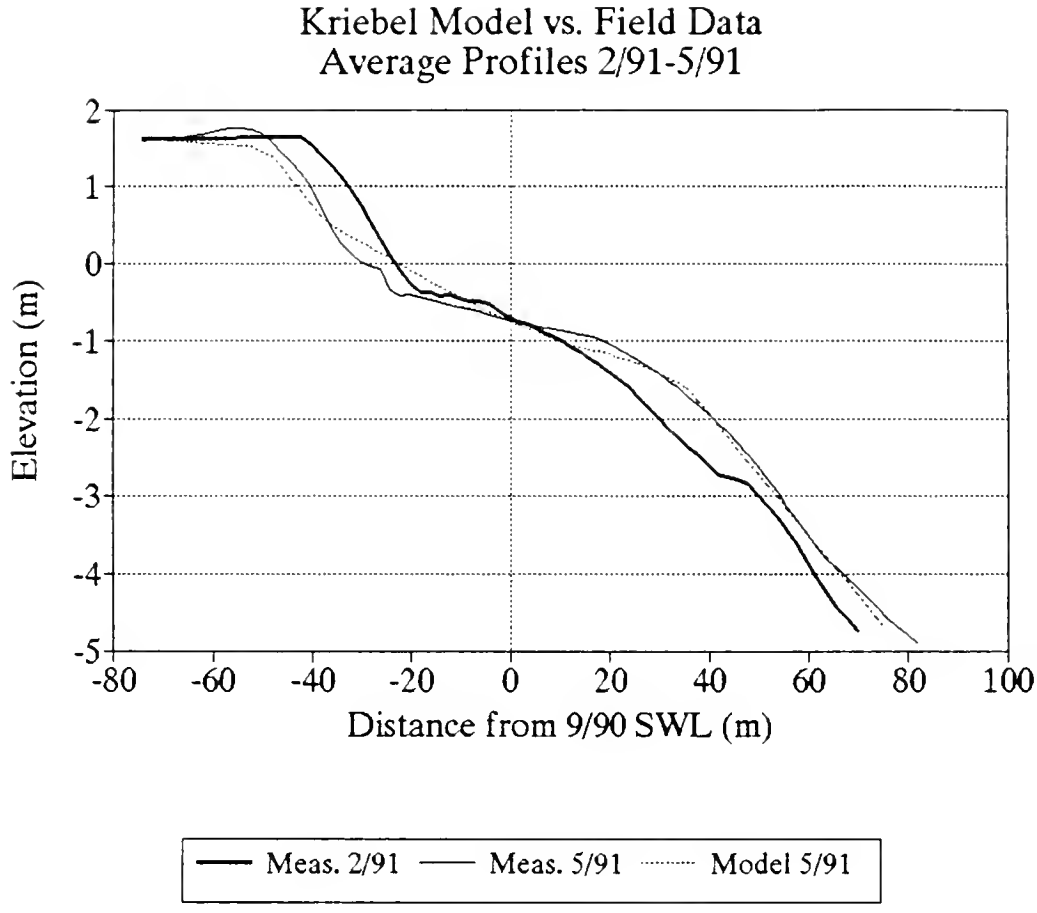

Figure 6.12: Modified Kriebel model vs. average nourished profiles based on measurements at Perdido Key, 2/91–5/91. K_{best}=2.0x10^{-6} m^4/N. R.M.S. error in depth=0.15 m.

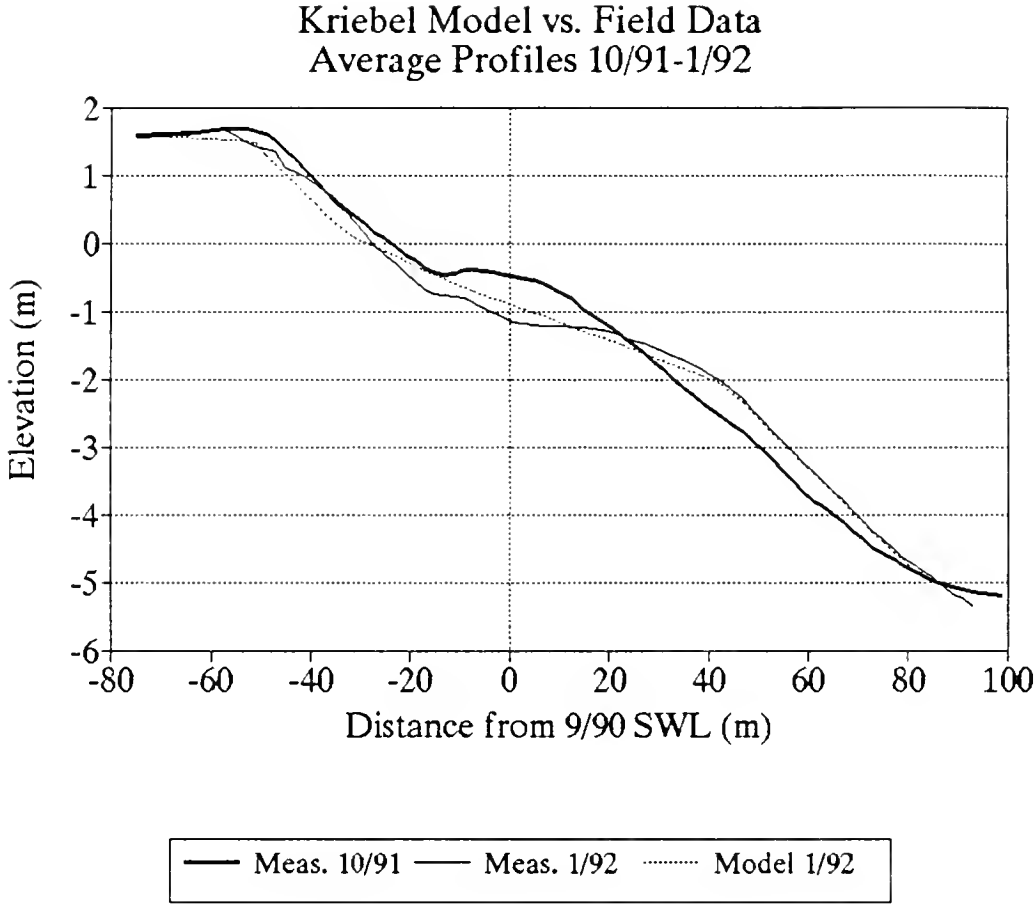

Figure 6.13: Modified Kriebel model vs. average nourished profiles based on measurements at Perdido Key, 10/91–1/92. K_{best}=0.2x10^{-6} m^4/N. R.M.S. error in depth=0.14 m.

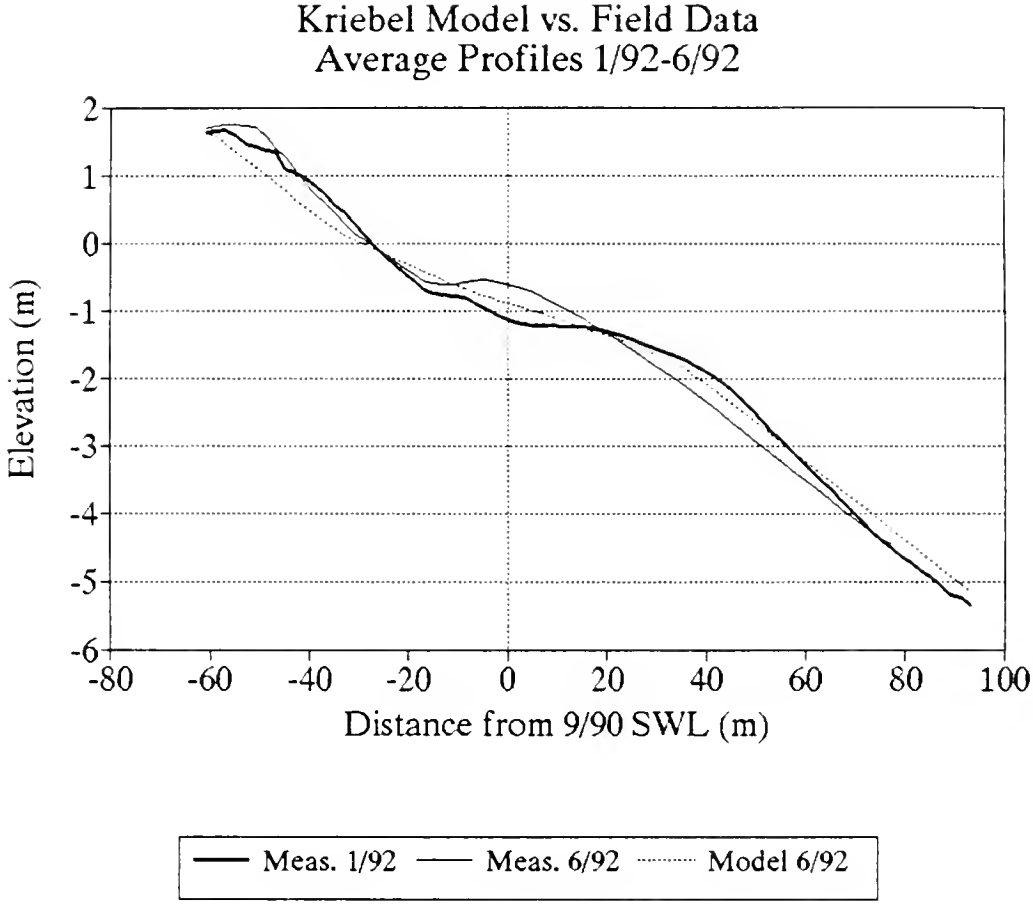

Figure 6.14: Modified Kriebel model vs. average nourished profiles based on measurements at Perdido Key, 1/92-6/92. K_{best}=0.1x10^{-6} m^4/N. R.M.S. error in depth=0.26 m.

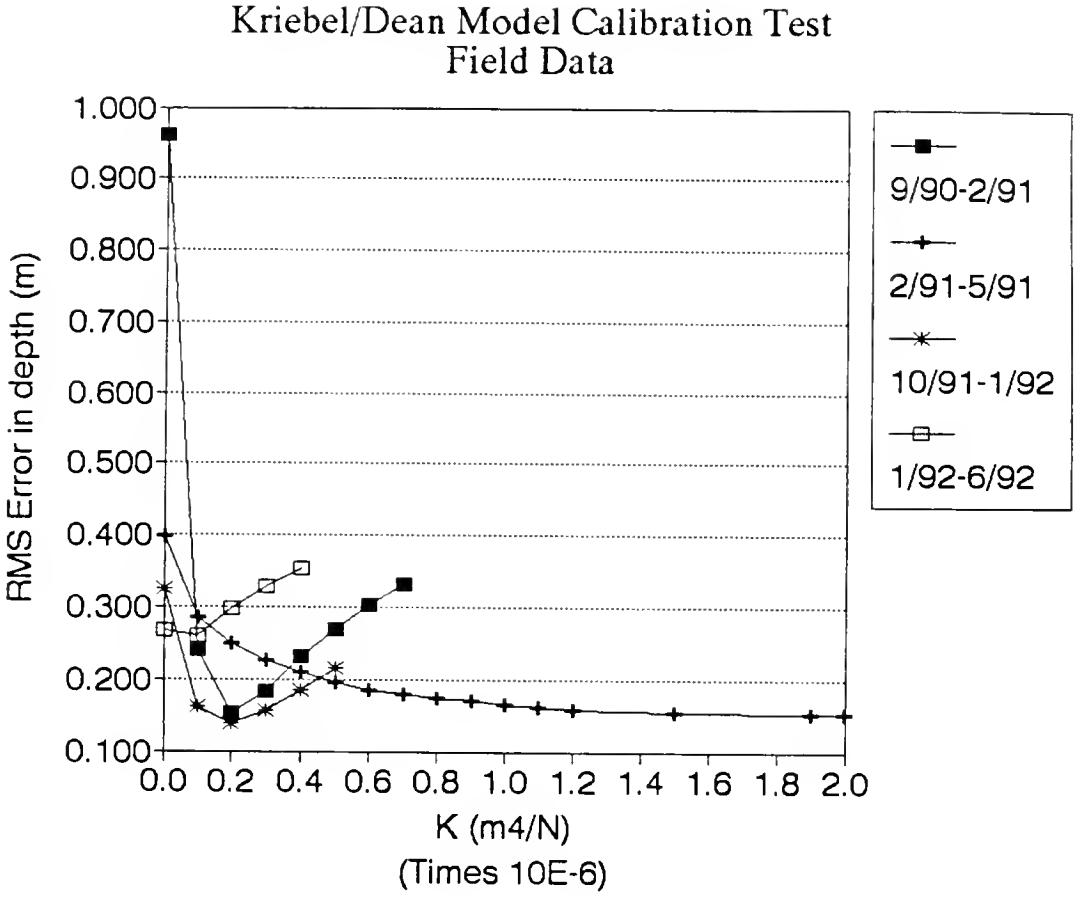

Figure 6.15: R.M.S. error in depth as a function of transport coefficient, K, for each field simulation. Note that K=0 corresponds to the R.M.S. depth change measured in the field over the given interval.

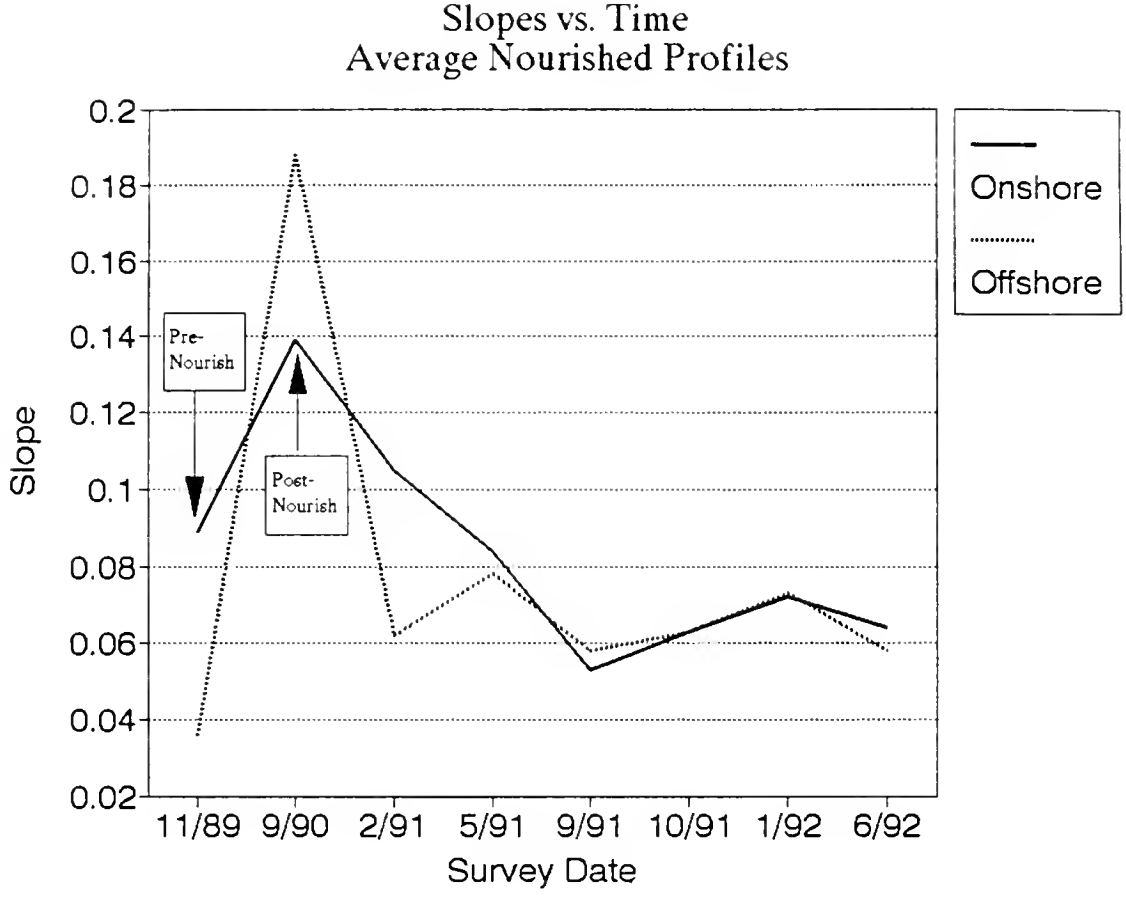

Figure 6.16: On- and offshore average slopes within nourished area, based on measurements at Perdido Key. Onshore slope defined by +1 m contour and waterline; offshore slope by -2 and -4 m contours.

$$\frac{H_o}{L_o} = 0.00070 \left[\frac{H_o}{wT}\right]^3 \tag{6.15}$$

where w is the sediment fall speed and T is the wave period. Mean wave height and period at the spectral peak were substituted to describe the waves in the field. Erosion occurred when the right-hand-side of Equation (6.15) exceeded the left.

A subtle modification was also made to the equation describing the magnitude of the cross-shore sediment transport rate:

$$q_y(y) = \begin{cases} K[D + \frac{\varepsilon}{K}\frac{\partial h}{\partial y} - D_*] & \text{for } D > D_* - \frac{\varepsilon}{K}\frac{\partial h}{\partial y} \\ 0 & \text{for } D < D_* - \frac{\varepsilon}{K}\frac{\partial h}{\partial y} \end{cases} \tag{6.16}$$

This modification is necessary to avoid a conflict in the predicted sediment transport direction that might arise using Equations (6.15) and (6.11). Upon first inspection, it would appear that Equation (6.11) predicts maximum onshore transport (<0) as the wave height goes to zero, since $D \rightarrow 0$ as $H \rightarrow 0$. With the similarity law employed to describe the wave height in the previous model, however, surf zone width also goes to zero as the wave height decreases.

Initial tests of the SBEACH model to simulate beach profile evolution in the field after nourishment indicated either onshore transport or no transport for almost all time steps. This prompted further inspection of Equation (6.15) governing the direction of transport. The two dimensionless numbers found in this equation were evaluated based on the mean monthly wave data measured in the field and the results plotted in Figure 6.17. Similar results were obtained using the six-hourly wave and water level data. Although computation of transport rates from the field data in each case involves averaging over several months, the data appear to indicate that erosion does correspond to larger values of the parameter H_o/wT. The coefficient in front of this term that defines the boundary between erosion and accretion would have to be changed, however, to reproduce the dominant offshore transport seen in the field.

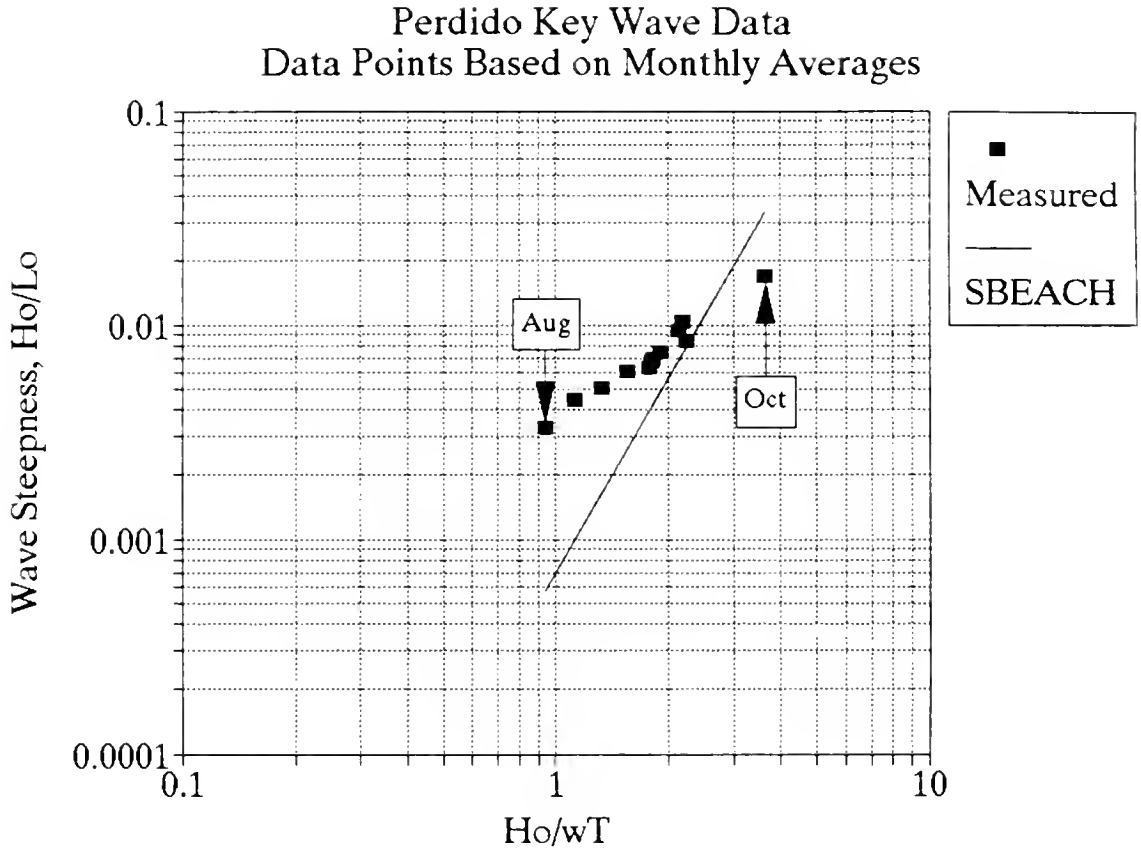

Figure 6.17: Deep water wave steepness, based on mean wave height (monthly average), vs. dimensionless fall speed. Solid line defines switch from offshore to onshore transport in SBEACH model.

Equation (6.16) includes the influence of gravity on the magnitude of the cross-shore sediment transport rate. The results presented here and the steep slopes found in the field immediately after nourishment suggest that the relation defining the sign of the cross-shore transport should also incorporate the effects of gravity, perhaps by inclusion of a slope term.

Documentation for the SBEACH program states that it should be applied only for short-term simulations, presumably because it has not been tested or calibrated against longer-term data sets. But if the governing equations are valid, and all important forcing described, it is reasonable to extend tests to longer simulation times. To test the behavior of the model and allow comparison to the previous results, the same simulations of the field conditions were attempted.

With the incorrect sign on the cross-shore sediment transport rate for much of the simulation, it should be expected that agreement between measured and modeled beach profiles will be poor for the first post-nourishment survey interval. Some effort was made to calibrate the model to yield the best agreement, but the coefficient governing the switch from onshore to offshore transport was not adjustable. Measured quantities were used as input where possible. Figure 6.18 shows the measured and modeled profiles for this first post-nourishment interval, using the "default" calibration factors. Despite the artificially steep initial profile, onshore transport is predicted even from the toe of the beachfill. Note that the net loss of 20 m^3/m of sediment due to longshore gradients of longshore sediment transport has not been accounted for in this result, but exerts a minor influence compared to changes due to cross-shore transport.

The case tested previously for which profile recovery was documented in the field was also tested with the SBEACH model. Results are shown in Figure 6.19. For this case, the measured longshore gradient of longshore sediment transport was negligible, and the two primary calibration factors (K and ε) were set to their minimum allowable

values (0.5×10^{-6} m^4/N and 0.001 m^2/s, respectively) to improve agreement between measurements and model results. The dominant bar predicted by the model for this case is not evident in the field.

6.7 Summary

Despite employing the same basic governing equation, the results of the two models for beach profile response investigated in this chapter differed markedly. The modified Kriebel model performed best for the first post-nourishment survey interval, when the beach profile deviated most strongly from its "natural" or "equilibrium" condition. Subsequent simulations yielded poorer results. The onshore transport observed in the field was not described by the model for the one case tested including profile recovery.

The drastically different results obtained through use of the SBEACH model (Larson and Kraus [1989]) are largely attributed to the relationship employed to determine the direction of cross-shore sediment transport. The results of this study suggest that the direction of the local cross-shore sediment transport rate is probably influenced by the local bottom slope. The SBEACH model incorporates a number of important differences that make it more realistic than the simpler, modified form of the model due to Kriebel [1982].

The tests highlighted in this study represent one of the few attempts to simulate the physical processes driving beach profile change over a time scale larger than that of a storm. Future studies at different sites, with different environmental conditions, will provide additional data that will allow calibration and testing of this and future generations of models.

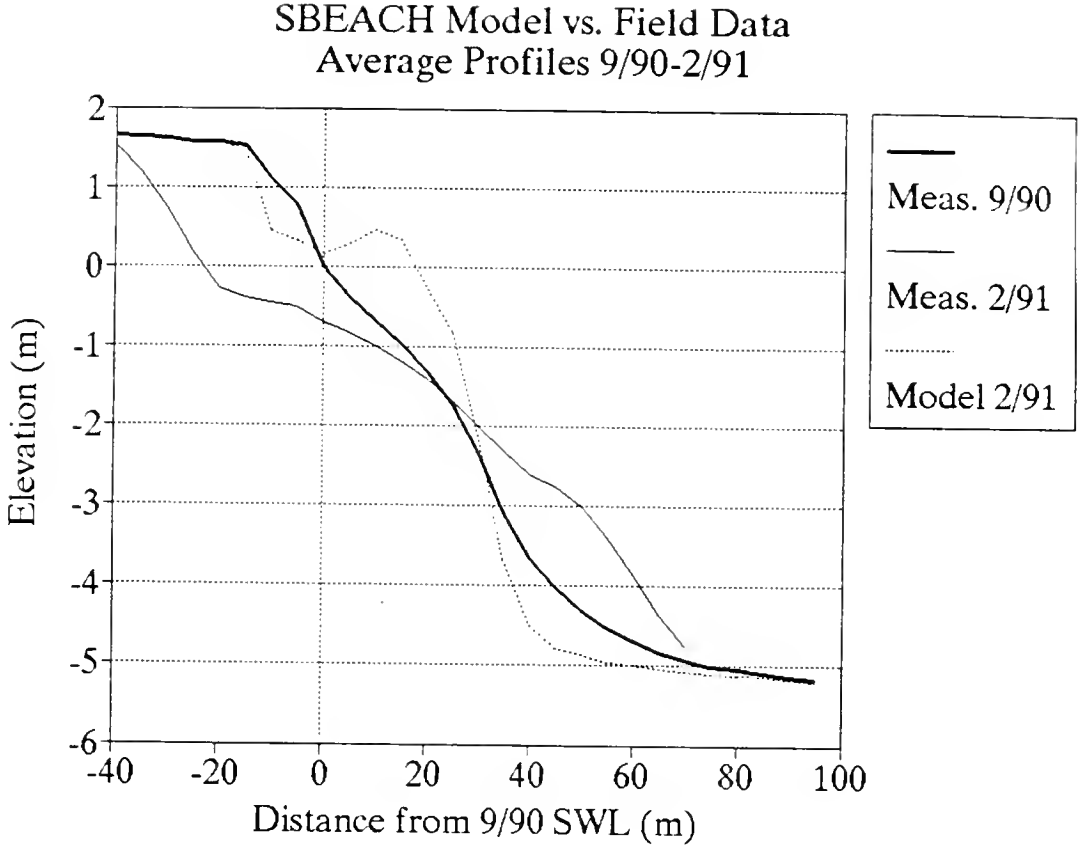

Figure 6.18: Measured and modeled beach profiles, first post-nourishment survey interval at Perdido Key. Model result is based on Larson and Kraus [1989]. K=1.5x10^{-6} m^4/N, ε=0.002 m^2/s.

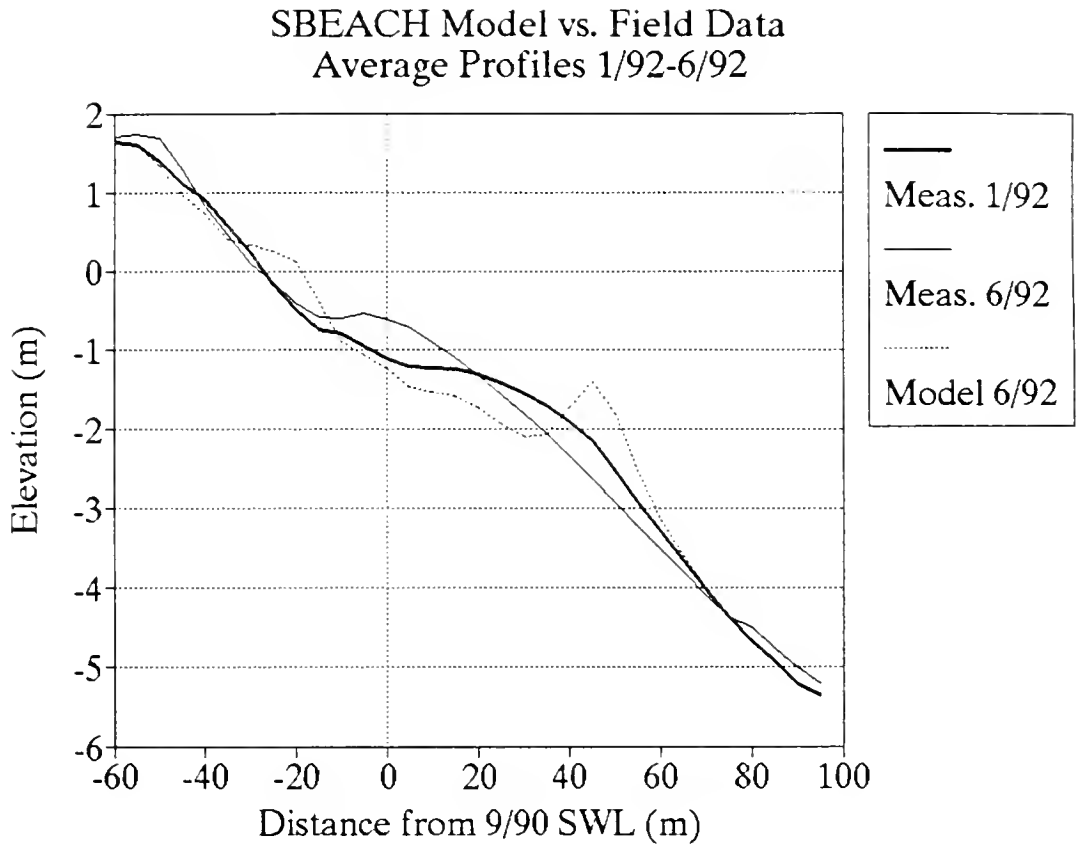

Figure 6.19: Measured and modeled beach profiles in field, profile recovery case. Model result is based on Larson and Kraus [1989]. K=0.5x10^{-6} m^4/N, ε=0.001 m^2/s.

CHAPTER 7
CONCLUSIONS

The results presented here have demonstrated that a beach nourishment project provides an excellent opportunity to observe and monitor nearshore sediment transport processes. The beach profile and planform perturbations produced by the construction of such projects lead to gradients in both the longshore and cross–shore sediment transport rates, causing changes obvious to even the casual observer. Given adequate data at sufficient resolution in both time and space, beach nourishment projects can be used to assess and advance the ability with which coastal engineers and scientists can predict nearshore sediment transport rates.

Considering the number of beach nourishment projects that have been undertaken, and the costs associated with monitoring studies relative to those for construction, it is somewhat surprising that no detailed description of the sediment transport processes at a nourished beach has previously been available. Many previous studies have focused attention only on the subaerial beach. For the project studied here, neglect of the subaqueous portion of the nourished beach would imply exclusion of over 75% of the active profile. Future studies that retain, or improve upon, the level of detail maintained for data collection at the Perdido Key beach nourishment site should provide valuable data describing both cross–shore and longshore sediment transport processes.

The success or failure of beach nourishment projects is often expressed solely in terms of the position of the waterline. The location of this contour is important, as it defines the dry beach width which has much recreational and psychological value. But landward movement of the waterline over the short term (weeks to months) after

placement should be expected when as-built slopes greatly exceed those associated with the pre-nourishment profile. This short-term, landward movement of the waterline, resulting primarily from cross-shore sediment transport, does not represent a volumetric loss, but is probably the source of statements claiming that beaches erode faster after nourishment than before. It should be remembered that beach nourishment is not a remedy for erosion, but instead postpones the adverse impacts of erosion.

Data collection at Perdido Key has provided a rich and unique data set, some of which is essentially untapped. A secondary wave gage recently installed near Pensacola Pass should help describe the spatial variation in the nearshore wave climate and the influence of both Caucus Shoal and tidal currents on the waves. Ongoing and future data collection at the site will ultimately yield a five-year description of the evolution of a large beach nourishment project on an open coast. The environmental parameters and physical dimensions monitored were found to be sufficient for the purposes of this study, although increased temporal and spatial resolution of the surveys would always be welcomed.

One aim of the preceding chapters was to demonstrate that repetitive bathymetric and topographic surveys can be used to infer both cross-shore and longshore sediment transport gradients when they are large enough to overwhelm potential error in the surveys. Beach nourishment projects typically cause such large planform and profile perturbations that the resulting sediment transport gradients are quite evident. In agreement with many previous studies, changes of the nourished beach attributable to cross-shore sediment transport became evident first, as the beach profile "equilibrated" to the incident waves. This "equilibrium" condition should not be construed as a static configuration that results in no further change, but is instead a conceptual tool that assists in predicting the rate of response of the beach when subjected to forcing.

The models employed here to describe, separately, the longshore and cross–shore sediment transport processes in the field after beach nourishment may be considered predictive tools that are under development. A lack of quality data sets from field sites has often forced application of beach planform and profile evolution models without sufficient prior verification.

Many nearshore phenomena have been addressed in the beach planform and profile evolution models discussed in this study, but some potentially important effects have been neglected. Wave–driven currents, temporally– and spatially–varying, have been included (implicitly), but currents driven by other forces have not. These additional driving forces include tides and winds, and their importance may at times approach that of the waves. This problem is complicated by the interaction between the winds, mean currents, and the waves. This interaction affects the nearshore velocity field as well as the mean and fluctuating water levels. Future models will have to consider the coupled effect of these forces, as well as the coupling between longshore and cross–shore motions.

One–line models for beach planform evolution have seen many applications in recent years. This type of model was found to give a reasonable description of the longshore gradient of longshore sediment transport subsequent to beach nourishment, after accounting for background erosion. It is necessary to use the longshore gradient of longshore sediment transport as the basis for model comparison to integrate out the effects of cross–shore sediment transport, which were found to be particularly important for roughly the first half–year after beach nourishment. The worst agreement between measurements and model was found near the "shoulders" of the beachfill. This is probably a result of inadequate description of the wave climate near these areas of strong longshore and cross–shore bathymetric gradients.

Models for cross–shore response of beaches when subjected to waves have traditionally been applied only over the time scale of a storm — hours to days. Marginal

understanding of the physics of the problem and a lack of suitable data have made extension to larger time scales risky and speculative. Yet some insight may be gained into the problem by attempting new tests of preceding models. The results presented here clearly indicate that at least two fundamental components of the cross-shore sediment transport problem remain unsolved: 1) the wave, sediment, and beach parameters that define the switch from onshore to offshore transport; and 2) the beach "recovery" process that follows when transport is predominately onshore. Existing models have had more success predicting volumetric changes when transport is predominately directed offshore, but the longshore bar formation process has not yet been adequately described. The increasing popularity of near-prototype scale experiments in large wave tanks should provide valuable data that will help solve these problems.

Beach nourishment has been and is expected to remain a popular remedy for coastal erosion. As the ability to describe the evolution of beach nourishment projects improves, more intelligent decisions can be made regarding how, when, and where to nourish. Monitoring studies such as the one documented here can add not only to the body of knowledge regarding beach nourishment projects, but also the more general problem of nearshore sediment transport.

REFERENCES

Abel, C.E., Tracy, B.A., Vincent, C.L., and Jensen, R.E., 1989. Hurricane hindcast methodology and wave statistics for Atlantic and Gulf Coast hurricanes from 1956–1975. WIS Report 19, U.S. Army Corps of Engineers, Coastal Engineering Research Center, Vicksburg, MS.

Abramowitz, M., and Stegun, I.A., 1972. Handbook of Mathematical Functions, Dover Publications, New York, NY.

Ashley, G.M., Halsey, S.D., and Farrell, S.C., 1987. A study of beachfill longevity: Long Beach Island, NJ. Proc. Coastal Sediments '87, Vol. 2, American Society of Civil Engineers, New York, NY, pp. 1188–1202.

Aubrey, D.G., and DeKimpe, N.M., 1988. Performance of beach nourishment at Jupiter Island, Florida. Proc. Beach Preservation Technology '88, Florida Shore and Beach Preservation Association, Tallahassee, FL, pp. 409–420.

Bagnold, R.A., 1963. Mechanics of marine sedimentation, in The Sea: Ideas and Observations, Vol. 3, Interscience, New York, NY.

Bailard, J.A., 1981. An energetics total load sediment transport model for a plane sloping beach. J. Geophys. Res., Vol. 86, No. C11, pp. 10,938–10,954.

Balsillie, J.H., 1975. Analysis and interpretation of Littoral Environment Observation (LEO) and profile data along the western Panhandle of Florida. Technical Memorandum No. 49, U.S. Army Corps of Engineers, Coastal Engineering Research Center, Ft. Belvoir, VA.

Balsillie, J.H., Chiu, T.Y, and Demirpolat, S., 1986. Long–term shoreline change rates for Escambia County, Florida. Beaches and Shores Technical Design Memorandum No. 86–2, Florida Department of Natural Resources, Tallahassee, FL.

Basco, D.R., and Yamashita, T., 1986. Toward a simple model of the wave breaking transition region in surf zones. Proc. Twentieth Coastal Engineering Conference, Vol. II, American Society of Civil Engineers, New York, NY, pp. 955–970.

Battjes, J.A., and Janssen, J.P.F.M., 1978. Energy loss and setup due to breaking of random waves. Proc. Sixteenth Coastal Engineering Conference, American Society of Civil Engineers, New York, NY, pp. 569–587.

Battjes, J.A., and Stive, M.J.F., 1985. Calibration and verification of a dissipation model for random breaking waves. J. Geophys. Res., Vol. 90, No. C5, pp. 9159–9167.

Blair, C., 1983. Tidal corrections in hydrographic surveying. J. Waterway, Port, Coastal and Ocean Engineering, Vol. 109, No. 1, American Society of Civil Engineers, New York, NY, pp. 31–40.

Bodge, K.R., 1986. Short term impoundment of longshore sediment transport. Ph.D. Dissertation, Coastal and Oceanographic Engineering Department, University of Florida, Gainesville, FL.

Bodge, K.R., and Kraus, N.C., 1991. Critical examination of longshore transport rate magnitude. Proc. Coastal Sediments '91, Vol. 1, American Society of Civil Engineers, New York, NY, pp. 139–155.

Börekçi, O.S., 1982. Distribution of wave–induced momentum fluxes over depth and application within the surf zone. Ph.D. Dissertation, Dept. of Civil Engineering, University of Delaware, Newark, DE.

Bruun, P., 1954. Coast erosion and the development of beach profiles. Technical Memorandum No. 44, Beach Erosion Board, Corps of Engineers, Department of the Army.

Childers, D.G., and Durling, A.E., 1975. Digital Filtering and Signal Processing, West Publishing Co., St. Paul.

Chu, Y.–H., and Posey, F.H., 1989. Beach erosion protection and beach nourishment at Tybee Island, Georgia. Proc. Beach Preservation Technology '89, Florida Shore and Beach Preservation Association, Inc., Tallahassee, Florida, pp. 67–74.

Clark, R.R., 1991. Beach conditions in Florida: a statewide inventory and identification of the beach erosion problem areas in Florida. Beaches and Shores Technical Design Memorandum 89–1, Third Edition, Florida Department of Natural Resources, Tallahassee, FL.

Clausner, J.E., Birkemeier, W.A., and Clark, G.R., 1986. Field comparison of four nearshore survey systems. Miscellaneous Paper CERC–86–6, U.S. Army Corps of Engineers, Coastal Engineering Research Center, Vicksburg, MS.

Combe, A.J., III, and Soileau, C.W., 1987. Behavior of man–made beach and dune, Grande Isle, Louisiana. Proc. Coastal Sediments '87, Vol. 2, American Society of Civil Engineers, New York, NY, pp. 1232–1242.

Dally, W.R., 1980. A numerical model for beach profile evolution. M.S. thesis, Department of Civil Engineering, University of Delaware, Newark, DE.

Dally, W.R., 1990. Random breaking waves: a closed–form solution for planar beaches. Coastal Engineering, Vol. 14, No. 3, pp. 233–263.

Dally, W.R., 1992. Random breaking waves: field verification of a wave–by–wave algorithm for engineering application. Coastal Engineering, Vol. 16, No. 4, pp. 369–397.

Dally, W.R., and Dean, R.G., 1984. Suspended sediment transport and beach profile evolution. J. Waterway, Port, Coastal and Ocean Engineering, Vol. 110, No. 1, American Society of Civil Engineers, New York, NY, pp. 15–33.

Dally, W.R., and Dean, R.G., 1986. Mass flux and undertow in the surf zone, by I.A. Svendsen — Discussion. Coastal Engineering, Vol. 10, No. 3, pp. 289–307.

Dally, W.R., Dean, R.G., and Dalrymple, R.A., 1984. A model for breaker decay on beaches. Proc. Nineteenth Coastal Engineering Conference, American Society of Civil Engineers, New York, NY, pp. 82–98.

Dally, W.R., Dean, R.G., and Dalrymple, R.A., 1985. Wave height variation across beaches of arbitrary profile. J. Geophys. Res., Vol. 90, No. C6, pp. 11917–11927.

Dean, R.G., 1977. Equilibrium beach profiles: U.S. Atlantic and Gulf coasts. Ocean Engineering Rep. No. 12, Department of Civil Engineering, University of Delaware, Newark, DE.

Dean, R.G., 1988. Recommendations for placement of dredged sand on Perdido Key, Gulf Islands National Seashore, Coastal and Oceanographic Engineering Department, University of Florida, Gainesville, FL.

Dean, R.G., 1991. Equilibrium beach profiles: characteristics and applications. J. of Coastal Research, Vol. 7, No. 1, pp. 53–84.

Dean, R.G., Berek, E.P., Gable, C.G., and Seymour, R.J., 1982. Longshore transport determined by an efficient trap. Proc. Eighteenth Coastal Engineering Conference, Vol. 2, American Society of Civil Engineers, New York, NY, pp. 954–968.

Dean, R.G., and Dalrymple, R.A., 1984. Water Wave Mechanics for Engineers and Scientists. Prentice-Hall, Englewood Cliffs, NJ.

Dean, R.G., and Grant, J., 1989. Development of methodology for thirty-year shoreline predictions in the vicinity of beach nourishment projects. Coastal and Oceanographic Engineering Department, University of Florida, Gainesville, FL.

Dean, R.G., and Lin, L.-H., 1990. The North Redington Beach nourishment project: comparison of measured and predicted performances. Beaches: Lessons of Hurricane Hugo, Proc. 1990 National Conference on Beach Preservation Technology, Florida Shore and Beach Preservation Association, Tallahasse, FL, pp. 86–99.

Dean, R.G., and Yoo, C.-H., in press. Beach nourishment performance predictions. J. of the Waterways and Harbors Div., American Society of Civil Engineers, New York, NY.

DeKimpe, N.M., Aubrey, D.G., and Fields, M.L., 1991. Performance of beach nourishment at Dead Neck barrier beach, Osterville, Cape Cod, Massachusetts. Preserving and Enhancing Our Beach Environment, Proc. of the 1991 National Conference on Beach Preservation Technology, Florida Shore and Beach Preservation Association, Tallahassee, FL, pp. 27–43.

de Lange, W.P., and Healy, T.R., 1990. Renourishment of a flood-tidal delta adjacent beach, Tauranga Harbor, New Zealand. J. of Coastal Research, Vol. 6, No. 3, pp. 627–640.

Dette, H.H., 1977. Effectiveness of beach deposit nourishment. Proc. Coastal Sediments '77, American Society of Civil Engineers, New York, NY, pp. 211–227.

Dixon, K.L., and Pilkey, O.H., 1991. Summary of beach replenishment on the U.S. Gulf of Mexico shoreline. J. of Coastal Research, Vol. 7, No. 1, pp. 249–256.

Downing, G.C., and Fagerburg, T.L., 1987. Evaluation of vertical motion sensors for potential application to heave correction in Corps hydrographic surveys. Technical Report HL-87-10, U.S. Army Corps of Engineers, Hydraulics Laboratory, Waterways Experiment Station, Vicksburg, MS.

Dyhr-Nielsen, M., and Sorensen, T., 1970. Some sand transport phenomena on coasts with bars. Proc. Twelfth Coastal Engineering Conference, American Society of Civil Engineers, New York, NY, pp. 855–865.

Emery, K.O., 1961. A simple method of measuring beach profiles. Limnol. and Oceanogr., v. 6, pp. 90–93.

Everts, C.H., DeWall, A.E., and Czerniak, M.T., 1974. Behavior of beach fill at Atlantic City, New Jersey. Proc. Fourteenth Coastal Engineering Conference, Vol. 2, American Society of Civil Engineers, New York, NY, pp. 1370–1388.

Ferrante, A., Franco, L., and Boer, S., 1992. Modelling and monitoring of a perched beach at Lido di Ostia (Rome). Book of Abstracts, Twenty-third Coastal Engineering Conference, American Society of Civil Engineers, New York, NY, pp. 553–555.

Fernández, A.J., Gómez-Pina, G., and Ramírez, J.L., 1992. A field experiment on a nourished beach. Book of Abstracts, Twenty-third Coastal Engineering Conference, American Society of Civil Engineers, New York, NY, pp. 551–552.

Fisher, J.S., and Felder, W.N., 1976. Cape Hatteras beach nourishment. Proc. Fifteenth Coastal Engineering Conference, Vol. 2, American Society of Civil Engineers, New York, NY, pp. 1512–1531.

Giardino, J.R., Bednarz, R.S., and Bryant, J.T., 1987. Nourishment of San Luis Beach, Galveston Island, TX: An assessment of impact. Proc. Coastal Sediments '87, Vol. 1, American Society of Civil Engineers, New York, NY, pp. 1012–1022.

Goda, Y., 1990. Distribution of sea state parameters and data fitting. In Handbook of Coastal and Ocean Engineering, Vol. 1: Wave Phenomena and Coastal Structures, J.B. Herbich, Ed., Gulf Publishing Co., Houston, TX.

Gorsline, D., 1966. Dynamic characteristics of Gulf Coast beaches. Marine Geology, 4:187–206.

Hall, J.V., 1952. Artificially nourished and constructed beaches. Technical Memorandum No. 29, Beach Erosion Board, Corps of Engineers, Department of the Army, Washington, D.C. Also Proc. Third Conference on Coastal Engineering, J.W. Johnson, Ed., Council on Wave Research, The Engineering Foundation, Berkeley, CA, pp. 119–136.

Hall, J.V., and Herron, W.J., 1950. Test of nourishment of the shore by offshore deposition of sand, Long Branch, New Jersey. Technical Memorandum No. 17, Beach Erosion Board, Corps of Engineers, Department of the Army.

Hanes, D.M., 1990. The structure of events of intermittent suspension of sand due to shoaling waves. Chapter 28 in The Sea: Ocean Engineering Science, Vol. 9, pp. 941–952, John Wiley and Sons, Inc.

Hansen, J.B., and Svendsen, I.A., 1984. A theoretical and experimental study of undertow. Proceedings of the Nineteenth Coastal Engineering Conference, American Society of Civil Engineers, New York, NY, pp. 2246–2262.

Harris, R.L., 1954. Restudy of test — shore nourishment by offshore deposition of sand, Long Branch, New Jersey. Technical Memorandum No. 62, Beach Erosion Board, Corps of Engineers, Department of the Army.

Hobson, R.D., 1981. Beach nourishment techniques. Report 3, Typical U.S. beach nourishment projects using offshore sand deposits. Technical Report H-76-13, Geotechnical Engineering Branch, U.S. Army Coastal Engineering Research Center, Fort Belvoir, VA.

Houmb, O.G., 1989. Basic wave statistics. In Port Engineering, Vol. 1, P. Bruun, Gulf Publishing Co., Houston, TX.

Hubertz, J.M., and Brooks, R.M., 1989. Gulf of Mexico hindcast wave information. WIS Report 18, U.S. Army Corps of Engineers, Coastal Engineering Research Center, Vicksburg, MS.

Hushla, F.L., 1982. Evaluating the performance of beach nourishment in Brevard County, Florida, through the use of aerial photography. M.S. thesis, Department of Oceanography and Ocean Engineering, Florida Institute of Technology, Melbourne, FL.

Ibe, A.C., Awosika, L.F., Ibe, C.E., and Inegbedion, L.E., 1991. Monitoring of the 1985/86 beach nourishment project at Bar Beach, Victoria Island, Lagos, Nigeria. Proc. Coastal Zone '91, American Society of Civil Engineers, pp. 534–552.

Jarrett, J.T., 1988. Performance of the Wrightsville Beach, North Carolina shore protection project. Proc. Beach Preservation Technology '88, Florida Shore and Beach Preservation Association, Tallahassee, FL, pp. 59–64.

Johnson, J.W., 1956. Dynamics of nearshore sediment movement. Am. Assoc. Pet. Geol. Bull., Vol. 40, pp. 2211–2232.

Jones, C.P., and Kana, T.W., 1988. Performance of beach nourishment at Myrtle Beach, South Carolina. Proc. Beach Preservation Technology '88, Florida Shore and Beach Preservation Association, Tallahassee, FL, pp. 75–86.

Kajima, R., Shimizu, T., Maruyama, K., and Saito, S., 1982. Experiments on beach profile change with a large wave flume. Proc. Eighteenth Coastal Engineering Conference, American Society of Civil Engineers, New York, NY, pp. 1385–1404.

Kamphius, J.W., 1991. Alongshore sediment transport rate distribution. Proc. Coastal Sediments '91, Vol. 1, American Society of Civil Engineers, New York, NY, pp. 170–183.

Kerckaert, P., Roovers, P.P.L., Noordam, A., and DeCandt, P., 1986. Artificial beach nourishment on Belgian east coast. J. of Waterway, Port, Coastal and Ocean Engineering, Vol. 112, No. 5, American Society of Civil Engineers, New York, NY, pp. 560–571.

Komar, P.D., 1991. Littoral sediment transport. In Handbook of Coastal Engineering, Vol. 2, J.B. Herbich, Ed. Gulf Publishing Co., Houston, TX.

Komar, P.D., and Inman, D.L., 1970. Longshore sand transport on beaches, J. Geophys. Res., Vol. 75, pp. 5914–5927.

Kramer, J., 1961. Beach-rehabilitation by use of beach fills and further plans for the protection of the Island of Norderney. Proc. Seventh Coastal Engineering Conference, Vol. 2, J.W. Johnson, Ed., Council on Wave Research, The Engineering Foundation, Richmond, CA, pp. 847–859.

Kramer, J., 1972. Artificial beach nourishment on the German North Sea coast. Proc. Thirteenth Coastal Engineering Conference, American Society of Civil Engineers, New York, NY, pp. 1465–1483.

Kraus, N.C., Isobe, M., Igarashi, H., Sasaki, T, and Horikawa, K., 1982. Field experiments on longshore sand transport in the surf zone. Proc. Eighteenth Coastal Engineering Conference, Vol. 2, American Society of Civil Engineers, New York, NY, pp. 969–988.

Kraus, N.C., and Larson, M., 1988. Beach profile change measured in the tank for large waves, 1956–1957 and 1962. Technical Report CERC–88–6, Coastal Engineering Research Center, U.S. Army Corps of Engineers, Vicksburg, MS.

Kriebel, D.L., 1982. Beach and dune response to hurricanes. M.S. thesis, Department of Civil Engineering, University of Delaware, Newark, DE.

Kriebel, D.L., 1986. Verification study of a dune erosion model. Shore and Beach, Vol. 54, No. 3, pp. 13–21.

Kriebel, D.L., and Dean, R.G., 1985. Numerical simulation of time–dependent beach and dune erosion. Coastal Engineering, Vol. 9, No. 3, pp. 221–245.

Kunz, H., 1990. Artificial beach nourishment on Norderney, a case study. Proc. Twenty–Second Coastal Engineering Conference, Vol. 3, American Society of Civil Engineers, New York, NY, pp. 3254–3267.

Larson, M., Hanson, H., and Kraus, N.C., 1987. Analytical solutions of the one–line model of shoreline change. Technical Report CERC–87–15, U.S. Army Corps of Engineers, Coastal Engineering Research Center, Vicksburg, Mississippi.

Larson, M., and Kraus, N.C., 1989. SBEACH: Numerical model for simulating storm–induced beach change. Report 1: Empirical foundation and model development. Technical Report CERC–89–9, U.S. Army Corps of Engineers, Coastal Engineering Research Center, Vicksburg, MS.

Larson, M., and Kraus, N.C., 1991. Mathematical modeling of the fate of beach fill. Coastal Engineering, Vol. 16, No. 1, pp. 83–114.

Larson, M., Kraus, N.C., and Byrnes, M.R., 1990. SBEACH: Numerical model for simulating storm–induced beach change. Report 2: Numerical formulation and model tests. Technical Report CERC–89–9, U.S. Army Corps of Engineers, Coastal Engineering Research Center, Vicksburg, MS.

Leonard, L., Clayton, T., and Pilkey, O.H., 1990. An analysis of replenished beach design parameters on U.S. East Coast barrier islands. J. of Coastal Research Vol. 6, No. 1, pp. 15–36.

Leonard, L., Dixon, K.L., and Pilkey, O.H., 1990. A comparison of beach replenishment on the U.S. Atlantic, Pacific, and Gulf coasts. J. of Coastal Research, SI 6, pp. 127–140.

Longuet–Higgins, M.S., 1953. Mass transport in water waves, Phil. Trans. of the Royal Society, London, England, Series A, Vol. 245, pp. 535–581.

Longuet–Higgins, M.S., 1983. Wave set–up, percolation, and undertow in the surf zone. Proc. Roy. Soc. Lond. A390, pp. 283–291.

Longuet-Higgins, M.S., and Stewart, 1962. Radiation stress and mass transport in gravity waves, with application to 'surf beats'. J. Fluid Mech., Vol. 13, No. 4, pp. 481–504.

Longuet-Higgins, M.S., and Stewart, 1964. Radiation stresses in water waves; a physical discussion, with applications. Deep Sea Research 11, pp. 529–540, 561–562.

Longuet-Higgins, M.S., Cartwright, D.E., and Smith, N.D., 1963. Observations of the directional spectrum of sea waves using the motions of a floating buoy. Ocean Wave Spectra, Proc. of a Conference, Prentice-Hall, Inc., Englewood Cliffs, NJ, pp. 111–132.

Mann, D.W., Curtis, L.W., and Daniel, T.H., 1992. Short beach nourishment fill performance on an irregular coastline. Proc. Coastal Engineering Practice '92, S.A. Hughes, Ed., American Society of Civil Engineers, New York, NY, pp. 104–119.

McCann, D.P., 1981. Beach changes at Atlantic City, New Jersey (1962–1973). Miscellaneous Report No. 81-3, Coastal Engineering Research Center, U.S. Army Corps of Engineers, Fort Belvoir, VA.

McCowan, J. 1894. On the highest wave of permanent type. Philos. Mag. J. Sci., Vol. 38.

Moore, B.D., 1982. Beach profile evolution in response to changes in water level and wave height. M.S. thesis, Department of Civil Engineering, University of Delaware, Newark, DE.

Nadaoka, K., and Kondoh, T., 1982. Laboratory measurements of velocity field structure in the surf zone by LDV. Coastal Engineering in Japan, Vol. 25, JSCE, pp. 125–145.

Nairn, R.B., and Riddell, K.J., 1992. Numerical beach profile modelling for beachfill projects. Proc. Coastal Engineering Practice '92, American Society of Civil Engineers, New York, NY, pp. 12–28.

Nairn, R.B., Roelvink, J.A., and Southgate, H.N., 1990. Transition zone width and implications for modelling surf zone hydrodynamics. Proceedings of the Twenty-Second Coastal Engineering Conference, Vol. 1, American Society of Civil Engineers, New York, NY, pp. 68–81.

Nordstrom, C.E., and Inman, D.L., 1975. Sand level changes on Torrey Pines Beach, California. Miscellaneous Paper No. 11-75, U.S. Army Corps of Engineers, Coastal Engineering Research Center, Vicksburg, MS.

Oertel, G.F., Chamberlain, C.F., Larsen, M., and Schaaf, W., 1977. Monitoring the Tybee beach nourishment project. Proc. Coastal Sediments '77, American Society of Civil Engineers, New York, NY, pp. 1049–1056.

Okayasu, A., Shibayama, T., and Horikawa, K., 1988. Vertical variation of undertow in the surf zone. Proceedings of the Twenty-First Coastal Engineering Conference, American Society of Civil Engineers, New York, NY, pp. 478–491.

Pelnard-Considère, R., 1956. Essai de théorie de l'evolution des forms de rivages en plage de sable et de galets. 4th Journées de l'Hydraulique, les Energies de la Mer, Question III, Rapport No. 1, pp. 289–298.

Perdikis, H.S., 1961. Behavior of beach fills in New England. J. of the Waterways and Harbors Div., Proc. of the American Society of Civil Engineers, Vol. 87, No. WW1, pp. 75–110.

Phillips, J.D., Psuty, N.P., and McCluskey, J.M., 1984. The impact of beach nourishment at South Beach, Sandy Hook, New Jersey. Center for Coastal and Environmental Studies, Rutgers — The State University of New Jersey, New Brunswick, NJ.

Phlegar, W.S., III, 1989. Performance prediction of beach nourishment projects. M.S. thesis, Coastal and Oceanographic Engineering Department, University of Florida, Gainesville, FL.

Pilkey, O.H., and Clayton, T.D., 1989. Summary of beach replenishment experience on U.S. East Coast barrier islands. J. of Coastal Research, Vol. 5, No. 2, pp. 147–159.

Psuty, N.P., 1987. Shoreline changes at Perdido Key, Florida. Center for Coastal and Environmental Studies, Rutgers University, New Brunswick, NJ.

Psuty, N.P., 1988. Balancing recreation and environmental system in a 'natural area', Perdido Key, Florida, USA. Ocean and Shoreline Management, 11(1988), pp. 395–408.

Roelvink, J.A., and Stive, M.J.F., 1989. Bar-generating cross-shore flow mechanisms on a beach. J. Geophys. Res., Vol. 94, No. C4, pp. 4785–4800.

Saville, T., Jr., 1957. Scale effects in two dimensional beach studies. Transactions from the 7th general meeting of the International Association of Hydraulic Research, Vol. 1, pp. A3-1–A3-10.

Saville, T., Jr., and Caldwell, J.M., 1953. Accuracy of hydrographic surveying in and near the surf zone. Technical Memorandum No. 32, Beach Erosion Board, Corps of Engineers, March, 1953. See also Proc. Third Coastal Engineering Conference, J.W. Johnson, Ed., Council on Wave Research, The Engineering Foundation, Berkeley, CA, pp. 31–47.

Seymour, R.J., and King, D.B., Jr., 1982. Field comparisons of cross-shore transport models. J. of Waterway, Port, Coastal and Ocean Division, Vol. 108, No. WW2, American Society of Civil Engineers, New York, NY, pp. 163–179.

Shemdin, O.H., Brooks, H.K., Ceylanli, Z., and Harrell, S.L., 1976. Comprehensive monitoring of a beach restoration project. Proc. Fifteenth Coastal Engineering Conference, Vol. 2, American Society of Civil Engineers, New York, NY, pp. 1477–1492.

Skrabal, T.E., Ramsey, K.A., and Henry, R.D., 1990. Monitoring results of a beach replenishment project at Fenwick Island, Delaware. Beaches: Lessons of Hurricane Hugo, Proc. 1990 National Conference on Beach Preservation Technology, Florida Shore and Beach Preservation Association, Tallahassee, FL, pp. 36–52.

Sorensen, R.M., Douglass, S.L., and Weggel, J.R., 1988. Results from the Atlantic City, NJ, beach nourishment program. Proc. Twenty-First Coastal Engineering Conference, Vol. 3, American Society of Civil Engineers, New York, NY, pp. 2806–2817.

Spadoni, R.H., 1992. Monitoring of the 1988 Boca Raton beach nourishment project. Proc. Coastal Engineering Practice '92, S.A. Hughes, Ed., American Society of Civil Engineers, New York, NY, pp. 120–136.

Stauble, D.K., Garcia, A.W., Kraus, N.C., Grosskopf, W.G., and Bass, G.P., 1992. Beach nourishment project response and design evaluation: Ocean City, Maryland. Report 1: 1988–1992 (Draft). Coastal Engineering Research Center, U.S. Army Corps of Engineers, in press.

Stauble, D.K., and Holem, G.W., 1991. Long term assessment of beach nourishment project performance. Proc. Coastal Zone '91, Vol. 1, American Society of Civil Engineers, New York, NY, pp. 510–524.

Stive, M.J.F., and Wind, H.G., 1986. Cross-shore mean flow in the surf zone. Coastal Engineering, Vol. 10, No. 4, pp. 325–340.

Stone, G.W., Stapor, F.W., Jr., May, J.P., and Morgan, J.P., 1992. Multiple sediment sources and a cellular, non-integrated, longshore drift system: Northwest Florida and southeast Alabama coast, USA. Marine Geology, 105: 141–154.

Svendsen, I.A., 1984a. Wave heights and setup in a surf zone. Coastal Engineering, Vol. 8, pp. 303–329.

Svendsen, I.A., 1984b. Mass flux and undertow in a surf zone. Coastal Engineering, Vol. 8, pp. 347–365. (Discussion, Coastal Engineering, Vol. 10, No. 3, pp. 289–299, 1986. Reply, Coastal Engineering, Vol. 10, No. 3, pp. 299–307, 1986.)

Svendsen, I.A., and Hansen, J.B., 1988. Cross-shore currents in surf-zone modeling. Coastal Engineering, Vol. 12, No. 1, pp. 23–42.

Thompson, E.F., and Harris, D.L., 1972. A wave climatology for U.S. coastal waters. Proc. of Offshore Technology Conference, Dallas, TX, pp. 675–688.

Thornton, E.B., and Guza, R.T., 1983. Transformation of wave height distribution. J. Geophys. Res., Vol. 88, No. C10, pp. 5925–5938.

University of Florida, 1971. Study report to determine behavior of project fill for beach erosion control, Treasure Island, Florida. Coastal and Oceanographic Engineering Laboratory, University of Florida, Gainesville, FL.

University of Florida, 1973. Performance predictions of planned beach fill at Delray Beach, Florida. Coastal and Oceanographic Engineering Laboratory, University of Florida, Gainesville, FL.

U.S. Army Corps of Engineers, 1972. Evaluation of weir jetty systems at Perdido Pass, Alabama, and East Pass, Florida. U.S. Army Corps of Engineers, Mobile District, Mobile, Alabama.

U.S. Army Corps of Engineers, 1984. Shore Protection Manual, Coastal Engineering Reseach Center, Vicksburg, MS.

U.S. Department of Commerce, National Oceanic and Atmospheric Administration, 1981. United States Coast Pilot, 5 - Atlantic Coast: Gulf of Mexico, Puerto Rico, and Virgin Islands, Fourteenth Edition.

U.S. Naval Weather Service Command, 1975. Summary of Synoptic Meteorological Observations, North American Coastal Marine Areas — Revised, Atlantic and Gulf Coasts, Volume 4. National Climatic Center, Asheville, NC.

Vesper, W.H., 1961. Behavior of beach fill and borrow area at Prospect Beach, West Haven, Connecticut. Technical Memorandum No. 127, Beach Erosion Board, Corps of Engineers, Department of the Army.

Walton, T.L., 1973. Littoral drift computations along the coast of Florida by means of ship wave observations. Coastal and Oceanographic Engineering Department TR-15, University of Florida, Gainesville, FL.

Walton, T.L., 1977. Beach nourishments in Florida and on the lower Atlantic and Gulf coasts. Florida Sea Grant Technical Paper No. 2, Coastal and Oceanographic Engineering Department, University of Florida, Gainesville, FL.

Watts, G.M., 1956. Behavior of beach fill at Ocean City, New Jersey. Technical Memorandum No. 77, Beach Erosion Board, Corps of Engineers, Department of the Army.

Watts, G.M., 1958. Behavior of beach fill and borrow area at Harrison County, Mississippi. Technical Memorandum No. 107, Beach Erosion Board, Corps of Engineers, Department of the Army.

Watts, G.M., 1959. Behavior of beach fill at Virginia Beach, Virginia. Technical Memorandum No. 113, Beach Erosion Board, Corps of Engineers, Department of the Army.

Weggel, J.R., 1972. Maximum breaker height. J. Waterway, Port, Coastal and Ocean Engineering, Vol. 98, No. WW4, American Society of Civil Engineers, New York, NY, pp. 529–548.

Winton, T.C., Chou, I.B., Powell, G.M., and Crane, J.D., 1981. Analysis of coastal sediment transport processes from Wrightsville Beach to Fort Fisher, North Carolina. Miscellaneous Report No. 81–6, Coastal Engineering Research Center, U.S. Army Corps of Engineers, Fort Belvoir, VA.

Work, P.A., and Dean, R.G., 1990. Even/odd analysis of shoreline changes adjacent to Florida's tidal inlets. Proc. Twenty–Second Coastal Engineering Conference, Vol. 3, American Society of Civil Engineers, New York, NY, pp. 2522–2535.

Work, P.A., and Dean, R.G., 1992. Perdido Key Beach Nourishment Project: Gulf Islands National Seashore. 1991 Annual Report. Coastal and Oceanographic Engineering Department, University of Florida, Gainesville, FL.

Work, P.A., Lin, L.–H., and Dean, R.G., 1990a. Perdido Key Beach Nourishment Project: Gulf Islands National Seashore. Pre–Nourishment Survey, Conducted October 28–November 3, 1989. Coastal and Oceanographic Engineering Department, University of Florida, Gainesville, FL.

Work, P.A., Lin, L.–H., and Dean, R.G., 1990b. Perdido Key Beach Nourishment Project: Gulf Islands National Seashore. First Progress Report. Coastal and Oceanographic Engineering Department, University of Florida, Gainesville, FL.

Work, P.A., Lin, L.–H., and Dean, R.G., 1991a. Perdido Key Beach Nourishment Project: Gulf Islands National Seashore. First Post–Nourishment Survey — Conducted September 22–26, 1990. Coastal and Oceanographic Engineering Department, University of Florida, Gainesville, FL.

Work, P.A., Lin, L.-H., and Dean, R.G., 1991b. Perdido Key Beach Nourishment Project: Gulf Islands National Seashore. 1990 Annual Report. Coastal and Oceanographic Engineering Department, University of Florida, Gainesville, FL.

Work, P.A., Charles, L., and Dean, R.G., 1991c. Perdido Key Historical Summary and Interpretation of Monitoring Programs. Coastal and Oceanographic Engineering Department, University of Florida, Gainesville, FL.

BIOGRAPHICAL SKETCH

Paul A. Work was born December 14, 1963, in Ann Arbor, Michigan, and spent much of his early life there, enjoying the lakes for summertime sailing and winter ice hockey games. His interest in practical science led to enrollment in the civil engineering program at the University of California at Berkeley. He graduated with a Bachelor of Science degree in civil engineering in 1986, and stayed at Berkeley for a Master of Science degree in the Hydraulic and Coastal Engineering division of the Civil Engineering Department, graduating in December, 1987.

The author was employed by the U.S. Army Corps of Engineers, Los Angeles District, through the summer of 1988, when he enrolled as a Ph.D. student in the Coastal and Oceanographic Engineering Department of the University of Florida. His 4-1/2 years at the University of Florida yielded a number of new experiences. Among these were many memorable, work-related field trips, sailing trips (non-work-related), three months on a farm in an Amish section of Pennsylvania during a semester visit to the University of Delaware, and employment as an instructor for a course on coastal engineering for high school students. He enjoys many watersports and plays a mean slide guitar.

I certify that I have read this study and that in my opinion it conforms to acceptable standards of scholarly presentation and is fully adequate, in scope and quality, as a dissertation for the degree of Doctor of Philosophy.

Robert G. Dean, Chairman
Graduate Research Professor of Coastal and Oceanographic Engineering

I certify that I have read this study and that in my opinion it conforms to acceptable standards of scholarly presentation and is fully adequate, in scope and quality, as a dissertation for the degree of Doctor of Philosophy.

Ashish J. Mehta
Professor of Coastal and Oceanographic Engineering

I certify that I have read this study and that in my opinion it conforms to acceptable standards of scholarly presentation and is fully adequate, in scope and quality, as a dissertation for the degree of Doctor of Philosophy.

Hsiang Wang
Professor of Coastal and Oceanographic Engineering

I certify that I have read this study and that in my opinion it conforms to acceptable standards of scholarly presentation and is fully adequate, in scope and quality, as a dissertation for the degree of Doctor of Philosophy.

Ulrich H. Kurzweg
Professor of Aerospace Engineering, Mechanics, and Engineering Science

This dissertation was submitted to the Graduate Faculty of the College of Engineering and to the Graduate School and was accepted as partial fulfillment of the requirements for the degree of Doctor of Philosophy.

December, 1992

for Winfred M. Phillips
Dean, College of Engineering

Madelyn M. Lockhart
Dean, Graduate School

UNIVERSITY OF FLORIDA
3 1262 08556 8607